A.G. Amelin

Theory of Fog Condensation

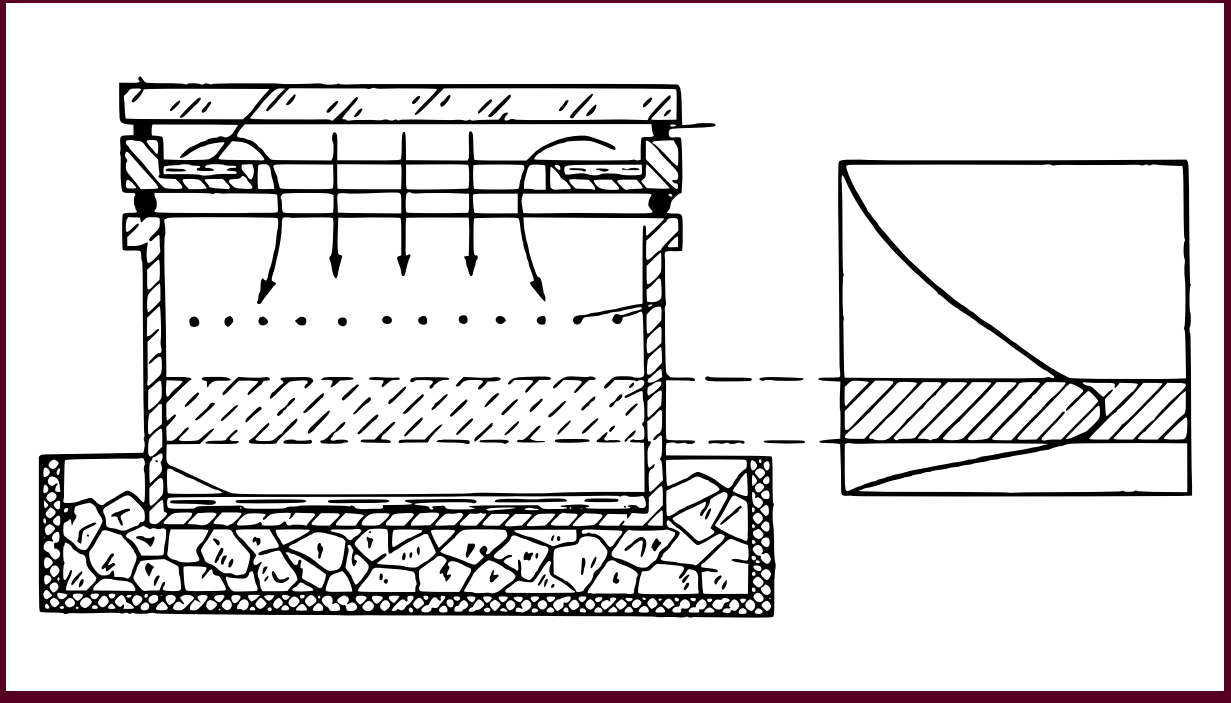

A. G. Amelin

THEORY OF FOG CONDENSATION

Second edition, augmented and revised
Edited by B. V. Deryagin

Translated from Russian
by Z. Lerman

Israel Program for Scientific Translations
Jerusalem 1967

This book is a translation of

TEORETICHESKIE OSNOVY OBRAZOVANIYA
TUMANA PRI KONDENSATSII PARA
Izdatel'stvo "Khimiya"
Moskva 1966

IPST Cat. No. 2186

Printed and Bound in Israel
Printed in Jerusalem by S. Monson
Wiener Bindery Ltd.

VI/10

TABLE OF CONTENTS

PREFACE vii

INTRODUCTION ix

CHAPTER ONE. GENERAL ASPECTS OF FOG CONDENSATION 1
Supersaturated vapor 1
Formation of liquid droplets in a gas 2
Vapor condensation on nuclei 3
Thermodynamic derivation of Kelvin equation . 7
Homogeneous condensation of vapor 9
Derivation of the formula for the rate of formation of embryos 9
New trends in the theory of homogeneous vapor condensation . 15
Critical vapor supersaturation 16
Methods for the determination of critical supersaturation . . . 17
Dependence of critical supersaturation on temperature . 19
Condensation nuclei 20
Experimental data on nucleation rates 24
Accommodation coefficients 27
Rate of vapor condensation on the surface of droplets 29
Temperature of a droplet in supersaturated vapor 31
Dispersity, number density, and mass concentration of fog . . 33
Mechanism of fog formation 35
References 39

CHAPTER TWO. FORMATION OF SUPERSATURATED VAPOR AND FOG BY ADIABATIC EXPANSION AND RADIATIVE COOLING 43
Fog formation in an adiabatically expanding vapor-gas mixture . . 43
Working formulas for supersaturation 43
Droplet size and number density of fog 47
Numerical calculation of fog formation by adiabatic expansion . . 51
Cloud chamber and its application 55
Adiabatic processes in nature and in industry 58
Fog formation by radiative cooling . . . 58
References 60

CHAPTER THREE. FORMATION OF SUPERSATURATED VAPOR AND FOG IN TURBULENT MIXING OF GASES 61
Derivation of working formulas for the supersaturation 61
Fundamental properties of turbulent jets 72
Drop size distribution and number density 80
Rate of nucleation and rate of growth of droplets in a jet . . . 83
Determination of critical supersaturation in a jet 85
Various cases of fog formation in turbulent mixing of gases . . . 87
References 92

CHAPTER FOUR. FORMATION OF SUPERSATURATED VAPOR AND FOG BY MOLECULAR DIFFUSION AND THERMAL CONDUCTION . . 94
Derivation of working formulas 94
The diffusion chamber 98
Preparation of metal powders 100
Formation of radiative fogs 101
References 103

CHAPTER FIVE. FORMATION OF SUPERSATURATED VAPOR AND FOG BY EDDY AND MOLECULAR DIFFUSION AND THERMAL CONDUCTION 105
Formation of supersaturated vapor during vapor condensation in a pipe 105
Formation of supersaturated vapor in a turbulent stream between surfaces of different temperature 113
Formation of supersaturated vapor in the boundary layer 115
Formation of fog during vapor condensation on a surface 117
Drop size distribution and number density of fog in pipe condensers 121
Calculation of drop size distribution and number density of fog forming when H_2SO_4 vapor condenses in a pipe 127
Prevention of fog during freezing out of vapor 141
Prevention of fog during the recovery of volatile solvents by condensation 147
Prevention of fog during vapor condensation in spray towers . . . 152
Prevention of fog during vapor condensation in bubblers 163
References 168

CHAPTER SIX. FORMATION OF SUPERSATURATED VAPOR AND FOG AS THE RESULT OF CHEMICAL REACTIONS OF GASES IN THE VOLUME 170
Derivation of working formulas for supersaturation 170
Formation of fog when SO_3 is absorbed by aqueous H_2SO_4 solutions 174
Photoelectric nephelometry 181
Formation of condensation nuclei in the atmosphere as the result of chemical reactions of gases in the volume 185

Production of soot, silica smoke, and Al_2O_3 powder 187
Various cases of fog formation as the result of chemical reactions of gases in the volume . . 195
References 199

CHAPTER SEVEN. FOGS WITH CONTROLLED NUMBER DENSITY AND DROP SIZE DISTRIBUTION 202
Drop size and number density as a function of supersaturation . . 202
Control of drop size distribution and number density of fogs . . . 206
Control of drop size in medical aerosols and pesticide sprays . . 208
Control of fog dispersity during vapor condensation on the surface 213
Generation of artificial condensation nuclei and monodisperse fog 216
References 220

APPENDIX I 222

APPENDIX II 223

APPENDIX III 224

APPENDIX IV 224

BIBLIOGRAPHY ON AEROSOLS 225

SUBJECT INDEX 229

LIST OF ABBREVIATION 235

PREFACE TO THE SECOND RUSSIAN EDITION

Although fog is a common phenomenon in nature, which is also often encountered in a variety of industrial processes and in research work, the theory of fog development is still at its infancy, and a lack of some basic data is often felt when dealing with practical applications.

This book presents the theoretical principles of fog formation. Fundamental formulas are derived for the prediction and, possibly, prevention of fog in various practical cases. The basic research on the subject is reviewed, and the theoretical findings are substantiated by comparing them with experimental data.

Since formation of fog by homogeneous vapor condensation is possible only in an atmosphere of supersaturated vapor, the different processes leading to the development of supersaturation are considered in some detail. The industrial mists are classified according to the processes responsible for the development of supersaturated vapor and are considered in the respective chapters. The practical application of the theoretical techniques for the prevention of fog formation is treated in ample detail.

One of the principal aims in writing this book was to familiarize the reader with methods for appraising the probability of fog formation in different particular cases and calculating the drop sizes and the number densities of mists. The examples are therefore largely based on cases of fog formation often encountered in practice.

The subject of this book is fog condensation, and the formation of mists by mechanical pulverization and spraying of liquids is not discussed. The physical mechanisms are entirely different for these two cases.

The number of theoretical and experimental researches on aerosols in general and fog in particular has been rapidly growing during the recent years and in preparing

the second edition of this book I have attempted to include the latest published data which pertain to formation of fog during vapor condensation. New theoretical and experimental data on rate of nucleation, critical supersaturation, rate of vapor condensation on droplets, etc., are included in Chapter One.

Chapter Five is of particular applied significance, since fog often forms in various industrial processes when a vapor-laden gas stream is cooled by contact with a colder surface. Particular cases of industrial mists, e.g., in the sulfuric acid manufacture, are therefore considered in great detail in parallel with theoretical results and laboratory findings. Sulfuric acid was chosen because its peculiar properties make it ideally suited for the investigation of the general features of aerosol systems. Sulfuric acid mist forms in different stages of the acid manufacturing process, and also when the acid is used in other industries.

Chapter Seven — "Fogs with Controlled Number Density and Drop Size Distribution" — analyzes the effect of various factors on drop sizes and number densities of fogs, and describes techniques for controlling these indices. Some practical examples of fog control are considered at the end of the chapter. The two principal indices of fog can always be controlled so as to alter the fog properties in the desired direction.

I am indebted to Prof. N. A. Fuks, Acad. S. I. Vol'fkovich, I. V. Petryanov, Corr. Member USSR Acad. Sci., G. K. Borekov, Corr. Member USSR Acad. Sci., Prof. S. B. Gorbachev, Prof. K. M. Malin and many other authorities on aerosols for valuable advice; my thanks are also due to the research workers M. I. Belyakov, E. V. Yashke, V. A. Petrovskii, Z. B. Borodastova, A. I. Baranova, and others who actively participated in various theoretical and experimental investigations of the process of vapor condensation and took the trouble to reduce the experimental findings.

I am particularly grateful to B V. Deryagin, Corr. Member USSR Acad. Sci., for his attention and help in the course of my research on fog development.

A. G. Amelin

Fog is a disperse system consisting of liquid droplets suspended in a gas. If the dispersed phase is a suspension of solid particles, we speak of smoke or dust. These different kinds of gaseous suspensions — fog, smoke, and dust — constitute what is generally known as aerosols (see Appendix I).

Fog develops due to condensation of vapor in a gas which remains noncondensible under the particular conditions (condensation fog); alternatively, fog can be formed by mechanical spraying of a liquid. These two cases of fog formation are considered separately because they are governed by different physical mechanisms.

Minute droplets of liquid are capable of considerable supercooling (e.g., water droplets can be supercooled to −40 °C). It has been therefore suggested (Ostwald) that the development of fog by homogeneous condensation of vapor in a noncondensible gas begins with the formation of liquid droplets which, upon being cooled further, may solidify. The theoretical principles of fog formation considered in this book are therefore applicable to the formation of aerosols in general. Moreover, the direct conversion of gas to solid phase in nature is also governed by the same laws as those which apply to the development of liquid embryos.

The peculiar properties of the aerosols are traced back to the high specific surface and a correspondingly high surface activity of a system of finely dispersed particles. The surface energy of particles increases with the degree of dispersion, since the surface-to-volume ratio is inversely proportional to the particle radius ($F/v = 3/r$).

Knowledge of the characteristic properties of aerosols, and of fog in particular, are often needed to solve a variety of applied problems. Lack of thorough understanding of the principles involved is an obvious obstacle, and detailed understanding of the theory is essential.

Let us consider a few examples which illustrate this point.

Clouds and fog lower the visibility in the atmosphere, thus interfering with normal flight schedules and with the timetables of ships, trains, automotive transport, etc. The meteorologists should learn to predict development of clouds and fogs in advance, and to devise appropriate preventive measures for these undesirable atmospheric phenomena. On the other hand, it is the clouds which are the source of atmospheric precipitation, sustaining animal and plant life everywhere on the earth. Artificial stimulation of cloud formation and precipitation is therefore of the utmost practical significance. Fairly efficient cloud seeding techniques have been developed in recent years, and their value to agriculture cannot be overestimated.

Aerosols are widely used in medicine: various infections in man and domestic animals are treated by applying the medicament as a fine spray. Disinfectants are also sprayed in a cloud of fine mist: the minute droplets penetrate into every nook and cranny, effectively destroying the disease carriers. Aerosol treatment ensures maximum speed of recovery and the patient is spared otherwise painful methods of topical or systemic application. The medicinal spray is naturally inhaled with the air the patient breathes. In the lungs the air comes in contact with the alveoli, having a total surface area of nearly 100 m^2. The spray is deposited on the surface of the alveoli and is readily absorbed into the blood.

Industrial emission gases, exhaust fumes of internal combustion engines, etc., contain a high proportion of suspended particles. In the air, these particles act as condensation nuclei and enhance the formation of fog (or rather "smog") in the ground layer, where it constitutes a considerable health hazard to man. The content of suspended pollutants in industrial emissions should therefore be minimized: the hazardous effect can be avoided by preventing fog formation altogether or, conversely, by stimulating development of aerosols which consist of particularly large particles that are easy to separate.

Agricultural diseases and pests are effectively suppressed by spraying the plants with a pesticide solution. A cloud of mist consisting of minute droplets of the liquid pesticide is generated and allowed to envelope the treated plants. The liquid droplets are deposited on the plant surface and begin to flow coalescing into a very thin film of the pesticide. This facilitates the absorption of the poison into the insect's system and ensures high efficacy of treatment.

When vapor condenses in a noncondensible gas, a case often encountered in a variety of industrial processes, the resulting supersaturation conditions almost inevitably lead to the development of fog. The manufacture of phosphoric, sulfuric, and many other acids is plagued by the formation of a highly stable corrosive mist, which readily passes through conventional filters and collectors to be emitted into the air as a harmful pollutant. It causes much damage in the neighborhood of the plant and actually poisons the atmosphere, not to speak of the substantial losses of the acid in the industrial process.

Powder metallurgy is a rapidly developing new industry. Metal powders are used in machine building and instrumentation, in the manufacture of various parts and components, and in many other branches of the national economy, where the high adsorptivity and chemical activity of the metal powders is employed to a considerable advantage. Some metals in a finely dispersed state can be effectively used in medicine and veterinary practice, and also for pest control in agriculture.

Finely divided and highly active metal powders are mostly generated by homogeneous condensation of the metal vapor. These powder-metallurgical methods are based on the general principles governing the development of supersaturated vapor in a noncondensible gas.

The theory of vapor condensation is also of considerable significance for the production of soot and "silica smoke" (extremely finely divided silica, known under a variety of names, e.g., Aerosil, Hi-Sil, Carb-O-Sil, and others).

Soot is manufactured by burning hydrocarbons to release elemental carbon into a gas medium. The conditions are further controlled to ensure that the vapor pressure of the released carbon is substantially higher than the saturated vapor pressure of carbon. High supersaturation develops, and carbon vapor condenses into soot particles. The particles become progressively smaller as the supersaturation is increased, and soot of correspondingly finer quality is obtained. Despite the widespread use of soot, the theory of its formation has been developed insufficiently, and soot manufacture is largely based on empirical techniques.

Silica smoke also requires highly supersaturated vapor in a noncondensible gas phase. Vapor is caused to condense spontaneously into minute spherical particles. The dispersity of the final product (which is an index of its quality) actually depends on the degree of supersaturation of the vapor. Again, no reliable theoretical data are available and the process is largely run by rule of thumb.

Dispersity (drop size distribution) and number density of a fog are the main indices which determine its specific properties. The two indices change continuously as the droplets coagulate, evaporate, or grow by vapor condensation on their surface. The properties of the fog are therefore also variable. The number density and the droplet size range between very wide limits which depend on the conditions of fog formation and the variation of different parameters with time. The smallest droplets are aggregates of a few molecules, whereas the largest droplets may have radii of a few millimeters; the number density may vary from 0 to 10^{12} droplets per 1 cm^3 of gas.

Fog condensation is invariably preceded by some process which raises the degree of supersaturation of the vapor. When the supersaturation exceeds some critical value (p. 16), which is dependent on the composition of the liquid and the temperature of the medium, fog starts forming at a perceptible rate. The conditions leading to an increase of vapor supersaturation are thus decisive for the development of fog, and considerable space is therefore devoted to this aspect of the theory. In practice, the degree of supersaturation is different at different points in the system. It reaches supercritical values at isolated regions, and fog starts forming locally.

Fog generally develops in a system where the concentration of the noncondensible gas is substantially higher than the concentration of the condensible vapor. It is this particular case of vapor-gas mixtures that is given the fullest treatment in this book.

Since the drop size and the number density are responsible for the characteristic properties of the fog, these indices should constitute the basis of any theoretical discussion of aerosols. The methods for the calculation of drop sizes and number densities are unfortunately highly inadequate, but nevertheless the theoretical data presented in the book give some idea of the extent to which different factors influence these fundamental fog indices. The numerical methods described in the book for the calculation of drop sizes and number densities, though obviously approximate, are quite sufficient for the majority of practical problems.

Chapter One

GENERAL ASPECTS OF FOG CONDENSATION

SUPERSATURATED VAPOR

When a liquid is allowed to remain in contact with its vapor in a closed space at a constant temperature, the so-called saturated vapor pressure is attained in the system after some time: this is a characteristic equilibrium parameter of each liquid. The slightest increase in vapor pressure above the liquid surface will result in immediate condensation of vapor on the surface, whereas the smallest decrease in pressure will produce additional evaporation of liquid from the surface. The saturated vapor pressure above convex and concave surfaces is respectively higher and lower than the pressure above a plane surface, and in this book we invariably operate with the saturated vapor pressure above a plane surface.

If the vapor pressure in the gaseous phase is higher than the saturated vapor pressure, the vapor is said to be supersaturated. The degree of vapor supersaturation is expressed by the equality

$$S = \frac{p}{p_\infty(T)} \tag{1.1}$$

where S is the supersaturation*, p vapor pressure in the gas phase, $p_\infty(T)$ saturated vapor pressure above a plane surface of the same liquid at the temperature T.

The dependence of the saturated vapor pressure on temperature for most liquids is expressed with varying degrees of accuracy by theoretical and empirical equations. In this book we adopt the simplified relation derived from the Clausius—Clapeyron equation, as it is fairly convenient in applications:

$$\ln p_\infty(T) = C - \frac{E}{T}; \quad p_\infty(T) = e^{C - \frac{E}{T}} \tag{1.2}$$

or

$$\lg p_\infty(T) = A - \frac{B}{T}; \quad p_\infty(T) = 10^{A - \frac{B}{T}} \tag{1.3}$$

where C, E, A, and B are coefficients.

* Clearly, $S > 1$ signifies that the vapor is supersaturated, $S = 1$ the vapor is saturated, and $S < 1$ unsaturated. The parameter $S = \frac{p}{p_\infty(T)}$ is therefore called supersaturation, although a more conventional term is saturation ratio.

In (1.2)

$$E = \frac{Q}{R} = \frac{ML}{8.314} = 0.12ML \tag{1.4}$$

where Q is the molar heat of evaporation, J/mole; M the mass of one mole; L the specific heat of evaporation, J/g; R the gas constant, $J \cdot deg^{-1} \times \times mole^{-1}$.

The numerical values of the coefficients A and B for various substances are given in standard reference books /1, 2/; some of the data are listed in Appendix II.

From equations (1.2) and (1.3) we have

$$C = 2.3A; \quad E = 2.3B \tag{1.5}$$

Inserting the expression for $p_\infty(T)$ from (1.2) in (1.1), we find

$$S = \frac{p}{f(T)} = \frac{p}{e^{C - \frac{E}{T}}} \tag{1.6}$$

In nature and in industrial processes, the vapor pressure in a gas and the temperature of the gas are normally variable with time, so that vapor supersaturation changes correspondingly. The general equation which expresses the dependence of S on time and temperature can be obtained by differentiating (1.6):

$$\frac{dS}{d\tau} = \frac{dp}{p_\infty(T)\,d\tau} - \frac{pE\,dT}{T^2 p_\infty(T)\,d\tau} \tag{1.7}$$

or

$$\frac{dS}{dT} = \frac{dp}{p_\infty(T)dT} - \frac{p\varepsilon}{T^2 p_\infty(T)} \tag{1.8}$$

FORMATION OF LIQUID DROPLETS IN A GAS

Condensation — the transition of vapor into liquid — may occur on a surface above which the saturated vapor pressure is less than the vapor pressure in the gas volume: the vapor condenses on the surface of condensation nuclei already present in the gas mixtures or on spontaneously forming embryos. As vapor condenses, suspended liquid droplets form in the gas which constitute the visible fog.

The distinction between condensation in a gas volume and condensation on a surface is arbitrary: in either case, vapor condenses on a surface. The condensation surface is normally provided by the container walls or a film of liquid, while in a gas volume vapor condenses on the surface of condensation nuclei, present in the form of suspended impurities or gas ions, or on the surface of embryos, molecular aggregates which arise spontaneously in the result of statistical fluctuations in the gas medium.

Above the convex surface of small liquid droplets (and of condensation nuclei in general), the saturated vapor pressure is higher than above a

plane surface: it increases as the radius of curvature is decreased. A necessary condition for the formation of fog by vapor condensation in a gas medium is therefore the presence of supersaturated vapor.

If the droplets are formed by vapor condensation on condensation nuclei or gas ions, the process is called heterogeneous condensation. If the droplets are formed in the result of vapor condensation on spontaneously forming embryos, the process is called homogeneous (spontaneous) condensation.

Heterogeneous vapor condensation can be divided into two stages: formation of supersaturated vapor and condensation of vapor on nuclei or gas ions which grow to the size of droplets.

Homogeneous condensation is substantially different from heterogeneous condensation. It consists of three stages: formation of supersaturated vapor; nucleation of embryos; condensation of vapor on the embryonic surfaces and the growth of embryos to the size of fog droplets.

Vapor condensation in a gas volume begins when a certain supersaturation, called critical supersaturation S_{cr} is attained (p. 16).

It follows from the preceding that, in principle, droplet formation follows the same course in both cases: vapor condenses on condensation centers present in the gas mixture. In homogeneous condensation, the priming centers are liquid embryos which form spontaneously; in heterogeneous condensation vapor condenses on nuclei — foreign particles or charged ions.

The conversion of vapor to fog, i.e., transition of matter from one qualitative state to another, is a discontinuous, abrupt process. The discontinuous transition occurs under critical conditions, when $S=S_{cr}$. Hence it follows that in order to establish the likelihood of fog formation and to develop preventive measures, one has to know the critical supersaturation of vapor (this is a characteristic parameter of each particular substance under a given set of condensation conditions) and the actually attainable supersaturation. The latter factor gives the maximum supersaturation of vapor, since fog condensation may set in locally, in isolated parts of the system, where the peak supersaturation has been attained.

VAPOR CONDENSATION ON NUCLEI

We first consider the simplest case when condensation nuclei are minute droplets of the condensing liquid.

When equilibrium has been established between the droplet and the surrounding medium, the vapor pressure p_r becomes equal to p, and we thus have

$$\frac{p_r}{p_\infty(T)} = \frac{p}{p_\infty(T)} = S$$

The relation of the saturated vapor pressure above the droplet and of the vapor supersaturation to the droplet radius is expressed by Kelvin's equation /3/

$$\ln S = \ln \frac{p_r}{p_\infty(T)} = \frac{2\sigma m}{kT\rho r} = \frac{2\sigma M}{RT\rho r} \qquad (1.9)$$

where S is the supersaturation corresponding to the equilibrium saturated vapor pressure above the droplet; p_r saturated vapor pressure above the droplet, mm Hg; $p_\infty(T)$ saturated vapor pressure above a plane surface, mm Hg; σ surface tension of the droplet, dyne/cm; m mass of vapor molecule, g; k Boltzmann's constant ($1.38 \cdot 10^{-16}$ erg/deg); T temperature, °K; ρ density of the liquid*, g/cm^3; r droplet radius, cm; M the mass of one mole of liquid; R the universal gas constant ($8.315 \cdot 10^7$ erg $\cdot$ deg^{-1} $\cdot$ mole^{-1}).

If the supersaturation in the gas mixture is greater than the value S calculated from (1.9), vapor will condense on the surface of the droplet and the droplet radius will increase. If, however, the vapor supersaturation in the gas mixture is less than S, vapor molecules will evaporate from the surface of the droplet and its radius will decrease. If the supersaturation in the gas mixture is equal to the S from (1.9), the processes of droplet growth and evaporation are equiprobable, i.e., given a sufficiently large population of droplets in the gas, half of them will grow by condensation and the other half will shrink by evaporation. The saturated vapor pressure above each droplet, and therefore the supersaturation expressed by equation (1.9), is thus metastable.

For water vapor in air at $T = 293$ °K we have from (1.9)

$$S = e^{\frac{1.07 \cdot 10^{-7}}{r}} \tag{1.10}$$

Table 1.1 lists the values of S calculated from (1.10) for various droplet radii.

TABLE 1.1. Saturated vapor pressure above water droplets

Droplet radius r, cm	Saturated vapor pressure p_r		Supersaturation S	Droplet radius r, cm	Saturated vapor pressure p_r		Supersaturation S
	N/m^2	mm Hg			N/m^2	mm Hg	
$1.0 \cdot 10^{-4}$	$2.33 \cdot 10^3$	17.5	1.001	$7.8 \cdot 10^{-8}$	$9.3 \cdot 10^3$	70	4.00
$1.0 \cdot 10^{-5}$	$2.36 \cdot 10^3$	17.7	1.01	$6.7 \cdot 10^{-8}$	$1.2 \cdot 10^4$	88	5.00
$1.0 \cdot 10^{-6}$	$2.61 \cdot 10^3$	19.6	1.12	$6.0 \cdot 10^{-8}$	$1.4 \cdot 10^4$	105	6.00
$2.3 \cdot 10^{-7}$	$3.7 \cdot 10^3$	28	1.60	$5.6 \cdot 10^{-8}$	$1.6 \cdot 10^4$	122	7.00
$1.9 \cdot 10^{-7}$	$4.1 \cdot 10^3$	31	1.78	$5.2 \cdot 10^{-8}$	$1.9 \cdot 10^4$	140	8.00
$1.0 \cdot 10^{-7}$	$7.1 \cdot 10^3$	53	3.00				

Curve 1 in Figure 1.1 plots the supersaturation corresponding to the equilibrium vapor pressure above a droplet of radius r as a function of the radius (for a droplet with $r = 5 \cdot 10^{-8}$ cm, $S = 9$).

The data of Table 1.1 for droplets of very small radius should be considered as tentative, since the surface tension σ decreases with decreasing droplet radius /4—8/.

No reliable data have been published on the relation of σ to r, and we must satisfy ourselves with the various theoretical formulas expressing the approximate dependence of surface tension on radius. Thus, from /9/

$$\sigma_r = \frac{\sigma_\infty}{1 + 2\frac{\delta}{r}} \tag{1.11}$$

* The density of vapor ρ_0 is ignored. Otherwise the difference $\rho - \rho_0$ should be substituted for ρ in (1.9).

or from /7/

$$\sigma_r = \sigma_\infty\left(1 - \frac{2}{kr}\right) \tag{1.12}$$

where σ_r and σ_∞ are the surface tension of a droplet and of a plane surface, respectively, dyne/cm; δ, k are coefficients.

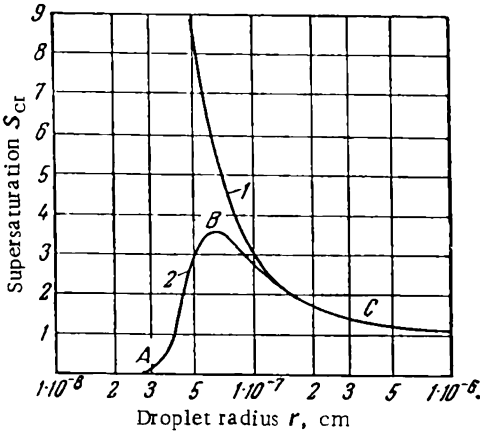

FIGURE 1.1. Equilibrium supersaturation near the surface of a water droplet vs. droplet radius:
1) electrically neutral droplet; 2) singly charged droplet.

It has been shown /10/ that simple substitution of σ_r for the tabulated values of σ_∞ in equation (1.9) does not solve the problem of variability of surface tension with droplet size: the equation itself should be radically modified.

If the droplets are electrically charged, the saturated vapor pressure above the droplets and the corresponding supersaturation are less than the respective quantities for electrically neutral droplets of the same radius. The dependence of vapor supersaturation above a droplet on its radius and electric charge is expressed by the equation

$$\ln S = \ln\frac{p_r}{p_\infty(T)} = \frac{M}{RT\rho}\left(\frac{2\sigma}{r} - \frac{e^2}{8\pi r^4}\right) \tag{1.13}$$

where e is the electric charge in ESU.

Table 1.2 lists the equilibrium pressure of water vapor in air above droplets at 293 °K and the equilibrium supersaturation calculated from (1.13) for droplets carrying the charge of one electron (Figure 1.1, curve 2). For droplet radii over 10^{-7} cm, the effect of this charge is negligible, but for smaller droplets electric charge has a considerable influence. For example, vapor supersaturation above an electrically neutral droplet grows steeply with decreasing radius, while for charged droplets supersaturation reaches a maximum of 3.6 for $r = 6.7\cdot10^{-8}$ cm and falls off for droplets of smaller radii (Figure 1.1). Uncharged droplets therefore cannot exist in an unsaturated gas mixture, while charged droplets may be present in saturated ($S = 1$) and even undersaturated ($S < 1$) vapor. Consequently, if ions are present in the gas mixture, minute droplets of liquid do not vaporize even if the vapor pressure is below saturation.

These droplets, however, cannot grow to a substantial size, since the droplet radius can increase only when $S > 1$ (Figure 1.1, curve 2, the ascending branch AB).

TABLE 1.2. Saturated vapor pressure above singly charged water droplets

Droplet radius r, cm	Saturated vapor pressure p_r		Supersaturation S	Droplet radius r, cm	Saturated vapor pressure p_r		Supersaturation S
	N/m^2	mm Hg			N/m^2	mm Hg	
$2.3 \cdot 10^{-7}$	$3.7 \cdot 10^3$	28	1.6	$5.6 \cdot 10^{-8}$	$7.9 \cdot 10^3$	59	3.4
$1.9 \cdot 10^{-7}$	$4.1 \cdot 10^3$	31	1.78	$5.2 \cdot 10^{-8}$	$7.2 \cdot 10^3$	54	3.1
$1.6 \cdot 10^{-7}$	$4.7 \cdot 10^3$	35	2.0	$5.0 \cdot 10^{-8}$	$6.8 \cdot 10^3$	51	2.9
$1.0 \cdot 10^{-7}$	$6.5 \cdot 10^3$	49	2.8	$4.3 \cdot 10^{-8}$	$4.0 \cdot 10^3$	30	1.7
$7.8 \cdot 10^{-8}$	$7.7 \cdot 10^3$	58	3.3	$3.9 \cdot 10^{-8}$	$1.87 \cdot 10^3$	14	0.8
$6.7 \cdot 10^{-8}$	$8.4 \cdot 10^3$	63	3.6	$3.6 \cdot 10^{-8}$	$9.2 \cdot 10^2$	7	0.4
$6.0 \cdot 10^{-8}$	$8.1 \cdot 10^3$	61	3.5				

If an appropriate supersaturation has been set up, so that the system occupies a position beyond the point B, vapor begins condensing on droplets and their radii increase by condensation (the BC branch of the curve). The larger the droplet, the smaller the saturated vapor pressure above its surface and the lower the supersaturation required for its continued growth. For water vapor in air in the presence of charged ions, the state B is attained at $S = 3.6$, so that fog should form abundantly at this supersaturation.

We thus conclude that the fog condensation in the presence of ions and in an ion-free gas is essentially governed by the same mechanism, but the supersaturation corresponding to the saturated vapor pressure is lower in ionized gas.

For most liquids, negative and positive ions have a different effect on critical supersaturation. The general reasons for this phenomenon are not clear /11/. It has been shown experimentally /12/ that in the system air — water vapor, negative ions act as condensation nuclei at $S = 4.2$, whereas condensation on positive ions commences at $S = 6$ (see Appendix IV). For many other vapors in air (acetic acid, amyl alcohol, ethyl iodide, ethyl alcohol, etc.), the condensation on positively charged nuclei occurs earlier than on negatively charged ones /13/; for some liquids (benzene and CCl_4), the condensation on positive and negative ions is nearly simultaneous /14/.

The different effect of positive and negative ions can be explained if we assume that the molecules which constitute the surface film of the droplet are so oriented that their negative charges are directed to the outside and the positive charges turn inward. The double electric layer formed in this way possesses a higher potential inside the droplet than outside, and this is responsible for the higher affinity of the droplets to negative, than to positive, ions /13, 15/.

The above mechanism of fog condensation applies also when the droplets suspended in the gas differ in their composition from the condensing liquid. However, all other conditions being equal, the supersaturation may prove to be different in the two cases. It is lower if the vapor reacts with the droplet (e.g., condensation of water vapor on droplets of sulfuric acid solution in water) or is soluble in the liquid. Vapor supersaturation is higher if the droplet surface is not wetted by the condensing liquid.

When vapor condenses on solid condensation nuclei, the mechanism of fog formation is the same as with liquid droplets, but the supersaturation corresponding to the saturated vapor pressure may differ for solid nuclei and droplets depending on the composition of the particles and their shapes. For example, if the condensation nuclei are made of chemically active substances (in relation to the condensing vapor), the conditions of equilibrium are substantially altered. If the condensation nuclei are porous, condensation is influenced by capillary forces.

Droplet formation on solid particles is the result of gradual accumulation of the condensing liquid. Regardless of the nucleus shape, the particle is gradually enveloped in a liquid film thus turning into a droplet. On first approximation, the suspended particles may be regarded as spherical; they are wetted by the liquid without interacting with it. The conditions for vapor condensation on these particles can be calculated from equations (1.9) and (1.13).

Thermodynamic derivation of the Kelvin equation

Consider a closed system at a temperature T containing vapor at a pressure p and a single liquid droplet of radius r; the droplet consists of g molecules, i.e., it has been formed when g vapor molecules have condensed to liquid. The total increment of free energy in condensation is given by the expression

$$\varphi = (\varphi_b - \varphi_a)\, g + F\sigma = (\varphi_b - \varphi_a)\, g + 4\pi r^2 \sigma \tag{1.14}$$

where φ_a, φ_b are the chemical potentials of each molecule in the vapor and the liquid phases, respectively; F the droplet surface; $4\pi r^2\sigma$ the free surface energy;

$$g = \frac{4}{3}\pi r^3 \frac{\rho}{m} = \frac{4}{3}\pi r^3 \frac{N\rho}{M} \tag{1.15}$$

where N is Avogadro's number.

In thermodynamic equilibrium, $d\varphi/dg=0$; therefore, inserting the expression for r from (1.15) in (1.14) and differentiating (σ is assumed to be independent of g, which holds true for sufficiently large r), we find

$$\frac{d\varphi}{dg} = (\varphi_b - \varphi_a) + \frac{2\cdot 4\pi\sigma}{3}\left(\frac{3M}{4\pi N\rho}\right)^{2/3} g^{-1/3} = 0 \tag{1.16}$$

or

$$\varphi_b - \varphi_a = -\frac{8\pi\sigma r^2}{3g} \tag{1.17}$$

Inserting the expression for g from (1.15), we find

$$\varphi_a - \varphi_b = \frac{2\sigma M}{N\rho r} \tag{1.18}$$

Further assuming that the vapor pressure changes slightly by dp and the temperature remains constant, we may write for the respective increments of molecular free energy in the gas and the liquid phases

$$d\varphi_a = v_a dp$$
$$d\varphi_b = v_b dp$$

where v_a, v_b is the volume occupied by a single molecule in vapor and liquid phases, respectively.

Subtracting the second equation from the first and seeing that $v_a \gg v_b$, we find (assuming the ideal gas law for the vapor)

$$d(\varphi_a - \varphi_b) = (v_a - v_b)\,dp = \frac{kT}{p}dp \tag{1.19}$$

Integrating equation (1.19) with the pressure varying from p_∞ to p, we find

$$\varphi_a - \varphi_b = kT \ln \frac{p}{p_\infty(T)} = kT \ln S = \frac{RT \ln S}{N} \tag{1.20}$$

Equating the right-hand sides of (1.18) and (1.20), we obtain

$$\ln \frac{p_r}{p_\infty(T)} = \ln S = \frac{2\sigma M}{RT\rho r} \tag{1.9}$$

The variation of free energy φ with the droplet radius is plotted in Figure 1.2 from equation (1.14). Curve 1 corresponds to saturated vapor, when $\varphi_a = \varphi_b$, and curve 2 to supersaturated vapor, when $\varphi_a > \varphi_b$. The free energy in a system with supersaturated vapor attains a maximum when g is equal to a certain critical value g^*. A droplet (or an embryo in homogeneous condensation, see p. 3) of critical size g^* is therefore in equilibrium with the vapor. This equilibrium is unstable, i.e., a slight increase in droplet radius (or an increase in supersaturation) lowers the free energy and the droplet starts growing. A slight reduction in droplet radius (or in supersaturation) raises the free energy and the droplet vaporizes.

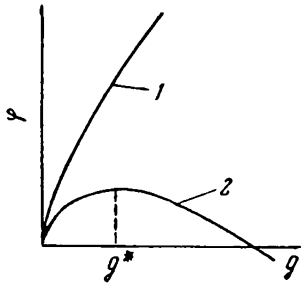

FIGURE 1.2. Free energy φ of a droplet consisting of g molecules: 1) in saturated vapor; 2) in supersaturated vapor.

The dependence of surface tension on droplet size (and thus on g) for very small droplets was given an analytical expression by Shcherbakov /10, 16–18/. When (1.14) is differentiated with respect to g, equality (1.16) is replaced with the equation

$$\frac{\partial \varphi}{\partial g} = \left[(\varphi_b - \varphi_a)\,4\pi r^2 \frac{N\rho}{m} + 8\pi r^2 \sigma + 4\pi r^2 \frac{\partial \sigma}{\partial r}\right]\frac{dr}{dg} = 0 \tag{1.21}$$

Hence for critical supersaturation, instead of (1.9) we have

$$\ln S = \frac{M}{RT\rho}\left(\frac{2\sigma}{r} + \frac{\partial \sigma}{\partial r}\right) \tag{1.22}$$

HOMOGENEOUS CONDENSATION OF VAPOR

The incessant statistical fluctuations in a vapor-gas mixture lead to the formation and rapid dissipation of multimolecular aggregates /19/. These aggregates have different sizes, and their relative content in the gas mixture decreases as the number of constituent molecules is increased.

Some of the aggregates grow to the critical size, and the associated saturated vapor pressure becomes equal to the vapor pressure in the gas medium, as expressed by equation (1.9). The molecular aggregates thus develop into embryos. Once a single vapor molecule has condensed on the surface of an embryo, the latter becomes a droplet whose radius grows by condensation at an accelerated rate (for $S = \text{const}$). If a single vapor molecule escapes from the surface of an embryo, it reverts to a simple multimolecular aggregate of subcritical size which inevitably vaporizes. Since embryo formation and dissipation are equiprobable, only half of the embyros grow into droplets.

As vapor supersaturation increases, the embryo radius decreases and the number of embryos rises, i.e., the rate of embryo formation becomes higher.

Derivation of the formula for the rate of formation of embryos

The work expended in the formation of a single embryo is the sum of the work done by the transition of particles from gas to liquid phase (in the case of supersaturated vapor this work is negative) and the work associated with the formation of a new embryonic surface. For embryos in unstable equilibrium with the supersaturated vapor, the total work according to Gibbs /20/ is given by

$$\Delta\varphi = \frac{1}{3}\sigma F \tag{1.23}$$

where F is the surface of the newly formed phase, cm^2.

For a spherical droplet

$$F = 4\pi r^2 \tag{1.24}$$

Inserting this expression for F in equation (1.23), we find

$$\Delta\varphi = \frac{4}{3}\pi r^2 \sigma \tag{1.25}$$

Inserting r from (1.9) in (1.25), we write

$$\Delta\varphi = \frac{16\pi m^2 \sigma^3}{3\rho^2 k^2 T^2 \ln S} \tag{1.26}$$

From the theory of fluctuations, the probability of formation of an embryo of a new phase in unit volume in unit time is

$$I = Ke^{-\frac{\Delta\varphi}{kT}} = Ke^{-A} \tag{1.27}$$

where I is the rate of formation of the embryos, $cm^{-3} \cdot sec^{-1}$, expressed by

$$I = \frac{dN}{d\tau} \tag{1.28}$$

K a kinetic factor; N number density (or concentration) of droplets, cm^{-3}; τ time, sec.

From (1.26) and (1.27) we have

$$A = \frac{16\pi}{3\ln^2 S}\left(\frac{m}{\rho}\right)^2\left(\frac{\sigma}{kT}\right)^3 = \frac{16\pi}{3\ln^2 S}\left(\frac{M}{\rho}\right)^2\left(\frac{\sigma}{T}\right)^3 = \frac{17.6}{\ln^2 S}\left(\frac{M}{\rho}\right)^2\left(\frac{\sigma}{T}\right)^3 \tag{1.29}$$

Equation (1.27) which expresses the nucleation rate in supersaturated vapor was originally derived by Volmer and Weber /21/. These authors considered isolated embryos: they ignored the reciprocal effects between growing and evaporating embryos. The theory of new-phase nucleation was subsequently refined and equations were derived for the rate of formation of embryos which contained the kinetic factor K in an explicit form.

Becker and Doering /22/ analyzed the steady-state case. Supersaturated vapor at a pressure p is enclosed in a container from which the growing aggregates are removed as soon as their radius surpasses the critical embryo radius. Constant vapor pressure is maintained by injecting vapor molecules from the outside. Under these conditions, the Becker-Doering equation takes the form

$$I = Ke^{-A\nu} \tag{1.30}$$

where K is the kinetic factor defined as

$$K = \frac{\alpha}{\rho}\left(\frac{2m\sigma}{\pi}\right)^{1/2}\left(\frac{p}{kT}\right)^2 \tag{1.31}$$

A is the power exponent expressed by (1.29);

$$\nu = 1 - 3g^{-2/3} + 2g^{-1} \tag{1.32}$$

where g is the number of molecules in the embryo; α the accommodation coefficient (p. 27).

From (1.9) and (1.15) it follows that

$$g = \frac{32\pi}{3\ln^3 S}\left(\frac{m}{\rho}\right)^2\left(\frac{\sigma}{kT}\right)^3 = \frac{35.2}{\ln^3 S}\left(\frac{M}{\rho}\right)^2\left(\frac{\sigma}{T}\right)^3 \tag{1.33}$$

For practical calculations, equation (1.30) can be written as

$$I = 10^{26} \cdot \frac{\alpha}{\rho}\left(\frac{p}{T}\right)^2 (M\sigma)^{1/2} e^{-A(1-3g^{-2/3}+2g^{-1})} \tag{1.34}$$

where α is the accommodation coefficient; ρ the density of liquid, g/cm^3; p vapor pressure, mm Hg; σ surface tension, dyne/cm; T temperature, °K; M molar mass.

Zel'dovich /23/, and then Frenkel /15/ proposed a more rigorous and illustrative derivation of the equation for the rate of nucleation. Frenkel in his derivation (which is also reproduced in some later works /24, 25/)

starts with the same assumption as Becker and Doering, namely that molecular aggregates of overcritical size are removed from the system and constant pressure is maintained.

We shall use the following symbols in the derivation:

g, g^*, G — the number of vapor molecules in an aggregate, an embryo, and a droplet;

N_g, N^*, N, N_∞ — the number of groups of size g, embyros, and vapor molecules in the gas mixture and the number of saturated vapor molecules above a plane surface ($N = SN_\infty$) in unit gas volume;

δ_g — the number of vapor molecules condensing in unit time on the surface of an aggregate of size g;

γ_g — the number of vapor molecules evaporating in unit time from the surface of an aggregate of size g.

The equilibrium size distribution of the aggregates in a system (in our case, 1 cm^3) containing N_∞ vapor molecules /26/ and N_g aggregates (of g molecules each) can be expressed by Frenkel's thermodynamic equation /15/

$$N_g = N_\infty e^{-\frac{\Phi}{kT}} = N_\infty e^{g \ln S - \frac{4\pi\sigma r^2 g}{kT}} \tag{1.35}$$

Figure 1.3 plots the equilibrium number of aggregates N_g as a function of aggregate size according to equation (1.35). We see from Figure 1.3 that for saturated vapor (curve 1) N_g monotonically decreases with increasing g. In supersaturated vapor, however, N_g initially decreases passing through a minimum at the critical size g^*.

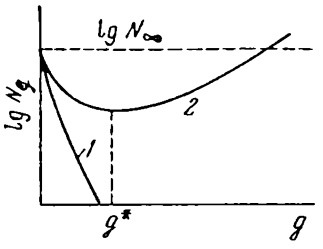

FIGURE 1.3. Equilibrium drop size distribution: 1) in saturated vapor; 2) in supersaturated vapor.

For $g \gg g^*$, N_g is greater than N_∞. This branch of curve 2 obviously does not represent a real situation, since equation (1.35) does not apply in supersaturated vapor at high values of g.

In studying the dynamic equilibrium between aggregates of size g, aggregates of size $g-1$, and vapor, we assume that the equilibrium distribution (1.35) is attained for a sufficiently high g. The equations then may be written in differential form.

The number of $g-1$ aggregates growing to g aggregates (due to condensation of vapor molecules on their surface) is $\delta_{g-1} N_{g-1}$ per second, and the number of g aggregates degrading to $g-1$ aggregates is $\gamma_g N_g$ per second. Since dynamic equilibrium is established, we have

$$\delta_{g-1} N_{g-1} = \gamma_g N_g \tag{1.36}$$

or

$$\ln \frac{\gamma_g}{\delta_{g-1}} = \ln N_{g-1} - \ln N_g = -\frac{d}{dg} \cdot \ln N_g \tag{1.37}$$

Inserting N_g from (1.35) in (1.37), we find

$$\frac{\gamma_g}{\delta_{g-1}} = e^{-\ln S + \frac{8\pi\sigma r^2}{3gkT}} \tag{1.38}$$

It follows from equation (1.38) that for very small aggregates the ratio γ_g/δ_{g-1} is very large (since $\frac{8\pi\sigma r^2}{3g} \approx \frac{1}{r}$) and the aggregates will readily evaporate. In this region dynamic equilibrium is maintained because the small aggregates are more numerous that the large ones (equation (1.29)). As g increases, the ratio γ_g/δ_{g-1} decreases to the limiting value of $1/S$. In supersaturated vapor ($S>1$), the ratio γ_g/δ_{g-1} for large aggregates is less than unity. The dynamic equilibrium is therefore maintained because N_g increases with increasing g (see Figure 1.3). For certain aggregates $\gamma_g/\delta_{g-1} = 1$. In this case $N_{g-1}=N_g$ (see equation (1.37)), which corresponds to the minimal N_g and an aggregate of the critical size g^* (an embryo).

The distribution of N_g in g expressed by equation (1.35) and curve 2 in Figure 1.3 is unattainable for $g>g^*$, because it requires the presence of an infinity of large aggregates (droplets). This state cannot be attained in practice, since as the embryos grow, the number of vapor molecules in the gas mixture decreases.

A nonequilibrium size distribution of aggregates is variable in time. Let f_g stand for this distribution; since it is different from the distribution N_g, equation (1.36) should be modified to

$$I_g = \delta_{g-1} f_{g-1} - \gamma_g f_g \tag{1.39}$$

where I_g is the number of aggregates passing from size $g-1$ to size g in 1 sec.

Initially f_g varies with time, i.e., $\frac{\partial f_g}{\partial \tau} = I_g - I_{g-1}$, but eventually a stable size distribution is attained and $I_g = I$ is a constant independent of g. Under these conditions the number of aggregates f_g remains constant, but there is a steady transition of smaller aggregates into larger ones. Indeed, the vapor condenses at a rate of I aggregates per second, and these aggregates grow passing through the entire spectrum of sizes until they evolve into an embryo and finally a visible droplet (with $r>r^*$). In other words, I may be interpreted as the current of embryos or the rate of nucleation.

To sustain the current I at small g, the steady-state distribution f_g should slightly deviate from the equilibrium distribution N_g (Figure 1.4). However, as g increases, N_g decreases, and to ensure a constant current f_g deviates progressively more from N_g. If in the process of growth some aggregates surpass the critical size (i.e., $g>g^*$), the ratio γ_g/δ_{g-1} (equation (1.37)) becomes less than unity. Further growth of these aggregates is thus more probable than their evaporation. The complexes grow to ever larger sizes, their number being inversely proportional to their lifetime, i.e., $f_g \approx 1/\delta_g$. Since δ_g increases in proportion to the surface of the aggregates, i.e., in proportion to $g^{2/3}$ (equation (1.15)), the number f_g of complexes of any size g drops as $g^{-2/3}$ (Figure 1.4).

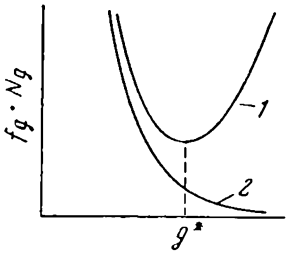

FIGURE 1.4. Equilibrium and steady-state drop size distributions in supersaturated vapor: 1) equilibrium distribution N_g; 2) steady-state distribution f_g.

To derive a differential equation for f_g, we transform equation (1.39) making use of (1.36)

and remembering that for large g the parameter δ_g approaches a constant value δ:

$$\delta = Fz = 4\pi r^2 p (2\pi m k T)^{-1/2} \tag{1.40}$$

where F is the droplet surface, cm^2; z the number of vapor molecules impinging on a unit liquid area in contact with vapor /15, 27/,

$$z = N \left(\frac{kT}{2\pi m}\right)^{1/2} = p (2\pi m k T)^{-1/2} \tag{1.41}$$

p vapor pressure in the gas.

It is further assumed that each vapor molecule hitting the surface of an aggregate sticks to it (the accommodation coefficient $\alpha = 1$, p. 27). The relevant equation thus takes the form

$$I_g = N_{g-1} \delta_{g-1} \left(\frac{f_{g-1}}{N_{g-1}} - \frac{f_g}{N_g}\right) = -\delta N_g \frac{d}{dg}\left(\frac{f_g}{N_g}\right) \tag{1.42}$$

If f_g is a steady-state distribution, I_g is equal to some constant I, so that

$$\frac{f_g}{N_g} = -\frac{I}{\delta} \int \frac{dg}{N_g} + A \tag{1.43}$$

To find A, consider the applicability of equation (1.43) at large g. Substituting N_g from (1.35) in (1.43), we write

$$\frac{f_g}{N_g} = A - \frac{I}{\delta N_\infty} \int e^{\frac{4\pi r^2 \sigma}{kT}} \cdot e^{-g \ln S} dg \tag{1.44}$$

At large g, the second exponential factor in the integrand is prevalent, so that

$$\frac{f_g}{N_g} \approx A - \frac{I}{\delta N_\infty} e^{\frac{4\pi r^2 \sigma}{kT}} \int e^{-g \ln S} dg = A + \frac{I}{\delta N_g \ln S} \tag{1.45}$$

On the other hand, for large g, f_g is proportional to $1/\delta$ and therefore $A = 0$. Equation (1.43) takes the form

$$\frac{f_g}{N_g} = \frac{I}{\delta} \int_g^\infty \frac{dg}{N_g} \tag{1.46}$$

Expression (1.46) satisfies the differential equation (1.43) and coincides with equation (1.45) for $g \to \infty$.

For $g \to 0$, the theory reveals an internal inconsistency; but when g is small, $f_g \to N_g$ (see Figure 1.4) and we may take $f_g / N_g = 1$ for $g \to 0$. From (1.46) we thus find

$$I = \frac{\delta}{\int_0^\infty \frac{dg}{N_g}} \tag{1.47}$$

Evaluating the integral in the right-hand side denominator of (1.47), we find /15, 24, 25, 28/

$$\int_0^\infty \frac{dg}{N_g} = \frac{3g^*}{2r^*N^*}\left(\frac{kT}{\sigma}\right)^{1/2} \tag{1.48}$$

From (1.13), (1.17), (1.27), and (1.35) we have

$$N^* = N_\infty e^{-A} = \frac{N}{S}e^{-A} \tag{1.49}$$

where N is the number density of vapor molecules in the gas, cm^{-3}:

$$N = \frac{p}{kT} \tag{1.50}$$

To expand equation (1.47), we substitute δ from (1.40), the integral from (1.48), and N^* from (1.49); introducing the accommodation coefficient, we write

$$I = \frac{a}{S\rho}\left(\frac{2m\sigma}{\pi}\right)^{1/2}\left(\frac{p}{kT}\right)^2 e^{-A} = \frac{a}{S}Z(4\pi r^2)\left(\frac{p}{(2\pi mkT)^{1/2}}\right)ne^{-A} \tag{1.51}$$

where Z is the Zel'dovich coefficient /23, 29/

$$Z = \frac{\rho \ln^2 S}{8\pi m}\left(\frac{kT}{\sigma}\right)^{3/2} \tag{1.52}$$

For practical purposes, the Frenkel equation may be written as

$$I = 10^{26}\frac{a}{S\rho}\left(\frac{p}{T}\right)^2 (M\sigma)^{1/2} e^{-\frac{17.6}{\ln^2 S}\left(\frac{M}{\rho}\right)^2\left(\frac{\sigma}{T}\right)^3} \tag{1.53}$$

or

$$I = Ke^{-A} \tag{1.54}$$

where K is the kinetic factor

$$K = 10^{26}\frac{a}{S\rho}\left(\frac{p}{T}\right)^2 (M\sigma)^{1/2} \tag{1.55}$$

and A is defined by (1.29).

Taking the logarithm of (1.53), we find

$$\ln I = 60 + \ln\left[\frac{a}{S\rho}\left(\frac{p}{T}\right)^2 (M\sigma)^{1/2}\right] - \frac{17.6}{\ln^2 S}\left(\frac{M}{\rho}\right)^2\left(\frac{\sigma}{T}\right)^3 \tag{1.56}$$

From (1.30), (1.31), (1.54), and (1.55) we have

$$I_B = I_F S e^{A(1-\nu)} \tag{1.57}$$

where I_B is the rate of nucleation in supersaturated vapor according to the Becker-Doering equation (1.34); I_F is the rate of nucleation from the Frenkel equation (1.53).

Since in homogeneous condensation $S > 1$, and $\nu < 1$, the Becker-Doering equation gives higher values of I than the Frenkel equation (e.g., for water at $T = 263.6$ °K and $S = 4.87$, $I_B = 4 \cdot 10^2$ cm^{-3} sec^{-1} while $I_F = 10^{-1}$ cm^{-3} sec^{-1}). The Frenkel equation is in better agreement with experimental data (see p. 26) than the other variants, and it is therefore recommended for practical calculations.

New trends in the theory of homogeneous vapor condensation

The process of nucleation of a new phase in general and homogeneous condensation in particular are of considerable applied interest and much effort is being devoted to the detailed study of these phenomena. The results of numerous theoretical and experimental investigations can be found in periodicals, topical collections, and books /28—38/. There are publications advocating different approaches to the problem /17, 18, 24, 25, 30, 39—41/ and review works which deal with the general theory of nucleation and various particular aspects /28, 29, 30, 42—46/.

The analysis of homogeneous vapor condensation generally starts with the assumption that density and temperature fluctuations in the medium lead to the formation of aggregates — minute liquid droplets which instantly evaporate (p. 2). It is also assumed that the thermodynamic and physical properties of these aggregates are close to those of large drops. This approach, however, is inaccurate, since the conventional thermodynamic concepts applicable to large drops (e.g., surface tension (p. 4), density, etc.) are meaningless as far as the minute aggregates are concerned.

Some recent publications have attempted to establish the relation of various thermodynamic parameters to embryo size and to introduce the actual physical conditions in calculations of the nucleation work. As an example, we consider the method which extends the thermodynamic approach to objects of very small size /10—14, 16—18, 47, 48/. It is based on a technique which has been previously used in calculations of thin liquid films /49/. The starting postulate maintains that for minute objects the excess of free energy is not localized in the object's surface, but is characteristic of the object as a whole. This novel approach automatically extends the applicability of thermodynamics to small objects where no clear distinction can be made between the bulk and the surface components. A consistent theoretical apparatus has been also developed for the derivation of fairly accurate thermodynamic characteristics of minute objects /50/.

An entirely different approach is manifested in the statistical theory of condensation /51—53/. In this theory, stable condensation embryos are not regarded as spherical liquid droplets and the equilibrium between the vapor phase and the embryo therefore is not considered.

There are also other vapor condensation theories /54, 55/, but these are still in the rudimentary stages of development and are as yet inadequate for the solution of applied problems.

Substantial additions to the theory of homogeneous vapor condensation have been made by quantum statistics /29, 56/. The nucleation energy is now determined with higher accuracy from the expression

$$\Delta\varphi' = \Delta\varphi + \Delta\varphi_S + \Delta\varphi_t + \Delta\varphi_r \qquad (1.58)$$

where $\Delta\varphi$ is the Gibbs nucleation work (equation (1.23)); $\Delta\varphi_s$ the change in free energy due to the separation of a group of molecules from a larger aggregate; $\Delta\varphi_t$ the change in free energy due to the activation of the translational degree of freedom; $\Delta\varphi_r$ the change in free energy to the activation of the rotational degree of freedom.

Substituting $\Delta\varphi'$ from (1.58) for $\Delta\varphi$ in (1.27), we write for (1.54)

$$I = K\Gamma e^{-A} \tag{1.59}$$

where Γ is Lothe and Pound's correction factor /56/. According to /29, 56/, $\Gamma = 10^{17}$ for water vapor at $T = 300\,°K$. The Frenkel equation, however, is consistent with the results of numerous experimental studies, and this exceedingly high value of the correction factor therefore remains unexplained.

CRITICAL VAPOR SUPERSATURATION

It follows from the preceding that vapor condensation in a gas volume commences at a certain critical supersaturation of vapor, S_{cr}. In other words, vapor may condense in a gas volume only if

$$S \geqslant S_{cr}$$

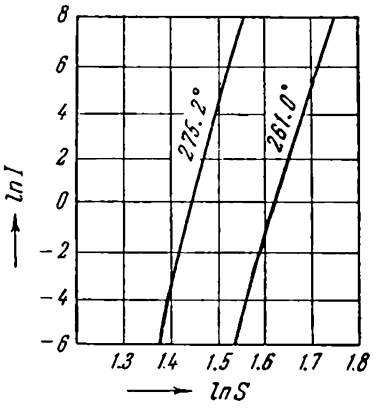

FIGURE 1.5. Rate of droplet formation vs. supersaturation (for water).

The critical supersaturation for homogeneous (spontaneous) condensation of vapor is defined as the supersaturation when embryos capable of further growth form at a rate of one per unit volume per unit time, i.e., when $I = 1\ cm^{-3}\ sec^{-1}$. This definition is apparently fairly arbitrary, since embryos will form even if $I < 1$, but the corresponding rates are too small to be seriously considered. Indeed, in (1.27) vapor supersaturation appears in a power exponent, and the rate of nucleation therefore increases very steeply with supersaturation (Figure 1.5). For water ($T = 293\,°K$), increasing vapor supersaturation from 3.4 to 3.6 raises the formation rate of stable nuclei capable of further growth from 1 to 120 (Table 1.3).

TABLE 1.3. Rate of water droplet formation as a function of supersaturation ($T = 293\,°K$)

Supersaturation s	Rate of droplet formation I (number of droplets in 1 cm^3 in 1 sec)	Supersaturation s	Rate of droplet formation I (number of droplets in 1 cm^3 in 1 sec)
3.2	$1.2 \cdot 10^{-4}$	4.0	$3.6 \cdot 10^{5}$
3.4	1.0	4.2	$8.9 \cdot 10^{6}$
3.6	$1.2 \cdot 10^{2}$	4.4	$1.3 \cdot 10^{8}$
3.8	$9.9 \cdot 10^{3}$		

Since the rate of nucleation is a rapidly ascending function of vapor supersaturation, the previous definition of critical supersaturation is quite adequate for all practical purposes: it provides a sufficiently reliable information on the probability of condensation.

Critical supersaturation for homogeneous condensation in an ion-free gas can be calculated from (1.27) and (1.29) putting $I = 1$ and $S = S_{cr}$:

$$\ln I = 0 = \ln K - \frac{17.6}{\ln^2 S_{cr}} \left(\frac{M}{\rho}\right)^2 \left(\frac{\sigma}{T}\right)^3 \tag{1.60}$$

or

$$\lg S_{cr} = \sqrt{\frac{1.44}{\lg K}} \cdot \frac{M}{\rho} \left(\frac{\sigma}{T}\right)^{3/2} = C \cdot \frac{M}{\rho} \left(\frac{\sigma}{T}\right)^{3/2} \tag{1.61}$$

where /57/

$$C = \sqrt{\frac{1.44}{\lg K}} = \frac{1.2}{\sqrt{\lg K}} \approx 0.242 \tag{1.62}$$

and K is the kinetic factor expressed by equations (1.31) and (1.55).

With liquid droplets suspended in the gas, vapor condensation commences when the supersaturation has reached the value expressed by (1.9); if ions are moreover present in the medium, the relevant supersaturation is expressed by (1.13). This is obviously the critical supersaturation of the given gas mixture, since it represents the onset of vapor condensation in the medium.

Atmospheric air and the gases involved in most industrial processes contain condensation nuclei with radii of $10^{-6} - 10^{-4}$ cm (see Figure 1.7). In accordance with equation (1.9) and Table 1.1, vapor starts condensing on the surface of these nuclei and fog forms when the supersaturation is 1.001 — 1.12. The condensation nuclei are often electrically charged and also contain hygroscopic substances which lower the saturated vapor pressure, so that vapor may start condensing on atmospheric nuclei even at lower supersaturations.

Methods for the determination of critical supersaturation

Critical supersaturation is commonly determined by the same methods, irrespective of whether the gas mixture contains condensation nuclei or the condensation is spontaneous (homogeneous) with the formation of embryos. In all the existing methods, the supersaturation of the vapor in the gas volume is increased until visible fog is formed (the fog is detected by inspecting the scattering of light in the volume). The vapor supersaturation at the instant of fog appearance is taken equal to S_{cr}.

This is an approximate technique, since the supersaturation of vapor at the instant of appearance of visible fog does not precisely correspond to the onset of vapor condensation on nuclei or embryos: it actually represents the time when the scattering of light by the forming droplets has become strong enough to be detected visually (and this obviously

depends on the number density of the droplets, their sizes, and some other factors as well). Considerable errors are incurred when an attempt is made to determine the S_{cr} of homogeneous condensation by this technique: while the number density of condensation nuclei in a given gas mixture is a constant quantity, the number of embryos which form by spontaneous condensation is variable with time. Moreover, condensation nuclei are larger than the embryos and their scattering power is correspondingly higher. The light scattering by the embryos (whose radii are substantially less than the wavelength in question) is proportional to the particle radius to the sixth power.

In what follows we consider the results of some experimental studies concerned with the determination of S_{cr} for homogeneous condensation; they also apply for certain S_{cr} in gas mixtures with condensation nuclei.

Most of the experimental determinations of S_{cr} have been made using the Wilson cloud chamber, where a vapor-gas mixture is allowed to expand adiabatically, so that the gas cools down, embryos form, and fog droplets eventually appear. Of particular interest are the results of Volmer and Flood /57/, which are listed in Table 1.4. Since the starting temperature conditions in these experiments were approximately constant and the S_{cr} of the various liquids were measured with the same equipment, the results are particularly convenient for comparative analysis.

TABLE 1.4. Critical vapor supersaturation of some liquids

Liquid	Temperature, T °K	Critical supersaturation s_{cr}			
		Experimental /34/	Calculated for $I = 10^2\ cm^{-3}\ sec^{-1}$		Calculated from Frenkel's equation (1.53) for $I = 1\ cm^{-3}\ sec^{-1}$
			Becker-Doering (1.34)	Frenkel (1.53)	
Water	263.7	4.85 ± 0.08	4.57	5.17	4.84
Methyl alcohol	270.0	3.20 ± 0.1	1.69	1.84	1.80
Ethyl alcohol	273.2	2.3 ± 0.05	2.22	2.32	2.24
n-Propyl alcohol	270.4	3.05 ± 0.05	3.19	3.41	3.24
Isopropyl alcohol	264.7	2.80 ± 0.07	2.82	2.99	2.86
n-Butyl alcohol	270.2	4.60 ± 0.13	4.27	4.83	4.52
Nitromethane	252.2	6.05 ± 0.75	5.73	6.67	6.18

The values of S_{cr} listed in Table 1.4 were calculated from equations (1.34) and (1.53) for $\alpha = 1$ and $I = 10^2\ cm^{-3}\ sec^{-1}$ (this I corresponds to the incipience of visible fog /11, 29/ in Volmer and Flood's experiments). For comparison purposes we also give the values of S_{cr} calculated from equation (1.53) for $I = 1\ cm^{-3}\ sec^{-1}$.

We see from Table 1.4 that neither formula is exact as far as representation of experimental findings is concerned, and we can hardly prefer one to another.

S_{cr} is difficult to determine with cloud chambers because of the insignificant light scattering by the minute embryos which form in homogeneous condensation of vapor ($\approx 10^{-7}$ cm). Therefore I cannot be determined for

the time when visible fog first appears. Moreover, the relatively warm walls of the chamber (which are maintained at a higher temperature than the filling gas), the presence of convection currents, and various other factors combine to make the cloud chamber insufficiently sensitive for the determination of S_{cr}.

The comparison of theoretical and experimental data is further complicated by the wide scatter of the different experimental values of the accommodation coefficient α for each liquid (p. 28).

The accuracy of the experimental values of S_{cr} listed in Table 1.4 is insufficient for the analysis of the nucleation rates and, in particular, for the evaluation of the theoretical formulas for I, since the apparently small fluctuations in the S_{cr} values in the table correspond to unacceptably large uncertainties in I. For example, the 0.05 deviation in the critical supersaturation of ethyl alcohol (see Table 1.4) is magnified to a 16-fold error in I.

Of considerable practical interest is the method whereby the critical supersaturation is determined by mixing a vapor-gas mixture with a cold indifferent gas in a free jet /58, 59/ (p. 83). The method is convenient because in turbulent mixing the maximum vapor supersaturation S_{max} in the field of the jet depends only upon the initial parameters of the mixing streams and can thus be calculated comparatively easily (Chapter Three). The initial parameters are easily controlled, and the maximum supersaturation, i.e., the supersaturation corresponding to fog formation in the jet, can therefore be assumed equal to the critical supersaturation of the vapor.

Unfortunately, this method has been hitherto applied only for the determination of the critical supersaturation of water vapor in homogeneous condensation at 41.2 °C. The result came out to be 2.73 (Chapter Three), while according to (1.61) the critical supersaturation for water at 41.2 °C is 2.72 (with K calculated from (1.56) for $\alpha = 1$).

The above method for the determination of S_{cr} in a free jet is fairly simple and convenient. It permits the measurements to be made continuously and is successfully used for the determination of S_{cr} in gases with condensation nuclei /60, 61/.

More reliable data on critical vapor supersaturation can apparently be obtained in diffusion chambers (Chapter Four), where the effect of the walls and the convection currents can be eliminated. A constant vapor supersaturation (varying in the vertical direction only) is set up between the plates of the diffusion chamber. The number of embryos forming in the supersaturated vapor, which rapidly grow and settle under their own weight and by thermophoresis, can be determined with fairly high accuracy (which favorably reflects on the precision with which I is found).

The rate of nucleation, as well as S_{cr}, can thus be found by direct experimental techniques.

Dependence of critical supersaturation on temperature

From equations (1.9), (1.13), and (1.61) and from experimental data we see that the critical supersaturation of vapor is a function of temperature.

This is a highly significant aspect which cannot be ignored in the solution of applied problems. As the temperature increases, the surface tension of liquids drops with the effect that the ratio σ/T entering equations (1.9), (1.13), and (1.61) falls off with rising temperature. For the same reason critical vapor supersaturation also decreases with temperature. The density of the liquid (which enters the denominator of the relevant equations) also decreases with increasing temperature, but its effect on S is less pronounced than the influence of the σ/T ratio.

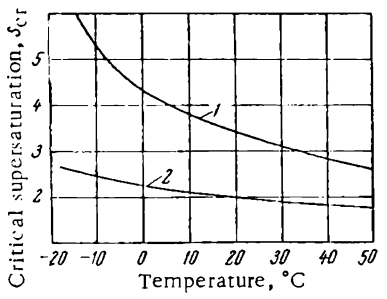

FIGURE 1.6. Critical supersaturation vs. temperature: 1) water vapor; 2) ethanol vapor.

Figure 1.6 plots the temperature variation of the critical supersaturation of water and ethanol vapors as calculated from equation (1.61) for homogeneous condensation in air.

Critical vapor supersaturation and the conditions of fog condensation are dependent on the nature of the indifferent gas, the character of the condensation nuclei, ambient temperature, electrical charges, and other environmental factors. It therefore follows from the preceding that the theoretical and experimental data available on critical vapor supersaturations are approximate and can hardly be used in the solution of various topical applied problems. Comprehensive investigations of the subject are therefore of considerable practical importance. In particular, it is necessary to establish the relation of the surface tension to droplet radius for minute (embryonic) droplets and to refine the Kelvin formula (1.9) for these exceedingly small particles.

CONDENSATION NUCLEI

We have previously observed that embryos and fog droplets will form in a clean, ion-free gas mixture only if the vapor pressure in the system is several times higher than the saturated vapor pressure. Such dust-free gas mixtures can be obtained only by artificial means, after special filtering and cleaning processes. In nature and in industry the gases invariably contain ions and minute liquid and solid particles in suspension; these are the condensation nuclei and it is on their surface that vapor first condenses to form fog droplets. This condensation begins at supersaturations which are substantially lower than those required for homogeneous condensation. According to published data /62/, free organic radicals and single molecules* may occasionally act as condensation nuclei.

Condensation nuclei (like aerosols in general) also form by spontaneous vapor condensation and in the result of mechanical breakup of solids and pulverization of liquids.

Condensation nuclei in atmospheric air. Quite a number of processes may lead to spontaneous condensation of vapor and to mechanical breakdown of matter in atmospheric air. For example, sunlight or

* Knof, H. — Geofis. pura e appl., 40:180. 1958; Bieber, W. — Ann. Phys., 39:1313. 1912.

spark discharges will cause some of the constituent atmospheric gases to react forming new compounds with low saturated vapor pressure. These compounds condense spontaneously and thus provide condensation nuclei for other vapors. The vapors of sulfuric and nitric acids — oxidation products of nitrogen and SO_3 by atmospheric oxygen — condense and form such nuclei (Chapter Four). The combustion gases released when fuel is burned, as well as the exhaust gases of various industrial processes contain a rich mixture of vapors (sulfuric acid, resins, oils, etc.) which upon mixing with the colder atmospheric air condense spontaneously and form minute droplets of liquid (Chapter Three).

Meteorites penetrating into the atmosphere heat up to very high temperatures and partially vaporize. This vapor mixes with the colder atmospheric air and condenses spontaneously into minute particles.

Condensation nuclei produced by mechanical fragmentation of solids and liquids come from a great variety of sources and are therefore difficult to classify. The earth's surface is subjected to continuous weathering and erosion, and the main proportion of condensation nuclei in this class are therefore inorganic substances. Swarms of condensation nuclei form when active volcanoes erupt (there are more than 500 active volcanoes in the world today). The cloud of dust hovering above Vesuvius normally rises to a height of over 1 km, but the volcanic ashes ejected by the volcano during its periods of activity reach heights greater than 20 km. The strong air currents prevailing at high altitudes carry the ash over great distances. For example, the explosion of Krakatoa on 26 August 1883 released nearly 6.5 km^3 of fine ash into the atmosphere to heights of up to 32 km. The cloud of dust floated in the atmosphere for many months, covering nearly all of the world and settling at a rate of some 70 m/day /63/.

Some condensation nuclei form from sea water. The spray which invariably accompanies the waves in the open sea and near the shoreline breaks into water drops with a radius of some 10^{-6} cm which evaporate and leave behind minute droplets of highly concentrated salt solutions.

Part of the condensation nuclei are of organic origin. Whole organisms (either living or dead) and fragments of bodies (scales, hairs, feathers, etc.) always float in the air. Microorganisms capable of withstanding long periods of dryness (bacteria and viruses) abound in great numbers in the atmosphere. On the average there are nearly 5000 microorganisms per 1 m^3 of ground air in urban areas. Seeds of the higher plants, pollen and spores, algae, molds, etc. invariably float in the air around us (the pollen of coniferous trees is often transported by wind over hundreds of kilometers).

The size distribution of atmospheric condensation nuclei, their number densities and chemical compositions are highly variable. Attempts have been made /64, 65/ to devise a consistent classification of condensation nuclei in terms of their size. Junge's classification /64/ is frequently used (Table 1.5), but there is no universal agreement on this point.

TABLE 1.5. Sizes of atmospheric condensation nuclei

Particle size r, cm	Name
$r \leqslant 0.2 \cdot 10^{-4}$	Aitken nuclei
$0.2 \cdot 10^{-4} < r < 1 \cdot 10^{-4}$ . . .	Large nuclei
$r \geqslant 1 \cdot 10^{-4}$	Giant nuclei

Condensation nuclei are detected by special counters (Aitken, Scholtz, etc.) which utilize the cloud chamber principle (p. 55). These are typically cylindrical containers whose walls are lined with moist filter (or blotting) paper. The air to be tested is pumped into the chamber, where it is saturated with water vapor and then allowed to expand to a known volume. Supersaturated vapor thus forms and water vapor condenses on the nuclei. The forming droplets settle on a stage provided at the bottom of the cylinder; the stage is extracted and the droplets on its surface are counted under suitable magnification.

The Nolan-Pollak counter /66/ has lately become popular. Here the number of water droplets forming due to adiabatic expansion of the air sample is determined by photoelectric measurement of the attenuation of transmitted light.

The number density of condensation nuclei in atmospheric air depends on a variety of factors; it is different in different geographical regions, sensitive to topographic and meteorological conditions, seasonal factors, etc. On mountaintops and in upper atmospheric layers the number density of condensation nuclei is lower than near the ground; above the sea it is lower than above dry land, and in daytime it is higher than at night.

The number density of condensation nuclei is substantially influenced by wind speeds and directions: it is not only that condensation nuclei are imported by incoming winds, they are generated in situ in the form of dust particles and water spray.

A particularly high concentration of condensation nuclei is observed in the air of large cities and industrial regions. This is the result of air pollution by the combustion gases of furnaces, the exhaust gases of automotive transport, and the industrial process gases.

TABLE 1.6. The content of condensation nuclei in the atmosphere in various areas

Sample area	Number of sampling points	Number of samples	Average number density, cm^{-3}
A large city	28	$2.5 \cdot 10^3$	$1.5 \cdot 10^5$
A small town	15	$4.7 \cdot 10^3$	$3.4 \cdot 10^4$
Country area	25	$3.5 \cdot 10^3$	10^4
Mountains (m)			
500—1000	13	$9 \cdot 10^2$	$6 \cdot 10^3$
1000—2000	16	$2 \cdot 10^2$	$2 \cdot 10^3$
Islands	7	$5 \cdot 10^2$	10^4
Oceans	21	$6 \cdot 10^2$	10^3

Table 1.6 lists the number densities of condensation nuclei in the air in various areas /28, 67/. Deviations from the mean number density are considerable. For a large city, e.g., the maximum number density is $4 \cdot 10^6\ cm^{-3}$, whereas the minimum number density is as low as $3.5 \cdot 10^3\ cm^{-3}$.

The size distribution of condensation nuclei depends on their origin. Some tentative results are presented by the curves in Figure 1.7 which plot the average data from /68, 69/. The peak count is observed for radii near $5 \cdot 10^{-6}$ cm. The maximum mass is concentrated in condensation nuclei with a radius of $3 \cdot 10^{-5}$ cm. The origin of atmospheric condensation

nuclei, their sizes, number densities, and mass concentrations are discussed in numerous experimental and review works /28, 63, 67, 69, 70/.

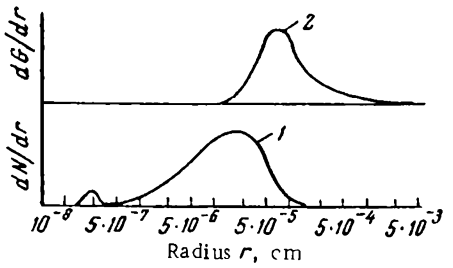

FIGURE 1.7. Distribution of atmospheric condensation nuclei:
1) size distribution; 2) mass distribution.

Cosmic rays and the radiations of radioactive elements in the earth's crust ionize a certain proportion of the molecules of the atmospheric gases producing positively and negatively charged ions. Light ions (i.e., singly charged ions) combine with the solid and liquid particles suspended in the air to form medium-weight and heavy ions. Particles with radii less than 0.01 μ acquire a single elementary charge, while larger particles will carry a multiple charge.

The number density of ions (in cm^{-3}) is represented by the following typical orders of magnitude:

	Ordinary air	Clean air
Light ions	a few hundreds	a few thousands
Medium-weight ions	up to 10^4	less than 100
Heavy ions	up to $5 \cdot 10^4$	0

Condensation nuclei in industrial process gases. Atmospheric air is widely used in various industrial processes as a source of oxygen or nitrogen, as a heating agent, as a coolant, etc. Air is often taken in without preliminary filtration, but even cleaned air carries a considerable number of condensation nuclei. Thus in all industrial processes using atmospheric air, the circulating process gases contain a high number of solid and liquid particles in suspension.

When air is used as a source of oxygen for fuel combustion, the temperature in the reaction space is sufficiently high to vaporize a considerable proportion of the suspended particles. Combustion processes also reduce the size of organic particles. In industrial processes the gases are passed through various pieces of equipment, heat exchangers, condensers; liquid-sprayed columns, contact apparatus with stationary and moving catalyst layers, filters, etc. The number density of condensation nuclei may drop due to their precipitation or, conversely, it may increase due to the additional intake of minute solid and liquid particles of the reagents which are entrained by the air stream. The fog potential of any particular industrial process thus depends not only on the number density of condensation nuclei in the initial gases, but also on the probable change in their number density during the processing of the gas; the conditions of fog

formation (and the weight concentration of fog) may change considerably depending on the size and the number density of the condensation nuclei.

EXPERIMENTAL DATA ON NUCLEATION RATES

The reliability of theoretical formulas can be confirmed only by experimental data, and the rates of nucleation obtained in actual tests are therefore primarily used in evaluating the accuracy of the various theoretical formulas that purport to predict the nucleation rate.

The research here branches in two directions. In the first group we have the various studies carried out under nearly critical conditions (with $S \approx S_{cr}$ and $I \approx 1$), which are regarded, by definition, as indicatory of the onset of homogeneous condensation. Critical supersaturation in this case is determined from equation (1.61). The fit of the theoretical and the experimental values of S is interpreted as a measure of reliability of the theoretical relations for the calculation of the nucleation rates.

The second group comprises the various investigations carried out for $S > S_{cr}$ and $I \gg 1$. The rate of nucleation is calculated from (1.28):

$$I = \frac{dN}{d\tau}$$

The results of these researches provide more accurate data on nucleation rates, since the derivative dI/dS decreases with increasing S and I is obtained with proportionately higher precision.

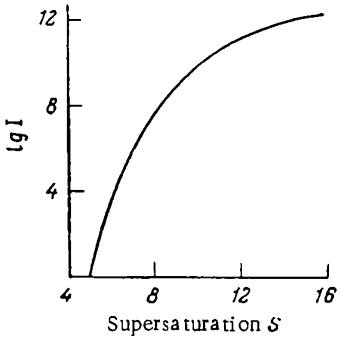

FIGURE 1.8. I vs. S for water vapor in an adiabatically expanding vapor-gas mixture.

Homogeneous condensation experiments have been discussed in connection with critical supersaturation (p. 17), and we do not propose to go again into this subject. Figure 1.8 plots the function $I = f(S)$ calculated from the Frenkel equation (1.53) for an adiabatically expanding vapor-gas mixture (initial temperature 291 °K). Table 1.7 lists the values of I calculated from (1.34) and (1.53) using the experimental findings of Volmer and Flood /57/ on supercritical supersaturations in a cloud chamber ($\alpha = 1$ was assumed). We see from Table 1.7 that the values of I calculated from different equations

are distinctly different and we cannot say which of the two equations should be preferred.

TABLE 1.7. Nucleation rates calculated from the experimental values of S_{cr}

Liquid	Temperature, °K	Nucleation rate I, $cm^{-3}sec^{-1}$, calculated according to	
		Becker and Doering (1.34)	Frenkel (1.53)
Water	263.7	$4.6 \cdot 10^{3}$	1.2
Methyl alcohol	270.0	$2.6 \cdot 10^{21}$	$4.3 \cdot 10^{19}$
Ethyl alcohol	273.2	$2.4 \cdot 10^{5}$	$2.6 \cdot 10^{2}$
n-Propyl alcohol	270.4	$1.4 \cdot 10^{2}$	3.7
Isopropyl alcohol	264.7	$1.9 \cdot 10^{3}$	4.7
n-Butyl alcohol	270.2	$2.7 \cdot 10^{3}$	0.7
Nitromethane.	252.2	$1.6 \cdot 10^{4}$	2.5

As we have previously observed, this is partly due to the low sensitivity of the cloud chamber technique, especially at the instant of incipient nucleation: the scattering of light is negligible due to the low number density of the nuclei and their small sizes, so that the exact time of incipient condensation is very difficult to pinpoint /24/. However, the numerical results listed in Table 1.7 for each of the two theoretical formulas reveal very substantial fluctuations in the orders of magnitude of I for different liquids. This apparently suggests that the formulas do not account comprehensively for the variety of factors influencing the rate of embryo formation. The observed scatter in the theoretical values of I may possibly be attributed to the substitution of $\alpha = 1$ in calculations: in reality, the values of this coefficient for different liquids range from 0.05 to 1 (p. 28).

Methods for the determination of nucleation rates at $S > S_{cr}$ may utilize any process which produces supersaturated vapor (p. 35). Radiative heat transfer, however, sets a definite limit to supersaturations attainable under laboratory conditions, and it is therefore difficult to develop an effective method for the determination of I.

In practice, I is determined with the aid of three processes: adiabatic expansion of the gas (p. 18), mixing of gases of different temperatures (p. 83), and vapor condensation on a surface (p. 126).

Let us consider the principal results obtained by these techniques. Conditions favoring high S and I can be set up in a cloud chamber, but this technique is deficient in that vapor expansion is not instantaneous: it takes a certain finite time.

When the adiabatically expanding vapor-gas mixture has reached the critical supersaturation, the number density N of the droplets starts increasing rapidly with further rise in S. Concurrently with the formation of new droplets, vapor condenses on already existing drops and promotes their steady growth. Vapor pressure in the system decreases owing to condensation and also because of adiabatic expansion; liberation of the latent heat of condensation warms the droplets to a temperature higher than the temperature of the gas. This temperature difference initiates a

transfer of heat from the droplets to the gas and eventually the entire condensation heat will have been deposited in the gas molecules.

The various processes involved are complexly related among themselves, and general equations are difficult to draw up. Simplified numerical techniques are therefore devised (p. 51). The theoretical results for water are plotted in Figure 1.9. Curve 1 corresponds to the results calculated from the Frenkel equation (1.53), and curve 2 represents the Becker-Doering equation (1.34).

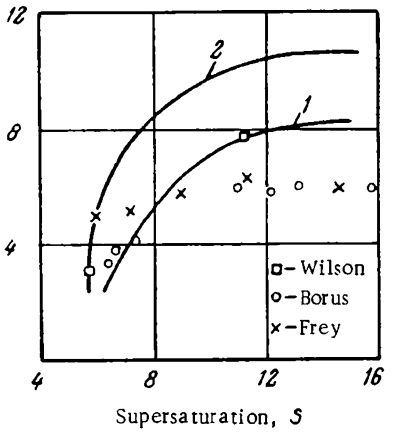

FIGURE 1.9. Number density of droplets in an adiabatically expanding gas as a function of final supersaturation: 1) calculated from the Frenkel equation; 2) calculated from the Becker-Doering equation.

Figure 1.9 also plots the experimental findings of some authors /71—74/. The theoretical curves and the experimental findings are in good agreement for low S, but there is considerable deviation at higher values of S. Curve 1 calculated from the Frenkel equation is closer to the experimental points than curve 2. It furthermore provides a better fit to Wilson's data /72/.

An analysis of the plot points to a satisfactory reliability of the Frenkel equation. In Wilson's experiments the gas was thoroughly cleaned and purified from suspended particles and gas ions, so that Wilson's data can be regarded as approximating to homogeneous (spontaneous) formation of embryos /29/. Most of the experimental data available, however, have been obtained for gas mixtures with a considerable content of suspended particles and gas ions, and they therefore represent processes of heterogeneous vapor condensation /29/.

The deviation of theory from experiment is partly attributable to the finite expansion time (more than 0.01 sec) in the experiments. If the expansion time in Frenkel's equation (1.53) is taken equal to 0.1 sec, and not 0.01 sec, curve 1 drops approximately by two orders of magnitude in the relevant region.

There are two published works on the determination of I for $S>S_{cr}$ where supersaturated vapor was produced by cooling a vapor-gas mixture by other than adiabatic means. The number density N of fog forming in a turbulent vapor-gas jet mixed with a colder indifferent gas (Chapter Three) is determined in /74/. The experimental findings of this source were applied to calculate the I from (1.28). The surface tension σ_{exp} was then calculated from (1.53) and the results were compared with the surface tension listed in Table 3.5. We see from this table that consistent data were obtained for dibutyl phthalate only; the figures for other liquids diverge considerably. This is particularly obvious from a comparison of the nucleation rates I_{exp} and I_{theor} calculated using σ_{exp} and σ_{table} (Table 3.5 lists the ratios of these nucleation rates). One of the reasons for the divergence in the nucleation rates is apparently the high variability of vapor supersaturation in the turbulent jet (see Figure 3.7).

More reliable data on nucleation rates for $S>S_{cr}$ were obtained in studies of the condensation of glycerine and sulfuric acid vapors on a

surface /75/. The vapor-gas mixture is passed through an externally cooled pipe (see Figure 5.7). High supersaturation is thus produced in the pipe, part of the vapor condenses spontaneously in the gas volume and fog is formed. The number density of the fog and the mean droplet radius are determined at the outlet. The results are compared with the theoretical data for nucleation rates /76/ obtained from equations (1.34) and (1.53).

Comparison of theoretical and experimental data (Table 5.8) shows that equation (1.53) provides a better approximation to the experiment. On the other hand, the discrepancies between the two sets of data necessitate additional studies in order to refine the thoery of homogeneous vapor condensation and to derive reliable equations for the calculation of nucleation rates, number densities, and size distribution.

ACCOMMODATION COEFFICIENTS

The number of vapor molecules impinging per unit surface area of the liquid in contact with its vapor is expressed by equation (1.41).

If p_∞ is the saturated vapor pressure above the liquid, the rate of condensation is proportional to W, as expressed by the equation /29, 77, 78/

$$W = (p - p_\infty)\,(2\pi m k T)^{-1/2} \tag{1.63}$$

However, not all the vapor molecules hitting the liquid surface "stick" to it permanently, and an additional fractional factor should be introduced in equation (1.63), which takes the form

$$W = \alpha\,(p - p_\infty)\,(2\pi m k T)^{-1/2} \tag{1.64}$$

where α is the accommodation coefficient: it expresses the fraction of impinging vapor molecules which stick to the liquid surface.

For the evaporation of the liquid we similarly write

$$W_v = \alpha_v\,(p_\infty - p)\,(2\pi m k T)^{-1/2} \tag{1.65}$$

where α_v is the evaporation coefficient.

It follows from the available experimental data that the coefficients α and α_v vary between wide limits depending on the particular liquid and the physical conditions in the system. The data of different authors, however, differ considerably (see Table 1.8), i.e., the numerical values of α and α_v obtained for the same liquids under identical conditions are all different /29/. The experimental material is insufficient to establish a strict correlation between the various data, and in what follows we do not distinguish between α and α_v, always referring to these quantities by a common name — accommodation coefficient.

Surface impurities in the liquid are one of the factors which lower the experimental values of α and cause its fluctuations between different samples of the same liquid. When the α of water is determined in a glass vessel, the rate of evaporation is lower because the water surface is

covered with a film of water-soluble components of the glass /90/ (mainly silicon oxide /91/). In experiments with mercury /87/ the coefficient α for a clean surface was equal to 1, while in the presence of some traces of impurities it was as low as 0.0005. We thus see that the measured α will increase if the experiment is conducted very carefully. Some authors therefore suggest /92/ that for clean surfaces the condensation coefficient is close to unity.

TABLE 1.8. Accommodation and evaporation coefficients α and α_v for some liquids

Liquid	Accommodation coef. α	Evaporation coef. α_v	References
Ethyl alcohol		0.02	/79/
Water		0.04	/79, 80/
		0.1, 0.24	/81, 82/
		0.03	/83/
Methyl alcohol		0.04	/79/
Chloroform		0.18	/79/
Toluene		0.55	/79/
Benzene		0.9	/79/
Glycerine	0.051*	0.052, 1.0	/84, 85/
Sulfuric acid	0.027*	—	
Mercury	0.92—1.0**	1.0	/87/
Carbon tetrachloride	—	1.0	/88/
Dibutyl phthalate	0.6—1.0*	1.0	/89/

* A. I. Baranova, A. G. Amelin, and N. M. Antonova.
** See /86/.

The effect of impurities on α may turn to be of considerable practical significance: in homogeneous vapor condensation the surface of the spontaneously forming embryos is impurity-free, and the kinetic factor K should therefore be calculated using numerical data for very clean liquids.

For some highly polar liquids (water, methanol and ethanol, glycerine, etc.), however, the experimental values of α are lower than the values obtained by the same experimenters for liquids with symmetric, nonpolar molecules (mercury, benzene, carbon tetrachloride, etc.). This suggests a certain dependence of α on the molecular structure of the liquid /79, 84/. The temperature dependence of α was also determined experimentally. For water /83/, the coefficient varies from 0.042 at 0 °C to 0.027 at 43 °C; for dibutyl phthalate the variation is from 0.95 at −3.2 °C to 0.24 at 50.2 °C.

There are some indications in the literature /88/ that α falls off if the vapor is mixed with molecules of an indifferent gas. This conclusion, however, requires further verification, as it has not been confirmed by experimental studies of mass transfer during vapor condensation in vapor-gas mixture /92/.

Theoretical and experimental determinations of α are reviewed in /29, 92—94/.

RATE OF VAPOR CONDENSATION ON THE SURFACE OF DROPLETS

The growth of nuclei and of embryos (in homogeneous condensation) by vapor condensation on their surfaces is the principal process which governs the dispersity, or the drop size distribution of the fog (p. 3).

The rate of condensation is a function of many variables:

$$\frac{dq}{d\tau} = f(T, r, p \text{ etc.}) \tag{1.66}$$

For a droplet suspended in a still gas, the rate of vapor condensation on droplet surfaces is expressed by the Maxwell formula /95/ with Fuks's correction /96—98/, which allows for the influence of the droplet radius:

$$\frac{dq}{d\tau} = \frac{4\pi D r M}{R T \varphi}[p - p_r(T_r)] \tag{1.67}$$

where q is the quantity of vapor in the gas, g; τ time, sec; D vapor diffusion coefficient, $cm^2\,sec^{-1}$; $p_r(T_r)$ equilibrium vapor pressure above the droplet (at the droplet temperature T_r), mm Hg; T the temperature of the gas mixture, °K; M the molar mass of the liquid, g/mole; R the universal gas constant, equal to $6.24 \cdot 10^4$ cm^3(mm Hg) $deg^{-1}\,mole^{-1}$; φ a coefficient /99/:

$$\varphi = \frac{D}{r\alpha\nu} + \frac{r}{r+\Delta} \tag{1.68}$$

$$\nu = \frac{w}{4} = 3643\sqrt{\frac{T}{M}} \tag{1.69}$$

where w is the mean velocity of the molecules and the vapor, cm/sec; α the accommodation coefficient (p. 27); Δ the thickness of the region adjoining the droplet where vapor molecules are exchanged freely, as in a vacuum, cm (we may approximately take $\Delta \approx l$, where l is the mean free path of the molecules, cm);

$$\frac{D}{\alpha\nu} = \frac{2.74 \cdot 10^{-4} D}{\alpha} \cdot \sqrt{\frac{M}{T}}$$

It follows from Figure 1.10 that as the droplet radius increases the coefficient φ decreases approaching unity for $r \gg l$. The Maxwell equation /95/ applies in this case:

$$\frac{dq}{d\tau} = \frac{4\pi D r M}{RT}[p - p_r(T_r)] \tag{1.70}$$

or

$$\frac{dr}{d\tau} = \frac{DM}{RTr}[p - p_r(T_r)] \tag{1.71}$$

For small droplets, all other conditions being constant, the coefficient φ increases in proportion to the ratio $D/\alpha\nu$, which may vary between wide limits (Table 1.9) because the accommodation coefficient α is sensitive to the molecular structure of the liquid (see Table 1.8).

The rate of vapor condensation on the surface of droplets is increased by the Stefan flow /100/. This increment is represented by an additional factor n in equation (1.67):

$$\frac{dq}{d\tau} = \frac{4\pi DrMn}{RT\varphi}[p - p_r(Tr)] \tag{1.72}$$

$$n = 1 + \frac{p_r(T_r) + p}{2P} \tag{1.73}$$

where P is the total pressure of the gas mixture, mm Hg.

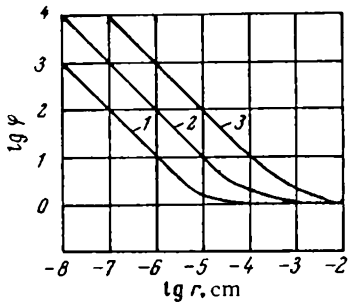

FIGURE 1.10. φ vs. r for various $\frac{D}{\alpha v}$:
1) $\frac{D}{\alpha v} = 10^{-5}$; 2) $\frac{D}{\alpha v} = 10^{-4}$;
3) $\frac{D}{\alpha v} = 10^{-3}$.

In practice, fog mostly forms when vapor condenses in the presence of large quantities of noncondensing gases, and the ratio

$$\frac{p_r(T_r)+p}{2P}$$

entering equation (1.73) is therefore small; the effect of the Stefan flow on condensation rates is consequently insignificant.

TABLE 1.9. The ratio $\frac{D}{\alpha v}$ for droplets suspended in the air for $\alpha = 1$

Liquid	$\frac{D}{\alpha v} \cdot 10^5$ at	
	273°K	373°K
Water	1.6	2.1
Ethyl alcohol	1.2	1.8
Benzene	1.1	1.7
Sulfuric acid	1.6	2.2

Fog droplets in a turbulent stream are entrained by the eddy pulsations and describe complex trajectories in the gas /101/. The droplets, however, are not fully entrained by the pulsations, and they additionally grow due to the intake of vapor transported by convective diffusion. The overall

diffusion coefficient is therefore higher than in a still medium. As the droplet radius decreases, the droplets are more readily entrained by the eddy pulsations and the contribution from convective diffusion decreases. For droplets with radii $r < 10^{-4}$ cm, the effect of diffusion in a turbulent stream can be completely ignored /101/.

TEMPERATURE OF A DROPLET IN SUPERSATURATED VAPOR

When vapor condenses on the surface of a droplet, the latent heat of condensation is released and the temperature of the droplet becomes higher than the temperature of the gas. The temperature difference results in a transfer of heat from the droplet to the gas. The quantity of heat released in a droplet per second is given by the relation

$$Q = \frac{dq}{d\tau} L \tag{1.74}$$

where L is the latent heat of condensation, cal/g.

The quantity of heat lost by the droplet to the gas molecules is expressed by an equation which is analogous to (1.67):

$$Q = \frac{4\pi r\lambda (T_r - T)}{\gamma} \tag{1.75}$$

where λ is the thermal conductivity of the gas around the droplet, cal·cm^{-1}× ×sec^{-1}deg^{-1}; T_r the surface temperature of the droplet, °K; T the temperature of the gas, °K; γ a coefficient defined by the equation

$$\gamma = \frac{\lambda}{r\beta m} + \frac{r}{r + \Delta} \tag{1.76}$$

where β is the thermal accommodation coefficient, i.e., the fraction of gas molecules which upon coming in contact with a droplet's surface acquire the temperature of that droplet; m a coefficient characterizing the contact of the gas with the droplet.

Since fog generally forms in the presence of large quantities of non-condensing gases, we may take

$$m = 0.0583 \cdot C_v P \sqrt{\frac{1}{M_g T}} \tag{1.77}$$

where C_v is the molar specific heat of the gas for constant volume, cal× ×mole^{-1} · deg^{-1}; M_g the molar mass of the gas; P the total pressure, mm Hg.

Equating the right-hand sides of (1.74) and (1.75) and substituting $dq/d\tau$ from (1.67), we find

$$T_r - T = \frac{DML[(p - p_r)(T_r)]}{RT\lambda Z} \tag{1.78}$$

where

$$Z = \frac{\varphi}{\gamma} \tag{1.79}$$

The droplet temperature T_r can be found from (1.78) by successive approximations; the droplet temperature is required if we are to determine the parameter $p_r(T_r)$ (see equation (1.9)) entering the numerator in the right-hand side of (1.78).

To simplify the calculations, Tunitskii /39/ assumes for the large droplets

$$p_r(T_r) \approx P_r(T)\left[1 + \frac{ML}{1.98\,TT_r}(T_r - T)\right] \tag{1.80}$$

Substituting $P_r(T_r)$ from (1.80) in (1.78), putting $T \cdot T_r \approx T^2$, and seeing that for small droplets $ML/1.98$ should be replaced with the difference $\frac{ML}{1.98} - \frac{2\sigma M}{R'\rho r}$ (where $R' = 8.314 \cdot 10^7\ \text{erg} \cdot \text{deg}^{-1} \cdot \text{mole}^{-1}$), we find /99/

$$T_r - T = \frac{p - p_r(T)}{\dfrac{RT\lambda Z}{DML} + \dfrac{ML - \dfrac{1.98 \cdot 2}{R'\rho r}}{1.98\,T^2}}\, p_r(T) \tag{1.81}$$

For droplets with $r > 10^{-7}$ cm, we have $\frac{ML}{1.98} \gg \frac{2\sigma M}{R'\rho r}$ and in practice the term $\frac{2\sigma M}{R'\rho r}$ can be omitted. The droplet temperature is thus calculated from the simple equation

$$T_r - T = \frac{p - p_r(T)}{\dfrac{RT\lambda Z}{DML} + \dfrac{ML p_r(T)}{1.98\,T^2}} \tag{1.82}$$

To form some idea of the dependence of the temperature difference between the droplet and the gas on the droplet radius, let us consider the magnitude of this difference for a sulfuric acid droplet suspended in air; the air temperature $T = 448.4$ °K ($t = 175.3$ °C), H_2SO_4 vapor pressure in air $p = 16.25$ mm Hg ($S = 5.0$). The constants entering equations (1.69), (1.68), (1.77), (1.76), (1.79), and (1.81) have the following values: $M = 98$, $D = 0.159\ \text{cm}^2/\text{sec}$, $\Delta \approx l = 10^{-5}$ cm, $C_v = 4.98$ cal/mole, $P = 760$ mm Hg, $M_r = 29$, $\lambda = 8.4 \cdot 10^{-5}\ \text{cal} \cdot \text{cm}^{-1} \cdot \text{sec}^{-1} \cdot \text{deg}^{-1}$, $\alpha = \beta = 1$, $P_\infty(T) = 3.24$ mm Hg, $\sigma = 50.2$ dyne/cm, $R = 6.24 \cdot 10^{-4}\ \text{cm}^3\,(\text{mm Hg})\ \text{deg}^{-1} \cdot \text{mole}^{-1}$, $R' = 8.314 \cdot 10^7$ erg× ×deg^{-1}·mole^{-1}, $L = 122$ cal/g, $\rho = 1.681\ \text{g/cm}^3$.

TABLE 1.10. Droplet parameters as a function of radius for $\Delta = 10^{-5}$ cm

Parameters	Radius r, cm						
	10^{-7}	$1.5 \cdot 10^{-7}$	10^{-6}	$5 \cdot 10^{-6}$	10^{-5}	10^{-4}	10^{-3}
$\varphi = \frac{D}{r\alpha_0} + \frac{r}{r+\Delta}$ . . .	204.4	—	20.6	—	2.54	1.11	1.01
$\gamma = \frac{\lambda}{r\beta m} + \frac{r}{r+\Delta}$	435.2	—	43.6	—	4.85	1.34	1.03
$Z = \frac{\varphi}{\gamma}$	0.470	—	0.471	—	0.524	0 828	0.978
$T_r - T$	0.64	9.1	17.9	19.0	17.3	11.6	10.0

Inserting these numerical values in the above equations, we find $r = 10^{-7}$ cm, $\nu = 7.78 \cdot 10^3$, $\varphi = 204.4$, $x = 1.93$, $\gamma = 435.2$, $Z = 0.470$, $T_r - T = 0.64$ °K.

Table 1.10 lists the data obtained for various r; we see from these data that the temperature difference between the droplet and the gas increases with increasing r to a certain maximum value and then subsides. This extremal variation is attributed to the fact that for small r, $p_r(T)$ is large, whereas the difference $p - p_r(T)$ is insignificant.

DISPERSITY, NUMBER DENSITY, AND MASS CONCENTRATION OF FOG

Dispersity is a measure of the drop size distribution of a fog. Monodisperse fog consists of droplets of equal radius and its dispersity is expressed unambiguously by the constant drop radius. The droplets in polydisperse fog have different radii and its dispersity (or rather polydispersity) is characterized by the actual drop size distribution, which is represented by different empirical and theoretical formulas /102—104/. Polydisperse fog is approximately described by the mean drop radius (arithmetic mean, root-mean-square, root-mean-cube, etc. /104/).

The monodispersity of a fog (like that of any aerosol) is expressed in terms of the ratio of the root-mean-cube radius to the arithmetic mean radius $\frac{\bar{r}}{r_a}$ or by the variability coefficient α /105/, i.e., the ratio of the rms deviation of σ of the drop radii to the arithmetic mean radius $\bar{r}_a$:

$$\alpha = \frac{\sigma}{\bar{r}_a} = \frac{\left[\frac{\Sigma_i N_i (r_i - \bar{r}_a)^2}{N}\right]^{1/2}}{\bar{r}_a} \qquad (1.83)$$

The smaller α, the higher the monodispersity of the fog; for $\alpha = 0$, all droplets have the same radius. Fog droplets normally have radii ranging between wide limits, from $5 \cdot 10^{-8} - 10^{-7}$ to $10^{-3} - 10^{-2}$ cm (see Appendix I).

The number density of fog, i.e., the number of droplets per unit gas volume, is generally denoted by n or N and expressed in cm^{-3} or m^{-3} at NTP. The number density at which the optical effect of the fog (i.e., the reduction of gas transparency) becomes visible to the naked eye depends on fog dispersity and on a variety of other factors (the thickness of the intervening gas layer, the position of the light source, etc.). For example, in atmospheric air, a slight fog is observed when $N = 0.5 \cdot 10^2 - 1 \cdot 10^2$ cm^{-3} /65/; heavy fog with a visibility of less than 200 m has $N = 5 \cdot 10^2 - 6 \cdot 10^2$ cm^{-3}. The mean drop size of atmospheric fog is $7 - 15\,\mu$. In a small volume (e.g., in a 1-liter glass flask) sulfuric acid fog with drops of radius $0.5\,\mu$ is visible to the naked eye when $N = 10^5$ cm^{-3}.

In nature, in laboratory work, and in industrial processes the number density of fog fluctuates between very wide limits. The number density is always variable in time. During nucleation, the number density of the fog is increased by the continued formation of new droplets and concurrently decreased coalescence. When the formation of new droplets has stopped,

the number density starts decreasing monotonically because of coalescence, droplet precipitation, and evaporation.

It follows from the above data that for each particular nucleation rate there is a definite limiting number density which can be found by combining the nucleation equation (1.27)

$$I = \frac{dN}{d\tau} = Ke^{-A} \tag{1.27}$$

with the equation of coalescence (coagulation)

$$\frac{dN}{d\tau} = -K_0N^2 \tag{1.84}$$

(here K_0 is the coalescence constant). Equating the absolute values of the right-hand sides of these equations, we find

$$N = \sqrt{\frac{K}{K_0}e^{-A}} = \sqrt{\frac{I}{K_0}} \tag{1.85}$$

The relaxation time τ (i.e., the time in which N attains a constant value) is expressed by the equation /97/

$$\tau = \frac{N}{I} = (IK_0)^{-1/2} \approx 10^5 \cdot I^{-1/2} \tag{1.86}$$

where $K_0 \approx 10^{-10}$.

Hence it follows, in particular, that the slope factor of the $N=f(S)$ curve decreases as S increases (since nucleation is offset by coalescence). This is consistent with the experimental findings /71, 72, 106/ which show that at high supersaturations the number of droplets increases insignificantly.

The mass concentration of fog (droplet mass in unit gas volume) is generally denoted by the symbol g or G and is expressed in g/cm^3 at NTP. In all fog condensation processes (with the exception of vapor condensation on a surface, see Chapter Four), the condensing vapor remains in the gas volume, and the mass concentration of the fog is therefore proportional to the vapor pressure difference in the initial and the final stages of fog formation.

If we assume that in the final stage of fog condensation the droplets in the system are sufficiently large and an equilibrium is established between the vapor pressure in the gas mixture and the saturated vapor pressure above the liquid drops, we may approximately write for the mass concentration of fog

$$G = \frac{M[p - p_\infty(T)]}{RT} = \frac{Mp_\infty(T)}{RT}(S - 1) \tag{1.87}$$

where p, $p_\infty(T)$ are the initial vapor pressure and saturated vapor pressure at the terminal temperature T, mm Hg; R is the gas constant, equal to $6.24 \cdot 10^4$ cm^3(mm Hg)$\cdot$deg$^{-1}\cdot$mole^{-1}.

The above assumption is valid for the majority of industrial processes, since once fog has formed, the supersaturation decreases because of vapor condensation on fog particles, which have a very large overall surface. The supersaturation falls off until an equilibrium is attained with vapor

supersaturation close to unity. The time to equilibrium depends on the nature of the condensation centers, their number density, the total vapor pressure, and the maximum supersaturation. Because of the high rate of fog condensation and the enormous overall surface of the fog particles, the above processes occur fairly rapidly and equation (1.87) can be reliably applied for practical calculations. If, however, p_∞ is interpreted as the saturated vapor pressure at the initial temperature of fog formation, equation (1.87) becomes markedly less accurate.

In practice, the mass concentration of fog is often comparatively low, and the heat of condensation released when fog particles form is small enough to be ignored. The mass concentrations are therefore calculated from equation (1.87) by substituting the supersaturations from the corresponding equations for each of the particular cases discussed in what follows (Chapters Two—Four).

Dispersity, number density, and mass concentration are related by the equation

$$\bar{r} = \left(\frac{3G}{4\pi\rho N}\right)^{1/3} \qquad (1.88)$$

where $\bar{r}$ is the root-mean-cube radius of the droplets, cm; G mass concentration of fog, g/cm^3(at NTP); N number density of fog, cm^{-3}(at NTP); ρ the density of the liquid, g/cm^3.

MECHANISM OF FOG FORMATION

It follows from the preceding that an increase in vapor supersaturation, either due to a reduction of temperature of the gas mixture with time ($dT/d\tau<0$) or to an increase of vapor pressure in the system ($dp/d\tau>0$), is prerequisite for fog formation.

The vapor-gas mixture cools by one of the following processes:

(1) adiabatic expansion;
(2) loss of heat by radiation;
(3) introduction of a cold indifferent gas to the mixture;
(4) contact with a cold surface.

Increase of vapor pressure leading to supersaturation may result from chemical reactions between mixing gas components or from the presence of various chemically activating agents (photosynthesis, radiation, etc.).

In practice the temperature and the pressure are normally both variable, and $dS/d\tau$ correspondingly changes with time. For example, adiabatic expansion of a vapor-gas mixture lowers the temperature and the pressure (because the volume increases, see Chapter Two). The equilibrium vapor pressure, however, is an exponential function of temperature (equation (1.2)), and the supersaturation of an adiabatically expanding vapor-gas mixture therefore shows a net increase.

The relation of temperature to pressure is different in different processes, and the supersaturation equation changes correspondingly. Each of the above variants of the formation of supersaturated vapor is therefore discussed in a separate chapter.

The mechanism of fog formation in a clean, ion-free gas (homogeneous condensation) reduces to an increase in the rate of nucleation with increasing supersaturation. Having nucleated, the embryos grow to fog droplets by condensation. When the size and the concentration of the droplets becomes high enough for the optical effect to be noticeable, we say that fog has formed.

The temperature of the gas mixture increases during the condensational growth of the droplets. Part of the vapor is removed from the gas mixture in the process and the latent heat of condensation is absorbed by the molecules: both these factors obviously lower the supersaturation. In the final account, the main process which raises the supersaturation is modified by the superposition of secondary processes which lower the supersaturation or stop further nucleation. Therefore, a clear distinction should be made in the study of the supersaturated vapor between the conditions before and after vapor condensation in the gas volume, i.e., between $S<S_{cr}$ and $S\geqslant S_{cr}$.

Figure 1.11 plots the supersaturation as a function of time without homogeneous condensation (curve 1) and taking account of homogeneous condensation (curve 2). Curve 2 is below curve 1 because embryos start forming for $\tau=\tau_1$, the rate of nucleation increasing with τ: the supersaturation S decreases due to vapor condensation on the embryos and the resulting liberation of the latent heat of condensation.

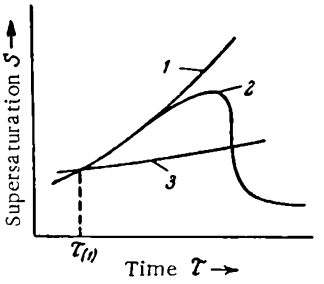

FIGURE 1.11. Supersaturation vs. time:
1) without nucleation; 2) with spontaneous formation of embryos; 3) critical supersaturation.

The sharp drop in S after the maximum is attributable to the steady increase in the rate of droplet growth by condensation on account of the increase in r and the reduction in φ (equation (1.67)).

It should be noted that according to some data supersaturation does not increase indefinitely: there is a certain upper limit to this quantity, known as the absolute supersaturation. The absolute supersaturation is attained when the work for the formation of critical embryo has decreased to zero /17/. The existence of the upper limit of supersaturation can also be deduced from the concepts of Van der Waals (as has been actually done by Buikov and Bakhanov).

The mechanism of fog formation in the presence of ions and condensation nuclei is essentially similar to the mechanism of homogeneous condensation, but droplets start forming at a lower supersaturation, i.e., as soon as the supersaturation has surpassed the equilibrium vapor pressure above the suspended condensation nuclei (see Table 1.1).

The rate of vapor condensation on the nuclei is determined by the diffusion of vapor to the surface (a comparatively slow process), and therefore at large $dS/d\tau$ (i.e., in processes associated with a rapid increase in supersaturation or involving low number densities of nuclei) the rate of diffusion may turn to be insufficient for equalizing the vapor pressure throughout the system. The vapor pressure in the gas phase may thus substantially differ from the vapor pressure near the surface of the nuclei. This obviously results in a high supersaturation, and homogeneous condensation may begin. This explains why homogeneous condensation, far from being an ideal process, may and often does occur in a variety of industrial media, despite the substantial content of condensation nuclei and gas ions in the real gases.

The above considerations are corroborated by experimental counts of fog droplets forming in adiabatic expansion of vapor-gas mixtures which contain dust particles and ions /73/. The results of the experiments show that as the expansion ratio (or the supersaturation) is increased, the number of fog droplets increases because vapor condenses on progressively smaller nuclei and embryos.

We thus distinguish between two cases depending on the relationship between $dS/d\tau$ and the number density of the nuclei (i.e., depending on the rate of growth of the derivative $dS/d\tau$ and the rate of vapor condensation on the nuclei):

(1) The rate of diffusion of the vapor to the condensation nuclei is high, supersaturated vapor does not form, and embryos do not nucleate.

(2) Vapor condensation on nuclei is insignificant, vapor supersaturation far from the nuclei attains the critical value, and homogeneous condensation sets in with embryos forming spontaneously.

The rate of nucleation is an exponential function of S (equation (1.53)), and the number density of the fog formed by homogeneous condensation is primarily dependent on S. It may be found from the equation

$$N(\tau) = \int_0^\tau I(S)\, d\tau \tag{1.89}$$

S is also a function of time (the main process whereby vapor supersaturation is raised being a function of time); it furthermore depends on drop size and concentration, because the condensation of vapor on the surface of the drops lowers the vapor pressure in the system. Equation (1.89) thus takes the form /107/

$$N(\tau) = \int_0^\tau I\{S[\tau, N(\tau)]\}\, d\tau \tag{1.90}$$

The solution of equation (1.90) involves considerable difficulties, since no sufficient data are available. We should therefore try to establish the dependence of the number density and the drop size on the principal indices of the process.

The rate of nucleation (conditioned by N and r) is primarily dependent on the supersaturation S, which falls off due to the condensational growth of droplets which proceeds at an ever increasing rate as long as the droplets remain in the region of supersaturated vapor. We may therefore write the following functional relations for the drop radius and the number density:

$$r = F(S); \quad r = f\left(\frac{dS}{d\tau}\right) \tag{1.91}$$

$$N = \psi(S); \quad N = \varphi\left(\frac{dS}{d\tau}\right) \tag{1.92}$$

As S and $dS/d\tau$ increase, r decreases and N rises. This point is illustrated by the various examples discussed in the following chapters.

The reduction of vapor concentration due to the formation of embryos is vanishingly small, since the radii of the embryos are small ($\approx 10^{-7}$ cm).

The dispersity of the fog forming by homogeneous condensation in its turn is dependent on the total amount of condensed vapor, the mass concentration of the fog (equation (1.87)), the number of droplets, and the number density of the fog (equation (1.89)). From (1.87) it follows that, other conditions being equal, the droplet radius increases with vapor pressure, since in homogeneous condensation p is several times higher than p_∞. The above considerations are all confirmed by experimental measurements of the radii of fog droplets forming when sulfuric acid vapor condenses /108/. The sulfuric acid vapor was obtained by mixing air with SO_3 and water vapor. As the vapor pressure of SO_3 and water increased, the droplets became progressively larger /108/:

Vapor pressure of sulfuric acid after mixing $p_{H_2SO_4}$, mm Hg	0.04	0.09	0.15	0.27	0.48	0.56	0.77
Mean drop radius $\bar{r} \cdot 10^6$, cm	1.4	1.6	2.4	2.8	2.9	3.2	3.1
Number density of droplets $N \cdot 10^{-10}$, cm^{-3}	—	—	2.6	3.6	3.9	4.6	5.5

These results can be expressed by the equation

$$\lg \bar{r} = 0.25 \lg p_{H_2SO_4}$$

The above considerations are also supported by experimental data on the dispersity of the fog which forms when the SO_3 gas (whose content in the air is 0.3%) is absorbed by sulfuric acid (with concentrations under 98.3%) (E. V. Yashke, A. G. Amelin, et al.). Fog will form in this case because water vapor is always present above sulfuric acid of these concentrations, its pressure increasing as the H_2SO_4 concentration is decreased (Chapter Six, p. 170). The water vapor interacts with SO_3 and forms sulfuric acid vapor which condenses into fog.

Figure 1.12 shows that the drop radius initially increases as the saturated vapor pressure above sulfuric acid (p_{H_2O}) is increased. When p_{H_2O} has reached the value of 0.06 mm Hg (see Figure 1.12) the drop radius remains constant with further increase of pressure because the flux of water molecules evaporating from the sulfuric acid surface is sufficient to bind all the SO_3 molecules.

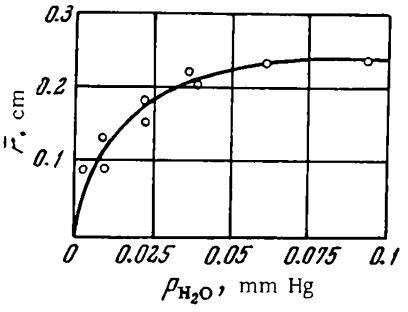

FIGURE 1.12. The mean drop radius $\bar{r}$ of fog vs. equilibrium vapor pressure of water p_{H_2O} above sulfuric acid (the SO_3 vapor pressure in air is 2.8 mm Hg).

The increase of the mean drop radius with the initial vapor pressure is also confirmed by calculations of the condensation of sulfuric acid vapor in a pipe (Chapter Five, p. 124).

If the gas temperature drops below the crystallization point of the liquid, the droplets solidify and the fog turns into dust. Minute droplets, however, withstand supercooling, and the freezing temperature of small droplets is therefore substantially lower than the tabulated figures for the same liquids in bulk. Water droplets, for example, can be supercooled to −40 °C /28/. Other liquids can be supercooled even to a higher degree. Indeed, the solid particles which form in homogeneous condensation of vapor at temperatures below freezing are

mostly spherical with a smooth surface (e.g., soot /109/, SiO_2 /110/, metal powder /111—112/, metal oxides /113, 114/, etc.).

According to Ostwald, the molecules of supersaturated vapor first condense into droplets of supercooled liquid, which eventually crystallize. There are indications, however, that in some cases the molecules pass directly from gas to solid state, without the intermediate stage of a liquid phase /15/.

REFERENCES

1. Tekhnicheskaya entsiklopediya. Spravochnik fiziko-khimicheskikh velichin (Technical Encyclopedia. Handbook of Physicochemical Constants), Vol. 5. 1930.
2. Spravochnik khimika (Chemist's Handbook), Vol. 1, p. 682. — Goskhimizdat. 1962.
3. KELVIN. — Proc. Roy. Soc. (London), 7:63. 1870.
4. GORBACHEV, S. V. — Izv. AN SSSR, math. and natural sci. section, p. 843. 1936.
5. MARTYNOV, V. — ZhFKh, 23:278. 1949.
6. LaMER, V. K. and G. M. POUND. — J. Chem. Phys., 17:1337. 1949.
7. TOLMAN, R. C. — J. Chem. Phys., 17:333. 1949.
8. BUFF, F. P. and J. G. KIRKWOOD. — J. Chem. Phys., 18:991. 1950.
9. KIRKWOOD, J. G. and F. P. BUFF. — J. Chem. Phys., 17:338. 1949.
10. SHCHERBAKOV, L. M. — Kolloidnyi Zhurnal, 14(5):379. 1952; 33:759. 1958.
11. KIP, L. B., A. F. LOEB, and A. W. EINARSSON. — J. Chem. Phys., 6:264. 1938.
12. WILSON, C. T. R. — Phil. Trans. Roy. Soc., 193:289. 1899.
13. LABY, T. H. — Phil. Trans. Roy. Soc., 208:445. 1908.
14. SCHARRER, L. — Ann. Phys., 35:619. 1939.
15. FRENKEL, J. Kinetic Theory of Liquids. — Dover Publ. Inc. 1955; Sobranie izbrannykh trudov (Collected Works), Vol. 3, Ch. 7. — Izdatel'stvo AN SSSR. 1959.
16. SHCHERBAKOV, L. M. — In: "Issledovaniya v oblasti poverkhnostnykh sil", p. 28. Izdatel'stvo AN SSSR. 1961.
17. SHCHERBAKOV, L. M., P. P. RYAZANTSEV, and N. L. FILIPPOVA. — Kolloidnyi Zhurnal, 23:338. 1961.
18. SHCHERBAKOV, L. M. — Kolloidnyi Zhurnal, 24:502. 1962.
19. LECENLY, R. E., E. J. ROBBINS, and P. A. TREVALION. — Proc. Roy. Soc., 280A:409. 1964.
20. GIBBS, J. W. Thermodynamic Papers [Russian translation]. — Gostekhizdat. 1950. [Also see GIBBS, W. Collected Works. — N. Y., Yale University Press. 1948.]
21. VOLMER, M. and A. WEBER. — Z. Phys. Chem., 119:277. 1926.
22. BECKER, R. and W. DOERING. — Ann. Phys., 24:719. 1935.
23. ZEL'DOVICH, Ya. B. — ZhETF, 12:325. 1942.
24. BARNARD, A. L. — Proc. Roy. Soc. (London), A 220:132. 1953.
25. FARLY, F. J. — Proc. Roy. Soc. (London), A 212:530. 1952.
26. COURTHEY, W. G. — J. Chem. Phys., 35:2249. 1964.
27. MOELWYN-HUGHES, E. D. Physical Chemistry. — Pergamon Press. 1961. [Russian translation. 1962.]
28. MASON, B. J. The Physics of Clouds. — Oxford. 1957. [Russian translation. 1961.]

29. HIRTH, I. P. and C. M. POUND. Condensation and Evaporation, Nucleation and Growth Kinetics. — Pergamon Press. 1963.

30. VOLMER, M. Kinetik der Phasenbildung. — Stenkopf, Dresden un Leipzig. 1939.

31. BRADLEY, R. S. — Quart. Rev., (London), 5 : 315. 1951.

32. FUKS, N. A. — UFN, 15 : 496. 1935.

33. STRANSKII, I. and R. KAISHEV. — UFN, 21 : 408. 1939.

34. Crystal Growth. — Disc. Faraday Soc., 5. 1949.

35. COURTHEY, W. G. — J. Chem. Phys., 38 : 1448. 1963.

36. HOLLOMON, D. N. and D. TARIBALL. — In: "Uspekhi fiziki metallov", Vol. 1, p. 304. Metallurgizdat. 1956.

37. The Physical Chemistry of Aerosols. — Disc. Faraday Soc., 30. 1960.

38. RUSANOV, A. I. — Uspekhi Khimii, 33 : 873. 1964.

39. TUNITSKII, N. N. — ZhFKh, 15 : 1061. 1941.

40. BRADLEY, R. S. — J. Coll. Sci., 15 : 525. 1960.

41. COURTHEY, W. G. — J. Chem. Phys., 36 : 2009, 2018. 1962.

42. LaMER, V. K. — Ind. Eng. Chem., 44 : 1270. 1952.

43. MASON, B. J. — Disc. Faraday Soc. , 30 : 8. 1960.

44. DUNNING, W. J. — Disc. Faraday Soc., 30 : 9. 1960.

45. ROSTOGI, R. P. and P. BASSI. — J. Sci. Ind. Res., A21 : 462. 1961.

46. DAVIES, C. N. Recent Advances in Aerosol Research. — Pergamon Press. 1964.

47. SHCHERBAKOV, L. M. — Kolloidnyi Zhurnal, 23 : 215. 1961.

48. SHCHERBAKOV, L. M. and V. I. RYKOV. — Kolloidnyi Zhurnal, 23 : 221. 1961.

49. DERYAGIN, B. V. — In: "Issledovaniya v oblasti poverkhnostnykh sil". Collection of papers presented at the Second Surface Activity Conference, B. V. Deryagin, ed. Nauka. 1964.

50. SHCHERBAKOV, L. M. Kapillyarnye effekty II roda i ikh rol' v termodinamike i kinetike fazovykh prevrashchenii v aerozol'nykh sistemakh (Capillary Effects of Second Kind and Their Role in Thermodynamics and Kinetics of Phase Transitions in Aerosol Systems). — Thesis. 1964.

51. MAYER, J. — J. Chem. Phys., 5 : 67. 1937; 5 : 87. 1938; 6 : 101. 1938.

52. MAYER, J. E. and M. G. MAYER. Statistical Mechanics. — N. Y., Wiley. 1940. [Russian translation. 1952.]

53. GEILIKMAN, B. T. Statisticheskaya teoriya fazovykh prevrashchenii (Statistical Theory of Phase Transitions). — Gostekhizdat. 1960.

54. HILL, T. L. Statistical Mechanics. — N. Y., McGraw-Hill. 1956. [Russian translation. 1960.]

55. UHLENBECK, G. E., ed. Studies in Statistical Mechanics. — New York, Interscience. 1962.

56. LOTHE, J. and G. M. POUND. — J. Chem. Phys., 36 : 2080. 1962.

57. VOLMER, W. and H. FLOOD. — Z. Phys. Chem., 170 : 273. 1934.

58. AMELIN, A. G. — DAN SSSR, 58 : 1673. 1947.

59. AMELIN, A. G. — Kolloidnyi Zhurnal, 10 : 169. 1948.

60. IZMAILOVA, G. I., P. S. PROKHOROV, and B. V. DERYAGIN. — Kolloidnyi Zhurnal, 19 : 556. 1957.

61. IZMAILOVA, G. I., P. S. PROKHOROV, and B. V. DERYAGIN. — Kolloidnyi Zhurnal, 19 : 556. 1957.

62. KOGAN, Ya. I. — DAN SSSR, 161 : 388. 1965.

63. KHRGIAN, A. Kh. Fizika atmosfery (Physics of the Atmosphere). — Fizmatgiz. 1958.

64. JUNGE, C. — Ber. Deutsch. Wetterdienst. U. S. Zone, 35 : 261. 1952.

65. TVERSKII, P. N. ed. Kurs meteorologii (A Course in Meteorology). — GIMIZ. 1951.

66. NOLAN, P. J. and L. W. POLLAK. — Proc. Roy. Irish Acad., A51 : 9. 1946.

67. LANDSBERG, H. — Kosm. Phys. (Leipzig, Akademische Verlagsgesellschaft), 3 : 207. 1938.

68. JANGE, C. — Ann. Met. (Beiheft), 5. 1952.

69. FETT, W. Der atmosphärische Staub. — Berlin, Deutscher Verlag der Wissenschaften. 1958.

70. GRABOVSKII, R. I. Atmosfernye yadra kondensatsiya (Atmospheric Condensation Nuclei). — Gidrometeoizdat. 1956.

71. BORUS, C. — Ann. Phys., 24 : 225. 1907.

72. WILSON, C. T. R. — Phil. Trans. Roy. Soc., A189 : 256. 1897; A192 : 403. 1899.

73. FREY, F. — Z. Physik. Chem., 13 : 49. 1941.

74. HIGUCHE, W. S. and C. T. O'KONSKI. — J. Coll. Sci., 15 : 14. 1960.

75. AMELIN, A. G. and E. V. YASHKE. — Kolloidnyi Zhurnal, 25 : 3. 1963.

76. AMELIN, A. G. and M. I. BELYAKOV. — Kolloidnyi Zhurnal, 24 : 374. 1962.

77. HERTZ, H. — Ann. Phys., 17 : 177. 1882.

78. KNUDSEN, M. — Ann. Phys., 29 : 179. 1909.

79. BARANAEV, M. — Uspekhi Khimii, 7 : 1231. 1938; ZhFKh, 13 : 1635. 1939.

80. ALTY, F. and C. A. MACKAY. — Proc. Roy. Soc., A149 : 104. 1935.

81. KAPPLER, E. and K. HAMMECK. — Forschungsber. Wirtschafts-und Verkehrsmin. NRW, 125. 1955.

82. HICKMAN, K. C. D. — Ind. Eng. Chem, 46 : 1442. 1954.

83. DELANEY, L. J., R. W. HOUSTON, and L. C. EAGLETON. — Chem. Eng. Sci., 19 : 105. 1964.

84. WYLLIE, G. — Proc. Roy. Soc., A197 : 383. 1949.

85. TREVOY, D. J. — Ind. Eng. Chem., 45 : 2366. 1953.

86. VOLMER, M. and J. ESTERMAN. — Z. Phys., 7 : 13. 1921.

87. KNUDSEN, M. — Ann. Phys., 47 : 697. 1915; 50 : 472. 1916.

88. BAER, E. and J. M. McKELEVEY. — A. I. Ch. E. Journal, 4 : 218. 1958.

89. BIRKS, J. and R. S. BRADLEY. — Proc. Roy. Soc. (London), A 198 : 226. 1949.

90. MACHE, H. — Z. Phys., 107 : 310. 1937.

91. HICKMAN, C. D. and W. A. FORPEY. — Ind. Eng. Chem., 46 : 1446. 1954.

92. BERMAN, L. D. — Trudy NIIKhIMMASh, 36 : 66. 1961.

93. PAYL, B. — ARS Journal, 32 : 1321. 1962.

94. COURTHEY, W. G. — ARS Journal, 31 : 751. 1961.

95. MAXWELL, C. — Coll. Sci. Paper, Cambridge, 11 : 625. 1890.

96. FUKS, N. A. — ZhETF, 4 : 7. 1934.

97. BRADLEY, R. S., M. G. EVANS, R. W. WHYTLAW-GRAY. — Proc. Roy. Soc. (London), 186 A : 368. 1946.

98. FUKS, N. A. Isparenie i rost kapel' v gazoobraznoi srede (Droplet Evaporation and Growth in a Gaseous Medium). — Izdatel'stvo AN SSSR. 1958.

99. AMELIN, A. G., E. V. YASHKE, and Yu. S. KURGIN. — Kolloidnyi Zhurnal, 23 : 652. 1961.

100. STEFAN, J. — Wien. Ber., 83 : 943. 1881.

101. LEVICH, V. G. Fiziko-khimicheskaya gidrodinamika (Physicochemical Hydrodynamics). — Fizmatgiz. 1959.

102. FUKS, N. A. Mekhanika aerozolei (Mechanics of Aerosols). — Izdatel'stvo AN SSSR. 1955.

103. SPURNÝ, K., Č. JECH, B. SEDLAČEK, and O. ŠTORCH. Aerozoli (Aerosols). Translation from Czech. — Atomizdat. 1964.

104. TSYURUPA, N. N. — Kolloidnyi Zhurnal, 26 : 117. 1964.

105. FUKS, N. A. and A. G. SUTUGIN. — Uspekhi Khimii, 34 : 276. 1965.

106. BYKOV, A. G. and E. N. TEVEROVSKII. — ZhETF, 19 : 328. 1949.

107. SEGAL', R. B. — ZhETF, 21 : 814. 1951.

108. PETRYANOV, I. V. and N. N. TUNITSKII. — ZhFKh, 13 : 1131. 1939.

109. KEL'TSEV, V. V. and P. A. TESNER. Sazha. Svoistva, proizvodstvo i primenenie (Soot. Properties, Production, and Applications). — Gostoptekhizdat. 1952.

110. NIKOLINA, V. Ya. — Khimicheskya Promyshlennost', No. 2 : 48. 1962.

111. JONES, W. D. Powder Metallurgy. — London, Arnold. 1960. [Russian translation. 1964.]

112. GEN, M. Ya., M. S. ZISKIN, and Yu. I. PETROV. — DAN SSSR, 127 : 366. 1959.

113. CAILLOT, R., J. P. CUERT, J. ELSTON, F. JUILLET, R. POINTUD, M. PRETTRE, and S. TEICHNER. — Bull. Soc. Chim. France, No. 1 : 152. 1959.

114. CUERT, J. P., J. ELSTON, and S. TEICHNER. — J. Bull. Soc. Chim. France, No. 1 : 81. 1961.

Chapter Two

FORMATION OF SUPERSATURATED VAPOR AND FOG BY ADIABATIC EXPANSION AND BY RADIATIVE COOLING

FOG FORMATION IN AN ADIABATICALLY EXPANDING VAPOR-GAS MIXTURE

Adiabatic processes are those which do not entail heat transfer between the system and the surrounding medium. Perfect thermal insulation of a system is unfeasible, but if a process is sufficiently fast (i.e., no significant heat transfer between the system and the medium can occur in the relevant time), it may be regarded as adiabatic even without perfect insulation.

Adiabatic expansion of a vapor-containing gas not only increases the volume of the gas mixture and lowers the vapor pressure, but also reduces the temperature of the mixture, since some of the internal energy of the gas is absorbed as the work of expansion. The saturated vapor pressure is a rapidly increasing function of temperature, and the reduction of temperature therefore raises the supersaturation despite the decrease in pressure by adiabatic expansion.

When S rises to a sufficiently high value ($S>S_{cr}$), homogeneous condensation sets in with the formation of embryos and then droplets. The vapor pressure in the system changes not only by expansion, but also due to vapor condensation, i.e., formation of embryos and their condensational growth. This process is accompanied by a release of the latent heat of condensation which is eventually deposited in the gas. Vapor condensation and the release of the latent heat both lower the supersaturation.

We shall first consider the formation of supersaturated vapor for $S<S_{cr}$ and then proceed to describe the conditions of supersaturation taking account of homogeneous condensation and droplet growth.

Working formulas for supersaturation

The first law of thermodynamics for ideal gases in an adiabatic process ($dQ = 0$) is expressed by the equation

$$PdV + C_v dT = 0 \qquad \text{(a)}$$

where P is the total pressure of the gas mixture; V the volume of the gas mixture; C_v the molar specific heat of the gas mixture for constant volume; T the absolute temperature.

Substituting in (a) $P=RT/V$, we obtain after simple manipulations

$$R\frac{dV}{V}+C_v\frac{dT}{T}=0 \qquad \text{(b)}$$

where $R=C_p-C_v$ (C_p is the molar specific heat of the gas mixture for constant pressure).

From (b) it follows that

$$(C_p-C_v)\frac{dV}{V}+C_v\frac{dT}{T}=0$$

or, dividing through by C_v,

$$(k-1)\frac{dV}{V}+\frac{dT}{T}=0$$

where k is the ratio of the specific heats C_p/C_v.

Integrating, we find

$$\ln V^{k-1}+\ln T=\text{const}$$

or

$$TV^{k-1}=\text{const} \qquad \text{(c)}$$

Substituting RT/P for V, we obtain

$$TP^{\frac{1-k}{k}}=\text{const} \qquad \text{(d)}$$

As the gas mixture expands adiabatically from the initial volume V_1 to the final volume V_2 (with temperature and pressure of T_2 and P_2, respectively), we find from equations (c) and (d)

$$TV^{k-1}=T_2V_2^{k-1}=\text{const}$$

$$T_1P_1^{\frac{1-k}{k}}=T_2P_2^{\frac{1-k}{k}}=\text{const}$$

whence

$$\frac{T_1}{T_2}=\left(\frac{V_1}{V_2}\right)^{1-k} \qquad (2.1)$$

$$\frac{T_1}{T_2}=\left(\frac{P_1}{P_2}\right)^{\frac{k-1}{k}} \qquad (2.2)$$

$$\frac{P_1}{P_2}=\left(\frac{V_2}{V_1}\right)^{k} \qquad (2.3)$$

For a vapor-gas mixture

$$\frac{P_1}{P_2}=\frac{p_1}{p_2} \qquad (2.4)$$

where p_1 and p_2 is the vapor pressure in the gas mixture before and after expansion.

From (2.2) and (2.4) we have

$$\frac{T_1}{T_2} = \left(\frac{p_1}{p_2}\right)^{\frac{k-1}{k}} \tag{2.5}$$

Since we are dealing with a mixture of gases, k should be calculated from the equation /1/

$$\frac{1}{k-1} = \frac{1}{k_v - 1} \cdot \frac{p_v}{P} + \frac{1}{k_g^{-1}} \cdot \frac{p_g}{P}$$

where p_v, k_v are the partial pressure and the ratio of the specific heats of the vapor in the system; p_g, k_g the partial pressure and the ratio of the specific heats of the noncondensing gas.

From (2.3), (2.4), and (2.5) we have

$$p_2 = p_1 \left(\frac{T_2}{T_1}\right)^{\frac{k}{k-1}} = p_1 \left(\frac{V_1}{V_2}\right)^k \tag{2.6}$$

Inserting in (1.1), we find

$$S = \frac{p_2}{p_\infty(T_2)} = \frac{p_1}{p_\infty(T_2)} \left(\frac{T_2}{T_1}\right)^{\frac{k}{k-1}} = \frac{p_1}{p_\infty(T_2)} \left(\frac{V_1}{V_2}\right)^k \tag{2.7}$$

where $p_\infty(T_2)$ is the saturated vapor pressure at the temperature T_2.

If prior to expansion the gas mixture contained saturated vapor (this is the case normally observed in a cloud chamber, see p. 55), we substitute $p_\infty(T_2)$ from (1.2) in (2.7) and write

$$S = \frac{p_2}{p_1} \cdot e^{E\left(\frac{1}{T_2} - \frac{1}{T_1}\right)} = \frac{P_2}{P_1} \cdot e^{E\left(\frac{1}{T_2} - \frac{1}{T_1}\right)} \tag{2.8}$$

or, making use of (2.1) and (2.3),

$$S = \left(\frac{V_2}{V_1}\right)^{-k} \cdot e^{\frac{E}{T_1}\left[\left(\frac{V_2}{V_1}\right)^{k-1} - 1\right]} \tag{2.9}$$

Differentiating (2.5) and putting $p_2 = p$, $T_2 = T$, we find

$$\frac{dp}{dT} = \eta T^{\frac{1}{k-1}} \tag{2.10}$$

where η is a constant:

$$\eta = \frac{k}{k-1} \cdot p_1 T_1^{\frac{k}{1-k}} \tag{2.11}$$

If the saturated vapor-gas mixture expands uniformly, i.e., $\frac{dV}{d\tau} = \text{const}$, the expansion ratio as a function of time is expressed by the equation

$$\frac{V}{V_1} = B\tau \tag{2.12}$$

where V is the gas volume at the time τ; B a coefficient defined by the expression

$$B = \frac{1}{t} \cdot \frac{V_2}{V_1} \tag{2.13}$$

here t is the time of expansion from the initial volume V_1 to the final volume V_2, which characterizes the rate of expansion.

Substituting these expressions in (2.9), we find

$$S = (B\tau)^{-k} \exp\left\{\frac{E}{T_1}[(B\tau)^{k-1} - 1]\right\} \tag{2.14}$$

or

$$\ln S = \frac{E}{T_1}[(B\tau)^{k-1} - 1] - k\ln(B\tau) \tag{2.15}$$

From (2.9) and (2.14) we see that the supersaturation in an adiabatically expanding vapor-gas mixture depends on the expansion ratio, the nature of the noncondensing gas (the coefficient k), and the nature of the vapor (the coefficient E). Table 2.1 lists the supersaturation as a function of the expansion ratio $\frac{V_2}{V_1}$. The calculations were made using equations (2.7) and (2.1) for the systems air—water vapor ($k = 1.4$) and air—ethanol vapor ($k = 1.37$). The initial temperature of the gas mixture was 293 °K, water vapor pressure 172 N·m^{-2} (17.54 mm Hg), ethanol vapor pressure 432 N·m^{-2} (44 mm Hg).

TABLE 2.1. Supersaturation vs. expansion ratio

System	Expansion ratio $\frac{V_2}{V_1}$				
	1.0	1.1	1.2	1.3	1.4
	Supersaturation				
Air—water vapor . .	1.00	1.78	2.96	5.52	9.14
Air—ethanol vapor .	1.00	1.62	2.55	4.15	6.94

We see from Table 2.1 that even a slight increase in expansion markedly raises the supersaturation, which of course depends on the composition of the vapor in the system.

Table 2.2 lists the calculated supersaturation for different noncondensing gases and different vapors for $\frac{V_2}{V_1} = 1.25$ and constant initial pressure $P = 1.47 \cdot 10^{-5}$ N·m^{-2} (1.5 atm).

TABLE 2.2. Supersaturation for different noncondensing gases and different vapors at $\frac{V_2}{V_1}=1.25$, $P_1=1.47\cdot10^{-5}$ N·m^{-2}

System	$k=\frac{c_p}{c_v}$	Gas temperature, °K		Supersaturation S
		before expansion, T_1	after expansion, T_2	
Argon—water vapor	1.66	293.1	252.8	15.6
Air—water vapor	1.40	293.1	267.2	4.2
Carbon dioxide—water vapor	1.31	293.1	273.4	2.8
Air—ethanol vapor	1.37	293.1	269.8	3.41

We see from Table 2.2 that when a monoatomic gas, e.g., argon, is substituted for air, the supersaturation increases. Indeed, for equal expansions, the supersaturation in the argon—water vapor system is 15.6, and that in the air—water vapor system is 4.2.

Droplet size and number density of fog

Fog forms in an adiabatically expanding clean, ion-free vapor-gas mixture because both the supersaturation S (equation (2.7)) and the rate of nucleation I (equation (1.53)) increase as the mixture expands. Vapor condenses on the surface of the spontaneously forming embryos and the latter grow into droplets. When the number density and the mass concentration of the droplets become sufficiently high, a distinct optical effect is observed in transmitted light (Tyndall effect).

The above considerations and analytical expressions apply for the case $S<S_{cr}$. If $S>S_{cr}$, the supersaturation is less than that obtaining from (2.9) because spontaneous condensation and the resulting heating of the gas mixture lower the supersaturation.

From (1.7) and (1.90) we see that for homogeneous condensation $S=f(T)=\varphi(\tau)$ is a complicated function of many variables, all of which influence to a certain degree the supersaturation S (P, p, T_r, N, r, φ, etc.). The solution of equations (1.7) and then (1.90) for adiabatic expansion therefore involves considerable difficulties and the various techniques of solution are highly approximate /2, 3/.

Some idea of the influence of various factors on the number density of droplets can be gained by a theoretical inspection of

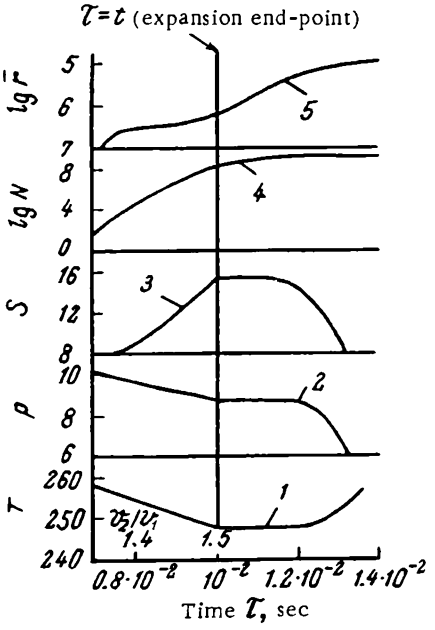

FIGURE 2.1. Variation of thermodynamic parameters during adiabatic expansion and after:
1) temperature T, °K; 2) vapor pressure p, mm Hg; 3) supersaturation S; 4) number density of droplets N, cm^{-3}; 5) mean droplet radius $\bar{r}$, cm.

the condensation process in adiabatically expanding vapor-gas mixtures /4, 5/ or by calculations /6—8/.

Figure 2.1 plots the homogeneous condensation of water vapor as calculated from the Frenkel equation (1.46) for an air-vapor mixture expanding adiabatically from an initial volume V_1 to a final volume V_2 in $\tau = t = 10^{-2}$ sec; here $V_2/V_1 = 1.5$. The initial temperature of the mixture is $T = 291$ °K, water vapor pressure $p = 15.33$ mm Hg. In these approximate calculations (which are reproduced in detail on p. 51) the total expansion time of the gas mixture from volume V_1 to V_2 and a certain additional period after the expansion end-point (e.g., from $\tau = 10^{-2}$ sec to $\tau = 1.4 \cdot 10^{-2}$ sec, as in Figure 2.1) are divided into i subintervals, each with constant supersaturation, constant nucleation rate, etc. The number of droplets forming in unit gas volume in each of these subintervals and the total number of droplets at the end of the process (i.e., the number density) are obtained from the equations

$$N = \sum_1^i N_i = \sum_1^i I_i \Delta\tau$$

The calculations are continued in a certain interval after the expansion end-point because in some cases spontaneous nucleation may persist even though the gas has stopped expanding.

Among the numerical factors which enter the calculations there are the heat released by the condensation of vapor on the droplets, the temperature of the droplets, and the dependence of the condensation rate on the droplet radius (which varies with time between wide limits).

We see from Figure 2.1 that the general trend of the temperature, vapor pressure, and supersaturation curves sharply changes at the expansion end-point. The curves of number density and droplet radius, on the other hand, have no distinct end-point, since the droplets continue forming and growing even when the expansion has stopped.

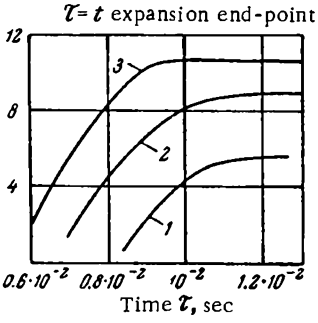

FIGURE 2.2. Variation of number density during adiabatic expansion and after:
1) calculated from the Frenkel equation (1.53) $\frac{V_2}{V_1} = 1.4$; 2) calculated from the Frenkel equation (1.53) for $\frac{V_2}{V_1} = 1.5$; 3) calculated from the Becker-Doering equation (1.34) for $\frac{V_2}{V_1} = 1.5$.

Figure 2.2 plots some curves which illustrate the dependence of the number density of droplets on the expansion ratio according to different theoretical relations for the nucleation rate I (in all cases, $t = 10^{-2}$ sec). We see from the figure that for an expansion ratio $V_2/V_1 = 1.4$ (curve 1) nucleation begins at $\tau \approx 8.2 \cdot 10^{-3}$ sec and goes on for $0.3 \cdot 10^{-2}$ sec after the expansion has stopped. The final number density of the droplets is $\sim 10^6$ cm^{-3}. For $V_2/V_1 = 1.5$ (curve 2), the nucleation process stops when the expansion stops.

Curve 3 is plotted according to the Becker-Doering equation (1.34), which gives higher values of I than equation (1.53). In this case nucleation stops while the gas is still expanding (at $\tau = 9.5 \cdot 10^{-3}$ sec): toward the end of the

expansion process and after the end-point the curve is parallel to the abscissa axis. The nucleation stops prematurely because by that time the weight concentration of the fog has risen considerably and the water vapor pressure in the air has dropped significantly (due to intensive vapor condensation). These factors combine with the heating of the vapor-gas mixture by the released latent heat of condensation to suppress the supersaturation S.

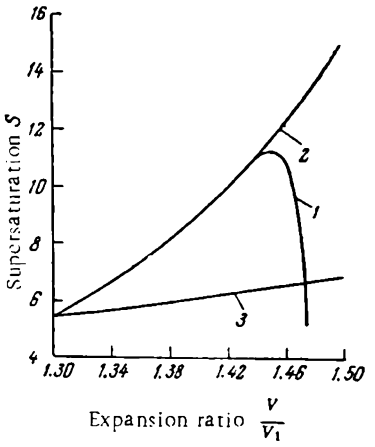

FIGURE 2.3. Supersaturation S during expansion ($\frac{V_2}{V_1}=1.5$): 1) $t=1$ sec ($\beta=1.5$); 2) $t=0.01$ sec ($\beta=150$) and $t=0$ ($\beta=\infty$); 3) critical supersaturation.

The trend of the $N=f(\tau)$ curves for an adiabatically expanding vapor-gas mixture is thus essentially dependent on the time t for the expansion of the mixture from volume V_1 to V_2, i.e., on the rate of expansion.

Supersaturation also depends on the rate of expansion. This is confirmed by the results plotted in Figure 2.3, which have been calculated for the same initial data as before, taking different values of t (and also of the coefficient β as expressed by equation (2.13)).

For $t=1$ sec (curve 1) nucleation begins at $V/V_1=1.30$; at first this process has an insignificant influence on S, since the embryos are small ($\approx 10^{-7}$ cm) and a small quantity of liquid has been tied up by their formation. Curve 1 and the curve which ignores nucleation therefore follow the same course during the initial stages.

As N and r increase, the rate of vapor condensation on the surface of droplets is accelerated (according to equation (1.67)) and the process exerts a progressively greater influence on the supersaturation S. For $V/V_1=1.45$ the supersaturation reaches a maximum, falling off steeply at higher expansion ratios.

Nucleation stops at $V/V_1=1.47$ (when $S=S_{cr}$). During the time from $V/V_1=1.3$ to $V/V_1=1.47$, two processes — nucleation and condensational growth of the embryos — occur simultaneously. The fog thus consists of larger particles, which have formed in the initial stages of the process, as well as fine particles which have formed in the late stages. Condensational growth of the large droplets and evaporation of the small droplets continue beyond the expansion ratio $V_2/V_1=1.47$, since the saturated vapor pressure above small droplets is higher than that above large droplets (isothermal distillation).

For $t=0.01$ sec (a higher expansion rate, curve 2), the maximum supersaturation rate increases, the rate of nucleation rises, and the number density of droplets becomes higher. The mean droplet radius should decrease, since less time is now available for condensational growth.

An analysis of the above data suggests that the main parameters specifying fog formation in an adiabatically expanding vapor-gas mixture are determined by the rate of expansion, i.e., the derivative $\frac{dv_2/v_1}{d\tau}$ or $dS/d\tau$ (making use of (2.9)). As $dS/d\tau$ increases S_{max} and N increase and $\bar{r}$ decreases.

To derive an equation for $dS/d\tau$, we should find the derivatives $dp/d\tau$ and $dT/d\tau$ and insert the corresponding expressions in (1.7). Making use of (1.54), we write for the rate of vapor condensation in a gas volume

$$\frac{dq}{d\tau} = \frac{4\pi MDrN}{RT\varphi}[p - p_r(T_r)] + \frac{4\pi r_c^3 \rho I}{3} \tag{2.16}$$

where q is the total quantity of condensed vapor in a unit gas volume at NTP, g/cm^3; τ time, sec; r the radius of droplets in the gas, cm; r_e the radius of the embryos, cm; N number density of droplets, cm^{-3}; φ a coefficient which allows for the dependence of the condensation rate on the droplet radius (equation (1.68)); I rate of nucleation, cm^{-3} sec^{-1}.

The first term in the right-hand side of (2.16) expresses the rate of vapor condensation on the surface of the droplets present in the gas mixture; the second term represents the rate of condensation by nucleation (i.e., conversion of vapor to liquid due to the formation of new embryos).

Since the embryos are minute particles ($\approx 10^{-7}$ cm), the quantity of liquid in these embryos is vanishingly small and the second term in (2.16) is generally ignored in practice.

Proceeding from the dependence between the amount of condensing vapor and the reduction in vapor pressure (equation (b), p. 106), we write (2.16) in the form

$$-\frac{dp}{d\tau} = A\frac{(P-p)^2}{P}\cdot\frac{DrN}{T\varphi}[p - p_r(T_r)] \tag{2.17}$$

where

$$A = \frac{4\pi M_v}{g_n R} \tag{2.18}$$

From (2.3), (2.4), and (2.12) we have

$$\frac{p_2}{p_1} = (B\tau)^{-k}$$

or

$$\frac{dp}{d\tau} = -\frac{p_1 k \tau^{-1-k}}{B^k} = \frac{\Pi}{\tau^{1+k}} \tag{2.19}$$

where

$$\Pi = -\frac{p_1 k}{B^k} \tag{2.20}$$

The vapor pressure thus decreases at the overall rate

$$-\frac{dp}{d\tau} = A\frac{(P-p)^2}{P}\cdot\frac{DrN}{T\varphi}[p - p_r(T_r)] - \Pi\tau^{-1-k} \tag{2.21}$$

Heat is released by condensation at a rate

$$\frac{dQ}{d\tau} = \frac{4\pi M_v DrNL}{RT\varphi}[p - p_r(T_r)] + \frac{4\pi r_{cr}^3 \rho IL}{3} \tag{2.22}$$

where Q is the total quantity of heat released in unit gas volume at NTP; L the latent heat of condensation.

The first term in the right-hand side of (2.22) expresses the quantity of heat released by vapor condensation on the surface of the droplets in the gas; the second term is the quantity of heat released when embryos form. The second term is again small in comparison with the first and is normally ignored.

Making use of the relation of the heat content of a gas to its temperature (equation (c) in Chapter Five, p. 106), we write for (2.22)

$$\frac{dT}{d\tau} \quad A\frac{P}{p_c}\cdot\frac{p}{T_\varphi}\cdot\frac{DrNL}{T_\varphi}[p - p_r(T_r)] \tag{2.23}$$

From equations (2.1) and (2.12), we have

$$\frac{T}{T_1} = (B\tau)^{1-k}$$

or

$$\frac{dT}{d\tau} = T_1(1-k)B^{1-k}\tau^{-k} = \Pi\tau^{-k} \tag{2.24}$$

where

$$\Pi = (1-k)T_1B^{1-k} \tag{2.25}$$

The total rate of cooling in this case is thus expressed by the equation

$$-\frac{dT}{d\tau} = \Pi\tau^{-k} - A\frac{P-p}{P\Pi}\cdot\frac{DrNL}{T_\varphi}[p - p_r(T_r)] \tag{2.26}$$

From (2.19) and (2.24) we have

$$\frac{dp}{dT} = \frac{A\dfrac{(P-p)^2}{P}\cdot\dfrac{DrN}{T_\varphi}[p - p_\infty(T_r) - \Pi\tau^{1-k}]}{\Pi\tau^{-k} - A\dfrac{P-p}{P\Pi}\cdot\dfrac{DrNL}{T_\varphi}[p - p_\infty(T_r)]} \tag{2.27}$$

Substituting $\frac{dp}{d\tau}$ and $\frac{dT}{d\tau}$ from (2.19) and (2.24) in (1.7), we find

$$\frac{dS}{d\tau} = \frac{A}{p_{\infty}(T)}\cdot\frac{(P-p)^2}{P}\cdot\frac{DrN}{T_\varphi}[p - p_r(T_r)] + \frac{\Pi}{p_\infty(T)\tau^{1+k}} - \\ - \frac{pE}{p_\infty(T)T^2}\left\{\Pi\tau^{-k} - A\frac{P-p}{P\Pi}\cdot\frac{DrNL}{T_\varphi}[p - p_r(T_r)]\right\} \tag{2.28}$$

If $S < S_{cr}$, equation (2.28) takes the simpler form

$$\frac{dS}{d\tau} = \frac{1}{p_\infty(T)\tau^k}\left[\frac{\Pi}{\tau} - \frac{pE\Pi}{T^2}\right] \tag{2.29}$$

Numerical calculation of fog formation by adiabatic expansion

Initial conditions. Initial temperature of the vapor-air mixture $T_0 = 291\ ^\circ K$; total initial pressure* $P_0 = 760$ mm Hg; water vapor pressure

* Conversion coefficient to SI units: mm Hg = 133 $N \cdot m^{-2}$; dyne $\cdot cm^{-2}$ = 0.1 $N \cdot m^{-2}$.

$p_0 = 15.33$ mm Hg; expansion ratio $\frac{V_2}{V_1} = \frac{V_f}{V_0} = 1.5$; expansion time $t = 0.01$ sec; $k = \frac{C_p}{C_v} = 1.4$; molecular weight of water $M = 18$; molecular weight of air $M = 29$; I calculated from (1.53).

The expansion time is divided into 11 intervals and all the parameters are assumed to remain constant over each of these intervals. The partial expansion time from interval n to $n+1$ is given by the equation

$$\Delta\tau_n = \frac{t}{\frac{V_f}{V_0} - 1}\left(\frac{V_{n+1}}{V_0} - \frac{V_n}{V_0}\right) = 0.02\left(\frac{V_{n+1}}{V_0} - \frac{V_n}{V_0}\right) \qquad \text{(a)}$$

The subscripts 0 and f refer to the initial and the end points of the expansion, respectively; the subscripts 1, 2, 3, . . . represent intermediate values in this order.

1st interval: $n = 1$, $\frac{V_1}{V_0} = 1.30$. From (2.1), (2.5), and (2.4) we have

$$T_1 = \frac{T_0}{\left(\frac{V_1}{V_0}\right)^{k-1}} = \frac{291}{1.3^{0.4}} = 262.7\ ^\circ\text{K}$$

$$p_0\left(\frac{T_1}{T_0}\right)^{\frac{k}{k-1}} = 15.33\left(\frac{262.7}{291.0}\right)^{\frac{1.4}{0.4}} = 10.72 \text{ mm Hg}$$

$$P_1 = P_0\frac{p_1}{p_0} = 760\cdot\frac{10.72}{15.33} = 531.5 \text{ mm Hg}$$

For $T_1 = 262.7\ ^\circ$K, saturated vapor pressure of water, $p_\infty(T_1)$, is 2.10 mm Hg; $S = \frac{p_1}{p_\infty(T_1)} = \frac{10.72}{2.10} = 5.11$ and $\sigma = 77.2$ dyne/cm.

Inserting in equation (1.53), we find

$$\ln I_1 = 60 - \ln\left[\frac{a}{S\rho}\left(\frac{p}{T}\right)^2 (M\sigma)^{1/2}\right] - \frac{17.6}{\ln^2 S}\left(\frac{M}{\rho}\right)^2\left(\frac{\sigma}{T}\right)^3 =$$

$$60 - \ln\left[\frac{0.1}{5.11\cdot 1}\left(\frac{10.72}{262.7}\right)^2 (18\cdot 77.2)^{1/2}\right] - \frac{17.6}{\ln^2 5.11}\left(\frac{18}{1}\right)^2\left(\frac{77.2}{262.7}\right)^3 = -0.498$$

whence $I_1 = 0.32\ \text{cm}^{-3}\,\text{sec}^{-1}$.

Since I_1 is small, the number of forming droplets is not determined.

2nd interval: $n=2$; $\frac{V_2}{V_0} = 1.32$; $T_2 = 260.4\ ^\circ$K; $p_2 = 10.39$ mm Hg; $P_2 =$ = 515 mm Hg; $p_\infty(T_2) = 1.75$; $S_2 = 3.95$; $\sigma_2 = 77.5$ dyne/cm; $I_2 = 3.1\cdot 10^2\ \text{cm}^{-3}\text{sec}^{-1}$.

Time for expansion from V_1/V_0 to V_2/V_0 from equation (a):

$$\Delta\tau_2 = 0.02\left(\frac{V_2}{V_0} - \frac{V_1}{V_0}\right) = 0.02(1.32 - 1.30) = 4\cdot 10^{-4} \text{ sec}$$

The number of droplets forming during the time $\Delta\tau_2$:

$$\Delta N_2 = I_2\Delta\tau_2 = 3.1\cdot 10^2\cdot 4\cdot 10^{-4} = 0.12\ \text{cm}^{-3}$$

The total number of droplets in the 2nd interval:

$$N_2 = N_1 + \Delta N_2 = 0 + 0.12 = 0.12 \text{ cm}^{-3}$$

The droplet radius is calculated from (1.9):

$$r_2 = \frac{2\sigma M}{RT\rho \ln S} = \frac{2 \cdot 77.5 \cdot 18}{8.315 \cdot 10^7 \cdot 260.4 \cdot 1 \cdot \ln 3.95} = 7.2 \cdot 10^{-8} \text{ cm}$$

The quantity of liquid in the droplets:

$$g_{d,2} = \frac{4}{3}\pi r^3 \rho \Delta N_2 = \frac{4}{3} \cdot 3.14 (7.2 \cdot 10^{-8})^3 \cdot 0.12 = 1.9 \cdot 10^{-22} \text{ g/cm}^3$$

3rd interval: $n=3$; $V_3/V_0 = 1.34$; $T_3 = 258.9°\text{K}$; $p_3 = 10.18$ mm Hg; $P_3 = 505$ mm Hg; $p_\infty(T_3) = 1.54$ mm Hg; $S_3 = 6.60$; $\sigma_3 = 77.8$ dyne/cm; $I_3 = 1.3 \cdot 10^4$; $\Delta\tau_3 = 4 \cdot 10^{-4}$ sec; $N_3 = 5.4 \text{ cm}^{-3}$; $r_3 = 6.9 \cdot 10^{-8}$ cm; $g_{d,3} = 7.3 \cdot 10^{-21}$ g/cm^3.

The quantity of liquid condensing on the ΔN_2 droplets during their stay in the 3rd interval ($\Delta\tau_3$) is calculated from equation (1.67). The coefficient φ and the equilibrium vapor pressure of water above the droplets at the temperature $T_r[p_r(T_r)]$, are determined before the actual calculations can be made.

The coefficient φ is obtained from the equations of Chapter One, putting $D = 0.30 \text{ cm}^2/\text{sec}$, $\Delta \approx l \approx 10^{-5}$ cm, $a = 1$.

$$\nu = 3643 \sqrt{\frac{T}{M}} = 3643 \sqrt{\frac{258.9}{18}} = 1.38 \cdot 10^4 \qquad (1.69)$$

$$\varphi = \frac{D}{ra\nu} + \frac{r}{r+\Delta} = \frac{0.30}{7.2 \cdot 10^{-8} \cdot 0.1 \cdot 1.38 \cdot 10^4} + \frac{7.2 \cdot 10^{-8}}{7.2 \cdot 10^{-8} + 10^{-5}} = 3019 \qquad (1.68)$$

To find the temperature of a droplet and then the pressure $p_r(T_r)$, we should first determine γ and the equilibrium vapor pressure of water above the droplets at the gas temperature, $-p_r(T)$, making use of the equations from Chapter One. Putting $C = 4.97$ cal/mole, $\beta = 1$, we find

$$m = 0.0583 \cdot C_v P \sqrt{\frac{1}{M_r T}} = 0.0583 \cdot 4.97 \cdot 505 \sqrt{\frac{1}{29 \cdot 258.85}} = 1.69 \qquad (1.77)$$

$$\gamma = \frac{\lambda}{r\beta m} + \frac{r}{r+\Delta} = \frac{5.1 \cdot 10^{-5}}{7.2 \cdot 10^{-8} \cdot 1 \cdot 1.69} + \frac{7.2 \cdot 10^{-8}}{7.2 \cdot 10^{-8} + 10^{-5}} = 419 \qquad (1.76)$$

$$Z = \frac{\varphi}{\gamma} = \frac{3019}{419} = 7.21 \qquad (1.79)$$

$$p_r(T) = p_\infty(T) \cdot e^{\frac{2\sigma M}{RTr}} = 154 \; e^{\frac{2 \cdot 77.8 \cdot 18}{8.3 \cdot 10^7 \cdot 258.9 \cdot 1 \cdot 7.2 \cdot 10^{-8}}} = 9.38 \text{ mm Hg} \qquad (1.3)$$

Inserting in (1.82), we obtain

$$T_r = T + \frac{p - p_r(T)}{\frac{RT\lambda Z}{DML} + \frac{ML p_r(T)}{1.98 T^2}}$$

$$T_r = 258.9 + \frac{10.18 - 9.38}{\frac{6.24 \cdot 10^4 \cdot 258.9 \cdot 5 \cdot 1 \cdot 10^{-5} \cdot 7.21}{0.30 \cdot 18 \cdot 600} + \frac{18 \cdot 600 \cdot 9.38}{1.98 \cdot 258.9^2}} = 259.2°\text{K}$$

and from (1.9) and (1.67) (seeing that for $T_r = 259.2\,°K$, $p_\infty = 1.56$ mm Hg)

$$p_r(T_r) = 1.56\, e^{\frac{2\cdot 77.8\cdot 18}{8.31\cdot 10^7\cdot 259.2\cdot 1\cdot 7.2\cdot 10^8}} = 9.48 \text{ mm Hg}$$

$$g_{2,3} = \frac{4\pi Dr\Delta N_2 \Delta\tau_3}{RTP\varphi}[p - p_r(T_r)] =$$

$$\frac{4\cdot 3.14\cdot 0.3\cdot 7.2\cdot 10^{-8}\cdot 18\cdot 0.12\cdot 4\cdot 10^{-4}}{82.06\cdot 258.9\cdot 505\cdot 3019}(10.18 - 9.48) = 5.1\cdot 10^{-21}\ \text{g/cm}^3$$

The total amount of liquid in the ΔN_2 droplets is

$$q_{2,3} = g_{d,2} + g_{2,3} = 1.9\cdot 10^{-22} + 5.1\cdot 10^{-21} = 5.3\cdot 10^{-21}\ \text{g/cm}^3$$

The droplets which formed in the 2nd interval will have grown to the following size by the end of the 3rd interval:

$$r_{2,3} = \sqrt[3]{\frac{3q_{2,3}}{4\pi\rho\Delta N_2}} = \sqrt[3]{\frac{3\cdot 5.3\cdot 10^{-21}}{4\cdot 3.14\cdot 1\cdot 0.12}} = 2.2\cdot 10^{-7}\,\text{cm}$$

The number density, the weight concentration of the fog, and the droplet radii for the 3rd interval are given by the following expressions:

$$N_3 = \Delta N_2 + \Delta N_3 = 0.12 + 5.36 = 5.48\ \text{cm}^{-3}$$

$$G_3 = q_{2,3} + q_{d,3} = 5.3\cdot 10^{-21} + 7.3\cdot 10^{-21} = 1.3\cdot 10^{-20}\ \text{g/cm}^3$$

$$\bar{r}_3 = \sqrt[3]{\frac{3G_3}{4\pi\rho N_3}} = \sqrt[3]{\frac{3\cdot 1.3\cdot 10^{-20}}{4\cdot 3.14\cdot 1\cdot 5.48}} = 8.3\cdot 10^{-8}\,\text{cm}$$

The calculations for all the following intervals, up to the 11th inclusive, follow the same general outline. New embryos continually form in each of the intervals and the number of droplets increases from one interval to the next. The calculations become more complicated, since each group of droplets (by group we mean all the droplets which have originated in the same interval) requires cumbersome manipulations. The problem is essentially simplified if a computer is used.

As V/V_1 increases, the ratio of the radii of droplets from different groups approaches unity. For simplicity, these groups are combined into one and the mean droplet radius is calculated. The accuracy is somewhat lowered, but since the droplets in question are all of nearly the same size, the error is insignificant and can actually be ignored for all practical purposes.

When the expansion of the gas mixture has stopped (for $\tau = t = 0.01$ sec), nucleation and condensational growth of droplets persist for some time. The time after adiabatic expansion is therefore divided into nine intervals and analogous calculations are carried out for each of them.

The effect of coalescence, however, is ignored in the calculations, since it follows from (1.86) that the relaxation time is $\tau = 10^5 I^{-1/2} = 0.3$ sec, while the entire process takes a mere 0.013 sec (Table 2.3).

The results of the calculations are listed in Tables 2.3 and 2.4; they are also plotted graphically in Figures 2.1 and 2.2 (curve 2). The calculated figures are compared with the experimental findings (cloud chamber

TABLE 2.3. Parameters of adiabatic expansion of an air—water vapor mixture

Number of intervals	τ_i sec	$\frac{V}{V_0}$	T °K	p mm Hg	$p_{\infty}(T)$ mm Hg	S	I $cm^{-3} \times sec^{-1}$	N cm^{-3}	r cm	Variability coefficient α (1.83)
0	0	1.0	291.0	15.33	15.33	1.0	—	—	—	—
1	$6.0 \cdot 10^{-3}$	1.30	262.7	10.72	2.10	5.11	—	—	—	—
2	$6.4 \cdot 10^{-3}$	1.32	260.4	10.35	1.75	5.95	$3.1 \cdot 10^{-2}$	0.1	—	—
3	$6.8 \cdot 10^{-3}$	1.34	258.9	10.18	1.54	6.60	$1.3 \cdot 10^{4}$	5.4	$6.5 \cdot 10^{-6}$	0.26
4	$7.2 \cdot 10^{-3}$	1.36	257.3	9.57	1.36	7.35	$4.1 \cdot 10^{5}$	$1.7 \cdot 10^{-2}$	$8.1 \cdot 10^{-8}$	0.34
5	$7.6 \cdot 10^{-3}$	1.38	255.8	9.77	1.20	8.12	$5.5 \cdot 10^{6}$	$1.7 \cdot 10^{-3}$	$2.7 \cdot 10^{-7}$	0.67
6	$8.0 \cdot 10^{-3}$	1.40	254.4	9.57	1.06	9.01	$6.1 \cdot 10^{7}$	$2.6 \cdot 6^{4}$	$2.5 \cdot 10^{-7}$	0.90
7	$8.4 \cdot 10^{-3}$	1.42	252.9	9.38	0.54	9.92	$4.1 \cdot 6^{8}$	$1.9 \cdot 10^{5}$	$3.4 \cdot 10^{-7}$	1.20
8	$8.8 \cdot 10^{-3}$	1.44	251.4	9.19	0.83	11.02	$2.7 \cdot 10^{9}$	$1.3 \cdot 10^{6}$	$3.6 \cdot 10^{-7}$	1.60
9	$5.2 \cdot 10^{-3}$	1.46	250.1	9.02	0.74	12.15	$1.3 \cdot 10^{10}$	$6.3 \cdot 10^{6}$	$4.2 \cdot 10^{-7}$	1.80
10	$9.6 \cdot 10^{-3}$	1.48	248.8	8.85	0.65	13.71	$1.8 \cdot 10^{10}$	$3.8 \cdot 10^{7}$	$4.6 \cdot 10^{-7}$	2.00
11	$1.0 \cdot 10^{-2}$	1.50	247.4	8.69	0.57	15.21	$2.8 \cdot 10^{11}$	$1.5 \cdot 10^{8}$	$6.5 \cdot 10^{-7}$	2.30
I	$1.04 \cdot 10^{-2}$		247.4	8.69	0.59	15.21	$2.8\ 10^{11}$	$2.6 \cdot 10^{8}$	$8.7 \cdot 10^{-7}$	2.20
II	$1.08 \cdot 10^{-2}$		247.4	8.69	0.59	15.21	$2.8 \cdot 10^{11}$	$3.8 \cdot 10^{6}$	$1.4 \cdot 10^{-6}$	2.10
III	$1.12\ 10^{-2}$		247.4	8.69	0.59	14.65	$1.4 \cdot 10^{11}$	$4.3 \cdot 10^{8}$	$2.4 \cdot 10^{-6}$	1.80
IV	$1.16 \cdot 10^{-2}$		247.5	8.66	0.60	14.58	$1.3 \cdot 10^{11}$	$4.5 \cdot 10^{6}$	$3.6 \cdot 10^{-6}$	1.10
V	$1.20 \cdot 10^{-2}$		247.7	8.57	0.61	14.26	$9.3 \cdot 10^{10}$	$5.2 \cdot 10^{8}$	$5.3 \cdot 10^{-6}$	1.00
VI	$1.24 \cdot 10^{-2}$		248.3	8.26	0.64	12.98	$1.8 \cdot 10^{10}$	$5.3 \cdot 10^{8}$	$6.4 \cdot 10^{-6}$	0.72
VII	$1.26 \cdot 10^{-2}$		249.4	7.71	0.70	10.99	$5.7 \cdot 10^{7}$	$5.3 \cdot 10^{8}$	$8.9 \cdot 10^{-6}$	0.66
VIII	$1.27 \cdot 10^{-2}$		251.5	6.68	0.84	7.99	$8.1 \cdot 10^{4}$	$5.3 \cdot 10^{8}$	$1.0 \cdot 10^{-5}$	0.56
IX	$1.28 \cdot 10^{-2}$		254.2	5.36	1.05	5.12		$5.3 \cdot 10^{6}$	$1.2 \cdot 10^{-5}$	0.51

TABLE 2.4. Drop size distribution in fog

Size distribution at expansion end-point		Size distribution after $1.28 \cdot 10^{-2}$ sec	
Droplet radius r, cm	Number of droplets N, cm^{-3}	Droplet radius r, cm	Number of droplets N, cm^{-3}
$1.2 \cdot 10^{-5}$	$1.7 \cdot 10^{3}$	$1.5 \cdot 10^{-5}$	$2.6 \cdot 10^{8}$
$4.3 \cdot 10^{-6}$	$1.9 \cdot 10^{5}$	$6.9 \cdot 10^{-6}$	$1.7 \cdot 10^{8}$
$1.8 \cdot 10^{-6}$	$1.1 \cdot 10^{8}$	$3.5 \cdot 10^{-6}$	$5.3 \cdot 10^{7}$
$6.8 \cdot 10^{-7}$	$5 \cdot 10^{6}$	$1.4 \cdot 10^{-6}$	$3.7 \cdot 10^{7}$
$1.4 \cdot 10^{-7}$	$3.1 \cdot 10^{7}$	$7.9 \cdot 10^{-7}$	$7.2 \cdot 10^{6}$
$5.2 \cdot 10^{-8}$	$1.1 \cdot 10^{8}$		
$r = 6.5 \cdot 10^{-7}$	$N = 1.5 \cdot 10^{8}$	$\bar{r} = 1.2 \cdot 10^{-5}$	$N = 5.3 \cdot 10^{6}$
$\alpha = 2.30$ (equation (1.83))		$\alpha = 0.51$ (equation (1.83))	

experiments) in Figure 1.9 (curve 1). The calculated number densities should be higher than the experimental data, since the supersaturation in the cloud chamber is lowered by the inevitable mass and heat transfer between the gas and the chamber walls.

CLOUD CHAMBER AND ITS APPLICATION

The cloud chamber was developed by the outstanding English physicist C. T. R. Wilson. He also carried out fundamental experiments with this chamber and studied fog formation in adiabatically expanding vapor-gas mixtures and the influence of various factors (e.g., the passage of electrically charged particles) on this process /9/. At present, the cloud

chamber is used in various researches and it still features as a fundamental tool for obtaining supersaturated vapor under laboratory conditions.

The vapor-gas mixture in the cloud chamber expands nearly instantaneously (0.01 — 0.001 sec). There is insignificant heat transfer between the gas and the chamber walls in this short time, and the conditions therefore approximate to those of an adiabatic process.

The chamber (Figure 2.4) is filled with air (or some noncondensing gas) which has been carefully cleaned from suspended particles and gas ions and then saturated with water vapor (or vapors of some other liquid). The volume of the vapor-gas mixture is increased by rapidly lowering the piston. The piston travels a certain distance and the vapor in the chamber attains a supersaturation S corresponding to the expansion ratio which has been achieved (equation (2.7)). Fog formation is observed visually or is detected with photographic equipment in parallel beams of transmitted light. Other transparency-measuring instruments can also be used to detect the fog.

As we have already observed, the expansion in the cloud chamber is not ideally adiabatic, since the chamber walls are warmer than the expanding vapor-gas mixture. The deviation from adiabaticity depends on chamber size and geometry and on the composition of the vapor-gas mixture. When expansion stops, the supersaturation drops due to heat transfer between the gas and the chamber walls, as well as due to vapor condensation and heat release (if fog has formed).

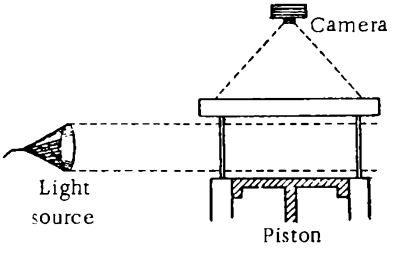

FIGURE 2.4. Schematic diagram of the cloud chamber.

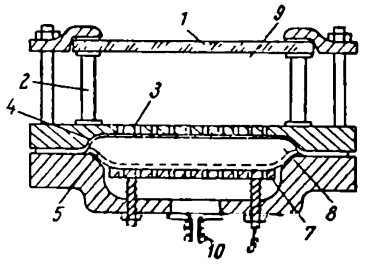

FIGURE 2.5. Schematic diagram of the modified expansion chamber with a rubber membrane: 1) glass top; 2) glass wall; 3) perforated plate; 4) position of membrane before air expulsion; 5) position of membrane after expulsion; 6) adjusting screws; 7) perforated disk; 8) subpiston space; 9) working space; 10) exhaust valve.

Figure 2.5 is a schematic diagram of a cloud chamber (originally proposed by Wilson) where the heavy piston (see Figure 2.4) has been replaced with a light-weight rubber membrane 4. Before expansion, the membrane is pneumatically pressed against a perforated plate 3; when the high-pressure air is expelled from the piston space 8, the membrane recoils toward the perforated plate 7. The expansion ratio $\left(\frac{V_2}{V_1}\right)$ can be varied by moving the disk 7 with the aid of adjusting screws 6.

The cloud chamber was instrumental to many outstanding discoveries in the physics of the atomic nucleus. Rutherford referred to the cloud chamber as "the most original and remarkable instrument in the history of science". The paths of electrons, nucleons, and other charged particles were first observed in the expansion chamber and it for the first time "displayed" their interactions and transformations. In nuclear physics experiments, the expansion of the chamber volume is chosen so that the resulting supersaturation is sufficient for vapor condensation in the presence of ions, while no vapor will condense if no ions are present. X rays or other energetic particles passing through the chamber volume ionize some of the gas molecules. The aggregates

which form in the gas because of statistical fluctuations acquire electrical charge, and the supersaturation proves to be sufficient for vapor condensation on these charged aggregates, though they are smaller than the embryos (see Figure 1.1). If strong lateral illumination is provided, fog streaks can be observed against a dark background. A typical photograph of the tracks left by alpha particles in a cloud chamber is shown in Figure 2.6.

An important addition to Wilson's technique is due to Academician D. V. Skobel'tsyn. Following his suggestion /10/, the cloud chamber is immersed in a magnetic field in which the paths of the charged particles are curved. The application of the magnetic field makes it possible to determine the sign and the magnitude of the electric charge, and to calculate the energy of the particles by measuring the length, the curvature, and the direction of the trajectories.

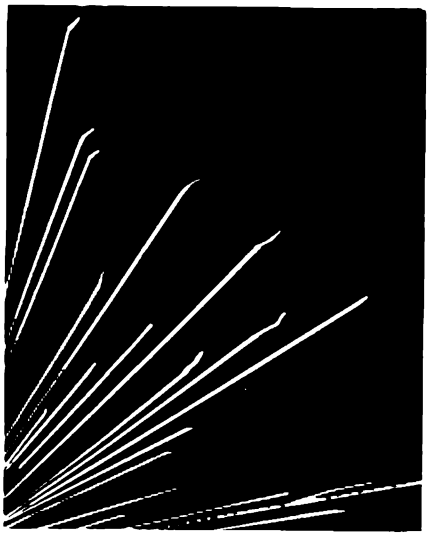

FIGURE 2.6. Tracks of alpha particles in nitrogen.

The tracks of charged particles in the cloud chamber are observed in the time interval between τ_1 and τ_2 (Figure 2.7), when the supersaturation lies between S_1 and S_2 and is sufficient for fog condensation on ions. This period is called the sensitive time of the chamber. It is proportional to the ratio $\left(\frac{V}{S}\right)^2$ (where V is the chamber volume and S the chamber surface), so that large-capacity chambers have a longer sensitive time.

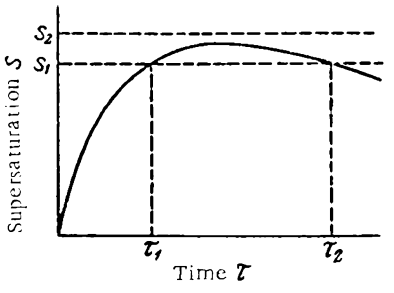

FIGURE 2.7. Supersaturation S in a cloud chamber vs. time.

The popularity of the cloud chamber in nuclear physics led to the development of various modified models /11—17/ with automatic electronic control and high sensitive times; simplified and portable chambers; high-pressure and variable-pressure high-capacity chambers (2 m^3); chambers for classroom experiments; etc. These chambers have been repeatedly used in various experiments on the conditions of fog formation along the path of a charged particle.

The results of the fundamental experiments on the formation of supersaturated vapor and homogeneous condensation of vapor in the cloud chamber have been discussed elsewhere (Chapter One) and we shall consider here only some studies which have a direct bearing on the particular aspects of Chapter Two.

Interesting results were obtained with cloud chambers on the conditions of supersaturation and homogeneous condensation of ethanol vapors /18/. In these experiments, the temperature was monitored with a resistance thermometer and a cathode ray oscilloscope which also displayed the

end-point in the release of the latent heat of condensation. The experimental results are consistent with the theoretical data obtained from the Frenkel equation (1.53) and with the theory and the actual findings in a second series of tests /19/, when vapor condensation on ions was studied.

The cloud chamber was also applied to investigate the homogeneous condensation of helium in a clean, ion-free medium /20/; it is in these studies that the dependence of critical supersaturation on temperature was established. The rate of formation of ice crystals in the presence of dry ice granules was seen to decrease steeply at temperatures above $-7\,^{\circ}C$ /21/. The condensational growth of water, ethanol, and methanol droplets was also investigated with the cloud chamber: the growth of the droplets was followed photoelectrically, by measuring the intensity of the scattered light. The experimental results were compared with theoretical calculations and the accommodation coefficients of 0.02, 0.01, and 0.004 were obtained for water, ethanol, and methanol, respectively.

ADIABATIC PROCESSES IN NATURE AND IN INDUSTRY

Adiabatic processes resulting in vapor supersaturation and fog formation are observed in nature and in various industrial processes. For example, the air rises from the lower atmospheric layers to higher altitudes, where the barometric pressure is lower, it expands adiabatically, and the air temperature drops approximately by $1\,^{\circ}C$ per 100 m of altitude. The supersaturation in the ascending air gradually rises from $S<1$ to $S = 1$ and fog droplets (clouds) form around the hygroscopic condensation nuclei which are inevitably present in the atmosphere (Chapter One).

When sound propagates in the air and in other gases, the temperature is higher than the average in the compressions and lower than the average in the rarefactions. No significant heat transfer may occur between the adjoining gas layers during the short period of the sound wave, and the process may therefore be regarded as an adiabatic one; the supersaturation of necessity increases in the rarefactions.

Adiabatic expansion is often observed in gas pumping. In some cases this may result in fog formation and interfere with the normal course of the work. For example, if a gas saturated or nearly saturated with liquid vapor is drawn into a compressor, the sudden drop in pressure will lead to fog formation. The liquid droplets settle on the walls and accumulate in the compressor enhancing corrosion.

When gas escapes into a relative vacuum, as the case is with a free jet (Chapter Three), the expansion is again very brief and therefore nearly adiabatic. An approximate theoretical analysis of this process /23/ shows that abundant condensation due to the expansion and the cooling of a vapor-gas mixture is possible only in nozzles $500-750$ mm in diameter in the presence of condensation nuclei with radii of $0.5-1\,\mu$.

FOG FORMATION BY RADIATIVE COOLING

Different gases differ in their capacity to absorb and to emit radiant energy. Monatomic and diatomic gases, in particular nitrogen, oxygen,

and hydrogen, have negligibly small emissivities and absorptivities; these gases are virtually transparent in the infrared. High emissivities and absorptivities, on the other hand, are observed for polyatomic gases, e.g., carbon dioxide, sulfuric oxide, ammonia, water vapor, etc. Therefore, if a gas mixture contains vapor molecules, which readily radiate heat, and is in contact with a relatively cold medium (the shell or the wall) the gas mixture will cool by giving off its excess heat. Since the vapor pressure remains constant in the process, the supersaturation must rise.

The attenuation of a flux of radiant energy in a gas is dependent on the number of molecules which intercept the impinging radiation; it is proportional to the path length l of the radiation in the gas and the partial pressure of the absorbing component p. The absorption of thermal radiation is furthermore proportional to the temperature of the gas, T.

The radiative heat transfer between the gas and the surrounding medium (the wall) is calculated from the following approximate equation /25/:

$$g = \varepsilon_g \varepsilon'_w C_0 \left[\left(\frac{T_g}{100} \right)^4 - \left(\frac{T_w}{100} \right)^4 \right] \tag{2.30}$$

where g is the radiated heat, $kJ \cdot m^2 \cdot hr$; ε_g the "blackness" (emissivity) of the gas; ε'_w the effective "blackness" of the wall; T_g, T_w the absolute temperature of the gas and the wall, °K; C_0 blackbody emissive power ($C_0 = 20.5\ kJ \times \times m^2 \cdot hr^{-1} \cdot °K^{-4}$).

The "blackness" ε_g of the gas depends on the thickness of the gas layer, its composition and temperature; it is read off the special nomograms which are plotted in advance for various gases /24, 25/. The effective "blackness" of the wall depends on its composition and temperature; it is expressed by the relation

$$\varepsilon'_w = 0.5 (\varepsilon_w + 1) \tag{2.31}$$

where ε_w is the wall "blackness" (listed in text-books /24/ and handbooks /25/).

For radiation into a vacuum (a blackbody at $T = 0$ °K) or into interplanetary space (e.g., radiation of heat by the earth's surface), the working equation takes the simpler form

$$g = \varepsilon_g C_0 \left(\frac{T_g}{100} \right)^4 \tag{2.32}$$

From (2.30) we see that a substantial radiative cooling and a considerable rise in supersaturation may occur only if both the temperature of the gas and the vapor pressure are high, e.g., as the case is with condensing metal vapors, in the focus of a nuclear explosion, and in stellar interiors.

Nuclear explosion produces a very high temperature, and all liquid and solid materials near the explosion focus are instantly vaporized. Then the gases rapidly cool off by radiative heat transfer (which is enormously high at the monstrous temperatures involved) and some other factors. The vapors condense into solid and liquid radioactive particles which coalesce into an aerosol cloud. This radioactive cloud rises to a great height and is then carried off by atmospheric currents over thousands of kilometers from the explosion site. Settling down, this radioactive fallout may cause fatal damage to man and animals.

Since high-temperature processes come into an ever wider use, the development of the theory of vapor supersaturation and fog formation by radiative cooling is a topical problem.

Thermal radiation plays an important role in the cooling of the earth's atmosphere and the formation of fog and clouds. Water and CO_2 vapor are the main atmospheric components which radiate heat. The atmospheric air thus absorbs the planetary heat radiated by the earth's surface, on the one hand, and loses part of the absorbed energy into the interplanetary space by radiation, on the other. The radiative cooling of a cloudy atmosphere is lower than that of a clear atmosphere, since clouds reflect radiant energy. Energy absorption and emission must be taken into consideration in rainfall and fog forecasting.

REFERENCES

1. RICHARZ, F. — Ann. Phys., 19:639. 1906.
2. TUNITSKII, N. N. — ZhFKh, 15:1061. 1941.
3. SEGAL', R. B. — ZhETF, 21:814. 1951.
4. WILLIAMS, E. J. — Proc. Camb. Phil., 35:512. 1939.
5. WAKESHIMA, H. — J. Phys. Soc. Japan, 9:400, 407. 1954.
6. MASON, B. J. — Proc. Phys. Soc., 64:773. 1951.
7. CORNER, G. — Proc. Roy. Soc. (London), A 211:417. 1952.
8. MASON, B. J. The Physics of Clouds. — Oxford. 1957. [Russian translation. 1961.]
9. WILSON, C. T. R. — Phil. Trans. Roy., 189:265. 1897; 192:403. 1899; 193:289. 1899; Phil. Mag., 7:681. 1904; Proc. Roy. Soc., 85:285. 1911; 87:277. 1912; 104:192. 1923.
10. PUTILOV, K. A. and V. A. FABRIKANT. Kurs fiziki (Textbook of Physics), Vol. 3. — Fizmatgiz. 1963.
11. WILSON, C. T. R. — Proc. Roy. Soc. (London), 142:88. 1933.
12. WILSON, C. T. R. and J. G. WILSON. — Proc. Roy. Soc., (London), 148:523. 1935.
13. VEKSLER, V., L. GROSHEV, and N. DOBROTIN. Eksperimental'nye metody yadernoi fiziki (Experimental Methods of Nuclear Physics). 1940.
14. DAS GUPTA, N. N. and S. K. GHOSH. The Cloud Chamber and Its Application in Physics. — [Russian translation. 1947.]
15. WILSON, J. G. The Principles of Cloud Chamber Technique. — Cambridge Univ. Press. 1951. [Russian translation. 1954.]
16. Spravochnik po fizike (Handbook of Physics). — Fizmatgiz. 1963.
17. BEKKERMAN, I. M. Nevidimoe ostavlyaet sled (Tracks of the Invisible). — Atomizdat. 1964.
18. STACHORSKA, D. — Ann. Univ. Curie-Skladowska, A12:143. 1960.
19. STACHORSKA, D. — Ann. Univ. Curie-Skladowska, A14:97. 1961.
20. EDWARDS, M. H. and W. C. WOODBURG. — Can. J. Phys., 38:335. 1960.
21. WILLIAM, I. E. and R. M. THOMAS. — Appl. Meteorol., 2:260. 1963.
22. WAKESHIMA, H. and K. J. TAKATA. — Appl. Phys., 2:792. 1963.
23. WILDE, K. J. — J. Appl. Phys., 30:577. 1959.
24. MIKHEEV, M. A. Osnovy teploperedachi (Principles of Heat Transfer). — Gosenergoizdat. 1956.
25. PERRY, D. G. Chemical Engineers' Handbook. — McGraw-Hill. 1950.
26. Meteorologiya i atomnaya energiya (Meteorology and Nuclear Energy). Translation from English, Fedorov, E. K., ed. — IL. 1959.

Chapter Three

FORMATION OF SUPERSATURATED VAPOR AND FOG IN TURBULENT MIXING OF GASES

Temperature and vapor pressure can be equalized by turbulent mixing of gases or by molecular diffusion and thermal conduction. Turbulent mixing of gases is a common occurrence in industrial processes; in these cases the rates of molecular diffusion and heat conduction are small in comparison with the speed of eddy mixing and are ignored in practical considerations.

The temperature of the mixture obtained when two volumes of gas are combined, as well as the vapor concentration and the supersaturation, are easily calculated if the initial volume, temperature, and vapor content are known for each of the mixing gases. The *I—T* diagram is used for these purposes, or simple calculations can be carried out by balancing the heat and mass transfer. The calculations show that the supersaturation varies with the volume ratio of the mixing gases and in some cases it reaches a maximum. The fog is therefore formed locally mainly in those regions of mixing where the supersaturation is highest.

DERIVATION OF WORKING FORMULAS FOR THE SUPERSATURATION

The relative role of eddy and molecular diffusion in the mixing of gases is determined by the radio $\frac{\omega}{D}$, where ω is the eddy diffusivity, D the molecular diffusivity. The ratio $\frac{\omega}{D}$ depends on the Reynolds number, fluctuating between 0.002 and 0.004 Re /1, 2/. Domkohler /3/ derived the following relation for gases:

$$\frac{\omega}{D} = 4\left(\frac{\mathrm{Re}}{\mathrm{Re}_{cr}}\right)$$

where Re_{cr} is the critical Reynolds number.

Analogous relations were derived for the relative contributions from eddy and molecular heat conduction. The significance of molecular processes for temperature and concentration equalization in turbulent flow is thus negligible for high Re.

The temperature and vapor pressure in the region of mixing depend on the mass ratio of the mixing gases:

$$n = \frac{g_2}{g_1} \tag{3.1}$$

where g_1 and g_2 are the component masses.

Balancing the masses we have

$$\frac{p_1 V_1}{P} + \frac{p_2 V_2}{P} = \frac{p(V_1 + V_2)}{P} \tag{3.2}$$

where p_1 and p_2 are the respective vapor pressures in the mixing gas streams; V_1 and V_2 the mixing volumes, reduced to NTP; p is the vapor pressure in the product mixture; P the total pressure.

From equation (3.2) we have

$$p = \frac{p_1 V_1 + p_2 V_2}{V_1 + V_2} \tag{a}$$

The mixing volumes can be expressed by the relations

$$V_1 = \frac{g_1 R T_0}{M_1} \quad \text{and} \quad V_2 = \frac{g_2 R T_0}{M_2} \tag{b}$$

where R is the gas constant; $T_0 = 273.1\ ^\circ\text{K}$; M_1 and M_2 the mean molar masses of the mixing gases. Inserting these expressions for the volumes in (a) and dividing through, we find

$$p = \frac{\frac{p_1 g_1}{M_1} + \frac{p_2 g_2}{M_2}}{\frac{g_1}{M_1} + \frac{g_2}{M_2}} \tag{c}$$

Multiplying the denominator and the numerator in the right-hand side of (c) by $\frac{M_1}{g_1}$, we obtain

$$p = \frac{p_1 + p_2 \frac{g_2}{g_1} \cdot \frac{M_1}{M_2}}{1 + \frac{g_2}{g_1} \cdot \frac{M_1}{M_2}} \tag{d}$$

Making use of (3.1) and putting

$$b = \frac{M_1}{M_2} \tag{3.3}$$

we obtain

$$p = \frac{p_1 + p_2 b n}{1 + b n} \tag{3.4}$$

From the heat balance equation we have

$$g_1 c_1 T_1 + g_2 c_2 T_2 = T(c_1 g_1 + c_2 g_2) \tag{3.5}$$

where c_1 and c_2 are the mean specific heats of the mixing gases; T_1 and T_2 the absolute temperatures of the mixing gases; T is the absolute temperature of the product mixture. From (3.5) we have

$$T = \frac{T_1 c_1 g_1 + T_2 c_2 g_2}{c_1 g_1 + c_2 g_2} \qquad \text{(e)}$$

Dividing the denominator and the numerator in the right-hand side of (e) by $c_1 g_1$, we write

$$T = \frac{T_1 + T_2 \cdot \frac{c_2}{c_1} \cdot \frac{g_2}{g_1}}{1 + \frac{c_2}{c_1} \cdot \frac{g_2}{g_1}} \qquad \text{(f)}$$

Making use of (3.1) and putting

$$a = \frac{c_2}{c_1} \qquad (3.6)$$

we write for (f)*

$$T = \frac{T_1 + T_2 an}{1 + an} \qquad (3.7)$$

The mean specific heat c and the mean molar mass M are calculated from the equations

$$c = \frac{c_n M_n}{M} + \frac{p}{PM}(c_v M_v - c_n M_n) \qquad (3.8)$$

$$M = M_n + \frac{p}{P}(M_v - M_n) \qquad (3.9)$$

where c_n is the specific heat of the noncondensing gas; M_n the molar mass of the noncondensing gas; c_v the specific heat of the vapor; M_v the molar mass of the vapor phase; P the total pressure.

Substituting p, p_n, and T from (3.4), (1.2), and (3.7) in equation (1.1), we find /4, 5, 6/

$$S = \frac{p_1 + p_2 bn}{(1 + bn)\, p_\infty (T)} = \frac{p_1 + p_2 bn}{(1 + bn) \exp\left(C - \frac{E}{\frac{T_1 + Tan}{1 + an}}\right)} \qquad (3.10)$$

All the quantities entering equations (3.4), (3.7), and (3.10) are constant for the mixing gas streams; the only exception is the parameter n, which is variable. Since the temperature, the pressure, and the supersaturation in the region of mixing are all functions of the parameter n, they are also variable.

From (3.4) and (3.7) we have

$$\frac{p_1 - p}{b(p - p_2)} = \frac{T_1 - T}{a(T - T_2)}$$

* The effect of temperature on the specific heat of the gas mixture is small enough to be ignored in the derivation of (3.7).

or, differentiating,

$$\frac{dp}{dT} = \mu \left(\frac{p - p_2}{T - T_2}\right)^2 \tag{3.11}$$

where μ is a constant:

$$\mu = \frac{b}{a} \cdot \frac{T_1 - T_2}{p_1 - p_2} \tag{3.12}$$

From (3.10) it follows that the functional dependence of supersaturation on the parameter n may have a maximum. The value of n corresponding to maximum supersaturation can be found from (3.10) in the usual way. The first derivative of the function $S = f(n)$ is

$$\frac{dS}{dn} = \frac{(1 + bn)\,[Ea\,(p_1 + p_2 bn)\,(T_1 - T_2) + p_2 bT^2\,(1 + an)^2]}{p_\infty(T)\,(1 + an)^2\,(1 + bn)^2 T^2} - \frac{bT\,(1 + p_2 bn)\,(1 + an)^2}{p_\infty(T)\,(1 + an)^2\,(1 + bn)^2 T^2}$$

Putting the first derivative equal to zero, we find

$$Ea\,(1 + bn)\,(p_1 + p_2 bn)\,(T_1 - T_2) + p_2 bT^2\,(1 + bn)\,(1 + an)^2 - bT^2\,(p_1 + p_2 bn)\,(1 + an)^2 = 0$$

or

$$\frac{E\,a\,(T_1 - T_2)}{b\,(p_1 - p_2)} - \frac{T^2\,(1 + an)^2}{(1 + bn)\,(p_1 + p_2 bn)} = 0$$

Substituting T from (3.7), we find

$$\frac{Ea\,(T_1 - T_2)}{b\,(p_1 - p_2)} - \frac{(T_1 + T_2\,an)^2}{(1 + bn)\,(p_1 + p_2 bn)} = 0$$

whence

$$n = -\frac{A}{2} \pm \sqrt{\frac{A^2}{4} - B} \tag{3.13}$$

where

$$A = \frac{E\,(T_1 - T_2)\,(p_1 + p_2) - 2\,T_1 T_2\,(p_1 - p_2)}{Ebp_2\,(T_1 - T_2) - aT_2^2\,(p_1 - p_2)} \tag{3.14}$$

$$B = \frac{Eap_1\,(T_1 - T_2) - bT_1^2\,(p_1 - p_2)}{ab\,[Ebp_2(T_1 - T_2) - aT_2^2(p_1 - p_2)]} \tag{3.15}$$

If the vapor pressure in the colder gas, p_2, is zero or small enough in comparison with p_1 to be neglected, equations (3.14) and (3.15) take the simpler form

$$A = \frac{2T_1 T_2 - E\,(T_1 - T_2)}{aT_2^2} \tag{3.14a}$$

$$B = \frac{bT_1^2 - Ea\,(T_1 - T_2)}{a^2 bT_2^2} \tag{3.15a}$$

If $a=b=1$, equations (3.4), (3.7), and (3.10) take the form

$$p = \frac{p_1 + p_2 n}{1 + n} \tag{3.4a}$$

$$T = \frac{T_1 + T_2 n}{1 + n} \tag{3.7a}$$

$$S = \frac{p_1 + p_2 n}{(1 + n) p_\omega (T)} \tag{3.10a}$$

The parameter n for maximum supersaturation is obtained from (3.13), and the coefficients A and B are calculated from (3.14) and (3.15). Since $a=b=1$, these equations can be written as

$$A = \frac{E(T_1 - T_2)(p_1 + p_2) - 2T_1T_2(p_1 - p_2)}{Ep_2(T_1 - T_2) - T_2^2(p_1 - p_2)} \tag{3.14b}$$

$$B = \frac{Ep_1(T_1 - T_2) - T_1^2(p_1 - p_2)}{Ep_2(T_1 - T_2) - T_2^2(p_1 - p_2)} \tag{3.15b}$$

If $p_2 = 0$ or negligible, we have

$$A = \frac{2T_1T_2 - E(T_1 - T_2)}{T_2^2} \tag{3.14c}$$

$$B = \frac{T_1^2 - E(T_1 - T_2)}{T_2^2} \tag{3.15c}$$

Substituting n in equation (3.10), we calculate the maximum supersaturation in the region of mixing. The magnitude of the maximum supersaturation depends on the vapor pressures in the mixing streams and on the temperatures of the components: the higher the temperature difference, the greater the maximum supersaturation.

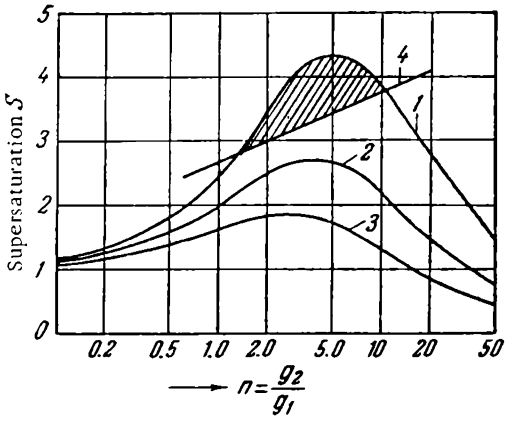

FIGURE 3.1. Supersaturation as a function of the mass ratio of the mixing gases for different temperatures of the cold gas:
1) $t_2 = 0°C$; 2) $t_2 = 10°C$; 3) $t_2 = 20°C$; 4) critical supersaturation.

Figure 3.1 plots the supersaturation as a function of the parameter n. These curves were calculated from equation (3.10) assuming constant

temperature and vapor pressure (water) for the first gas stream (air) ($t = 80\,°C$ and $p_1 = 355.1$ mm Hg) and putting 0, 10, and 20 °C for the temperature of the second gas stream (dry, vapor-free air).

Curve 4 (Figure 3.1) calculated from equation (1.61) corresponds to the critical vapor supersaturation, where the rate of nucleation cannot be ignored ($I \approx 1$).

The section of curve 1 between its intersection points with curve 4 is purely theoretical, since the corresponding state applies only if vapor does not condense spontaneously. In reality, the supersaturation in this region is higher than the critical value ($S > S_{cr}$), so that embryos form and the supersaturation falls below the values calculated from the preceding equations.

The results lead to a significant conclusion: if the composition of the mixing gases, their temperatures, and the vapor pressures are known, the probability of fog formation on mixing can be determined from equations (3.13) and (3.10) without going into complex calculations of local temperatures and concentrations. It should also be noted that in some cases the function $S = f(n)$ does not display a maximum. The parameter n normally varies from 0 to $+\infty$, and therefore if the two values of n calculated from (3.13) are negative, the function is without a maximum.

The validity of the above theoretical conclusions was confirmed by experiments with fog formation in a free jet /5, 6/. The hydrodynamics of jets permit a detailed study to be made of the influence of various factors on the formation of supersaturated vapor and fog in mixing gases.

A free jet is a high-speed stream of gas ejected from a pipe (a nozzle) into a stationary gas medium (Figure 3.2). Upon emerging from the nozzle, the gas stream creates a relative vacuum and the static gas is drawn into the jet, where the two gases are mixed. The velocity of the gas in the jet decreases with the distance from the nozzle, the moving gas increases in bulk, and the jet becomes broader.

Let T_1 stand for the temperature of the gas (or the gas mixture) in the jet, p_1 its vapor pressure, and S_1 the supersaturation. The jet is ejected into a gas medium having the temperature T_2, the vapor pressure p_2, and the supersaturation S_2.

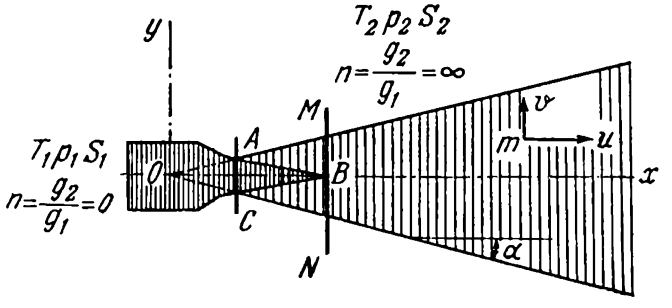

FIGURE 3.2. Schematic diagram of a jet.

In the initial section of the jet, from the orifice A—C to the plane through M—N, ABC is the central cone of constant flow velocities. The outer jet boundaries are straight lines diverging at an angle 2α from the pole O.

In the following, the origin of the coordinates is taken to coincide with the jet pole.

The central cone ABC has the thermodynamic parameters T_1, p_1, S_1 which are equal to the corresponding parameters of the initial gas stream issuing from the nozzle. For the original gas stream, the parameter n is zero, since the quantity of the foreign gas in the nozzle is zero. In the stationary gas medium, on the other hand, the parameter n is infinitely large, since the content of the primary gas there is zero. The parameter n thus varies from zero to infinity, running over all the positive values in the region of mixing between the jet boundaries.

The experiments were made with air jets containing water vapor. Water vapor or vapor-saturated air is injected into a cooler air mixture and a free jet is obtained. Given favorable conditions, fog will form in the region of mixing of the two gases. Having established the conditions corresponding to the incipient fog, one proceeds to calculate the critical supersaturation (i.e., the supersaturation for spontaneous vapor condensation) from the above equations.

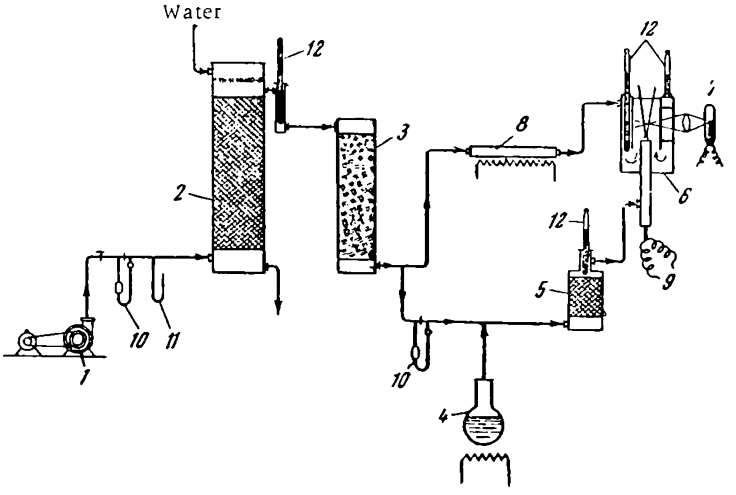

FIGURE 3.3. Schematic diagram of the laboratory setup:
1) air pump; 2) scrubbing tower; 3) filter; 4) boiling water flask; 5) spray trap; 6) mixing chamber; 7) point source; 8) gas heating and ionization; 9) thermocouple; 10) flowmeter; 11) pressure gage; 12) thermometer.

A schematic diagram of the laboratory setup is shown in Figure 3.3. Compressed air is forced through a spray scrubbing tower 2 and is then delivered to the filter 3 (absorbing cotton wool). The cleaned and filtered air is directed through two channels into the mixing chamber 6: this is a double-walled cylinder with a 100 mm bore and 250 mm height. The first stream ($V = 1.2\ m^3/hr$) is saturated with water vapor from a boiling water flask and issues from a 3.6 mm nozzle in the form of a jet. The second stream provides the medium into which the vapor-saturated jet is injected. The initial appearance of fog in the jet is detected with the aid of the Tyndall effect. The illumination of the mixing chamber is provided by a point source whose position can be changed at will.

The temperature of the mixture fed to the nozzle is maintained constant during each run. The initial temperature of the air into which the jet issues is high enough to preclude fog formation in the region of mixing; in this case the maximum of the supersaturation curve lies below the critical supersaturation line. The temperature of the air medium is gradually lowered until fog appears in the jet; the temperature of the air is noted. At this point, the maximum of the supersaturation curve will have risen to intersection with the critical supersaturation line (see Figure 3.1). The air temperature is then raised until the fog dissipates and the temperature is again noted. The average of the two temperature readings (visual appearance of fog and fog dissipation) is taken as the point of incipient fog.

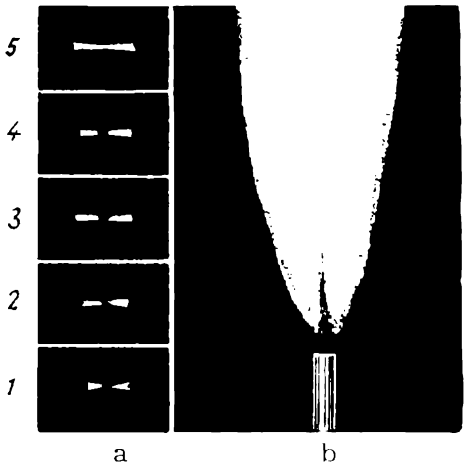

FIGURE 3.4. Fog zone in a free jet:
a—light beam at various distances from the nozzle: 1) 9 mm, 2) 15 mm, 3) 18 mm, 4) 30 mm, 5) 40 mm;
b—general aspect of the illuminated jet.

Figure 3.4a shows some photographs of the light beam in the jet at various distances from the nozzle. A bright luminous band is seen in the region of fog formation, and its width is indicatory of the width of the fog zone. Figure 3.4b is a general photograph of the illuminated jet; it is composed of several bands part of which are shown in Figure 3.4a.

In the first experiment (Table 3.1) the air was thoroughly cleaned by filtration and vapor therefore condensed on embryos which formed spontaneously due to pressure and temperature pulsations in the medium (homogeneous condensation). The parameter n was calculated from (3.13)

TABLE 3.1. Critical supersaturation of water and ethanol vapor determined by the mixing technique

Parameters	Water				Ethanol
	Runs				
	1	2	3	4	5
Air temperature (°C)					
in the nozzle t_1	99.2	70.6	88.8	99.7	52.5
in the medium t_2	21.2	38.3	51.0	58.3	16.2
Vapor pressure, mm Hg					
in the nozzle p_1	740	240	502	752	250
in the medium p_2	0	16	16.1	18.1	0
Total pressure P, mm Hg	740	737	737	752	747
Values of n for maximum supersaturation	5.8	0.75	0.72	0.70	0.47
Gas mixture temperature at maximum supersaturation, °C	41.2	58.3	74.2	88.9	42.7
Critical (maximum) supersaturation	2.72	1.09	1.07	1.05	1.025

for the point of incipient fog, the result was substituted in the supersaturation equation (3.10), and the maximum supersaturation was calculated (this figure was treated as the critical supersaturation). The details of the calculation are given below.

Details of calculation. Conversion coefficient to SI units:

$$1\ \text{mm Hg} = 133\ \text{N}\cdot\text{m}^{-2},\ 1\ \text{kcal} = 4.19\ \text{kJ}.$$

In run 1,

$$t_1 = 99.2\,^\circ\text{C},\ \text{or}\ T_1 = 372.3\,^\circ\text{K}$$
$$t_2 = 21.2\,^\circ\text{C},\ \text{or}\ T_2 = 294.3\,^\circ\text{K}$$
$$p_1 = 740\ \text{mm Hg}$$
$$p_2 = 0$$
$$P = 740\ \text{mm Hg}$$
$$c_n = c_2 = 0.241\ \text{cal/g}$$
$$c_v = c_1 = 0.482\ \text{cal/g}$$
$$M_1 = 18;\ M_2 = 29$$

From (3.6) and (3.3) we have

$$a = \frac{c_2}{c_1} = \frac{0.241}{0.482} = 0.5;\ b = \frac{M_1}{M_2} = \frac{18}{29} = 0.62$$

Taking 41 °C as the point of incipient fog (determined in preliminary calculations), we have $L = 574$ cal/g and from (1.4)

$$E = 0.12 \cdot 4.19 \cdot 18 \cdot 574 = 5190$$

Substituting in (3.14), (3.15), and (3.13), we find

$$A = \frac{5190\,(372.3 - 294.3)\,(740 + 0) - 2 \cdot 372.3 \cdot 294.3\,(740 - 0)}{5190 \cdot 0.62 \cdot 0\,(372.3 - 294.3) - 0.5 \cdot 294.3^2\,(740 - 0)} = -4.3$$

$$B = \frac{5190 \cdot 0.5 \cdot 740\,(372.3 - 294.3) - 0.62 \cdot 372.3^2\,(740 - 0)}{0.5 \cdot 0.62\,[5190 \cdot 0.62 \cdot 0\,(372.3 - 294.3) - 0.5 \cdot 194.3^2\,(740 - 0)]} = -8.7$$

$$n = \frac{4.3}{2} \pm \sqrt{\frac{4.3^2}{4} + 8.7} = 5.8$$

The temperature of the gas mixture at maximum supersaturation is found from (3.7):

$$T = \frac{T_1 + T_2 an}{1 + an} = \frac{372.3 + 294.3 \cdot 0.5 \cdot 5.8}{1 + 0.5 \cdot 5.8} = 314.3\,^\circ\text{K}\ \ (t = 41.2\,^\circ\text{C})$$

At this temperature, the saturated vapor pressure of water is $p_\infty = 59$ mm Hg. S_{max} is obtained from (3.10):

$$S_{max} = \frac{740}{(1 + 0.621 \cdot 5.8)\,59} = 2.72$$

Making the calculations according to (1.61) and (1.62), we find $S_{cr} = 2.77$ at 41.2 °C, i.e., equation (3.10) is consistent with the experimental findings.

In other runs the cleaned and filtered air was brought in contact with an incandescent platinum filament or magnesium oxide before being delivered into the mixing chamber /7/. The air was thus enriched in minute charged particles (condensation nuclei) on which the vapor actually condensed. In runs 2—5 (see Table 3.1) the supersaturation was nearly unity, and the preceding equations are seen to provide a satisfactory approximation to the true state of things.

In run 2,

$$t_1 = 70.6\,^{\circ}\text{C}, \text{ or } T_1 = 343.7\,^{\circ}\text{K}$$
$$t_2 = 38.3\,^{\circ}\text{C}, \text{ or } T_2 = 311.4\,^{\circ}\text{K}$$
$$p_1 = 239.7 \text{ mm Hg}$$
$$p_2 = 16.0 \text{ mm Hg}$$
$$P = 737 \text{ mm Hg}$$
$$c_n = 0.241 \text{ cal/g}$$
$$c_v = 0.482 \text{ cal/g}$$
$$M_n = 29;\ M_v = 18$$

From (3.9), (3.3), (3.8), and (3.6) we find

$$M_1 = 29 + \frac{239.7}{737}(18 - 29) = 25.42$$

$$M_2 = 29 + \frac{16}{737}(18 - 29) = 28.76$$

$$\frac{M_1}{M_2} = \frac{25.42}{28.76} = 0.885$$

$$c_1 = \frac{29 \cdot 0.241}{25.42} + \frac{239.7}{737 \cdot 25.42} = (18 \cdot 0.482 - 29 \cdot 0.241) = 0.295 \text{ cal/g}$$

$$c_2 = \frac{29 \cdot 0.241}{28.76} + \frac{16}{737 \cdot 28.76}(18 \cdot 0.482 - 29 \cdot 0.241) = 0.244 \text{ cal/g}$$

$$a = \frac{0.244}{0.295} = 0.827$$

We assume that fog starts forming at $t = 58$ °C (the point of incipient fog is again determined in preliminary calculations). Then $L = 564$ cal/g and from (1.4) we have

$$E = 0.12 \cdot 4.19 \cdot 18 \cdot 564 = 5100$$

Substituting in (3.14), (3.15), and (3.13), we find

$$A = 0.356;\ B = -0.822;\ n = 0.75$$

The temperature of the gas mixture at maximum supersaturation according to (3.7) is

$$T = \frac{343.7 + 311.4 \cdot 0.827 \cdot 0.75}{1 + 0.827 \cdot 0.75} = 331.4\,^{\circ}\text{K or } t = 58.3\,^{\circ}\text{C}$$

The saturated vapor pressure at this temperature is $p_\infty = 138$ mm Hg. From (3.10) we now find

$$S_{max} = \frac{239.7 + 16 \cdot 0.885 \cdot 0.75}{(1 + 0.885 \cdot 0.75)\,138} = 1.09$$

We see from Table 3.1 that in all cases (with the exception of run 1) fog formation starts at supersaturations slightly higher than unity (this is reasonable, since vapor condenses on suspended charged particles). The excess supersaturation can be attributed to the finite time of growth of the condensation nuclei: in regions of maximum supersaturation (when vapor condenses on the nuclei) the flow rates along and across the jet are comparatively high and the condensation nuclei take some time to grow to the size of fog droplets creating a noticeable optical effect. For fog to form, the gas mixture should remain for a certain time in the region of maximum supersaturation, and the zone of fog formation should therefore have a finite thickness. As the sensitivity of the optical detector is increased, the measurements yield progressively lower values of S_{max}. *

The above data on the formation of supersaturated vapor in mixing gases and the working formulas derived in the preceding are consistent with the findings of other authors /9, 10, 11/.

Experimental data on the limiting conditions of glycerine fog formation were obtained by Levine and Friedlander /9/ who used a setup not unlike the one shown in Figure 3.3. A free jet of dust-free gas-air mixture with glycerine vapor is injected into a colder air. Fog formation is detected by examining the content of fog droplets in a gas sample withdrawn from the jet and by visual observations. The effect of ions on fog formation is established by passing the gas mixture through a discharge tube.

The experimental findings indicate that fog formation in a jet occurs at a higher supersaturation than the calculated figures. Other conditions being constant, the fog cloud observed in the jet receded from the orifice as the flow velocity increased and dissipated completely at high velocities.

Taking $a=b=1$ and assuming that no condensation occurred, the authors derived the following equations:

$$\frac{C-C_2}{C_1-C_2} = \frac{T-T_2}{T_1-T_2} \qquad \text{(a)}$$

$$S_{max} = \frac{T_{max}-T_2}{T_1-T_1} \cdot \frac{C_{max}}{e^{E\left(\frac{1}{T_b}-\frac{1}{T_{max}}\right)}} \qquad \text{(b)}$$

where C_1, C_2, C, C_{max} are the mass concentrations of the vapor in the nozzle, in the gas medium, in the jet, and in region of maximum supersaturation (in g per kg of mixture); T_1, T_2, T, T_{max} are the corresponding absolute temperatures; S_{max} the maximum supersaturation in the jet; T_b the boiling

* The above concepts and equations are also valid for the various phenomena occurring when solutions of liquid or solid substances are mixed. Heat and mass transfer in this mixing can be similarly balanced. The solution temperature and the solute concentration after mixing are then expressed by equations (3.4) and (3.7) with concentrations substituted for pressures. The solubilities of numerous substances are likewise determined by equation (1.2) /8/. Equations (3.10) and (3.13) can thus be applied to determine the supersaturation of a solute when two solutions having different temperatures are mixed and to establish the conditions for maximum supersaturation.

point of the liquid at the total pressure of the system; E a coefficient defined by equation (1.4).

For the above conditions ($a=b=1$), equation (a) can be derived from (3.4) and (3.9) (see equation (3.40)), and equation (b) is analogous to (3.10) if we remember that

$$\frac{T_{max}-T_2}{T_1-T_2}=\frac{1}{1+n_{max}}$$

where n_{max} is a coefficient representing the quantitative ratio of the mixing gases at maximum supersaturation (equation (3.1)).

Interesting experimental studies of the nucleation rates in a jet /10/ were carried out on a setup like the one shown in Figure 3.3. A vapor-gas jet was mixed with a cold air under conditions ensuring fog formation. The number density of fog droplets was determined in the emerging stream. The experimental findings were compared with the results obtained by hydrodynamic jet calculations. The authors arrived at a satisfactory agreement of the theory with experiment for dibutyl phthalate only; for the other liquids the two sets of data displayed considerable divergence (see Table 3.5). One of the reasons for this was apparently the considerable variation of the supersaturation along the x and y axes of the jet, which made impossible precise determination of the nucleation rate and the number density of fog droplets.

Some results of laboratory experiments with fog formation in a free jet are also presented in /11/. The effect of temperature and vapor concentration on the limits of fog formation upon mixing of glycerine and dibutyl phthalate vapors with air was established photographically and by visual observations. The results were compared with theoretical findings. The point of incipient fog was determined by introducing solid bodies into the jet and injecting foreign particles into the region of mixing.

FUNDAMENTAL PROPERTIES OF TURBULENT JETS

Fog formation in a jet is frequently observed in practice; knowledge of the flow velocity of the gas, the temperature, the vapor pressure, and the supersaturation is therefore often required for various sections of the jet.

Let u and v be the longitudinal and the transverse velocity components at some point m in the jet (see Figure 3.2); the flow velocity along the x axis is always positive, while the velocity along the y axis is positive near the jet axis and negative near the jet boundary. The ambient gas is thus inducted into the jet and mixing occurs.

Various experimental works have established that the dimensionless flow velocity in the jet retains a constant value and it can be represented by the equation

$$\frac{u}{u_m}=f\left(\frac{y}{x}\right) \qquad (3.16)$$

where u is the flow velocity at some point in the jet; u_m the flow velocity on the jet axis; y the ordinate of the point, i.e., its distance from the jet axis; x the abscissa of the point, i.e., its distance from the pole.

The flow velocity on the axis of a circular jet is a function of the distance from the pole only:

$$u_m = \frac{\text{const}}{x}$$

Inserting this expression in (3.16) we obtain a general equation for the flow velocity in the principal section of a circular jet:

$$u = \frac{\text{const}}{x} f\left(\frac{y}{x}\right) \tag{3.17}$$

Making use of the theory of an eddy source, Abramovich /12/ derived the dependence $f\left(\frac{y}{x}\right)$ and obtained the following equation for the axial flow velocity in the main section of a circular jet:

$$\frac{u_m}{u_1} = \frac{0.96}{\frac{a' x}{r}} \tag{3.18}$$

where u_1 is the nozzle velocity; a' an experimental constant; r the initial radius of the jet (the nozzle radius).

For circular jets, $a' \sim 0.07 - 0.08$. In the transition plane $M-M$, where the principal section starts, the axial flow velocity is equal to the mean efflux velocity

$$\frac{u_m}{u_1} = 1$$

and therefore

$$x_0 = \frac{0.96 r}{a'} \tag{3.19}$$

where x_0 is the abscissa of the principal section.

The equations for the flow velocity in any section along the jet or in the radial direction have the form

$$\frac{u}{u_m} = \frac{F'(\varphi)}{\varphi}$$

$$\frac{v}{a' u_m} = \left[F'(\varphi) - \frac{F(\varphi)}{\varphi}\right]$$

where u is the flow velocity along the x axis; v the radial velocity, i.e., flow velocity along the y axis; φ a nondimensional variable,

$$\varphi = \frac{y}{a' x} \tag{3.20}$$

The solution of these equations is presented in Table 3.2.

At the jet boundary, $\varphi_b = 3.4$ (see Table 3.2), and from (3.20) we therefore have

$$\frac{y}{x} = \varphi_b a' = \operatorname{tg} \alpha = 3.4\, a' \tag{3.21}$$

In the initial section, the lines of equal velocity (isotachs) are straight lines issuing from the nozzle perimeter and terminating in the transition plane; the velocity distribution over the transition cross section can be calculated from the figures of Table 3.2.

TABLE 3.2. Flow velocity, temperature, and concentration for various φ

ψ	$\frac{u}{u_m} = \frac{F1(\varphi)}{\varphi}$	$\frac{v}{a' u_m}$	$\frac{\Delta T}{\Delta T_m} = \frac{\Delta C}{\Delta C_m} = \sqrt{\frac{u}{u_m}}$
0	1	0	1
0.2	0 958	0.100	0.979
0.4	0.884	0.174	0.941
0.6	0.725	0.220	0.892
0.8	0.700	0.240	0 837
1.0	0.606	0.225	0.779
1.2	0.510	0.190	0.714
1.4	0.425	0.140	0.652
1.6	0.340	0 080	0.583
1.8	0.265	0	0.515
2.0	0.198	—0.066	0 445
2.2	0.140	—0.140	0 374
2.4	0.094	—0.219	0.307
2.6	0.059	—0.270	0.243
2.8	0.034	—0.310	0.185
3.0	0.017	—0.334	0.131
3.2	0.007	—0.345	0.085
3.4	0.000	—0.335	0.000

The relation of vapor concentration and temperature across the jet to the vapor concentration and temperature along the axis is given by the equations

$$\frac{\Delta T}{\Delta T_m} = \frac{\Delta C}{\Delta C_m} = \sqrt{\frac{u}{u_m}} \tag{3.22}$$

$$\frac{\Delta T_m}{\Delta T_1} = \frac{\Delta C_m}{\Delta C_1} = \frac{0.7}{\frac{a' x}{r}} \tag{3.23}$$

whence

$$\frac{\Delta T}{\Delta T_1} = \frac{\Delta C}{\Delta C_1} = \frac{0.7}{\frac{a' x}{r}} \sqrt{\frac{u}{u_m}} \tag{3.24}$$

In these equations

$$\Delta T = T - T_2 \tag{3.25}$$

$$\Delta T_m = T_m - T_2 \tag{3.26}$$

$$\Delta T_1 = T_1 - T_2 \tag{3.27}$$

$$\Delta C = C - C_2 \tag{3.28}$$

$$\Delta C_m = C_m - C_2 \tag{3.29}$$

$$\Delta C_1 = C_1 - C_2 \tag{3.30}$$

where T_1, T_2, T, T_m are the absolute temperatures of the gas in the nozzle, the gas around the jet, the gas mixture in the jet, and the gas mixture

on the jet axis; C_1, C_2, C, C_m are the corresponding mass concentrations of the vapor (in g per kg of mixture).

At the inlet of the principal section (M—N)

$$\frac{\Delta T_m}{\Delta T_1} = \frac{\Delta C_m}{\Delta C_1} = 1$$

and therefore

$$x_0 = \frac{0.7r}{a'} \tag{3.31}$$

Comparison of equations (3.19) and (3.31) shows that in terms of temperature and concentration distribution the principal section is closer to the nozzle than the corresponding velocity profile.

The last column of Table 3.2 lists some figures which can be used for calculating temperatures and concentrations from flow velocities (equation 3.22).

To establish the supersaturation in various sections of the jet, we have to change over from mass concentration to vapor pressure in mm Hg. The mass concentration of vapor in g per kg of mixture can be written as

$$C = \frac{g_v \cdot 10^3}{g_n + g_v}$$

or

$$C = \frac{p M_v \cdot 10^3}{P\left[M_n + \frac{p}{P}(M_v - M_n)\right]} \tag{3.32}$$

where g_v and g_n are the masses of the vapor and the noncondensing gas, kg; p is the vapor pressure in the gas mixture, mm Hg; P the total pressure; M_v and M_n the molecular weights of the vapor phase and the noncondensing gas. Making use of (3.9), we write (3.32) in the form

$$C = \frac{pM_v \cdot 10^3}{PM} \tag{3.33}$$

where M is the molecular weight of the gas mixture.

Dividing through equation (3.28) by equation (3.30) and inserting C from (3.33) we find

$$\frac{\Delta C}{\Delta C_1} = \left[\frac{pM_v \cdot 10^3}{PM} - C_2\right] : \left[C_1 - C_2\right]$$

whence

$$\frac{pM_v \cdot 10^3}{PM} = \frac{\Delta C}{\Delta C_1}(C_1 - C_2) + C_2 \tag{3.34}$$

From (3.25) and (3.27) we have

$$\frac{\Delta T}{\Delta T_1} = \frac{T - T_2}{T_1 - T_2} \tag{3.35}$$

and hence

$$T = \frac{\Delta T}{\Delta T_1}(T_1 - T_2) + T_2 \tag{3.36}$$

Once the vapor pressure and temperature have been determined from (3.34) and (3.36), we can easily find the supersaturation in various sections of the jet.

The mixing formulas and the relations derived from jet hydrodynamics /12, 13/ are in reciprocal correspondence. This suggestion is confirmed by the following considerations: from (3.4) we have

$$p - p_2 = \frac{p_1 + p_2 bn}{1 + bn} - p_2$$

or

$$\frac{p - p_2}{p_1 - p_2} = \frac{\Delta p}{\Delta p_1} = \frac{1}{1 + bn} \tag{3.37}$$

Making use of (3.9), (3.28), (3.30), and (3.33), we find from (3.37)

$$\frac{\Delta C}{\Delta C_1} = \frac{M_1}{M} \cdot \frac{\Delta p}{\Delta p_1} = \frac{M_1}{M} \cdot \frac{1}{1 + bn} \tag{3.38}$$

From (3.7), (3.25), and (3.27) we similarly find

$$\frac{\Delta T}{\Delta T_1} = \frac{1}{1 + an} \tag{3.39}$$

The left-hand sides of equations (3.38) and (3.39) are equal to each other according to Abramovich's data; the right-hand sides, however, are equal only if Abramovich's assumption /12, 13/ is satisfied:

$$a = \frac{c_2}{c_1} = 1 \quad \text{and} \quad b = \frac{M_1}{M_2} = 1$$

In this case

$$\frac{\Delta T}{\Delta T_1} = \frac{\Delta C}{\Delta C_1} = \frac{1}{1 + n} \tag{3.40}$$

The equations of mixing thus fully correspond to Abramovich's analytical equations; they moreover complement these equations in cases when the mixing gas streams have different specific heats and molecular weights.

From (3.38) and (3.39) we have

$$\frac{M_1}{M} \cdot \frac{1}{1 + bn} = \frac{1}{1 + an} \tag{3.41}$$

Tables 3.3 and 3.4, together with Figures 3.5, 3.6, and 3.7, represent the results of the calculations of the temperature t, the vapor pressure p, the flow velocities u (along the x axis) and v (along the y axis), and the supersaturation S for the cross sections M—N (the initial section), K—L (the section where the supersaturation along the x axis is maximal), and P—Q distant 16.8, 28, and 42 mm from the jet pole; the axial variation of the

parameters in application to run 2 (see Table 3.1) is also listed. These data are presented in order to give some idea of the jet field in various sections. The calculations have been made for the following constants: $r = 1.8$ mm, flow rate of humid air at 70.6 °C 1.87 m^3/hr, $a' = 0.075$, $a = \frac{c_2}{c_1} = 1$, $b = \frac{M_1}{M_2} = 1$, $\frac{\Delta C}{\Delta C_1} = \frac{\Delta p}{\Delta p_1}$; the other parameters are listed in Table 3.1.

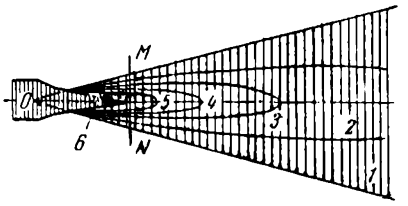

FIGURE 3.5. Isolines in the jet: 1) jet boundary, $n=\infty$; 2) $n = 4$; 3) $n = 1.5$; 4) $n = 0.67$; 5) $n = 0.25$; 6) central cone, $n = 0$.

TABLE 3.3. The values of p, t, S in the jet for run 2 (see Table 3.1)

$\frac{\Delta p}{\Delta p_1} = \frac{\Delta T}{\Delta T_1}$	$n = \frac{g_2}{g_1}$	Temperature of gas mixture, °C	Vapor pressure in gas mixture p		Saturated vapor pressure of water p_∞		Supersaturation S	Curves in Figure 3.5
			N·m^{-2}	mm Hg	N·m^{-2}	mm Hg		
0	∞	38.3	$2.1 \cdot 10^3$	16	$6.8 \cdot 10^3$	51	0.32	1
0.2	4	44.8	$8.1 \cdot 10^3$	61	$9.5 \cdot 10^3$	71	0.85	2
0.4	1.5	51.2	$1.4 \cdot 10^4$	106	$1.3 \cdot 10^4$	97	1.10	3
0.6	0.67	57.7	$2.0 \cdot 10^4$	150	$1.9 \cdot 10^4$	134	1.12	4
0.7	0.43	60.9	$2.3 \cdot 10^4$	173	$2.1 \cdot 10^4$	156	1.11	—
0.8	0.25	64.1	$2.6 \cdot 10^4$	195	$2.4 \cdot 10^4$	180	1.08	5
1.0	0	70.6	$3.2 \cdot 10^4$	240	$3.2 \cdot 10^4$	240	1.00	6

TABLE 3.4. Supersaturation of water vapor and flow rates for various jet sections

$\frac{\Delta p}{\Delta p_1} = \frac{\Delta T}{\Delta T_1} = \frac{1}{1+an}$	Section $M-N$, $x = 16.8$ mm		Section $K-L$, $x = 28$ mm				Section $P-O$, $x = 42$ mm			
	Distance from jet axis y, mm	Supersaturation S	Distance from jet axis y, mm	Supersaturation S	Velocity, m/sec		Distance from jet axis y, mm	Supersaturation S	Velocity, m/sec	
					u	v			u	v
0	4.3	0.32	7.1	0.32	0	−1.05	10.7	0.32	0	−0.7
0.2	3.5	0.85	5.0	0.85	4.5	−0.63	5.8	0.85	7.0	−0.03
0.4	2.7	1.10	2.8	1.10	19.7	+0.50	0	1.10	28.0	0
0.6	2.0	1.12	0	1.12	42.0	0	—	—	—	—
0.8	1.2	1.08	—	—	—	—	—	—	—	—
1.0	0	1.00	—	—	—	—	—	—	—	—

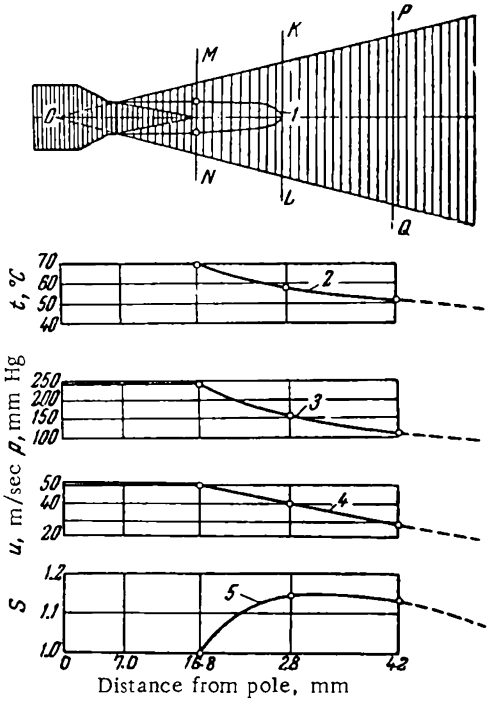

FIGURE 3.6. Axial values of t, p, u, and S: 1) maximum supersaturation in the jet; 2) temperature; 3) vapor pressure; 4) axial velocity; 5) supersaturation.

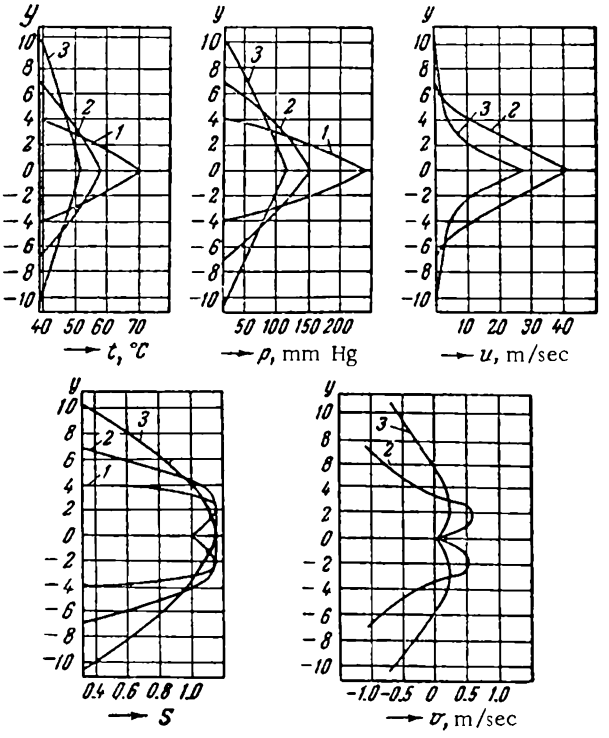

FIGURE 3.7. Values of t, p, u, v, and S in various jet sections: 1) M–N; 2) K–L; 3) P–Q.

The values 0 and 1 of the ratio $\Delta p/\Delta p_1 = \Delta T/\Delta T_1$ in Table 3.3 and Figure 3.5 correspond to the gas mixture outside the jet bounds (designated by the subscript 2) and to the gas mixture just emerging from the nozzle (subscript 1). For $\Delta p/\Delta p_1 = \Delta T/\Delta T_1 = 0.2$, we have from (3.40) $n = 4$. Inserting the results in (3.41) and (3.42), we find $t = 44.8$ °C and $p = 61$ mm Hg.

The axial values of t and p plotted in Figure 3.6 were calculated from equation (3.23); the flow velocity u was calculated from equation (3.18).

The parameters listed in Table 3.4 (and used in the construction of the curves in Figure 3.7) were calculated from equation (3.20) with the aid of the data from Table 3.2. For the section $M—N$ ($x = 28$ mm), taking $\Delta T/\Delta T_1 = 0.2$, we find from (3.24)

$$\sqrt{\frac{\overline{u}}{u_m}} = \frac{\Delta T}{\Delta T_1} \cdot \frac{a'x}{0.7r} = \frac{0.2 \cdot 0\ 075 \cdot 28}{0.7 \cdot 1.8} = 0.333$$

For this value we have from Table 3.2 $\varphi = 2.35$. Inserting the numerical results in (3.20), we find

$$y = \varphi a' x = 2.35 \cdot 0.075 \cdot 28 = 5.0$$

The axial flow velocity u_m is calculated from (3.18); then making use of the result $\sqrt{\frac{\overline{u}}{u_m}} = 0.333$ ($\frac{u}{u_m} = 0.110$) and taking $\frac{v}{a'u_m} = -0.18$ (Table 3.2), we find the velocities u and v.

We see from Figure 3.5 that the isolines in the jet field issue from the nozzle perimeter and close on the jet axis. Along the axis (Figure 3.6) the jet parameters vary smoothly starting at the initial section $M—N$, with the exception of the supersaturation S which first rises to a maximum and then subsides.

The temperature, vapor pressure, and flow velocity in the various jet sections all follow the same general trend (Figure 3.7): these parameters fall off uniformly from the jet axis to the wall. The magnitude of these parameters also decreases along the axis with the distance from the jet pole (see Figure 3.6).

The supersaturation has a maximum along the jet axis and in each cross section; between sections $M—N$ and $K—L$ there are even two maxima. Curve 1 (see Figure 3.6) specifies the position of the maximum supersaturation in the jet.

The variation of the flow velocity along the y axis is approximately the same in all sections. The transverse velocity is zero on the jet axis; it rises to a maximum somewhere along the jet radius and falls off to negative values at the boundary.

The above considerations apply to turbulent jets, where the mixing is governed by eddy diffusion and eddy heat conduction. Some results indicate /10/ that these conditions are observed for $\mathrm{Re} \geqslant 3000$ (in calculating Re, the nozzle diameter d is taken equal to $2r$). Fog obviously forms first in those points where the supersaturation is maximal (the region inside curve 1 in Figure 3.6); the region of maximum supersaturation in a jet generates a surface and a luminous cone of fog is thus seen in visual observations.

If a pure vapor or a vapor-containing gas mixture ($S \leqslant 1$) is fed into the nozzle, supersaturated vapor will form in the jet only if the supersaturation curve across the jet has a maximum. The region of supersaturated vapor is then limited by two curves of zero supersaturation. The position of these curves can be found from (3.10):

$$S = 1 = \frac{p_1 + p_2 bn}{(1 + bn)\exp\left(c - \frac{E}{T}\right)} \tag{3.42}$$

whence

$$\frac{p_1 + p_2 bn}{1 + bn} = \exp\left(c - \frac{E}{T}\right) \tag{3.43}$$

For given T_1, T_2, p_1, p_2, this equation yields two values of the parameter n; once these values have been found, the position of the curves enclosing the region of supersaturated vapor can be easily established.

It follows from the preceding that the maximum supersaturation in the jet is independent of the nozzle velocity, i.e., of the gas flow rate; it depends only on the temperature and the vapor pressure of the mixing streams. The flow velocity along the x and y axes in different sections varies in proportion to the nozzle velocity, since the experimental constant a' is independent of the Reynolds number. Increasing the nozzle velocity, however, has no effect on the parameters $\Delta C/\Delta C_1$, $\Delta T/\Delta T_1$, and n throughout the jet.

DROP SIZE DISTRIBUTION AND NUMBER DENSITY

The properties of turbulent jets discussed in the previous section apply for $S < S_{cr}$. It follows from the above that the flow velocity u, the gas temperature T, the vapor pressure p, and the supersaturation S at any point of the jet are functions of position, i.e., of the coordinates x and y:

$$u = u_1 f(x, y) \quad \text{(a)}$$
$$T = T_1 \varphi(x, y) \quad \text{(b)}$$
$$p = p_1 \Phi(x, y) \quad \text{(c)}$$
$$S = F(x, y) \quad \text{(d)}$$

where u_1, u are the nozzle and jet velocities; T_1, T, the nozzle and jet temperatures; p_1, p the nozzle and jet pressures.

The parameters u, T, p, and S are mutually independent. However, for $S > S_{cr}$, T and p (and therefore S also) are affected not only by the parameter n, but also by spontaneous vapor condensation. As u increases, the embryos and the droplets move progressively faster through the supersaturated region and the condensational growth of drops correspondingly decreases. The process thus shifts in the direction of nucleation, i.e., toward higher N and smaller r. For $S > S_{cr}$ the right-hand sides of equations (b), (c), and (d) above are thus functions of the nozzle velocity u_1, as well as the coordinates x and y. It follows from the preceding that, other

conditions being constant, an increase in u_1 raises the supersaturation, reduces the average droplet radius, and increases the number density of the fog.

Curve 1 in Figure 3.8 plots the supersaturation as a function of n neglecting the formation of embryos (see Figure 3.1, curve 1); curves 2 and 3 represent the same function with nucleation. The higher the nozzle velocity u_1, the greater the derivative $dS/d\tau$ and the higher the maximum supersaturation, the dispersity, and the number density of the fog.

Since $dS/d\tau$ increases with u_1, in some cases it is convenient to change over from u_1 to $dS/d\tau$, writing the general functional relations for the droplet radius and the number density in the following form:

$$\bar{r} = f\left(\frac{dS}{d\tau}\right) \tag{1.91}$$

$$N = \varphi\left(\frac{dS}{d\tau}\right) \tag{1.92}$$

Polydisperse fog always forms in the jet, since different supersaturations obtain in different sections. A droplet remains a progressively shorter time in the zone of supersaturated vapor as the nozzle velocity is increased; the terminal radius of the droplets correspondingly diminishes. This is also confirmed by experimental data /14, 15/.

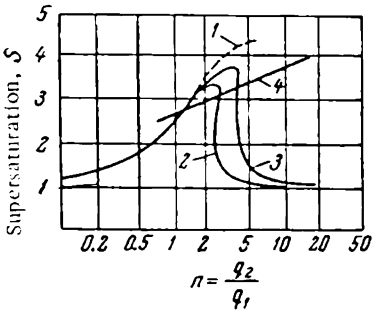

FIGURE 3.8. Supersaturation as a function of the mass ratio of the mixing gases for various nozzle velocities:
1) calculated ignoring nucleation; 2, 3) calculated with nucleation at velocities u_1' and u_1'' ($u_1'' > u_1'$); 4) critical supersaturation.

Taking account of all the factors which govern the process of fog formation by turbulent mixing (hydrodynamic factors, rates of nucleation and condensational growth of droplets, coalescence, pollution with condensation nuclei, etc.), we can calculate the droplet radius and the number density of the fog. This is actually confirmed by the results of experimental studies /10/ carried out on a setup like that shown in Figure 3.3. In these experiments a vapor-gas jet was mixed with colder air under conditions favoring fog formation. The number density of the fog was determined in the emerging stream. The experimental findings were compared with the rates of nucleation and condensational growth calculated from the hydrodynamics of free jets. The theoretical data for dibutyl phthalate were found to fit the experimental results (p. 26). This indicates that the calculated and the actual values of S in the field of a jet are sufficiently close to each other.

The supersaturation has a decisive influence on the rate of nucleation, and even a slight error in S is magnified to considerable proportions as far as the accuracy of number density is concerned. Inaccuracies in supersaturation in the jet are apparently one of the principal reasons for the discrepancies between the experiment and the theory in various cases (see Table 3.5).

The mass concentration of the fog which forms when vapor-gas streams are mixed can be approximately determined from (1.87), if S is inserted from (3.10):

$$G = \frac{M}{RT}\left[\frac{p_1 + p_2 bn}{1 + bn} - p_\infty(T)\right] \tag{3.44}$$

An analysis of equation (3.44) shows that the maximum mass concentration of fog can be achieved for n values which differ from those corresponding to maximum supersaturation. The derivative of $G=f(n)$ from (3.44) is expressed by a complicated equation which is difficult to use in applied calculations of maxima. However, if the temperature in the denominator in the right-hand side of (3.44) is taken equal to a constant value $T_{av} = \frac{T_1+T_2}{2}$ (which is permissible if the difference between T_1 and T_2 is small), the parameter n for the maximum mass concentration of the fog G_{max} is obtained from the equation

$$\frac{Eap_\infty(T_{av})(T_1 - T_2)}{b(p_1 - p_2)} = \left(\frac{T_1 + T_2 an}{1 + bn}\right)^2 \tag{3.45}$$

A more accurate value of n corresponding to G_{max} can be found by graphical methods or by the method of successive approximations, which also yields the temperature at which G_{max} is attained. In the zeroth approximation, the value of n calculated for T_{av} is substituted in equation (3.7) and the temperature T is found; the result is then used to find $p_\infty(T)$. Equation (3.45) is applied to calculate the next approximation to n. If the result is substantially different from the n calculated from T_{av}, the procedure is repeated.

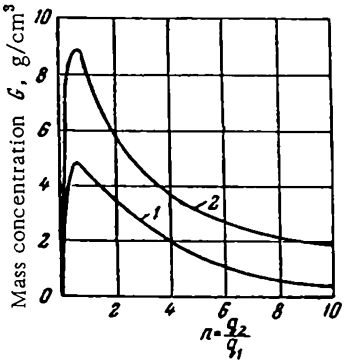

FIGURE 3.9. Mass concentration of fog as a function of the mass ratio of the mixing gases at different temperatures of the colder gas: 1) $T_2 = 253°K$; 2) $T_2 = 223°K$.

Figure 3.9 shows the results obtained for the mass concentration of the fog which forms when water-saturated air ($T_1 = 293°K$, $p_1 = 17.54$ mm Hg) is mixed with dry air ($p_2 = 0$) at $T_2 = 223$ and $253°K$. We see from the figure that G increases as T_2 decreases. At $T_2 = 223°K$ the maximum mass concentration is attained for $n = 0.54$ and is equal to $G_{max} = 8.9\ g/m^3$. The maximum supersaturation of vapor under these conditions is attained for $n = 5.7$.

RATE OF NUCLEATION AND RATE OF GROWTH OF DROPLETS IN A JET

Although the process of nucleation of a new phase is of obvious scientific interest, no reliable experimental data are available at present for direct determination of the rates of formation of embryos in homogeneous condensation.

The preceding data on fog formation in a turbulent jet can be applied for the determination of nucleation rates and of the rates of growth of droplets in supersaturated vapor. In experiments with critical supersaturation of water /4, 5/ and glycerine /9/ vapors in a free jet, fog was observed at some distance from the nozzle (see Figure 3.4). On the other hand, it follows from the hydrodynamics of free jets /12, 13/ that mixing occurs in the initial section also. The line of maximum supersaturation also issues from the nozzle (see Figure 3.6, curve 1). The absence of fog in the initial section despite the adequate supersaturation (as is evident from the formation of fog in the principal section) is attributable to the high flow velocities along the x and y axes near the orifice. The flow velocities being high, the vapor-gas mixture does not remain in the region of maximum supersaturation long enough for embryos to form and subsequently to grow to visible droplets.

The available results are sufficient for calculating the fields of temperature, concentration, and supersaturation in the jet and the flow velocities in the initial and the principal sections. The distance from the nozzle to the trailing fog line, the radius of fog droplets, and the number density of the fog in the jet can be determined experimentally. Comparison of theoretical and experimental findings provides an adequate test for the evaluation of the various relations used in the calculation of nucleation rates, evaporation and condensation rates, and rates of other concurrent processes.

The first attempt to determine the rates of nucleation in a turbulent jet is due to Higuchi and Konski /10/). The experimental number densities of the fog forming in a jet were compared with the results of calculations based on the hydrodynamics of jets and the theoretical formulas proposed for the determination of nucleation rates. The experiments were made with four compounds: dibutyl phthalate, triethyleneglycol, octadecane, and sulfur.

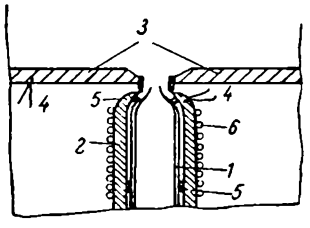

FIGURE 3.10. Nozzle and lower part of the mixing chamber:
1) glass nozzle; 2) copper tube; 3) copper bottom of mixing chamber; 4) thermocouple; 5) thermally insulated Teflon seal; 6) chromel winding (heater).

The mixing chamber used by the authors (Figure 3.10) is designed along the same lines as the setup shown in Figure 3.3. The carrier gas (nitrogen) and the gas into which the jet is injected (air) are filtered through two layers of asbestos paper and dried. The gases are heated, nitrogen is saturated with the vapor, and mixing is allowed to occur in the chamber 6 (see Figure 3.3). Special measures are taken to eliminate heat losses and to ensure high-precision measurements of the gas temperature. The nozzle 1 (Figure 3.10) is housed in a copper pipe 2, which is maintained at the same temperature as the gas; the temperature of the copper bottom in the mixing chamber 3 is equal

to the temperature of the gas into which the jet is injected. Joints between differently heated components are protected by thermally insulated Teflon seals 5.

The number density of the fog (and thus the number of forming embryos) is determined by measuring the scattering of light with a special instrument. The experimental data on number densities are reduced by graphical methods and the rates of nucleation are determined for each run. The surface tension σ is then computed from equations (1.53) and (1.60) and the results are compared with tabulated figures.

As we have previously remarked, dibutyl phthalate was the only substance which ensured a satisfactory agreement of the theory with the experiment, and this compound was therefore studied most intensively. For other substances the divergence between the theoretical and the experimental data was very substantial; the discrepancies were particularly pronounced in the case of the nucleation rates calculated from the experimental and the tabulated values of surface tension (the ratios of these nucleation rates are given in the last column in Table 3.5).

TABLE 3.5. Rates of nucleation in a jet /10/

Compound	Surface tension, dyne/cm		Ratio of nucleation rates I_{exp}/I_{table}
	experimental σ_{exp}	tabulated σ_{table}	
Dibutyl phthalate . .	28.8	29.4	15
Triethyleneglycol . .	36.8	42.8	$2.3 \cdot 10^{9}$
Octadecane	24	26.1	$2.8 \cdot 10^{5}$
Sulfur	54	67.6	$2.4 \cdot 10^{15}$

We have already noted that one of the reasons for these discrepancies is apparently the considerable variation of the supersaturation along the x and y axes in the jet (Figures 3.5 and 3.6), which makes accurate and reproducible measurements of nucleation rates and number densities nearly impossible.

The rate of growth of the droplets can also be measured using the setup schematically shown in Figure 4.1 (p. 94). Supersaturated vapor is formed between wetted plates which are maintained at different temperatures. The supersaturation results in spontaneous vapor condensation and formation of liquid droplets. The number of forming droplets depends on the degree of supersaturation, i. e., on the temperature difference between the plates. By varying the temperature of the plates, one adjusts the supersaturation to a value when the number of droplets can be counted, and the nucleation rate is thus found. In the same experiment one also measures the drop radii, the rates of growth of the droplets, and the rates of heat and mass transfer. If ions are present in the mixture, the droplets are electrically charged and their settling rates can be controlled by altering the electric field strength between the plates.

The formation of supersaturated vapor by turbulent mixing of gases is utilized for obtaining large condensation nuclei in KUST-2 and KUST-4 nucleus counters /16/. In these counters, a jet of the sample gas containing

condensation nuclei is mixed with a warm air saturated with vapors which are to condense on the nuclei. The supersaturation is controlled by altering the velocity ratio of the mixing streams so as to ensure homogeneous condensation. The number density of the nuclei which have grown to an appreciable size by condensation of vapor on their surfaces is determined by measuring the scattering of light.

Initial tests with the KUST-2 counter have shown that the radius of the grown particles is independent of the original size of the nuclei and their number density as long as it is less than $10^{-3}\,cm^{-3}$. The sensitivity of the counter in relation to the smallest nuclei is $10^{-20}\,g/cm^3$.

DETERMINATION OF CRITICAL SUPERSATURATION IN A JET

Critical supersaturation is commonly determined by inducing fog formation in a vapor-saturated gas mixture which is cooled by adiabatic expansion in a cloud chamber /17, 18/. The same chamber is also used for detecting condensation nuclei in the gas and studying the properties of charged particles. The expansion chamber, however, poses certain experimental difficulties, particularly at high temperatures. Among the principal shortcomings of the chamber we should mention two points: (a) the operation of the chamber is essentially periodic, and (b) the supersaturation diminishes rapidly because the vapor is heated by the chamber walls.

Supersaturated vapor, which is prerequisite for fog formation, can be obtained by alternative techniques, and not only by adiabatic expansion, as in the cloud chamber. Simpler, continuously sensitive instruments can therefore be used.

The experiments described in the preceding were carried out in order to study the conditions of formation of supersaturated vapor when vapor-containing gases of different temperatures are mixed (see Table 3.1). The critical supersaturation (for water and ethanol vapors) was determined by examining a free jet for incipient fog. This simple method is highly sensitive, since temperature is the only variable parameter and it can be controlled with great precision.

Figure 3.11 is a schematic diagram of a setup used in the determination of the critical supersaturation of sulfuric acid vapor. Dry, carefully filtered air is fed through two channels into the installation. The first stream is delivered to the evaporator 1 where it is saturated with sulfuric acid vapor and then ejected through a nozzle into the mixing chamber 3. The second stream is delivered directly to the mixing chamber where it creates the background medium for the free jet. The mixing chamber is enclosed in a thermostat which maintains constant temperature. The temperature of the two streams is measured by thermoelectric elements 6 which consist of four serially connected copper-constantan thermocouples. The incipient fog is detected by means of the Tyndall effect which is observed in the light from a point source 4 illuminating the jet.

The temperature of the gas stream reaching the nozzle and the content of sulfuric acid in the gas remain constant during the experiment. The

temperature of the air medium in the mixing chamber is initially high enough to preclude fog formation in the region of mixing (the maximum supersaturation is less than the critical figure). As the air temperature is lowered, the maximum supersaturation in the region of mixing increases until fog is detected. It is assumed that incipient fog forms at the midpoint between the points of visible fog and fog dissipation.

The point of incipient fog is substituted in equation (3.13) to find the parameter n corresponding to maximum supersaturation. The result is inserted for n in equation (3.10) to find the maximum supersaturation which is adopted as the critical figure. The procedure is the same as that employed to reduce the data listed in Table 3.1. In the treatment stage allowance must be made for the fact that the degree of dissociation of the sulfuric acid vapor increases with temperature and the average molecular weight of the gas mixture correspondingly decreases.

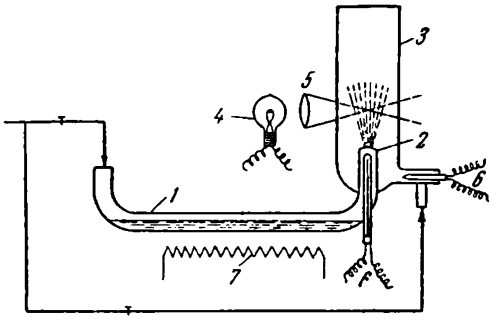

FIGURE 3.11. Schematic diagram of the setup for the determination of the critical supersaturation: 1) evaporator saturating the gas with liquid vapor; 2) nozzle; 3) mixing chamber; 4) point source; 5) lens; 6) thermocouples; 7) electric heating element.

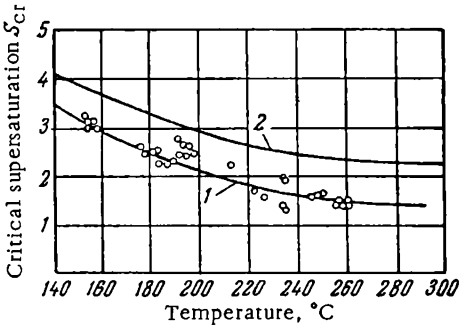

FIGURE 3.12. Critical supersaturation of sulfuric acid vapor vs. temperature: 1) experimental; 2) calculated.

In Figure 3.12 curve 1 represents the experimental findings, and curve 2 plots the critical supersaturation of sulfuric acid vapor calculated from (1.61) putting $c = 0.242$. We see from the figure that the experimental data are somewhat lower than the theoretical figures. This is partly due to the fact that the air was not perfectly ion-free in the experiments, whereas equation (1.61) applies for ion-free gas mixtures only.

Experiments with fog formation in exhaled air and above the surface of water also suggest that critical supersaturation can indeed be determined by monitoring fog formation in mixing gases.

Measurements of critical supersaturation in mixing gases can also be applied to determine the dependence of this parameter on temperature, pressure, and other factors and to detect the presence of condensation nuclei, in particular ions, in gases.

The supersaturated vapor forms in a free jet and the supersaturation remains constant during the experiment, so that, unlike the cloud chamber, this technique can be used in continuous measurements. The supersaturation is easily controlled by adjusting the temperatures of the mixing gases and the vapor pressures. The condensation nuclei can be removed from the gas mixture by filtration or electrostatic precipitation before it reaches

the mixing chamber; at this stage the mixture can also be treated in an appropriate way so that the initial conditions at the entrance to the mixing chamber will be accurately known. The formation of ions can furthermore be automatically monitored by measuring the light scattering in the fog with a phototube or some other photoelectric device.

VARIOUS CASES OF FOG FORMATION IN TURBULENT MIXING OF GASES

Formation of supersaturated vapor and fog in mixing gases often occurs in nature in a variety of processes encountered in everyday practice. The high temperatures developing when fuel is burned in the furnaces of central heating installations, locomotives, ships, and various factories are sufficient to vaporize some of the fuel components and the combustion products. Furnace gases emitted into the atmosphere are mixed with the colder air and supersaturated vapor forms locally in regions of mixing. The supersaturated vapor naturally registers as visible fog.

The existence of an upper limit for the supersaturation enables us to predict the probability of formation of supersaturated vapor and fog when vapor-containing gases are mixed without taking account of the actual quantities of gases that are mixed.

Equations (3.10) and (3.13) can be applied to calculate fog formation above graduating towers and other installations, i.e., whenever water vapor or warm, vapor-containing air masses are mixed with the colder ambient air.

Fog formation is particularly frequent in various chemical processes: in the production of sulfuric acid, sulfur, phosphorus, organic products, etc. Very stable fog forms when the vapors of a high-boiling liquid are mixed with a cold gas, because the rate of droplet evaporation decreases as the saturated vapor pressure of the liquid is decreased.

Turbulent mixing of gases in a free jet is also applied for cloud seeding: crystallization nuclei form which act as condensation centers for the droplets and thus promote artificial precipitation. Considerable efforts are being currently devoted to the study of vapor condensation on crystallization nuclei of various substances and some field experiments have been carried out on production of artificial precipitation by the seeding of atmospheric clouds (which consist of supercooled droplets) with crystallization nuclei /19, 20/. Silver iodide and lead iodide, which are typically injected into the exhaust gases of aircraft, proved to be the most effective seeding agents of this class. These compounds vaporize at high temperatures and are ejected with combustion gases through the exhaust pipe into the atmosphere. The exhaust gases are cooled by mixing with air, and silver iodide (or lead iodide) condense to form minute crystal nuclei. The structure of silver iodide and lead iodide crystals is analogous to the structure of ice crystals, and water vapor therefore condenses and freezes on these seeds despite the fact that the saturated vapor pressure above supercooled water droplets is higher than above ice crystals. The condensational growth of the crystals lowers the vapor pressure in the air and the supercooled droplets start evaporating. This *isothermal distillation* continues until all the droplets will have evaporated.

Since the seeding crystals are comparatively few, they grow to a substantial size by accruing the multidue of the cloud droplets and precipitate as snow flakes or rain drops.

Clouds and fog sometimes form in the atmosphere when air currents of different temperatures are mixed. For example when warm tropical air penetrates into the northern latitudes and collides with cold masses of arctic air, the denser cold air remains closer to the ground cutting as an enormous wedge into the oncoming warm air (Figure 3.13). The interface between the two air masses, known to meteorologists as a frontal surface or, briefly, a front (shown by the double line in Figure 3.13), slopes slightly with a gradient of 1—2 km per 100—200 km. Different cloud systems form along the frontal surface: cirrostratus clouds are the first to appear at altitudes of 7—8 km; they give way to altostratus and finally to nimbostratus clouds (Figure 3.13a).

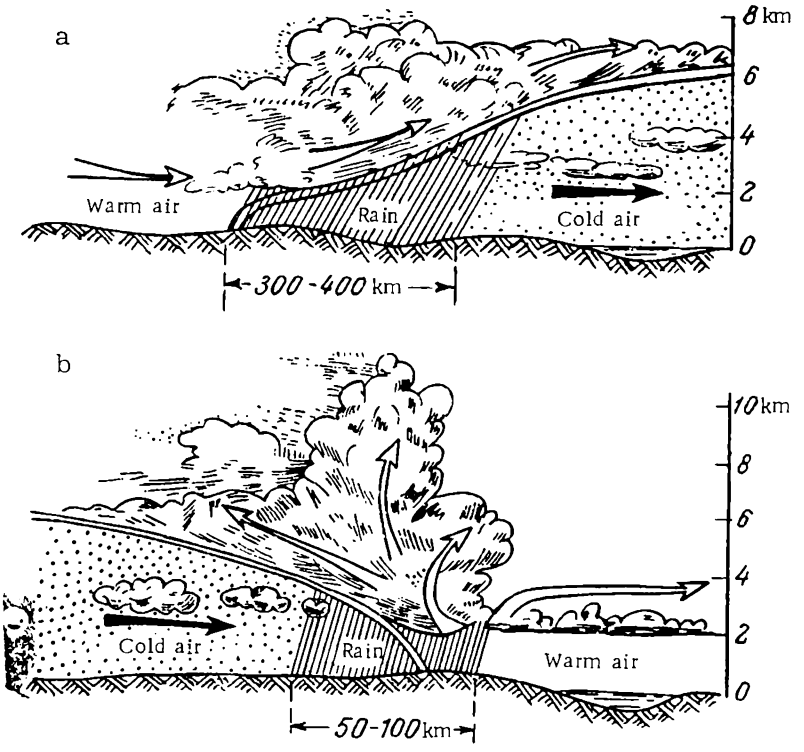

FIGURE 3.13. Cloud and fog formation along the frontal surface: a) warm front; b) cold front.

When cold air advances into a generally warm region, the frontal surface between the two air masses — a cold front — slopes at a larger angle (Figure 3.13b). Small clouds first appear in the sky, which rapidly grow to thick thunderstorm clouds.

The probability of cloud and fog formation in cold and warm fronts can be predicted without taking account of the quantitative ratio of the mixing air masses, since the coefficient n (equation (3.1)) may assume any value from 0 to ∞ in the region of mixing. If the maximum supersaturation calculated from equations (3.10) and (3.13) is greater than unity, vapor

will inevitably condense in the gas volume and clouds will appear. Additional calculations should be carried out in order to establish the number density and the mass concentration of the fog.

A white trail of fog is often visible in the wake of high-altitude aircraft; it is seen from far away and pinpoints the position of the aircraft. The formation of these aircraft trails is explained as follows: the combustion of 1 g of liquid aviation fuel releases nearly 1.5 g of water vapor, which is emitted into the atmosphere with the exhaust gases. The hot exhaust gases mix with the cold ambient air, the supersaturation of water vapor increases presumably reaching the critical figure, and visible fog condenses in a trail behind the aircraft.

The persistence of this cloud trail depends on air currents and air humidity. If the winds are slow, the trail takes some time to dissipate and the fog is comparatively stable. If the air humidity is increased, the rate of evaporation of the water droplets diminishes and the lifetime of the fog trail again increases. Knowing the composition of the aviation fuel and the temperature of the exhaust gases, as well as the air temperature and composition, we can predict the probability of fog formation in the wake of a flying aircraft and develop special measures for its prevention.

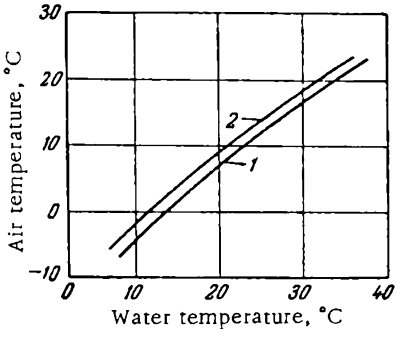

FIGURE 3.14. Initial conditions of fog formation above a water surface: 1) air humidity 60%; 2) air humidity 80%.

The mechanism of fog formation in air exhaled on cold premises was established by special experiments, in which the exhaled air was assumed to be saturated with water vapor /21/. The temperature of the ambient air was altered in the course of the experiments.

In some cases fog will form above a liquid whose temperature is higher than the ambient temperature. The air layer near the liquid surface is warmed to the temperature of the liquid and is saturated with its vapors. Fog forms when this warm, vapor-saturated layer is subsequently mixed with the colder overlying air by convection currents. The low-lying fog over rivers, lakes, and other bodies of water forms in this way. In daytime, the water is warmed by the sunlight and at night the air cools more rapidly than the water, so that in the morning the temperature of the water is noticeably higher than the air temperature, this frequently resulting in the formation of fog.

The validity of the preceding considerations is confirmed by experimental data /5, 6/. The temperature of water in a thermostat is slowly raised until visible fog appears above the water surface. The temperature of the water at the instant of fog appearance and the air temperature and humidity in the thermostat are noted. These data are substituted in equation (3.13) to calculate the parameter n corresponding to maximum supersaturation of the water vapor; the supersaturation at the point of incipient fog is then calculated from equation (3.10). In these calculations it is again assumed that the air adjoining the surface of the water is saturated with vapor and its temperature is equal to that of the water.

Experiments show that the point of incipient fog above the surface of warm water corresponds to a supersaturation of 1.01, which is equal to

the critical supersaturation of water vapor in uncleaned air with suspended particles larger than 10^{-5} cm.

Figure 3.14 plots the initial conditions for fog formation in atmospheric air above the surface of water, calculated for air humidities of 60 and 80%. The calculations are made as follows. Several points corresponding to various air temperatures are laid off along the ordinate axis and equations (3.45), (3.13), (3.46), and (3.47) are then applied to calculate the temperatures of the vapor-saturated air near the water surface which ensure a maximum supersaturation of 1.01 in the region of mixing. The calculated results are then plotted in a graph. It should be noted, however, that the critical supersaturation varies depending on air purity.

Table 3.6 lists the points of incipient fog above a water surface for various critical supersaturations. We see from the table that the point of incipient fog is highly sensitive to the critical supersaturation: a change of 0.01 in the supersaturation shifts the point of incipient fog approximately by 2 °C.

TABLE 3.6. Initial conditions of fog formation above a water surface for various critical supersaturations

Water temperature t_1, °C	Relative humidity 60%			Relative humidity 80%		
	S=1.00	S=1.01	S=1.02	S=1.00	S=1.01	S=1.02
	ambient temperature t_2, °C					
10	−1.3	−4.4	−7.2	+1.9	−2.0	−5.8
20	8.4	5.2	2.3	11.1	9.0	7.0
30	17.4	15.6	13.5	20.2	18.0	16.0
40	26.5	24.8	23.0	—	—	—

A method for producing dense fog with a high mass concentration has been proposed in /22/. The liquid of interest is brought almost to boil and another liquid with a considerably lower boiling point is poured on its surface. The low-boiling liquid starts evaporating vigorously and breaks up into spheroidal droplets on the surface of the first liquid. Observations indicate that fog forms in the clearance between the spheroid and the depression in the liquid surface in which the spheroid rests. Here the vapor of the high-boiling liquid is mixed with the colder vapor of the low-boiling liquid, supersaturated vapor forms, and fog subsequently condenses in the gas volume. The degree of supersaturation and the parameter n corresponding to the maximum supersaturation can be calculated from equations (3.10) and (3.13). The applicability of this method is also confirmed by measurements of the electric charge of the forming droplets /22/.

The mass concentration of the fog which forms in mixing gases can be found from equation (1.87). It is directly proportional to the supersaturation. Since the supersaturation increases with the temperature difference and the vapor pressure difference between the mixing gases, the mass concentration of fog also depends on these parameters. However, the vapor pressure of the first liquid (p_1) is a function of its temperature T_1 and the partial vapor pressure of the first liquid in the vapors of the second liquid (p_2) is zero. The mass concentration therefore increases as T_1 is increased

and T_2 — the temperature of the second liquid — is decreased (see Figure 3.9). This condition is also confirmed by experimental findings /22/.

The above considerations are illustrated by the data in Table 3.7, which lists the calculated maximum mass concentrations of the mist forming when transformer oil vapor is mixed with cold air and carbon dioxide. The calculations were made from equations (3.10) and (3.13).

TABLE 3.7. Maximum mass concentration of transformer oil mist

Temperature of transformer oil t_1, °C	Vapor pressure of transformer oil p_1		Temperature t_2, °C		Maximum mass concentration of mist, g/m³
	N/m²	mm Hg	air	carbon dioxide	
280	$5.2 \cdot 10^4$	388	−180	—	1220
280	$5.2 \cdot 10^4$	388	—	−78	1190
280	$5.2 \cdot 10^4$	388	+20	—	492
158	1467	11	−180	—	43.9
158	1467	11	—	−78	35.5
158	1467	11	+20	—	8.4

We see from the table that the maximum mass concentration depends on the temperature of the mixing gases, i.e., on their vapor content. It is also sensitive to the composition of the indifferent gas.

The above method was applied in a somewhat modified form to produce cold, highly disperse fog with a high mass concentration (liquid water content) /23/ by immersing dry ice in warm water. In the range of water temperatures from 30 to 50 °C the mass concentration (liquid water content) of the fog was 200 g/m³, with a mean drop radius of nearly 1 μ. The mass concentration and the mean drop radius both increased with the temperature of the water.

Agricultural crops are protected against various diseases and pests by spraying with chemical poisons — pesticides. Harmful weeds are also killed by spraying them with chemicals /24/. Application of pesticides and insecticides by spraying with fine aerosols was proved as the most effective technique of crop protection. The aerosol particles hover as a cloud of mist above the plants and gradually settle on the surface of leaves and stems.

Aerosols used in agriculture are produced by three principal techniques:

(1) mechanical;

(2) thermal;

(3) thermomechanical.

In mechanical spraying, the insecticide solution is pulverized in the air into minute droplets which form a mist cloud. In thermal spraying, the insecticides are first warmed until vapor has formed, and the vapor is then mixed with the colder atmospheric air. The vapor cools and condenses into minute droplets in the gas volume. The thermomechanical techniques combine mechanical breakup with thermal evaporation.

Various spray guns are currently available for routine production of aerosol and fog. The functional diagram of the Soviet-made AG-UD-2 aerosol generator is shown in Figure 3.15. Liquid fuel mixed with air is delivered by the supercharger 3 to the combustion chamber 7. The

exhaust gases are delivered to the diffuser 9 simultaneously with the insecticide solution. The fast moving exhaust gases pulverize the liquid which then evaporates in the diffuser 11. The vapor-gas mixture issuing from the diffuser 11 is mixed with atmospheric air (see Figures 3.2, 3.5). Highly supersaturated solvent vapors are formed in the jet and the active agent condenses into minute droplets, i.e., into a cloud of mist.

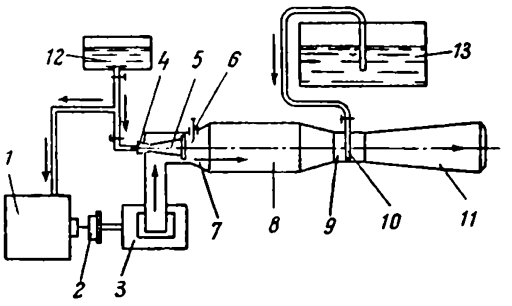

FIGURE 3.15. AG-UD-2 aerosol generator: 1) motor; 2) clutch; 3) supercharger; 4, 10) jet tubes; 5) burner; 6) spark plug; 7) combustion chamber; 8) fire tube; 9, 11) diffuser; 12) liquid fuel; 13) insecticide solution.

If the fuel is not burned, the liquid is pulverized in the nozzle, but it does not evaporate. The fog is thus generated by mechanical means.

Thermomechanical spraying would call for the burning of a small quantity of fuel, so that only part of the droplets would evaporate.

A variety of spray guns and aerosol generators designed on the same principle /24—28/ are widely used in agriculture and livestock breeding (to kill bacteria and insects).

REFERENCES

1. BAUM, V. A. Dissertation. Available at the ENIN AN SSSR Library. 1945.
2. D'YAKONOV, G. K. Voprosy teorii podobiya v oblasti fiziko-khimicheskikh protsessov (Similarity Theory in Physicochemical Processes). — Izdatel'stvo AN SSSR. 1956.
3. DOMKOHLER, G. — Themi—Ingenier, 3. 1939.
4. AMELIN, A. G. — DAN SSSR, 68 : 1673. 1947.
5. AMELIN, A. G. —Kolloidnyi Zhurnal, 10 : 169. 1948.
6. AMELIN, A. G. — In: "Novye idei v oblasti izucheniya aerozolei". Izdatel'stvo AN SSSR. 1949.
7. DESSAUER, F. Dosierung und Wesen der Rontgenstrahlenwirkung in der Tiefentherapie vom physikalischen Standpunkt. — Dresden, Steinkopff. 1923.
8. Tekhnicheskaya entsiklopediya. Spravochnik fiziko-khimicheskikh velichin (Technical Encyclopedia. Handbook of Physicochemical Constants), Vol. 1. 1930.
9. LEVINE, D. G. and S. K. FRIEDLANDER. — Chem. Eng. Sci., 13 : 49. 1960.
10. HIGUCHI, W. J. and C. T. KONSKI. — J. Coll. Sci., 15 : 14. 1960.
11. HIDY, G. M. and S. K. FRIEDLANDER. — A. I. Ch. Eng. Journal, 10 : 115. 1964.

12. ABRAMOVICH, G. N. Teoriya turbulentnykh strui (Theory of Turbulent Jets). — Fizmatgiz. 1960.

13. ABRAMOVICH, G. N. Prikladnaya gazovaya dinamika (Applied Gas Dynamics). — Tekhteoretizdat. 1953.

14. LANGMUIR, I. — UFN, 37:349. 1949.

15. AMELIN, A. G. and M. I. BELYAKOV. — Kolloidnyi Zhurnal, 17:1463. 1955.

16. KOGAN, Ya. I. and Z. A. BURNASHOVA. — ZhFKh, 24:2630. 1960.

17. PUTILOV, K. A. and V. A. FABRIKANT. Kurs fiziki (Textbook of Physics), Vol. 3. — Fizmatgiz. 1963.

18. WILSON, J. G. The Principles of Cloud Chamber Technique. — Cambridge Univ. Press. 1951. [Russian translation. 1954.]

19. MASON, B. J. The Physics of Clouds. — Oxford. 1957.

20. SHISHKIN, N. S. Oblaka, osadki i grozovoe elektrichestvo (Clouds, Precipitations, and Thunderstorm Electricity). — Gidrometeoizdat. 1964.

21. KERRIDGE, P. M. T. Principles of Physical Chemistry for Medical Students. — London, Oxford Univ. Press. 1927.

22. SMIRNOV, N. S. — Kolloidnyi Zhurnal, 10:448. 1948; In: "Novye idei v oblasti izucheniya aerozolei". Izdatel'stvo AN SSSR. 1949.

23. SOLYANEK, E. G., K. A. ZAITSEV, and V. N. ORLOV. — Kolloidnyi Zhurnal, 25:234. 1963.

24. KOROTKIKH, G. I. Aerozoli v sel'skom khozyaistve (Aerosols in Agriculture). — Sel'khozgiz. 1960.

25. PRONIN, A. F. Mashiny dlya bor'by s vreditelyami i boleznyami sel'skokhozyaistvennykh kul'tur (Machinery for Combating Pests and Diseases of Agricultural Crops). — Izdatel'stvo Vysshaya Shkola. 1964.

26. Primenenie aerozolei v sel'skom khozyaistve (Application of Aerosols in Agriculture). Collection of translations. — IL. 1955.

27. Aerozoli v sel'skom khozyaistve (Aerosols in Agriculture). Collection of papers. — Sel'khozgiz. 1956.

28. Aerozoli i ikh primenenie (Aerosols and Their Application). Collection of papers. — Izdatel'stvo Ministerstva Sel'skogo Khozyaistva. 1959.

Chapter Four

FORMATION OF SUPERSATURATED VAPOR AND FOG BY MOLECULAR DIFFUSION AND THERMAL CONDUCTION

DERIVATION OF WORKING FORMULAS

The relation of vapor pressure to temperature can be derived from the general differential equations of molecular diffusion and thermal conduction:

$$\frac{\partial p}{\partial \tau} = D\left(\frac{\partial^2 p}{\partial x^2} + \frac{\partial^2 p}{\partial y^2} + \frac{\partial^2 p}{\partial z^2}\right) \tag{4.1}$$

$$\frac{\partial T}{\partial \tau} = a\left(\frac{\partial^2 T}{\partial x^2} + \frac{\partial^2 T}{\partial y^2} + \frac{\partial^2 T}{\partial z^2}\right) \tag{4.2}$$

where p and T are the vapor pressure and temperature; D the diffusivity; a thermal diffusivity; τ time; x, y, z rectangular coordinates.

These equations cannot be applied for the solution of particular problems without proper initial and boundary conditions. If we assume that the pressure and temperature along the y and z axes are constant, equations (4.1) and (4.2) take the simpler form

$$\frac{\partial p}{\partial \tau} = D\frac{\partial^2 p}{\partial x^2} \tag{4.3}$$

$$\frac{\partial T}{\partial \tau} = a\frac{\partial^2 T}{\partial x^2} \tag{4.4}$$

These simplified equations describe the thermodynamic state of the material layer between two surfaces which are maintained at different temperatures (Figure 4.1). The temperatures T_1 and T_2 of the upper and the lower surfaces are constant, and $T_1 > T_2$. The two surfaces are wetted by a liquid; the saturated vapor pressure of the liquid at the temperature T_1 is p_1 and at T_2 it is p_2. The space between the two planes, h, is filled with a gas which does not condense under the particular set of conditions. The liquid and the noncondensing gas are chosen so that the density of the vapor-gas mixture decreases from the bottom to the top surface. The system is free from convection in this case.

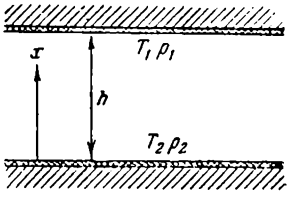

FIGURE 4.1. The principle of the diffusion cloud chamber.

Under steady-state conditions

$$D\frac{d^2p}{dx^2}=0 \tag{4.5}$$

$$a\frac{d^2T}{dx^2}=0 \tag{4.6}$$

Equation (4.5) is divided through by D and integrated to give

$$p=C_1x+C_2 \tag{4.7}$$

The integration constants are determined by putting $p=p_2$ at $x=0$ and $p=p_1$ at $x=h$. Equation (4.7) thus takes the form

$$p=p_2+\frac{p_1-p_2}{h}x \tag{4.8}$$

From (4.6) we similarly have

$$T=T_2+\frac{T_1-T_2}{h}x \tag{4.9}$$

Inserting these expressions for vapor pressure and temperature in (1.2), we can find the supersaturation along the entire height between the two surfaces. Wherever the supersaturation exceeds the critical figure, vapor condenses and fog forms locally.

The probability of fog formation can be established by a simpler technique, specifically by measuring the maximum supersaturation arising between the surfaces. Indeed, if the maximum supersaturation is higher than the critical value, vapor will inevitably condense in the gas volume. Otherwise, no condensation will occur throughout the volume.

To find the maximum supersaturation, we eliminate the variable x between (4.8) and (4.9). The resulting expression relates the vapor pressure to temperature at any point of the gas volume for the given boundary values of p and T:

$$p=\left(\frac{T-T_2}{T_1-T_2}\right)(p_1-p_2)+p_2 \tag{4.10}$$

The differential equation relating vapor pressure to temperature thus takes the form

$$\frac{dp}{dT}=\frac{p_1-p_2}{T_1-T_2}=\text{const} \tag{4.11}$$

i.e., the derivative $\frac{dp}{dT}$ is graphically represented by a straight line.

Substituting p from (4.10) in (1.1), we find

$$S=\left(\frac{T-T_2}{T_1-T_2}\right)\left(\frac{p_1-p_2}{p_\infty(T)}\right)+\frac{p_2}{p_\infty(T)} \tag{4.12}$$

The temperature corresponding to maximum supersaturation can be found by examining the functional dependence $S=f(T)$. Differentiating, making use of (2.7), and writing T_{max} for the absolute temperature at which

the maximum supersaturation is attained, we obtain the following equation:

$$\frac{T_{max}^2}{E(T_1 - T_2)} - \frac{p_2}{p_1 - p_2} \cdot \frac{T_1 - T_2}{T_{max} - T_2} - 1 = 0 \qquad (4.13)$$

Substituting this T_{max} in (4.12), we may also find the magnitude of the maximum supersaturation.

When solving equations (4.5) and (4.6), the diffusivity and the thermal diffusivity are assumed constant across the layer, i.e., these coefficients are independent of both temperature and gas mixture composition. In more exact calculations this dependence cannot be ignored and the working equations for vapor pressure, temperature, and supersaturation across the layer become correspondingly more complex.

Figure 4.2 plots the results of calculations for ethanol vapor in the air layer between two parallel plates maintained at different temperatures. We see from the figure that as the temperature of the bottom plate is decreased and that of the upper plate is increased, the maximum supersaturation rises and may reach values substantially higher than the critical supersaturation.

All the preceding remains in force when $T_2 > T_1$, $p_2 > p_1$, and diffusion proceeds in the upward direction. The condition that the density of the gas mixture decreases from bottom to top, however, should be observed.

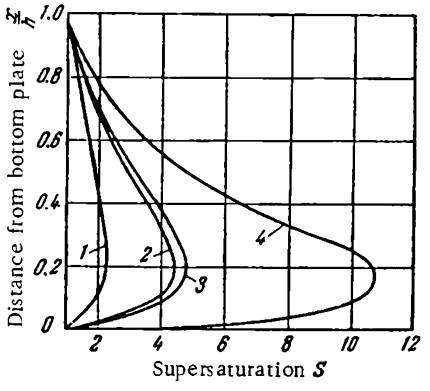

FIGURE 4.2. Supersaturation of ethanol vapor between two plates:
1) $t_1 = 20°$, $t_2 = -20°$; 2) $t_1 = 40°$, $t_2 = -20°$;
3) $t_1 = 10°$, $t_2 = -40°$; 4) $t_1 = 30°$, $t_2 = -40°$C.

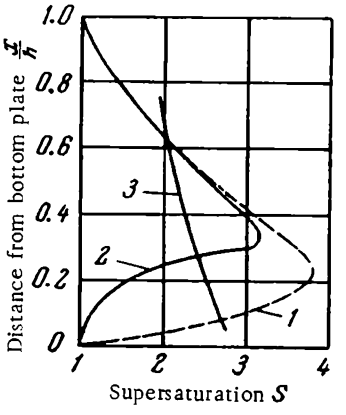

FIGURE 4.3. Supersaturation of ethanol vapor between two plates: 1) vapor condenses without nucleation; 2) true supersaturation (approximate); 3) critical supersaturation.

For the curves in Figure 4.2 having $S_{max} > 2$, the theoretical results are meaningless, since equation (4.12) applies only for $S < S_{cr}$. The dependence for $S > S_{cr}$ is radically different. Figure 4.3 shows some curves for ethanol vapor in air ($t_1 = 35\,°C$, $t_2 = -20\,°C$, $p_1 = 103.7$ mm Hg, $p_2 = 2.5$ mm Hg, $E = 5100$). Curve 1 has been plotted for $S = f(x/h)$ neglecting spontaneous condensation of vapor (it has been calculated from (4.12)). Curve 3 plots the critical supersaturation according to equation (1.61) for $c = 0.242$. Curve 2 traces the approximate true variation of the supersaturation

$S=f(x/h)$. The position of this curve depends on the applicable physical conditions, on the rate of nucleation, and the rate of condensational growth of the embryos.

The formation of fog droplets in this case depends on the variety of factors which govern the number density of the fog and its drop size distribution. The formation of embryos (which grow into droplets) begins at the intersection point of curves 1 and 3 for $h \approx 0.6$ (Figure 4.3). The rate of this nucleation (determined by the supersaturation S) initially increases, reaches a maximum, and then steeply diminishes due to the reduction in S, mainly because of vapor condensation on the surface of the droplets (the embryos are very small, having radii of the order of 10^{-7} cm, and their nucleation does not cause a noticeable reduction in vapor pressure). The droplets are propelled by thermophoretic and diffusive forces to the cold surface, on which they settle. While moving through the medium, the droplets grow by condensation and coalescence. All the parameters in (1.46) and (1.55) which influence the nucleation of new embryos and their condensational growth (S, N, φ, T, $P-p_r(T_r)$, etc.) are therefore variable with time, and general relations for droplet radii and number densities are difficult to derive. In what follows we are only able to analyze the effect of separate factors on these parameters.

The time a droplet spends in supersaturated vapor and the final size of the droplet both depend on its velocity (i.e., thermophoretic and diffusive forces) and the path length l from the nucleation site to the cold surface; clearly, $l=f(h)$. Thermophoresis and diffusion in their turn are determined by the temperature and vapor pressure gradients /1—4/.

Some data on the variation of droplet radii and number densities emerge from the experiments with condensation of aluminum /5/. A sample of aluminum (100 mg) was placed on a tungsten wire loop at the center of a glass flask 8 cm in diameter. The air was pumped out to a vacuum of $\sim 10^{-5}$ mm Hg and the pressure in the flask was then raised to a required level by admitting argon, helium, or hydrogen. When electric current was passed through the tungsten wire, the aluminum sample vaporized completely in 2 min. The processes taking place between the hot wire and the flask wall are entirely analogous to the processes which have been previously described for two plates at different temperature (see Figure 4.1). The aluminum vapor thus condenses spontaneously in the gas volume into minute spherical particles, which settle on the flask's inner walls.

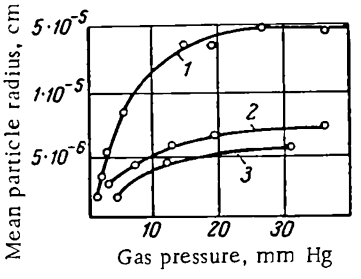

FIGURE 4.4. Mean radius of aluminum droplets as a function of gas pressure;
1) A; 2) H_2; 3) He.

Convection currents arise in the flask, however, because of the high temperature difference between the wire and the glass wall and the large gas volume. These currents have a substantial influence on the nucleation and the condensational growth of the embryos.

An analysis of the experimental data indicates that the mean drop size increases with the pressure of the indifferent gas (Figure 4.4). This phenomenon can be attributed to diffusion, since its rate decreases with increasing pressure.

The relative arrangement of the experimental curves from helium to argon is apparently attributable to the reduction in thermal diffusivity a, which is the highest for helium and the lowest for argon.

The formation of supersaturated vapor and liquid droplets between wetted surfaces of different temperature is applied for the determination of nucleation rates and critical supersaturations. The droplets initially form in regions of maximum supersaturation. If the number of these droplets is insignificant, the maximum supersaturation and the distance of the supersaturated pocket from the cold surface can be found from the preceding equations. The number of droplets settling per unit time on the lower surface can be converted into the rate of nucleation and S_{cr} is thus found.

Fog formation due to vapor condensation on a cold surface in a still medium is encountered fairly seldom, since turbulent streams generally interfere with the normal course of the process. In thin layers, e.g., in the boundary layer in the case of vapor condensing in a pipe (p. 105), eddy diffusion and thermal conduction have a negligible effect on heat and mass transfer. High temperature and vapor pressure gradients may produce highly supersaturated vapor, which will condense to fog.

THE DIFFUSION CHAMBER

In the expansion cloud chamber, where vapor is cooled by adiabatic expansion (p. 55), the supersaturation is nonuniform across the chamber and variable with time (see Figure 2.6). It is therefore not disputed that other, better experimental instruments should be used.

In the diffusion chamber /6—8/ supersaturated vapor is formed in a still gas mixture between two wetted surfaces maintained at different temperatures. The first satisfactory results were obtained in a chamber designed along the lines of the general sketch shown in Figure 4.1. This chamber was a closed vessel with a cooled bottom, and the top surface was maintained at a higher temperature /9/. The simple design and the steady supersaturation make the diffusion chamber particularly suitable for continuous observations, unlike the expansion chamber whose operation is inherently periodic.

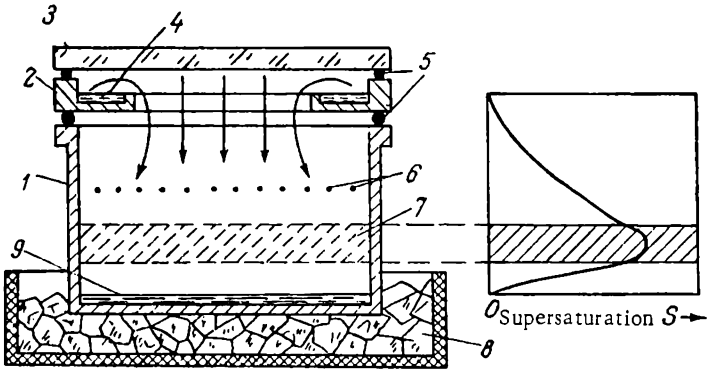

FIGURE 4.5. Schematic diagram of the diffusion chamber and vertical variation of supersaturation in the chamber:
1) glass vessel; 2) metallic pan; 3) glass top; 4) heated liquid layer; 5) rubber seals; 6) filament providing cleansing electrostatic field; 7) sensitive volume; 8) dry ice; 9) condensed liquid.

A functional diagram of a diffusion cloud chamber is shown in Figure 4.5. It generally comprises a glass container 1, a metallic pan 2, and a glass top 3; the joints are sealed with rubber gaskets 5. The pan 2 contains some liquid 4 which is heated by hot water circulating in a metallic tube. The heated liquid vapor diffuses downward to the bottom of container 1, which is immersed in a dry ice bath, and supersaturated vapor is obtained.

The curve in the right-hand part of Figure 4.5 plots the vertical variation of supersaturation in the chamber.

Diffusion chambers are normally filled with air or argon at atmospheric pressure. Methanol or ethanol serve as the vapor-forming liquid. The bottom is typically cooled with dry ice (solid CO_2) which is either in direct contact with the bottom or is circulated through cooling pipes in a mixture with acetone.

If the chamber is set up in the vertical field of a solenoid /10/, equilibrium conditions are established 5—10 min after the cooling of the bottom is begun and tracks of ionizing particles can be observed in the sensitive layer (where $S>1$). This setup can be used in observations of nuclear reactions and in monitoring the radiations of very weak artificial and natural radioactive samples. A more sophisticated diffusion chamber which operates on the same principle has been designed for operation with a cyclotron /11/. Diffusion chambers built for observing nuclear reactions in gases are made of stainless steel and filled with 15 atm of hydrogen /12/. Numerous glass windows are provided for illumination and viewing of particle tracks.

Diffusion chambers have also been described with vapor diffusing in the upward direction through the noncondensing gas /13, 14/. In these chambers it is easier to maintain a constant volume of working liquid, since the vapors condensing on the chamber top drop back to the bottom. However, the danger of convection currents which may arise if the top surface is cooled excessively make this chamber inadequate for operation at low temperatures, where the best track photographs are normally obtained.

Since a stable supersaturated vapor is formed in diffusion chambers, the droplets rapidly grow by condensation and settle to the bottom. Experience shows that this shower of droplets does not interfere with observations of particle tracks.

Diffusion chambers are currently used for the determination of critical supersaturation /15/ and for other researches which require supersaturated vapor. Diffusion chambers have been most instrumental in studying the conditions of cloud formation in the atmosphere. The effectiveness of various inorganic condensation nuclei produced by sublimation on a chrom-nickel spiral was investigated in these chambers /16/. The critical supersaturation of vapor on LiCl, NaCl, $CaCl_2$, MnCl, $CuSO_4$, and AgI nuclei is respectively equal to 1.02, 1.06, 1.06, 1.07, 1.11, and 1.12.

Critical supersaturation, as well as other effects, can be studied by an alternative technique: supersaturated vapor is formed in a gas mixture moving slowly between two surfaces which are maintained at different temperatures. The actual setup depends on the aim of the experiment and the method has certain advantages in various cases. For example, vapor condensation on nuclei can be investigated in a laminar flow of clean, filtered air between two parallel horizontal surfaces of unequal temperature (see Figure 4.1) /17/. A thin (~ 0.1 mm) jet of clean air

which contains the relevant condensation nuclei is passed exactly at the middle between the two surfaces. The temperature of the surfaces at the time of fog appearance is noted and the critical supersaturation is calculated from equation (4.12). The results are plotted as a curve of nucleus distribution vs. supersaturation.

If the wetted parallel surfaces (Figure 4.1) are cooled and heated alternately (at intervals not exceeding 1 sec), a constant and uniform supersaturation is set up between the plates /18/. This method can be applied for reproducing and investigating slow processes of atmospheric condensation.

PREPARATION OF METAL POWDERS

Finely divided metals possess certain specific properties /2, 19—21/ which make them particularly attractive for use in various branches of industry. In metallurgy metal powders are employed in manufacturing certain products that cannot be made by alternative techniques. The use of powders lowers the cost of some products, since no production wastes are involved and the finished part need not be machined /22, 23/. In machine-building industry metal powders are used in the production of gears, filters, piston rings, porous bearings, electrical contacts, refractory components, in jet engines, hard alloys, etc. Powdered ferromagnetic metals and alloys are used in the production of permanent magnets and cores for various induction coils. Some metallic powders act as catalysts in the synthesis, hydration, and oxidation of various organic materials. Numerous metals have bactericidal properties, which are particularly pronounced if the metal is applied in powder form (superfine powders). The metal particles react with the organic tissues and form a multitude of exceptionally long-lived foci; the metal ions given off by these foci are continually replenished in vanishingly small concentrations around each colloidal particle.

Fine metal powders are prepared preferably by homogeneous condensation of the metal vapor in a gas volume. The condensational techniques of metal powder production are divided into two groups depending on the particular method employed for the generation of supersaturated vapor: in the first group the supersaturated vapor is formed by vaporizing the metal from a hot surface and cooling the vapor or the vapor-gas mixture (the distillation technique); in the second group the supersaturated vapor is obtained by a chemical reaction which takes place in the gaseous phase and releases metal molecules (the chemical technique).

Theoretically, any metal can be obtained in powder form by the above methods: if heated to a sufficiently high temperature, the metal inevitably vaporizes, while metal compounds can always be decomposed into constituent elements. In practice, however, the applicability of these methods is limited by technical considerations, i.e., by the exceedingly high temperatures and the special equipment required.

The distillation technique is realized by heating the metal in a vacuum or in an inert gas medium and causing the vapor to condense on a cooled surface or in a special condenser /21/. The temperature of the condensation surface is always below the melting point of the metal. Many metals

can be prepared in powder form by distillation at temperatures under 1500 °C and pressures under 10^{-3} atm. It should be noted, however, that the rate of vaporization of the metals is often too low for commercial applications of the technique. The distillation method is now industrially employed in the production of zinc and cadmium powder /20/.

Metal powders are prepared by distillation in a stationary indifferent gas or in a slowly moving vapor-gas mixture. This process is governed by molecular diffusion and thermal conduction. Currents of heat and vapor pass between the surface of the metal and the condensation surface, the supersaturation changes and metal particles form. The process is carried out at a large difference of temperatures between the metal and the condensation surface; therefore at a certain distance from the metal surface critical supersaturation is attained and embryos form and grow into droplets in the supersaturated vapor. The metal particles are propelled by thermophoresis and diffusion to the cold surface on which they settle and solidify.

Laboratory tests and experience gained in industrial installations indicate that the metal particles become progressively finer as the temperature difference is increased. This is attributable to the higher supersaturation (p. 96), i.e., a state when the particles do not grow to a substantial size.

Preparation of metal powders by the chemical technique is discussed in Chapter Six.

FORMATION OF RADIATIVE FOGS

Radiative fogs generally form at the end of a cloudless night in regions of stagnant air: in troughs, in forest clearings, etc. The formation of these fogs can be explained as follows. In daytime, the soil heats up more readily than the air, but after sunset the earth's surface loses heat by intensive radiation and it cools below the air temperature. Heat is therefore transferred from the ground air layer to the soil. Radiation losses of air are insignificant and can be ignored. The vapor pressure of water in the air does not change at first, but when the temperature of the earth drops below the dew point, water vapor starts condensing on the surface /23/. The process is thus entirely analogous to that observed between two surfaces of unequal temperature (see Figure 4.1). The formation of radiative fogs, however, is complicated by the fact that the temperature of the earth is variable with time, whereas the vapor pressure in the air remains constant until the earth temperature has dropped to the dew point and then starts decreasing in accordance with the rate of vapor condensation on the surface, whose temperature is diminishing. It can be said /23/ that to first approximation the cooling of the earth at night is represented by a linear relation

$$T(0, \tau) = T(0,0) - k\tau$$

where $T(0, 0)$ is the absolute surface temperature of the soil at sunset; $T(0, \tau)$ the absolute surface temperature of the soil after a time τ; k is a proportionality coefficient.

The following boundary conditions should be assumed for the solution of equation (4.4):

$$T(0,\tau) = T_0 \text{ for } \tau = 0$$
$$T(0,\tau) \neq T_0 - k\tau \text{ for } \tau > 0$$

where T_0 is the initial temperature of the earth and of the ground air layer ($\tau = 0$).

Making use of a well-known equation /24/ we find

$$T(x,\tau) = \frac{2}{\sqrt{\pi}} \int_0^{\infty} f\left(\tau - \frac{x^2}{4a\xi^2}\right) e^{-\xi^2} d\xi \qquad \text{(a)}$$

where

$$f\left(\tau - \frac{x^2}{4a\xi^2}\right) = f(u) = T_0 \quad \text{for } u \leqslant 0$$
$$f(u) = T_0 - ku \quad \text{for } u > 0$$

ξ is an auxiliary function. After some manipulations, we write (a) in the form

$$T(x,\tau) = T_0 - k\tau \left\{ \left(1 + \frac{z^2}{2}\right)\left[1 + \Phi\left(\frac{z}{2}\right)\right] - \frac{z}{\sqrt{\pi}} e^{-\frac{z^2}{4}} \right\} \qquad (4.15)$$

where $\Phi(z)$ is Kramp's transcendental function and

$$z = \frac{x}{\sqrt{a\tau}}$$

(a is the thermal conductivity, x the distance from the earth's surface).

To determine the vapor pressure of water in the ground layer, we have to assume that at night the saturated vapor pressure near the ground varies linearly. Therefore, when the ground temperature decreases to the dew point after some time τ, the solution of equation (4.3) takes the form (4.15):

$$p = p_0 - n(\tau - \tau_0) \left\{ \left(1 - \frac{y^2}{2}\right)\left[1 - \Phi\left(\frac{y}{2}\right)\right] - \frac{y}{\sqrt{\pi}} e^{-\frac{y^2}{4}} \right\} \qquad (4.16)$$

where

$$y = \frac{x}{\sqrt{D(\tau - \tau_0)}} \qquad (4.17)$$

D is the diffusivity, τ_0 the time when vapor starts condensing on the ground; n a coefficient.

Equation (4.3) can now be solved approximately under this assumption. To obtain more precise results, the entire time interval should be divided into several subintervals and the variation of the saturated vapor pressure near the ground in each of these subintervals is then calculated from the linear relation.

Table 4.1 lists the results of some calculations for the following conditions:

Surface temperature, °C:
ground and air at sunset . . . . . $t_1 = 15$
ground after 10 hrs . . . . . $t_2 = 5$
Vapor pressure of water in the air at sunset, mm Hg $p_1 = 11.5$
Relative air humidity, % 90
Diffusivity of water vapor in the air, m^2/hr . . . . $D = 0.0846$
Thermal diffusivity, m^2/hr . . . . . $a = 0.0727$

TABLE 4.1. Supersaturation of water vapor in the ground air layer 10 hours after sunset

Height above ground x, m	Air temperature, °C	Vapor pressure of water in the air		Supersaturation s
		mm Hg	N/m^2	
0	278.1	6.54	872	1
0.05	278.76	6.84	912	0.99
0.1	279.36	7.14	952	1.0
0.15	279.93	7.44	992	1.001
0.2	280.45	7.69	1052	0.99
0.3	281.52	8.15	1087	0.98

We see from Table 4.1 that the supersaturation attained after 10 hrs at a height of 0.15 m is greater than unity, and fog will therefore be observed at that height. Experiments show /25/, however, that under the particular conditions chosen for the calculations fog should start forming earlier and at a lower height. This discrepancy is possibly attributable to the implicit assumption that the critical supersaturation is 1. In reality it is less than unity, since the air invariably contains active condensation nuclei. The calculations have furthermore neglected eddy diffusion and thermal conduction, which substantially raise the diffusivity and the thermal diffusivity of the atmospheric air. We see from equations (4.15) and (4.17) that if these coefficients are increased, other conditions remaining constant, the height x will increase proportionally to the square root of the total increment of diffusivity and thermal diffusivity.

REFERENCES

1. DERYAGIN, B. V. and S. P. BAKANOV. — DAN SSSR, 117:959. 1957.
2. BAKANOV, S. P. and B. V. DERYAGIN. — Kolloidnyi Zhurnal, 21:377. 1959.
3. DERYAGIN, B. V. and S. P. BAKANOV. — DAN SSSR, 147:139. 1962.
4. DERYAGIN, B. V. and Yu. I. YALAMOV. — DAN SSSR, 155:886. 1964.
5. GEN, M. Ya., M. S. ZISKIN, and Yu. I. PETROV. — DAN SSSR, 127:366. 1959.
6. HOXTON, L. G. — Proc. Virginia Acad. Sci. Absr., 9:23. 1933—1934.
7. VOLLRATH R. E. — Rev. Sci. Instr., 7:409. 1936.
8. LANGSDORF, A. — Rev. Sci. Instr., 10:91. 1939.
9. AMELIN, A. G. Soviet patent No. 80708, 31 May 1948. — Byulleten' Izobretenii, No. 6:67. 1950.

10. NEEDELS, T. S. and C. E. NIELSEN. — Rev. Sci. Instr., 21 : 976. 1950.

11. COWAN, E. W. — Rev. Sci. Instr., 21 : 991. 1950.

12. MILLER, D. H., E. C. FOWLER, and R. P. SHUTT. — Am. Phys. Soc., New York Meeting, Feb. 1951.

13. WEEDLE, O. H. and C. E. NIELSEN. — Phys. Rev., 81 : 324. 1951.

14. NIELSEN, C. E., T. S. NEEDELS, and O. H. WEEDLE. — Rev. Sci. Instr., No. 9 : 22. 1951.

15. FRANCK, G. P. and H. G. HIRTZ. — Z. Phys., 143 : 559. 1956.

16. SCHIFF, D. et al. — Can. J. Chem., 31 : 1108. 1953.

17. STAROZHILOVA, A. I. — In: "Issledovaniya v oblasti poverkhnostnykh sil", p. 209. Izdatel'stvo AN SSSR. 1961.

18. DERYAGIN, B. V., P. S. PROKHOROV, M. V. VELICHKO, and L. F. LEONOV. — In: "Issledovaniya v oblasti poverkhnostnykh sil". Izdatel'stvo AN SSSR. 1961.

19. NATANSON, E. M. Kolloidnye metally (Colloidal Metals). — Kiev, Izdatel'stvo AN UkrSSR. 1959.

20. JONES, W. D. Powder Metallurgy. — London, Arnold. 1960. [Russian translation. 1964.]

21. PETROV, Yu. I. Stroenie i teplovye svoistva aerozol'nykh chastits metallov (Structure and Thermal Properties of Metal Aerosols). — Dissertation. 1965.

22. FEDORCHENKO, I. M. and R. A. ANDRIEVSKII. Osnovy poroshkovoi industrii (Foundations of Powder Industry). — Kiev, Izdatel'stvo AN UkrSSR. 1963.

23. RAKOVSKII, V. S. and V. V. SAKLIKSKII. Poroshkovaya metallurgiya v mashinostroenii. Spravochnik (Powder Metallurgy in Machine Building. A Handbook). — Mashgiz. 1963.

24. AMELIN, A. G. — DAN SSSR, 77 : 249. 1951.

25. WEBSTER, A. G. and G. SZEGÖ. Partielle Differentialgleichungen der mathematischen Physik. — Leipzig, Teubner. 1930.

26. LYUTERSHTEIN, P. G. and A. F. CHUDNOVSKII. — Trudy NIU GUGMS, Ser. 1, No. 28. 1946.

Chapter Five

FORMATION OF SUPERSATURATED VAPOR AND FOG BY EDDY AND MOLECULAR DIFFUSION AND THERMAL CONDUCTION

In common industrial processes the rates of eddy and molecular diffusion are comparable. The temperature and vapor-pressure equalizing action of these mechanisms is manifested in a variety of phenomena, such as condensation and evaporation of liquids in scrubbing towers, in bubbling equipment, in systems employing sprayed liquids, in coil pipe condensers, in installations where boiling and foaming are used, etc.

The relation of vapor pressure to temperature (which determines the degree of vapor supersaturation in the system) can be derived from the equations of heat and mass transfer, which have been established for a wide range of processes by theoretical analysis, laboratory tests, and industrial experiments. These equations are strictly empiric: they are normally derived by making use of the basic similarity concepts and thus represent the overall effect of eddy and molecular diffusion and heat conduction on the processes of heat and mass transfer.

In the following we consider some typical cases which are frequently encountered in practice.

FORMATION OF SUPERSATURATED VAPOR DURING VAPOR CONDENSATION IN A PIPE

In a turbulent vapor-gas mixture moving along a cold surface, the vapor is transported by molecular diffusion across the boundary layer, where it cools and condenses on the wall. The vapor-gas mixture is additionally cooled by molecular heat conduction. In the turbulent core of the stream, on the other hand, the concentration and temperature are equalized by turbulent mixing. The processes are thus governed by eddy, as well as molecular, diffusion and heat conduction.

The supersaturation obtaining when vapor condenses on the wall is calculated from the well-known equations of heat and mass transfer /1, 2/:

$$dg_v = \beta_p F (p - p_2)\, d\tau \qquad (5.1)$$

$$dQ = \alpha F (T - T_2)\, d\tau \qquad (5.2)$$

where g_v is the mass of vapor in the gas, g; β_p the mass transfer coefficient of vapor, $g \cdot cm^{-2} \cdot sec^{-1} (mm\ Hg)^{-1}$; F the condensation area, cm^2; p vapor pressure in the gas mixture, mm Hg; p_2 vapor pressure near the condensation

surface, mm Hg; τ time, sec; Q the heat lost by the cooling gas, cal; α heat transfer coefficient, cal·cm^{-2}·sec^{-1}·deg^{-1}; T the absolute temperature of the gas mixture, °K; T_2 the absolute temperature of the condensation surface, °K.

The mass of vapor in the gas mixture can be expressed by the equation

$$g_v = \frac{gM_v p}{MP}$$

where g is the mass of the gas mixture, g; M_v the molar mass of the vapor phase; M the mean molar mass of the gas mixture; P the total pressure, mm Hg.

Since

$$\frac{g}{M} = \frac{g_n P}{M_n (P - p)}$$

we have

$$g_v = \frac{g_n M_v p}{M_n (P - p)} \qquad (a)$$

where g_n is the mass of the noncondensing gas, g; M_n the molar mass of the noncondensing gas.

Differentiating equation (a) and remembering that p diminishes as the vapor condenses, we write

$$dg_v = -\frac{g_n M_v P dp}{M_n (P - p)^2} \qquad (b)$$

The quantity of heat lost by the cooling gas is written as

$$dQ = -gcdT = -\frac{g_n P M c}{M_n (P - p)} dT \qquad (c)$$

where c is the specific heat of the gas mixture, cal·g^{-1}·deg^{-1}.

Inserting these expressions for dg_v and dQ in (5.1) and (5.2) and dividing the first equation by the second, we obtain after some manipulations

$$\frac{dp}{dT} = \frac{Mc(P - p)}{M_v} \cdot \frac{\beta_p}{\alpha} \cdot \frac{p - p_2}{T - T_2}$$

Putting

$$\delta = \frac{Mc(P - p)}{M_v} \cdot \frac{\beta_p}{\alpha} \qquad (5.3)$$

we find

$$\frac{dp}{dT} = \delta \frac{p - p_2}{T - T_2} \qquad (5.4)$$

When the pressure of the condensing vapor is low (this is a particularly relevant case, since supersaturated vapor forms mainly in the presence of a large excess of noncondensing gas), we may take

$$P - p \approx P$$

Since

$$\beta_p = \frac{\beta M_v}{RT} \qquad (5.5)$$

and

$$\rho = \frac{MP}{RT}$$

we obtain from equation (5.3)

$$\delta = \rho c \frac{\beta}{\alpha} \tag{5.6}$$

where β is the coefficient of mass transfer, cm/sec; ρ the density of the gas mixture g/cm^3; R the universal gas constant, $6.24 \cdot 10^4$ (mm Hg) $\times$ $\times$cm^3 mole^{-1} deg^{-1}. The coefficient δ is a nondimensional quantity, and for low vapor concentrations it may be taken constant.

Equation (5.4) gives the relation of vapor pressure to temperature in the course of vapor condensation on a cold surface. This equation can be integrated if the condensation surface is maintained at a constant temperature or if the temperature of the gas mixture is known as a function of the temperature of the condensation surface. If this function cannot be established, the solution is obtained by an approximate numerical technique, whereby the height of the condensation layer is divided into several intervals, each with a constant temperature of the condensation surface. The calculations are then made using equation (5.4).

If the temperature of the condensation surface is constant, the vapor pressure near that surface is also constant. Thus, integrating equation (5.4) from p_1 to p and from T_1 to T, we find

$$p = \left(\frac{T - T_2}{T_1 - T_2}\right)^{\delta} (p_1 - p_2) + p_2 \tag{5.7}$$

Dividing both sides of equation (5.7) by the saturated vapor pressure (at the gas temperature T) and making use of equation (1.1), we find

$$S = \left(\frac{T - T_2}{T_1 - T_2}\right)^{\delta} \frac{p_1 - p_2}{p_\infty(T)} + \frac{p_2}{p_\infty(T)} \tag{5.8}$$

where S is the final supersaturation; T, T_1, T_2 are respectively the final temperature of the gas mixture, the initial temperature of the gas mixture, and the temperature of the condensation surface; p_1 the initial vapor pressure in the gas mixture; p_2 the vapor pressure near the condensation surface; $p_\infty(T)$ the saturated vapor pressure above the condensation surface.

It follows from (5.8) that the function $S=f(T)$ has a maximum. The determination of the maximum supersaturation which obtains during vapor condensation on a cold surface is of considerable practical significance, since it enables us to predict fog formation without going into detailed calculations of the condensation process. Substituting $p_\infty(T)$ from (1.2) in (5.8) and examining the function for a maximum in the ordinary way, we find

$$\frac{\delta T_{\max}^2}{E(T_{\max} - T_2)} - \frac{p_2}{p_1 - p_2}\left(\frac{T_1 - T_2}{T_{\max} - T_2}\right) - 1 = 0 \tag{5.9}$$

where p_1, p_2 are the initial vapor pressure in the gas mixture and the vapor pressure near the condensation surface; $T_{\max}$, T_1, T_2 are respectively the temperature of the gas mixture near the supersaturation maximum, the initial temperature, and the temperature near the condensation surface; E the coefficient defined by equation (1.4); δ the coefficient defined by equation (5.6).

Equation (5.9), generally solved by successive approximations, gives the temperature at which the maximum supersaturation is attained. Substituting this temperature in equation (5.8), we find the maximum supersaturation which arises during vapor condensation on a cold surface.

If the vapor pressure near the condensation surface is zero or is very small in comparison with the vapor pressure in the gas stream (this is often the case in practice), the second term in equation (5.8) is less than unity. Equation (5.9) then takes the simpler form

$$\delta T_{\max}^2 - ET_{\max} + ET_2 = 0 \tag{5.10}$$

whence

$$T = \frac{E \pm \sqrt{E^2 - 4\delta ET_2}}{2\delta}$$

The terminal vapor pressure and supersaturation depend on the coefficient δ. This coefficient can be determined from various theoretical and empirical formulas representing heat and mass transfer processes.

For example, in a turbulent gas flow in a pipe

$$\mathrm{Nu}_D = \frac{\beta d}{D} = B\mathrm{Re}^l \cdot \mathrm{Pr}_D^m \tag{5.11}$$

$$\mathrm{Nu} = \frac{\alpha d}{\lambda} = B\mathrm{Re}^l \cdot \mathrm{Pr}^m \tag{5.12}$$

where Nu_D, Nu are the Nusselt numbers of mass and heat transfer, respectively; β the mass transfer coefficient; α the heat transfer coefficient; D the diffusivity; d the pipe diameter; Re the Reynolds number

$$\mathrm{Re} = \frac{wd\rho}{\mu} \tag{5.13}$$

(w is the gas velocity, ρ its density, μ viscosity); Pr_D, Pr are the Prandtl numbers of mass and heat transfer, respectively

$$\mathrm{Pr}_D = \frac{\mu}{\rho D} \tag{5.14}$$

$$\mathrm{Pr} = \frac{c\mu}{\lambda} \tag{5.15}$$

(B, l, m are coefficients; c is the specific heat, λ the thermal conductivity).

Dividing (5.11) by (5.12), we find

$$\frac{\beta}{\alpha} = \frac{D}{\lambda}\left(\frac{\lambda}{\rho c D}\right)^m = \frac{D}{\lambda}\left(\frac{a}{D}\right)^m$$

where a is the thermal diffusivity.

Making use of this expression for $\frac{\beta}{\alpha}$, we write (5.3) and (5.6) in the form

$$\delta = \frac{cM(P-p)}{RT} \cdot \frac{D}{\lambda}\left(\frac{a}{D}\right)^m = \frac{P-p}{P}\left(\frac{D}{a}\right)^{1-m} \tag{5.16}$$

$$\delta = \left(\frac{\rho c D}{\lambda}\right)^{1-m} = \left(\frac{D}{a}\right)^{1-m} \tag{5.17}$$

Equation (5.5) was used in the derivation of (5.16).

For turbulent gas flow in a pipe, we may take $m = 0.4$ /3—5/, and thus

$$\zeta = \left(\frac{D}{a}\right)^{0.6} \tag{5.18}$$

The ratio $\left(\frac{D}{a}\right)^{0.6}$ does not change much with temperature, and it can be assumed constant between narrow temperature limits (Table 5.1).

As the Reynolds number increases, the coefficient m in (5.17) approaches unity /6/, and therefore for $\mathrm{Re} \to \infty$, $\zeta = 1$. The dependence of vapor pressure on temperature (which for a condensation surface of constant temperature is expressed by equation (5.7)) therefore approaches a straight line at high Re, irrespective of the composition of the gas medium and the condensing vapor.

TABLE 5.1. The ratio $\left(\frac{D}{a}\right)^{0.6}$ for various media

Noncondensing medium	Water vapor		Sulfuric acid vapor		
	0°C	100°C	0°C	100°C	200°C
Hydrogen	0.60	0.58	0.42	0.40	—
Air	1.07	1.01	0.58	0.55	0.53
Water vapor.	—	—	1.14	1.02	0.92
Sulfur dioxide	2.13	1.82	1.10	0.93	—

The following differential equation was derived /7/ for the relation of the condensing vapor pressure to temperature in a two-vapor mixture:

$$\frac{dp}{dT} = \frac{\mathrm{Pr}^{2/3}}{\mathrm{Pr}_D^{2/3}} \cdot \frac{l^b - 1}{b} \cdot \frac{p - p_2}{T - T_2}$$

Substituting appropriate expressions for the Prandtl number, we obtain

$$\zeta = \left(\frac{D}{a}\right)^{2/3} \frac{l^b - 1}{b} \tag{5.19}$$

here

$$b = \left(\frac{D}{a}\right)^{2/3} \frac{c_l}{c} \ln \frac{P - p}{P - p_2}$$

where c is the specific heat of the gas mixture; c_l the specific heat of the condensate; P the total pressure of the gas mixture.

Equation (5.19) differs from equation (5.18) in that it contains the factor $\frac{l^b - 1}{b}$, which is greater than unity for a gas mixture with a high content of the condensing vapor. If the vapors are highly diluted by the noncondensing gas ($p < 0.1$ atm), this factor is close to unity and (5.19) reduces to (5.18).

For laminar gas flow /3, 4/

$$\mathrm{Nu} = B\mathrm{Re}^{2/3} \cdot \mathrm{Pr}^{1/3} \left(\frac{d}{L}\right)^{1/3}$$

where B is a coefficient and L the length of the pipe. Proceeding as in the derivation of (5.18) we obtain

$$\delta = \left(\frac{D}{a}\right)^{0.7} \tag{5.20}$$

The coefficient δ for vapor condensation on the external surface of pipes and for other particular cases can be found similarly.

We see from equation (5.17) that the coefficient δ is a function of diffusivity. The diffusivity decreases as the molecular weight is increased; the coefficient δ diminishes appropriately and the maximum supersaturation therefore increases.

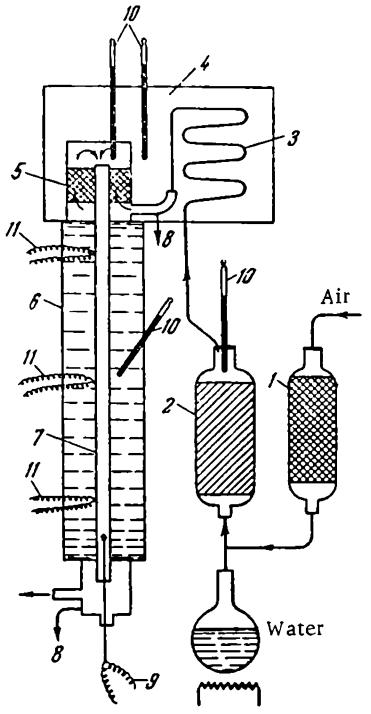

FIGURE 5.1. Setup for measuring supersaturation during vapor condensation on a surface: 1) filter; 2) spray trap; 3) coil pipe; 4) air thermostat; 5) filtering layer; 6) liquid thermostat; 7) condensation pipe; 8) condensed liquid out; 9) temperature and supersaturation probe; 10) thermometer; 11) thermocouples.

It also follows from equation (5.7) that if the thermal conductivity of the condensing gas is high, the coefficient δ is small; this explains the high supersaturation of the vapor condensing on the surface which promotes fog formation.

We see from Table 5.1 that the value of the coefficient δ for water vapor in a turbulent hydrogen medium is half the corresponding value for water vapor in an SO_2 medium.

The validity of the above results is qualitatively confirmed by the high frequency of fog formation during condensation of liquids with high molecular weights and high boiling points. Qualitative corroboration is also provided by other experiments with the condensation of different vapors /8/.

When vapor condenses in a turbulent gas in a pipe, the gas temperature and the vapor pressure fall off in the radial direction from the pipe center to the wall /4/; this variation, however, becomes less pronounced as the Re is increased. The supersaturation displays an opposite trend, i.e., initially it increases from the pipe center to the walls (p. 116). In laminar flow the two trends (the radial decrease of gas temperature and vapor pressure and the radial increase of supersaturation) are more pronounced than in turbulent flow.

The formation of supersaturated water vapor was investigated using the setup shown in Figure 5.1 /2/. Cleaned, water-saturated air was passed through an externally cooled copper pipe. The coolant water was stirred vigorously, and the coefficient of heat transfer between the pipe and the water medium was thus sufficiently high. The pipe wall was therefore maintained at a nearly constant temperature over its length.

The temperature and the humidity of the incoming and the outgoing air was measured in each experiment; the pipe wall temperature was also noted. The coefficient δ was calculated from equation (5.7), and the result was applied to find the supersaturation of the issuing vapor.

In the first series of experiments the air admitted into the condensation pipe was saturated with water vapor; in the second series relatively dry air was passed through. The results of these experiments (Table 5.2) show that the supersaturation invariably increased. The experimental values of δ are in fairly close agreement with the results calculated from the above relations.

When cleaned air was delivered into the pipe, no fog formation was observed in the outgoing air, irrespective of whether supersaturated vapor was present or not. The maximum supersaturation attained in these experiments was less than the critical supersaturation required for the onset of spontaneous condensation. If, however, normal polluted air was used, fog was observed in the emerging stream.

TABLE 5.2. Supersaturation measured during vapor condensation on a surface (1 mm Hg = 133 N/m^2)

Temperature of vapor-air mixture, °C		Vapor pressure in the mixture, mm Hg		Wall temperature, °C	Total pressure P, mm Hg	Reynolds number Re	Supersaturation		δ	
in	out	in	out				S_1 (in)	S_2 (out)	exp.	theor.
24.97	16.40	23.74	15.84	3.6	747	3520	1.00	1.13	1.14	1.07
32.05	20.95	35.70	23.22	4.9	750	3550	1.00	1.25	1.06	1.06
37.05	24.55	47.07	29.66	6.0	737	3570	1.00	1.28	1.15	1.06
34.45	22.20	15.74	11.67	4.7	751	2700	0.39	0.59	1.08	1.08
39.95	25.60	15.84	11.94	4.1	739	3470	0.20	0.49	1.04	1.08
35.10	22.30	16.40	12.10	4.9	748	4330	0.39	0.60	1.03	1.08
40.10	24.69	15.85	12.24	4.0	750	6160	0.30	0.53	1.00	1.08

Table 5.3 lists the values of δ calculated from equation (5.7) using the experimental data published in /9, 10, 11/. The results of the experiments actually correspond to $\delta = 1.07$, and the slight discrepancies are apparently attributable to inaccuracies in measurements of the water content: even small errors in gas humidity have a substantial influence on the coefficient δ as calculated from equation (5.7).

TABLE 5.3. The coefficient δ for water vapor in air (calculated from published data)

Re	δ	Reference	Re	δ	Reference
6 250	1.04	/10, 11/	1 710	1.14	/9/
6 320	1.14	/10, 11/	3 320	0.97	/9/
10 060	1.27	/10, 11/	4 600	0.92	/9/
10 540	1.17	/10, 11/	6 130	0.94	/9/
24 270	1.22	/10, 11/	7 150	0.93	/9/
24 390	1.17	/10, 11/			

It follows from equation (5.8) that, other conditions being constant, the maximum supersaturation decreases as the coefficient δ and the temperature of the condensation surface are increased. Indeed, the ratio

$$\frac{T - T_2}{T_1 - T_2} \tag{5.21}$$

entering equation (5.8) is always less than unity; the factor $\left(\frac{T-T_2}{T_1-T_2}\right)^{\delta}$ in equation (5.8) therefore decreases with increasing δ and the supersaturation diminishes correspondingly. As the temperature is increased, the ratio (5.21) decreases and the supersaturation again diminishes.

The supersaturation in an externally cooled pipe can be substantially lowered by injecting condensation nuclei into the vapor-air mixture. The heat of condensation is released and the temperature of the nucleus surface becomes higher than the temperature of the gas mixture. The warm nuclei enhance further condensation of vapor on their surface.

If the air is seeded with condensation nuclei, an additional factor should be introduced in the right-hand side of equation (5.4) which takes the form /1/

$$\frac{dp}{dT} = K\delta \frac{p-p_2}{T-T_2} \tag{5.22}$$

where K is a coefficient specifying the relative quantity of vapor condensing on the nuclei. This coefficient can be calculated from the formula

$$K = 1 + \frac{p-p_\infty}{p-p_2} \cdot \frac{F_n}{F_w} \tag{5.23}$$

where p_∞ is the saturated vapor pressure above the heated nucleus; F_n the surface of the nuclei per unit pipe length; F_w the wall surface per unit pipe length.

If the temperature of the gas mixture and the supersaturation are known, p_∞ can be determined. Since $K \geqslant 1$, seeding invariably reduces the supersaturation.

A method for the prevention of fog formation has been described in /9/. The gas is heated in a condensation pipe by a wire which is passed axially through the entire pipe. The dependence of vapor pressure on temperature in this case is described by equation (5.22), where the coefficient K is replaced with K_1:

$$K_1 = \frac{\alpha}{d - d_f \frac{t_f - t}{t - t_2}} \tag{5.24}$$

where d is the pipe diameter; d_f the diameter of the heating filament; t_f the temperature of the filament.

It should be noted that equations (5.3), (5.5), and (5.11) can be applied to extend the various results of heat transfer investigations to mass transfer processes (and vice versa). This conversion does not require complex calculations, since the ratios β/α (or β_ρ/α) normally vary between narrow limits. For example, in the common case of evaporative cooling by circulating water /12/

$$\frac{\beta_\rho}{\alpha} = 2.9 - 3.0$$

FORMATION OF SUPERSATURATED VAPOR IN A TURBULENT STREAM BETWEEN SURFACES OF DIFFERENT TEMPERATURE

Stable supersaturated vapor also forms when a vapor-gas mixture is passed between two wetted surfaces of different temperature (see Figure 4.1) /13/. We now consider the processes of mass and heat transfer in a turbulently moving gas between two surfaces. The symbols and notations are as in Chapter Four.

Since turbulent gas flow entails intensive mixing, we may assume to first approximation that T and p are constant across the turbulent core, changing downstream only /3/. Similar assumption applies for the supersaturation S.

The quantity of vapor condensing on the upper and the lower surfaces, dg_1 and dg_2, and the quantities of heat dQ_1 and dQ_2 are expressed by equations (5.1) and (5.2):

$$dg_1 = \beta_p f_1 (p_1 - p)\, d\tau \qquad dQ_1 = \alpha f_1 (T_1 - T)\, d\tau$$

$$dg_2 = \beta_p f_2 (p_2 - p)\, d\tau \qquad dQ_2 = \alpha f_2 (T_2 - T)\, d\tau$$

where f_1 and f_2 are the areas of the upper and the lower surfaces.

Adding dg_1 and dg_2, dQ_1 and dQ_2 and remembering that $f_1 = f_2 = F/2$, we obtain the following expressions for the quantities of vapor (dg) and heat (dQ) released into the gas stream in the time $d\tau$:

$$dg = \beta_p F (\bar{p} - p)\, d\tau \tag{5.25}$$

$$dQ = \alpha F (\bar{T} - T)\, d\tau \tag{5.26}$$

where

$$\bar{p} = \frac{1}{2}(p_1 + p_2) = \frac{1}{2}[p_\infty(T_1) + p_\infty(T_2)] \tag{5.27}$$

$$\bar{T} = \frac{1}{2}(T_1 + T_2) \tag{5.28}$$

It follows from (5.25) and (5.26) that mass and heat transfer between the gas stream and the two surfaces of different temperature is expressed by the same equations as in the case of two surfaces of equal temperature, provided that the mean vapor pressure $\bar{p}$ at the surface and the mean temperature $\bar{T}$ of the surface are substituted in the appropriate places.

At a fairly large distance from the gas inlet, the vapor pressure, the temperature, and the supersaturation are all constant. The constant vapor pressure $\bar{p}$ is expressed by equation (5.27), the temperature $\bar{T}$ by equation (5.28), and the constant supersaturation S_v is expressed by the relation

$$S_v = \frac{p_\infty(T_1) + p_\infty(T_2)}{2p_\infty(T)} \tag{5.29}$$

The length l of the initial section, where the thermodynamic parameters have not yet attained the constant values of $\bar{p}$, $\bar{T}$, and S_v, can be found from the following equation, which has been derived /13/ on the basis of data on mass /4/ and heat /3/ transfer:

$$p = p + (p_0 - \bar{p})\, l^{-M_D l/h} \tag{5.30}$$

$$T = T + (T_0 - \bar{T})\, l^{-Ml/h} \tag{5.31}$$

where p_0 and T_0 are the initial vapor pressure and gas temperature:

$$M_D = 0.023\ \mathrm{Re}^{-0.2} \cdot \mathrm{Pr}_D^{-0.6};$$
$$M = 0.023\ \mathrm{Re}^{-0.2} \cdot \mathrm{Pr}^{-0.6};$$

Pr_D and Pr the Prandtl numbers of heat and mass transfer (equations (5.14) and (5.15)); h the distance between the two surfaces. In a highly turbulent flow M_D and M are equal to a few hundreds, and the region of constant supersaturation is therefore established at a distance of a few h from the gas inlet.

The formation of supersaturated vapor between two surfaces of different temperature is utilized in the design of a current-type diffusion cloud chamber. At a certain distance from the inlet orifice of the chamber forms a zone of stable supersaturation, which is homogeneous in the longitudinal and the radial directions.

Table 5.4 gives the supersaturation of the water vapor in the stable zone as calculated from equation (5.29) for various temperatures of the upper and the lower surfaces /13/. We see that the supersaturation between the two surfaces may reach substantial values, exceeding S_{cr}.

TABLE 5.4. Supersaturation between wetted surfaces of different temperature

Temperature of lower surface t_2, °C	Supersaturation for various temperatures of the upper surface t_1, °C			
	40	60	80	100
+ 20	1.1	1.5	2.0	2.6
0	1.7	2.5	3.2	4.1
- 20	3	4.3	5.6	6.9

Experiments have shown /13/ that the current-type diffusion chamber is a highly effective filter for the cleaning of air or gases: it traps the intractable minute particles precipitating, in particular, the fine silicate dust. In the supersaturated vapor of the diffusion chamber the suspended particles grow rapidly by vapor condensation and then settle under their own gravity or are separated in gas filters. For example, if the distance between the cold and the hot walls is 5 cm, the channel length 200 cm, the air velocity 5 m/sec, $t_1 = 50$ °C, and $t_2 = 15$ °C, the dust is converted into a monodisperse fog with droplets of $\sim 5\mu$ radius.

The current-type diffusion chamber can be used to obtain monodisperse fogs and to investigate the properties of aerosols and ionizing particles. The condensational growth of suspended particles in a turbulent supersaturated medium (with constant mixing along the stream and constant turbulence parameters) was actually investigated in a diffusion chamber of this kind.

FORMATION OF SUPERSATURATED VAPOR IN THE BOUNDARY LAYER

The processes occurring in the boundary layer of a turbulent stream have been insufficiently studied and it is therefore impossible to establish the variation of supersaturation across the boundary layer and to determine the conditions of nucleation of a new phase. We therefore proceed with a qualitative treatment of the boundary layer which may help in practical considerations and analysis.

The motion of the gas in the boundary layer is the subject of numerous theories and hypotheses. It has been suggested /14/ that the turbulent flow does not disappear abruptly in the boundary layer (the viscous lamina adjoining the wall), but decays gradually toward the channel wall. No eddy pulsations originate in the boundary layer: they are injected from the outside, propagating from the turbulent core. The gas temperature in the boundary layer, T_b, and the vapor pressure p_b are highly variable across the layer. At the outer surface of the boundary layer $x=z$ (where x is the distance from the condensation surface and z the thickness of the boundary layer), the temperature T and the vapor pressure p have the same values as in the turbulent stream. Near the condensation surface ($x = 0$), the gas temperature is equal to the temperature T_2 of the condensation surface and the vapor pressure is the saturated vapor pressure above the condensation surface (p_2). In the first approximation, T_b and p_b are linear functions of x (in reality, however, these are not perfect linear functions, since the gas velocity in the boundary layer $w \neq 0$). The dependence of supersaturation on temperature (and thus on x) in the boundary layer is expressed by the equation

$$S = \frac{T_b - T_2}{T - T_2} \cdot \frac{p - p_2}{p_\infty(T_b)} - \frac{p_2}{p_\infty(T_b)} \qquad (4.12)$$

where $p_\infty(T_b)$ is the saturated vapor pressure above a plane surface at the temperature T_b.

It follows from (4.12) (see p. 95) that the supersaturation is variable across the boundary layer, passing through a maximum. Since the gas temperature and the vapor pressure in the turbulent core and near the condensation surface vary along the pipe, the supersaturation profile in the boundary layer and the coordinate x at which the maximum supersaturation S_{max} is attained are different in different sections of the pipe; the value of S_{max}, however, remains constant. As the gas moves along the cooled surface, the zone of maximum supersaturation shifts toward the turbulent core (Figure 5.2a), and supersaturations $S<S_{max}$ are gradually established in the boundary layer.

In laminar flow the processes which have been described for the boundary layer extend over the entire pipe cross section (Figure 5.2b).

If $S_{max}>S_{cr}$, embryos form in the boundary layer and fog droplets appear in the initial section (at $l = 0$), before the section with $S \approx S_{cr}$ is reached.

The conditions of fog formation in the boundary layer can be expressed to first approximation by the relations which have been derived in Chapter Four for the condensation of vapor between two plates of different temperature (see Figures 4.1 and 4.3). Fog formation in the boundary layer enhances the rates of mass and heat transfer in the layer, which is confirmed by the following considerations.

The diffusive current of vapor from the turbulent core to the condensation surface is intensified by the formation of liquid droplets and their condensation growth. The droplets are incapable of penetrating from the boundary layer into the turbulent core, and they settle on the pipe wall due to thermophoresis, diffusion, and Stefan flow /15—17/. In a turbulent flow with Re > 10,000 (the case of greatest practical significance) the boundary layer is very thin /3/:

$$z = 64.2 \frac{d}{\mathrm{Re}^{7/8}}$$

where d is the pipe diameter, m. The temperature and vapor concentration gradients in this layer are high, and the thermophoretic and diffusive forces driving the droplets to the wall are correspondingly strong /18/. The precipitation of the droplets on the pipe wall is also enhanced by the decaying eddy pulsations which infiltrate into the boundary layer from the turbulent core /14/.

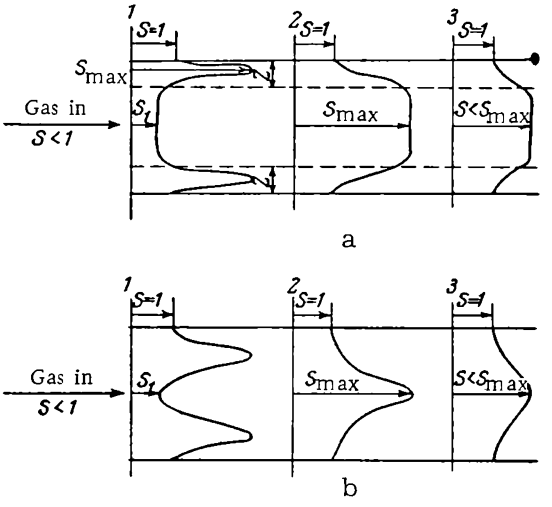

FIGURE 5.2. Supersaturation across the pipe for turbulent (a) and laminar (b) flow:
1) inlet section; 2) section with $S = S_{max}$ at midstream;
3) section with $S < S_{max}$ at midstream.

The rate of heat transfer is increased by the heat of condensation which is released in the gas volume and the heating of the gas in the boundary layer. These factors increase the temperature difference between the gas and the condensation surface.

As Re is decreased, the boundary layer becomes thicker and some droplets may start escaping into the turbulent stream. If in the turbulent stream $S < S_r$ (where S_r is the equilibrium supersaturation above a droplet), the escaping droplets will evaporate, the rate of condensation will diminish, and the total quantity of fog will increase. On the other hand, if $S > S_r$, the droplets will grow in the turbulent stream by condensation, and the supersaturation will correspondingly decrease.

When the liquid evaporates from the surface ($T_2 > T$), the droplets forming in the boundary layer are driven by thermophoresis, diffusion,

and Stefan flow away from the condensation surface and into the turbulent core of the stream. Depending on the S in the turbulent core, these droplets evaporate suppressing further condensation, or grow and intensify the rate of condensation.

FORMATION OF FOG DURING VAPOR CONDENSATION ON A SURFACE

Vapor condensation on a surface is very frequently observed in nature, in the laboratory, and in various industrial processes. It is often accompanied by the formation of supersaturated vapor and fog, but this aspect of the matter is generally ignored. It should be noted that the calculations of the condensation of water vapor from a vapor-air mixture /19/ and of ethyl acetate vapor from its mixture with nitrogen /20/ gave inaccurate results because the formation of supersaturated vapor was neglected. In those calculations, the entire condensation column was divided into several arbitrary sections and the equations of mass and heat transfer were solved for each of these sections separately. It was always assumed that the saturation point was reached after the particular section being considered, and yet supersaturated vapor actually formed in the first few sections, the degree of supersaturation varying along the column. The calculations failed to take this factor into consideration and the results are therefore inaccurate.

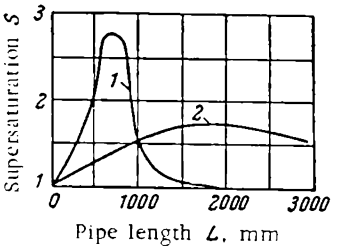

FIGURE 5.3. Supersaturation along the condenser pipe: 1) temperature of coolant water 20 °C; 2) temperature of coolant water 40 °C.

Equation (5.4) which expresses the dependence of vapor pressure on the temperature of the gas mixture is applicable when $S<S_{cr}$ and the formation of embryos can be neglected. The curves plotted in Figure 5.3 correspond to these particular conditions; they trace the supersaturation as a function of cooling and condensation. The curves represent the results of calculations for water vapor condensing from an air mixture in a pipe; the temperature of the gas mixture at the inlet is 95 °C, the water vapor pressure 608 mm Hg (saturated vapor), the total pressure 760 mm Hg, the temperature of the coolant water 20 and 40 °C.

We see from Figure 5.3 that the supersaturation first increases, reaches a maximum and then falls off; the peak value of the supersaturation is higher when the coolant temperature is lower.

The conditions are entirely different for $S>S_{cr}$, since p and T change additionally due to the nucleation of embryos and their condensational growth. This aspect is confirmed by the curves in Figure 5.4 which plot the supersaturation of sulfuric acid vapor condensing in a pipe (p. 136). We see from the figure that curve 1, which corresponds to hypothetical condensation without nucleation, and curve 2, representing the true process, diverge at the point $L = 640$ mm where curves 1 and 3 meet (when $S=S_{cr}$).

Once the maximum true supersaturation has been attained (curve 2), S decreases rapidly due to the reduction of vapor pressure and the increase of temperature with the condensational growth of the embryos and the droplets.

Fog formation as the result of vapor condensation on a surface is complicated by the superposition of several processes, and the general expressions for S, p, and T are therefore difficult to derive. These simultaneous processes have been studied insufficiently and no satisfactory theory is available.

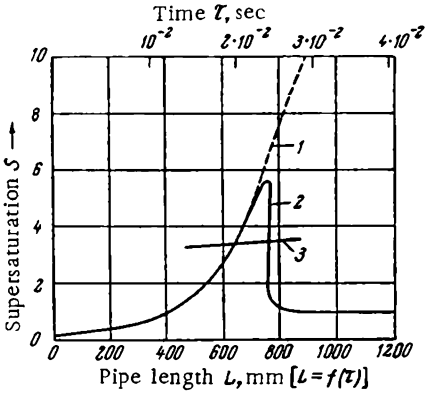

FIGURE 5.4. Variation of supersaturation along the pipe:
1) supersaturation calculated ignoring nucleation (from (5.4)); 2) true supersaturation; 3) critical supersaturation.

We shall now derive an equation for dp/dT which gives some idea of the relation among the process indices during vapor condensation in an externally cooled pipe with $S>S_{cr}$.

The combined rate at which vapor is converted to liquid by simultaneous condensation in the gas volume and on the surface is /21, 22/

$$\frac{dg}{d\tau} = \beta_p F [p - p_\infty(T_2)] + \frac{4\pi M_V D r v N}{RT\varphi} [p - p_r(T_r)] + 4\frac{\pi r_e^3 \rho v I}{3} \qquad (5.32)$$

where g is the mass of condensed vapors, g; τ time, sec; β_p mass transfer coefficient, $g \cdot cm^{-2} \cdot sec^{-1} (mm\ Hg)^{-1}$; F the condensation surface, cm^2; r the radius of the droplets in the gas, cm; r_e the radius of the embryos, cm; v the volume of gas passing through the pipe, cm^3; N the number of droplets per unit gas volume (the number density of the droplets), cm^{-3}; φ a coefficient which allows for the effect of the droplet radius on the rate of vapor condensation on the droplet surface (equation (1.68)); I the rate of nucleation, $cm^{-3} sec^{-1}$,

$$I = \frac{dn}{d\tau} \qquad (5.33)$$

(n is the number of droplets, in cm^{-3}, which form in a certain time).

The first term in the right-hand side of (5.32) is the rate of vapor condensation on the wall surface, the second term is the rate of condensation on the surface of the existing droplets in the gas mixture, and the third term is the rate at which vapor is converted to liquid by the nucleation mechanism. Since the embryos are very small (with a radius of some 10^{-7} cm), the quantity of liquid tied up as embryos is insignificant and the last term in the right-hand side of (5.32) is normally omitted.

Making use of the dependence of the vapor mass on the partial pressure (equation (a), p. 106), we write (5.32) in the form

$$\frac{dp}{d\tau} = \frac{M_{\Pi}(P-p)^2}{g_{\Pi}M_V P}\left\{\beta_p F\left[p - p_{\infty}(T_2)\right] + \frac{4\pi DrvN}{RT\varphi}\left[p - p_r(T_r)\right]\right\} \tag{5.34}$$

The rate at which the gas loses heat is expressed by the equation

$$\frac{dQ}{d\tau} = \alpha F(T - T_2) - \frac{4\pi M_V DrvNL}{RT\varphi}\left[p - p_r(T_r)\right] - \frac{4\pi r_c^3 \rho v l L}{3} \tag{5.35}$$

where Q is the total quantity of heat lost by the cooling gas, cal; α the heat transfer coefficient, cal·cm^{-2}·sec^{-1}·deg^{-1}; L the latent heat of condensation, cal/g.

The first term in the right-hand side of (5.35) is the quantity of heat lost by the gas to the cooling surface; the second term is the heat of condensation released by the vapor condensing on the surface of the existing droplets in the gas; the third term is the heat of condensation released by nucleation. The third term is negligible in comparison with the first two terms.

Making use of the relation of the heat lost by the gas to its temperature T (equation (c), p. 106), we write (5.35) in the form

$$\frac{dT}{d\tau} = \frac{M_{\Pi}(P-p)}{g_{\Pi}PcM}\left\{\alpha F(T - T_2) - \frac{4\pi M_V DrvNL}{RT\varphi}\left[p - p_r(T_r)\right]\right\} \tag{5.36}$$

From (5.34) and (5.36) we have

$$\frac{dp}{dT} = \frac{Mc_p^{\beta}(P-p)}{M_V^{a}} \cdot \frac{\left[p - p_{\infty}(T_2)\right] - \dfrac{4\pi M_V DrvN}{RT\varphi\beta_p F}\left[p - p_r(T_r)\right]}{(T - T_2) - \dfrac{4\pi M_V DrvNL}{RT\varphi\alpha F}\left[p - p_r(T_r)\right]} \tag{5.37}$$

For a pipe

$$F = \pi dl \tag{a}$$

$$v = \frac{\pi d^2 w}{4} \tag{b}$$

$$\beta_p = b\frac{D}{d}\mathrm{Re}^m \cdot \mathrm{Pr}_D^n = bD\mathrm{Pr}_D^n \frac{w^m}{\nu^m d^{1-m}} \tag{c}$$

$$\alpha = b\frac{\lambda}{d}\mathrm{Re}^m \cdot \mathrm{Pr}^n = b\lambda\mathrm{Pr}^n \frac{w^m}{\nu^m d^{1-m}} \tag{d}$$

where d is the internal diameter of the pipe, cm; w the gas velocity, cm/sec; Pr_D,Pr the Prandtl numbers for mass and heat transfer, respectively; ν the kinematic viscosity of the gas, cm^2/sec; b, m, n constant coefficients.

Making use of equation (5.3) and substituting the various parameters from equations (a)—(d) in (5.37), we obtain after some manipulations

$$\frac{dp}{dT} = \delta\frac{\left[p - p_{\infty}(T_2)\right] + AC}{(T - T_2) - BC} = \delta\frac{\left[p - p_{\infty}(T_2)\right]}{(T - T_2)} \cdot \frac{1 + \dfrac{AC}{p - p_{\infty}(T_2)}}{1 - \dfrac{BC}{T - T_2}} \tag{5.38}$$

$$A = \frac{M_V \pi \nu^m w^{1-m} d^{2-m} r N}{RT\varphi b \mathrm{Pr}_D^n l} \tag{5.39}$$

$$B = \frac{M_V \pi D \nu^m w^{1-m} d^{2-m} r N L}{RT\varphi b \lambda \mathrm{Pr}^n l} \tag{5.40}$$

$$C = p - p_r(T_r) \tag{5.41}$$

The following ratios entering equations (5.39) and (5.40) remain constant during nucleation:

$$\frac{M_V \pi \nu^m}{RTb\mathrm{Pr}_D^m} = \varepsilon \tag{e}$$

$$\frac{M_V T \gamma^m DL}{RTb\lambda \mathrm{Pr}^n} = \varepsilon^1 \tag{f}$$

For a turbulent flow of a gas, $m = 0.8$. Therefore

$$A = \frac{\varepsilon w^{0.2} d^{1.2}}{l} \cdot \frac{rN}{\varphi} \tag{g}$$

$$B = \frac{\varepsilon' w^{0.2} d^{1.2}}{l} \cdot \frac{rN}{\varphi} \tag{h}$$

When S is low and no embryos are present in the gas, $AC=BC=0$. In this case equation (5.38) reduces to equation (5.4) which has been analyzed previously (p. 112). It follows from this analysis that the supersaturation is decreased by increasing either the temperature of the condensation surface T_2 or the temperature of the incoming gas.

The formation of droplets raises the derivative dp/dT and lowers the supersaturation S, so the rate of nucleation decreases. The products AC and BC are initially small and do not have a noticeable influence on the resulting supersaturation. However, as N and r increase and φ decreases, AC and BC increase substantially. The supersaturation S sharply subsides and the nucleation stops abruptly. Depending on vapor concentration and the cooling arrangement, AC and BC may become quite high, possibly surpassing $p-p_\infty(T_2)$ and $T-T_2$ in equation (5.38).

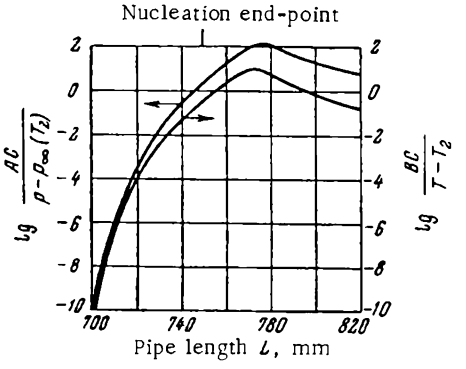

FIGURE 5.5. Variation of $\frac{AC}{p-p_\infty(T_2)}$ and $\frac{BC}{T-T_2}$ along the pipe.

Figure 5.5 plots the variation of the two ratios $\frac{AC}{p-p_\infty(T_2)}$ and $\frac{BC}{T-T_2}$ along a pipe in which sulfuric acid vapor condenses (p. 126). The first of the two

quantities is the mass ratio of the vapor condensing on the droplets to the vapor condensing on the pipe surface; the second is the ratio of the heat of condensation released in the droplets to the quantity of heat transferred to the condensation surface. We see from Figure 5.5 that the two ratios continue increasing when the nucleation has stopped. This is explained by the intensive condensation of vapor on the surface of the droplets. When the nucleation stops (750 mm downstream along the pipe), the quantity of vapor condensing on the droplets is approximately equal to that condensing on the pipe wall. At a distance of 775 mm from the inlet, nearly 100 times as much vapor condenses on the droplets as on the pipe wall. The ratio of the quantity of heat released in the droplets to the quantity of heat transferred to the walls behaves analogously.

If the gas carries condensation nuclei (dust and various suspended particles) and the rate of nucleation is negligible, the number density N remains constant. All the droplets grow by condensation to a substantial size and eventually acquire a nearly constant radius, so that $\varphi \approx 1$. Equation (5.38) is simplified and can be integrated without difficulty.

Equation (5.38) applies not only for a condenser pipe, but also for other kinds of condensers (packed spray towers, bubbling equipment, grid towers, froth systems, etc.) provided that appropriate conversion coefficients are introduced in the equations.

The equation for dp/dT is derived above by a fairly cumbersome method and its solution involves considerable difficulties. The relation of S to τ is even more complicated, because condensation of vapor on a surface occurs simultaneously with fog formation. In order to find the derivative $dS/d\tau$, the derivatives $dp/d\tau$ and $dT/d\tau$ should be inserted from equations (5.34) and (5.36) into (1.7).

DROP SIZE DISTRIBUTION AND NUMBER DENSITY OF FOG IN PIPE CONDENSERS

The theoretical results of the previous section are sufficient to determine the conditions under which any given proportion of vapor will condense without fog formation. However, it is often more economic to speed up the process, so that part of the vapor condenses in the gas volume and fog forms. The fog is then separated by porous, fibrous, centrifugal (cyclones), or electrostatic filters and precipitators. The filtering efficiency, however, increases with droplet radius. Therefore, if fog formation is not prevented, the actual conditions should favor the formation of large droplets, which are easily trapped by the filters.

Although the gas normally contains condensation nuclei (dust particles, liquid droplets, etc.), they do not have a noticeable influence on fog formation in industrial processes, since the concentration of suspended particles seldom exceeds $10^4\,cm^{-3}$. Highly supersaturated vapor therefore forms in the large spaces between the nuclei and homogeneous condensation begins (p. 36): the concentration of the primary droplets which form in this way is thousands and even hundreds of thousands of times greater than the original number density of the condensation nuclei. In industry the number of condensation nuclei is additionally reduced when the gas is being processed

(in heat exchangers, scrubbing towers, etc.). The incoming gases are sometimes specially cleaned and filtered, so that all things considered, the content of condensation nuclei in the process gas is ignored in all what follows.

Vapor is condensed in apparatus of three main types: pipe (or surface) condensers, packed spray towers, and bubblers (bubble caps, bubbling pipes, grid-packed towers, froth systems, etc.).

The mechanism of vapor condensation is the same whether a pipe condenser, a spray tower, or a bubbler is used: the gas is invariably cooled by contact with the surface of a colder liquid. In a pipe condenser this surface is provided by the film of the condensed liquid which forms on the pipe walls and drips in the downward direction; in spray towers the spray provides the cold condensation surface; in bubblers the vapor condenses on the inner surface of the gas bubbles rising through the liquid layer.

In these various systems, the supersaturation increases as the gas is cooled; if the supersaturation becomes sufficiently high vapor will start condensing spontaneously or on existing condensation nuclei. The liquid droplets forming in the gas volume will grow into fog.

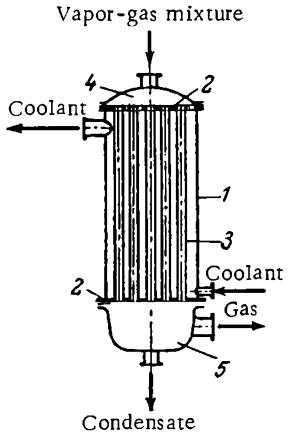

FIGURE 5.6. Pipe condenser: 1) body; 2) grids; 3) pipes; 4) upper chamber; 5) lower chamber.

Although in principle the mechanism of fog formation is the same in the different condensers, each has its own specific features which cannot be ignored.

Pipe condensers are widely used in industry for the separation of vapor from gas, since they are simple in design, highly efficient, and offer low hydraulic resistance to the gas stream. Figure 5.6 is a schematic diagram of a pipe condenser. The vertical cylindrical body 1 has two grids 2 to which the pipes 3 are attached. The vapor-gas mixture is delivered to the upper chamber 4; it passes through the pipes to the lower chamber 5, and leaves through a lateral pipe. The liquid condensing in the pipes is collected in the lower chamber and drained. A gas or liquid coolant circulates between the pipes, in parallel with the gas stream or countercurrently. The condenser components are manufactured from different materials, depending on the particular coolant to be employed; in some cases the surface which comes in direct contact with the gas mixture or the coolant is protected by a coat of varnish, enamel, etc.

The process can be speeded up by providing special turbulizing devices in the pipes or between them. These devices do not alter the basic processes which take place in the condenser. They only change the supersaturation, which is made to rise until it reaches a certain maximum, and then decreases (see Figure 5.3). If the maximum supersaturation is sufficiently high, homogeneous condensation begins and embryos start forming. Some vapor is converted to liquid by this spontaneous mechanism and more condensate forms on the surface of the pipes and the surface of the embryo droplets. Figure 5.7 schematically illustrates the condensation of vapor on the wall of the condenser pipe simultaneously with its condensation in the gas volume, on the spontaneously forming embryos.

We see from the above data that the various process parameters are complexly related among themselves; no satisfactory analytical expressions are available for this relation, so it is hardly possible to proceed with rigorous calculations of drop size distribution and number density of the fog forming under these conditions. And yet these data are highly significant for the solution of various practical problems. We therefore give in the next subsection a detailed description of the approximate numerical technique /19, 21/ for the calculation of drop size distributions and number densities of the fog in a pipe. The accuracy of this technique is sufficient for the purposes of various technological processes. (The approximate numerical technique for adiabatic expansion is described on p. 51.)

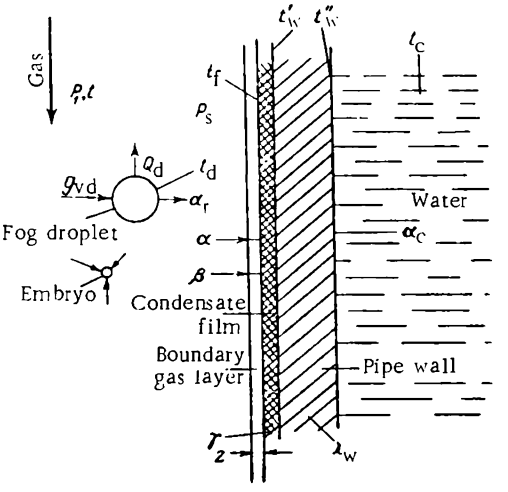

FIGURE 5.7. Vapor condensation on the pipe wall and on spontaneously forming embryos: α is the coefficient of heat transfer from the gas to the pipe; α_r the coefficient of radiative heat transfer from the droplets to the pipe; α_c the coefficient of heat transfer from the pipe to the coolant; β vapor condensation coefficient; τ thermal conductivity of the liquid film; λ_w thermal conductivity of the pipe wall; t, t_f, t'_w, t''_w, t_c, t_d the temperatures of the gas, the liquid film, the internal and the external pipe walls, the coolant, and the droplet, respectively; p_1, p_s vapor pressure in the gas and near the condensation surface; g_{vd} mass of vapor condensing on the surface of the droplets; q_d the quantity of heat transmitted from the droplets to the gas; z the thickness of the boundary layer.

In these calculations the entire height of the pipe (the calculations are made for a single pipe in the condenser) is divided into several sections (layers), each characterized by constant thermodynamic indices. The sections have different lengths: the shortest section is that where nucleation occurs (droplets form and grow by condensation), since homogeneous condensation is characterized by a fairly rapid variation of the process parameters along the pipe. Since the rate of droplet formation is essentially dependent on the degree of supersaturation, we first determine the

supersaturation of the vapor entering each successive section and then decide on the convenient length of that section.

This approximate technique was applied to calculate the condensation of glycerine and sulfuric acid vapors in a water-cooled pipe. The calculations were made twice: using the nucleation rates from the Frenkel equation (1.53) and from the Becker-Doering equation (1.34). The details are reproduced in the next subsection, p. 127.

Table 5.5 lists the initial data used in the calculations, and Table 5.6 presents the results of the calculations. We see from Table 5.6 that the number density of the fog obtained using the Becker-Doering equation is substantially higher than the number density obtained using the Frenkel equation.

TABLE 5.5. Initial data for the calculation of glycerine and sulfuric acid condensation

	Glycerine	H_2SO_4
Gas temperature at pipe inlet t_0, °C	265	300
Vapor pressure at gas inlet p_0, mm Hg	5.35	30.2
Gas volume at pipe inlet v_0, m^3/hr (at NTP)	6.560	7.815
Total gas pressure P, mm Hg	760	760
Internal pipe diameter d, mm	13	13
Temperature of condensation surface, °C	40	40

TABLE 5.6. Results of calculations for the condensation of glycerine and sulfuric acid vapors in a pipe

	Glycerine		Sulfuric acid	
	Frenkel equation (1.53)	Becker-Doering equation (1.34)	Frenkel equation (1.53)	Becker-Doering equation (1.34)
Number density of fog N, cm^{-3} (NTP)	$1.7 \cdot 10^8$	$1.2 \cdot 10^{10}$	$1.6 \cdot 10^8$	$7.5 \cdot 10^8$
Droplet radius (mean) $\bar{r}$, cm	$1.2 \cdot 10^{-5}$	$2.8 \cdot 10^{-6}$	$4.5 \cdot 10^{-5}$	$2.6 \cdot 10^{-5}$
Mass concentration of fog g, g/cm^3 (NTP)	$1.5 \cdot 10^{-6}$	$1.4 \cdot 10^{-6}$	$1.1 \cdot 10^{-4}$	10^{-4}
Maximum supersaturation S_{max}	122	45	5.7	4.8
Maximum nucleation rate I_{max}, $cm^{-3} \cdot sec^{-1}$	$1.9 \cdot 10^{10}$	$3.3 \cdot 10^{12}$	$3.1 \cdot 10^{11}$	$1.1 \cdot 10^{13}$

As the vapor pressure at the pipe inlet decreases (other conditions being constant), the number density of the fog increases and the mean droplet radius diminishes. The following data were obtained for the sulfuric acid vapor of 300 °C initial temperature entering a pipe with wall temperature of 40 °C:

	H_2SO_4 vapor pressure in the gas at pipe inlet, mm Hg			
	0.1	1.0	5.0	30.2
Number density of fog N, cm^{-3}	$1.7 \cdot 10^6$	$4 \cdot 10^{10}$	$5.9 \cdot 10^9$	$1.6 \cdot 10^8$
Mean droplet radius $\bar{r}$, cm	$1.1 \cdot 10^{-6}$	$1.8 \cdot 10^{-6}$	$7.1 \cdot 10^{-6}$	$4.5 \cdot 10^{-5}$

This dependence is explained by the following fact: at low p, nucleation starts later and persists for a longer time, since the droplets grow slowly, and the maximum supersaturation reaches a higher peak value (Figure 5.8).

At a certain p, the number density N reaches a maximum and then drops to $N = 0$ when p is further decreased. This is so because at the particular p the maximum supersaturation $S_{max} < S_{cr}$.

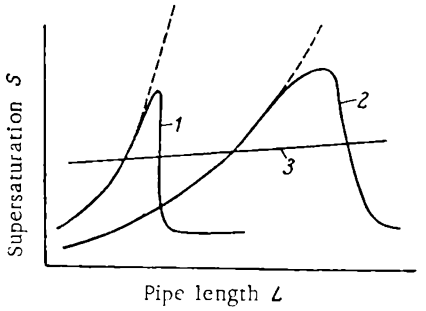

FIGURE 5.8. Variation of supersaturation along the pipe for different initial vapor pressures:
1, 2) supersaturation for p_1' and p_1'' ($p_1' > p_1''$);
3) critical supersaturation.

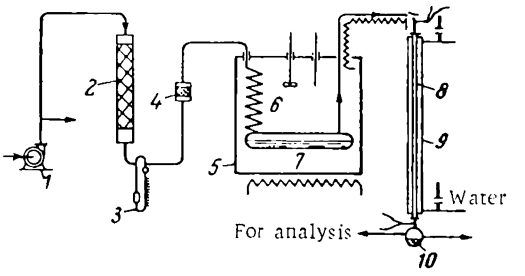

FIGURE 5.9. Laboratory setup for investigating vapor condensation in a pipe:
1) air pump; 2) cotton wool filter; 3) flowmeter; 4) metal grid filter; 5) thermostat; 6) coil pipe; 7) evaporator; 8) pipe condenser; 9) coolant; 10) condensate.

Several experiments were carried out in order to assess the accuracy of the calculations (and the reliability of the approximate numerical technique) and to determine which of the two theoretical equations for the nucleation rate I is the more reliable. In these experiments, the setup shown in Figure 5.9 was used to measure the number density and the mean radius of the fog droplets forming in the pipe condenser /23/. The experimental conditions were consistent with the initial data of the calculations (see Table 5.5).

A measured air volume is cleaned from suspended particles and ions in the cotton wool filter 2 and in the metal grid filter 4; the cleaned air is delivered to the thermostat 5 where it is heated in the coil pipe 6 and saturated with vapor in the evaporator 7. The air is then passed through a heated glass pipe to the condenser 8 (a pipe 2 m long, with an internal diameter of 13 mm and an external diameter of 16 mm) which is enclosed in a cooling jacket 9 (with an internal diameter of 45 mm). Water circulates in the upward direction in the space between the jacket and the condenser pipe. The condensate is collected in the container 10, and the noncondensing gases are ejected into the atmosphere.

The temperature of the condensation surface was calculated from the temperature difference of the incoming and the outgoing coolant water. It follows from the calculation that the temperature of the condenser surface is nearly constant along the pipe; the constancy of the wall temperature is particularly significant in the region of nucleation.

The vapor content is measured in the air entering the condenser 8, whereas the mass concentration and the number density of the fog are determined at the outlet (the samples are withdrawn from the container 10). Since the number density of the fog at the pipe outlet is high (approximately 10^8 cm^{-3}), the gas sample is diluted in a proportion of 1 part to 300—400 parts of clean air and is then delivered to the ultramicroscope /24/ for the counting of the fog droplets. The root-mean-cube radius of the fog droplets is calculated from the measured mass concentration and number density.

The completeness of the separation of the suspended particles and gas ions in filters 2 and 4 is not controlled in these experiments. That the separation is effective follows from the results of calculations which show that a residual content of up to 10^4 particles per cm^3 in the air has no substantial effect on the number density of droplets at the outlet, which is of the order of $10^8\ cm^{-3}$ (Table 5.7).

TABLE 5.7. Experimental data on the condensation of glycerine and sulfuric acid vapors in a pipe

	Glycerine	H_2SO_4
Number density of fog N, cm^{-3} (NTP)	$4.5 \cdot 10^7$	$8.1 \cdot 10^8$
Mean droplet radius $\bar{r}$, cm	$3.3 \cdot 10^{-5}$	$2.5 \cdot 10^{-5}$
Mass concentration of fog g, g/cm^3 (NTP)	$8.8 \cdot 10^{-6}$	10^{-4}
Gas temperature at pipe inlet, °C	265	309
Vapor pressure at pipe inlet, mm Hg	5.0	27.4

The results of the experiments with glycerine and sulfuric acid in a pipe cooled to 40 °C are presented in Table 5.7. Table 5.8 gives some calculated and experimental data for comparison purposes.

TABLE 5.8. Calculated and experimental data on condensation in a pipe

	Experimental	Calculated	
		Frenkel (1.53)	Becker-Doering (1.34)
Glycerine			
Number density of droplets N, cm^{-3}	$4.5 \cdot 10^7$	$1.7 \cdot 10^8$	$1.2 \cdot 10^{10}$
Mean droplet radius $\bar{r}$, cm	$3.3 \cdot 10^{-5}$	$1.2 \cdot 10^{-5}$	$2.8 \cdot 10^{-6}$
Sulfuric acid			
Number density of fog N, cm^{-3}	$8.1 \cdot 10^8$	$1.6 \cdot 10^8$	$7.5 \cdot 10^8$
Mean droplet radius $\bar{r}$, cm	$2.5 \cdot 10^{-5}$	$4.5 \cdot 10^{-5}$	$2.6 \cdot 10^{-5}$

The experimental results show that the number density decreases and the droplet radius increases as the temperature of the condensation surface is increased (other conditions being constant). These results are consistent with the theoretical analysis of equation (5.4).

We see from Table 5.8 that the experimental data for glycerine are in better agreement with the Frenkel equation, while the data for sulfuric acid are better approximated with the Becker-Doering equation.

In evaluating these results we should remember that the saturated vapor pressure above 96.5% H_2SO_4 used in the calculations is not exact: it has been arrived at by interpolation of unverified data /25/.

The experimental and the theoretical figures show a satisfactory fit. We must remember that from the time when nucleation begins and to the end-point where the number density is measured the volume of the embryos

will have increased approximately by a factor of 10^8 due to their condensational growth. Therefore, even slight inaccuracies in each of the numerous equations used to determine the quantity of vapor condensing on the droplets, the temperature of the droplets, etc., eventually lead to a noticeable divergence between the theoretical and the experimental data.

Calculation of drop size distribution and number density of fog forming when H_2SO_4 vapor condenses in a pipe

Conversion coefficient to SI units: 1 mm Hg = 133 N/m^2, 1 kcal = 4.19 kJ, 1 dyne = 10^{-5} N. The initial data and symbols are listed in Table 5.5 and additionally defined in text, if necessary.

Sulfur trioxide and water vapor occur in dissociated form at high temperature. When the gas mixture is cooled, SO_3 and water vapor combine to form sulfuric acid vapor which gradually condenses. This process is represented by the equations

$$SO_3 + H_2O_{gas} = H_2SO_{4\,gas} + 29.83\ \text{kcal/mole} \qquad (5.42)$$

$$H_2SO_{4\,gas} \rightarrow H_2SO_{4\,liq.} + 11.98\ \text{kcal/mole} \qquad (5.43)$$

Reaction (5.42) — formation of sulfuric acid vapor — takes place in the gaseous phase; the reaction heat is absorbed by the gas. The average temperature difference between the gas and the condensation surface (the inner pipe wall) is therefore higher than the difference which is obtained from the conventional formulas, and the rate of heat transfer is correspondingly altered.

TABLE 5.9. Gas composition at pipe inlet for completely associated H_2SO_4 vapor

Components	Intake			
	% by vol.	mm Hg	m^3/hr at NTP	kg/hr
H_2SO_4	3.97	30.2	0.315	1.373
Air	95.24	723.8	7.438	9.616
H_2O	0.79	6.0	0.062	0.050
	100.00	760.0	7.815	11.039

The H_2SO_4 vapor pressure p_0 and the total gas volume listed in Table 5.5 correspond to completely associated H_2SO_4 vapor. The corresponding composition of the gas at the pipe inlet is listed in Table 5.9. The concentration of the condensing sulfuric acid in this case is 96.5%.

The coefficients of mass and heat transfer, β_p and α, at the pipe inlet and outlet are calculated from equations (5.11) and (5.12). The constant parameters entering these equations have the following values:

	In	Out
g, kg·hr^{-1}	11.039	9.616
μ, kg·m^{-1}·hr^{-1}	0.107	0.079
c, kcal·kg^{-1}·deg^{-1}	0.250	0.244
λ, kcal m^{-1}·hr^{-1}·deg^{-1}	0.0369	0.0264
D, m^2·hr^{-1}	0.081	0.044
ρ, kg·m^{-3}	0.67	0.946
T, °K	573	373
Re	10,500	12,100
Pr	0.722	0.722
Pr_D	2.13	1.90
B	0.023	0.023
l	0.8	0.8
m	0.4	9.4

Inserting these numerical values in (5.11) and (5.12), we obtain at the pipe inlet

$$\beta_{p,\,in} = \frac{0.023 \cdot 98 \cdot 0.081}{62.4 \cdot 573 \cdot 0.013} \cdot 10\,150^{0.8} \cdot 2.13^{0.4} = 0.78 \text{ kg} \cdot \text{m}^{-2} \cdot \text{hr}^{-1} (\text{mm Hg})^{-1}$$

$$\alpha_{in} = \frac{0.023 \cdot 0.0369}{0.013} \cdot 10\,150^{0.8} \cdot 0.722^{0.4} = 92.3 \text{ kcal} \cdot \text{m}^{-2} \cdot \text{hr}^{-1} \cdot \text{deg}^{-1}$$

At the pipe outlet

$$\beta_{p,\,out} = 0.74 \text{ kg} \cdot \text{m}^{-2} \cdot \text{hr}^{-1} (\text{mm Hg})^{-1}$$

$$\alpha_{out} = 76.8 \text{ kcal} \cdot \text{m}^{-2} \cdot \text{hr}^{-1} \cdot \text{deg}^{-1}$$

For the intermediate sections, we take the average values

$$\beta_p = \frac{0.78 + 0.74}{2} = 0.76 \text{ kg} \cdot \text{m}^{-2} \cdot \text{hr}^{-1} \cdot \text{deg}^{-1}$$

$$\alpha = \frac{92.3 + 76.8}{2} = 84.6 \text{ kcal} \cdot \text{m}^{-2} \cdot \text{hr}^{-1} \cdot \text{deg}^{-1}$$

The technique for the calculation of the fundamental process parameters is illustrated by the numerical examples for sections 1, 8, and 9. For the 1st section (the initial stage of the process) we calculate the cooling of the gas and the condensation of the sulfuric acid vapor on the pipe wall; for the 8the section we additionally calculate the nucleation parameters, since the rate of nucleation is by no means negligible ($I = 1.2 \cdot 10^2$); the calculations made for the 8th section are then repeated for the 9th section, where we also calculate the condensation of vapor on the surface of the embryos that have formed in the 8th section.

1st section. The supersaturation is calculated from equation (1.1) for the initial conditions $p_0 = 30.2$ mm Hg and $T_0 = 573.1$ °K.

For 96.5% H_2SO_4 we have from equation (2.9) and from interpolated data of Table 5.14

$$\lg p_\infty(T) = 8.402 - \frac{3617}{T} = 8.402 - \frac{3617}{573.1} = 2.090 \qquad (5.44)$$

or

$$p_\infty(T) = 123.0 \text{ mm Hg}$$

Thus

$$S_0 = \frac{p_0}{p_\infty(T)} = \frac{30.2}{123.0} = 0.246$$

Since $S_1 < 1$, no spontaneous condensation of vapor occurs and no droplets form. Vapor condenses only on the pipe wall, and as the gas cools reaction heat is released according to (5.42). Taking $l = 0.1$ m as the length of the 1st section, we obtain the corresponding wall surface

$$F_1 = \pi dl \qquad F_1 = 0.004084 \text{ m}^2$$

The quantity of heat transmitted by the gas to the surface is

$$Q_T = \alpha F (T - T_f) \tag{5.45}$$

where T_f is the temperature of the condensed film or of the condensation surface, °K.

Preliminary calculations have shown that when the coolant temperature changes from 20 °C (or 293 °K) at the inlet to 25 °C at the outlet, T_f changes insignificantly and it is thus assumed to remain constant along the entire pipe (313 °K or 40 °C). From (5.45) we have

$$Q_T = 84.6 \cdot 0.004084 (300 - 40) = 89.83 \text{ kcal/hr}$$

The quantity of sulfuric acid vapor condensing on the pipe wall is given by the equation

$$\Phi = \beta_p F [p - p_\infty(T_f)] \tag{5.46}$$

where $p_\infty(T_f)$ is the saturated vapor pressure of sulfuric acid above a plane surface at the appropriate temperature, mm Hg.

From equation (5.44) for $T_f = 313$ °K we have

$$\lg p_\infty(T_f) = 8.402 - \frac{3617}{313} = -3.150$$

or

$$p_\infty(T_f) = 0.001 \text{ mm Hg}$$

Inserting in (5.46) we find

$$K_1 = 0.76 \cdot 0.004084 [30.2 - 0.001] = 9.373 \cdot 10^{-2} \text{ kg/hr}$$

The H_2SO_4 vapor pressure in the gas leaving the 1st section is

$$p_1 = p_0 - \Delta p = p_0 - \frac{KRTP}{MV} \tag{5.47}$$

where p_0 is the H_2SO_4 vapor pressure in the gas entering the 1st section, mm Hg; V the flow rate, m^3/hr.

The flow rate at the pipe inlet for completely associated sulfuric acid vapor (at NTP) is $V_{in} = 7.815\ m^3/hr$. The flow rate decreases as the sulfuric acid vapor condenses, dropping to $V_{out} = 7.500\ m^3/hr$ at the outlet. Since the difference between V_{in} and V_{out} is insignificant, we adopt a constant average for all the sections:

$$V = \frac{V_{in} + V_{out}}{2} = \frac{7.815 + 7.500}{2} = 7.658\ m^3/hr\ (NTP)$$

For the 1st section from (5.47) we thus have

$$p_1 = 30.2 - \frac{9.373 \cdot 10^{-2} \cdot 22 \cdot 4 \cdot 760}{98 \cdot 7.658} = 28.074\ mm\ Hg$$

The gas temperature at the end of the section is

$$T_1 = T - \Delta T = T_0 - \frac{Q_T - Q_{frm} - Q_c}{Vc_g} \qquad (5.48)$$

where Q_{frm} is the heat of formation of sulfuric acid vapor according to equation (5.42), cal/hr; Q_c the heat of condensation of the vapor in the gas volume (released when new droplets form and when vapor condenses on already existing droplets), kcal/hr; c_g the specific heat of the gas at NTP, 0.33 kcal/m^3.

The degree of association of the sulfuric acid vapor in the gas stream leaving the 1st section is unknown, and we therefore initially take $Q_{frm} = 0$. Then

$$T_1' = 573 - \frac{89.83 - 0}{7.658 \cdot 0.33} = 537.45\ °K$$

To determine the quantity of heat Q_{frm} released when sulfuric acid vapor is formed, we should first find the true vapor pressure of H_2SO_4 and then the degree of association of SO_3 and water vapor in the incoming and the outgoing gas:

$$\varphi = \frac{x}{p} \qquad (5.49)$$

where φ is the degree of association; x the true vapor pressure of H_2SO_4 in the gas, mm Hg; p the H_2SO_4 vapor pressure when the association is complete, mm Hg.

The true vapor pressure of sulfuric acid in the gas can be found by examining the equilibrium between the H_2SO_4 vapor, SO_3, and water vapor. The equilibrium constant of the reaction (5.42) is expressed by the equation /25/

$$K_p = \frac{(p - x)(p_{H_2O} + p - x)}{x} \qquad (5.50)$$

where p_{H_2O} is the excess water vapor pressure in the gas, mm Hg (in our case, $p_{H_2O} = 0.2\,p$).

The equilibrium constant (5.50) is also expressed by the formula /25/

$$\lg K_p = 5.881 - \frac{500}{T} + 1.75 \lg T - 5.7 \cdot 10^{-4} T \qquad (5.51)$$

From (5.50) we have

$$x = a \pm \sqrt{a^2 - b} \tag{5.52}$$

where

$$a = \frac{K_p + 2p + p_{H_2O}}{2} = \frac{K_p + 2.2\,P_\infty}{2} \tag{5.53}$$

$$b = p^2 + p \cdot p_{H_2O} = 1.2\,p^2 \tag{5.54}$$

For a gas with an initial temperature of 300 °C (T = 573.1 °K), we have from equation (5.51) $K_p = 45.37$. From equations (5.52), (5.53), and (5.54) we thus obtain

$$a = \frac{45.37 + 2 \cdot 30.2 + 6}{2} = 55,88$$

$$b = 30.2^2 + 30.2 \cdot 6 = 1092.04$$

$$x = 55.88 \pm \sqrt{55.88^2 - 1092.04} = 10.84 \text{ mm Hg}$$

From (5.49) we thus have for the incoming gas

$$\varphi_0 = \frac{10.84}{30.2} = 0.359$$

At the end of the 1st section T_1 = 537.45 °K and we have

$$K_p = 11.07 \quad a = 36.42; \quad b = 945.85 \quad \text{and} \quad x = 16.913 \text{ mm Hg}$$

Hence

$$\varphi_1 = \frac{16.913}{28.074} = 0.602$$

The quantity of heat released when sulfuric acid vapor forms is expressed by the equation /21/

$$Q_{frm} = \frac{ML_{frm}v}{RTP}[(p_0 + p_1)(1 - \varphi_0) + p_1(\varphi_1 - \varphi_0)] \tag{5.55}$$

where L_{frm} = 296 kcal/kg is the heat of formation of sulfuric acid. Inserting the numerical values for the 1st section, we find

$$Q_{frm} = \frac{98 \cdot 296 \cdot 7.658}{22.4 \cdot 760}[(30.2 - 28.074)(1 - 0.359) + 28.074\,(0.602 - 0.359)] =$$

$$= 107.06 \text{ kcal/hr}$$

Making use of this $Q_{frm,1}$, we find from (5.48)

$$T_1'' = 573 - \frac{89.83 - 107.06}{7.658 \cdot 0.33} = 579.82 \text{ °K}$$

This temperature is substantially different from the temperature that we have assumed in our calculations (T_1 = 537.45 °K), and the entire procedure is therefore repeated in the same order, starting with a new temperature reading equal to the average of the two figures:

$$T_1'' = \frac{573.45 + 579.82}{2} = 558.64 \text{ °K}$$

At this temperature, $K_p=26.39$; $a=44.08$; $b=945.88$; $x=12.503$ mm Hg; $\varphi_1=0.445$ and $Q_{frm.1}=13.049[(30.2-28.074)(1-0.359)+28.074(0.445-0.359)]=49.46$ kcal/hr. Hence

$$T_1 = 573 - \frac{89.83 - 49.46}{7.638 \cdot 0.33} = 557.03\,°\text{K}$$

Since this T_1 is close to the average temperature assumed in the calculations, no further refinement of T_1 is attempted.

According to (5.44), the saturated vapor pressure at $T_1 = 557.03$ °K is $p_\infty = 81.6$ mm Hg, and therefore

$$S_1 = \frac{p_1}{p_\infty(T_1)} = 0.34$$

The calculations are made along the same lines for sections 2 through 7, where the supersaturation does not reach the critical value and no homogeneous condensation is observed (see Table 5.10).

8th section. The principal parameters of the gas leaving the 7th section are as follows:

$$T_7 = 472.05\,°\text{K};\quad p_7 = 18.809\ \text{mm Hg};\quad \varphi_7 = 0.906$$

At 472.05 °K, $p_\infty(T_7) = 5.492$ mm Hg (calculated from (5.44)), and the supersaturation is

$$S_7 = \frac{p_7}{p_\infty(T_7)} = 3.425$$

Under these conditions we have $T=472.05$ °K; $p(T)=5.492$ mm Hg; $\sigma = 51.04$ dyne/cm; $\alpha=1$; $M=98$; $\rho=1.658$ g/cm^3; $S=3.425$. Inserting these numerical constants in Frenkel's equation (1.53), we find

$$\lg I = 26 + \lg\left[\frac{1}{3.425 \cdot 1.658}\left(\frac{18.809}{472.05}\right)^2 (98 \cdot 51.04)^{1/2}\right] - \left[\frac{0.434 \cdot 3.32}{\lg^2 3.425}\left(\frac{98}{1.658}\right)^2\left(\frac{51.04}{472.05}\right)^3\right] = 2.08895$$

or

$$I = 1.23 \cdot 10^2\ \text{cm}^{-3}\ \text{sec}^{-1}$$

Since the calculated rate of droplet formation is fairly high, we take this particular section to be shorter than the previous sections:

$$l_8 = 0.02 \quad \text{and} \quad F_8 = 8.168 \cdot 10^{-4}\text{m}^2$$

The number of droplets forming in this section is given by

$$N = I\tau \tag{5.56}$$

where τ is the time it takes the gas to cross the section, sec. To find τ, we first calculate the velocity of the gas in the pipe:

$$w_8 = \frac{VT_8}{3600 \cdot 273.1 f} = \frac{7.658 \cdot 472.05}{3600 \cdot 273.1\ \dfrac{3.14 \cdot 0.013^2}{4}} = 27.75\ \text{m/sec}$$

$$\tau_8 = \frac{l_8}{W_8} = \frac{0.02}{27.75} = 7.22 \cdot 10^{-4} \text{ sec} \qquad (5.57)$$

$$N_8' = I\tau_8 = 1.23 \cdot 10^2 \cdot 7.22 \cdot 10^{-4} = 8.86 \cdot 10^{-2} \text{ cm}^{-3}$$

or at NTP

$$N_8 = \frac{N_8 \cdot T_8}{273.1} = \frac{8.86 \cdot 10^{-2} \cdot 472.05}{273.1} = 0.15 \text{ cm}^{-3}$$

The size of the embryos is determined from equation (1.9):

$$r_8 = \frac{2 \cdot 51.04 \cdot 98}{8.315 \cdot 10^7 \cdot 472.05 \cdot 1.658 \cdot 1.231} = 1.25 \cdot 10^{-7} \text{ cm}$$

The total mass of the liquid in the droplets is therefore

$$g_{d,8} = \frac{4}{3} \pi r^3 \rho N = \frac{4}{3} \cdot 3.14 (1.25 \cdot 10^{-7})^3 \cdot 1.658 \cdot 0.15 =$$

$$= 2 \cdot 10^{-21} \text{ g/cm}^2 \text{(NTP)} \qquad (5.58)$$

or

$$g_{d,8}' = g_{d,8} V \cdot 10^3 = 2 \cdot 10^{-21} \cdot 7.658 \cdot 10^3 = 1.5 \cdot 10^{-17} \text{ kg/hr}$$

From (5.45) and (5.46) we have

$$Q_{T,8} = 84.6 \cdot 8.168 \cdot 10^{-4} (471.95 - 313) = 10.984 \text{ kcal/hr}$$

$$\Phi_8' = 0.76 \cdot 8.168 \cdot 10^{-4} (18.809 - 0.001) = 1.168 \cdot 10^{-2} \text{ kg/hr}$$

It now remains to find p_8. First we calculate the total quantity of condensed vapor (on the pipe wall and in the gas volume):

$$\Phi_8 = \Phi_8' + g_8' = 1.168 \cdot 10^{-2} + 1.5 \cdot 10^{-17} \approx 1.168 \cdot 10^{-2} \text{ kg/hr} \qquad (5.59)$$

Substituting this result in (5.47) we obtain

$$p_8 = 18.809 - \frac{1.168 \cdot 10^{-2} \cdot 22.4 \cdot 4.760}{98 \cdot 7.658} = 18.545 \text{ mm Hg}$$

To obtain the temperature of the gas at the end of the particular section, we first calculate the quantity of heat released by vapor condensation in the gas volume:

$$Q_c = Lg_d' = 122 \cdot 1.5 \cdot 10^{-17} = 1.8 \cdot 10^{-15} \text{ kcal/hr} \qquad (5.60)$$

where L is the latent heat of condensation of sulfuric acid, kcal/kg.

Now we proceed as in the calculations of the 1st section, putting $Q_{frm} = 0$ in equation (5.48). Then

$$T_8' = 571.55 - \frac{10.984 - 0 - 1.8 \cdot 10^{-15}}{7.658 \cdot 0.33} = 467.61 \text{°K}$$

For $T_8' = 467.61$ °K and $p_8 = 18.545$ mm Hg we have

$$K_p = 0.395; \quad a = 20.60; \quad b = 412.69;$$

$$x = 17.201; \quad \varphi = 0.928$$

Inserting the result in equation (5.55), we find

$$Q_{frm}=\frac{98\cdot296\cdot7.658}{22.4\cdot760}[(18.809-18.545)(1-0.906)+$$
$$+18.545(0.928-0.906)]=5.581\ \text{kcal/hr}$$

Refining the temperature, we find

$$T_8''=471.95-\frac{10.984-5.581-1.8\cdot10^{-15}}{7.658\cdot0.33}=469.81\ ^\circ\text{K}$$

As the next higher approximation, we obtain

$$T_8=469.50\ ^\circ\text{K}$$

At this temperature $p_\infty(T_8)$=5.008 mm Hg; σ=51.14 dyne/cm; ρ=1.663 g/cm^3 and correspondingly S=3.709; $I_8=1.8\cdot10^4$ cm^{-3}sec^{-1}.

9th section. We take l_9=0.02 m, $F=8.168\cdot10^{-4}$ m^2, so w_9=27.60 m/sec; $\tau_9=7.26\cdot10^{-4}$ sec; N_9=22.4 cm^{-3}; $r_9=1.18\cdot10^{-7}$ cm; $g_9=2.55\cdot10^{-19}$ g/cm^3 at NTP.

The quantity of sulfuric acid vapor condensing on the droplets imported from the preceding section (g_f, g/cm^3) is calculated from equation (1.67), provided that the temperature of the droplets has been determined from equation (1.81).

The numerical constants entering these equations are as follows: c_v=4.97 cal/mole; $\lambda=8.4\cdot10^{-5}$ cal·cm^{-1}·sec^{-1}·deg^{-1}; $M_2=M_{air}$=29; $\Delta\approx l=10^{-5}$ cm; σ=51.14 dyne/cm; D=0.170 cm^2/sec; α=1; β=1; P=760 mm Hg; T=469.60 °K.

From (1.68), (1.69), (1.77), (1.76), and (1.79) we find

$$\nu=3643\sqrt{\frac{469.60}{98}}=7.975\cdot10^3$$

$$\varphi=\frac{0.170}{1.25\cdot10^{-7}\cdot7.975\cdot10^3}+\frac{1.25\cdot10^{-7}}{1.25\cdot10^{-7}+10^{-5}}=171$$

$$m=0.0583\cdot4.97\cdot760\sqrt{\frac{1}{29\cdot469.60}}=1.89$$

$$\gamma=\frac{8.4\cdot10^{-5}}{1.25\cdot10^{-7}\cdot1.89}+\frac{1.25\cdot10^{-7}}{1.25\cdot10^{-7}+10^{-5}}=356$$

$$Z=\frac{\varphi}{\gamma}=\frac{171}{356}=0.48$$

Since $p_\infty(T_8)$=5.008 mm Hg, from (1.9) we have

$$p_r(T_g)=5.008\ e^{\frac{2\cdot51.14\cdot98}{8.315\cdot10^7\cdot469.60\cdot1.663\cdot1.25\cdot10^{-7}}}=17.218\ \text{mm Hg}$$

Substituting in (1.87), we obtain

$$T_{r,8,9}=469.50+\frac{18.545-17.218}{\frac{6.24\cdot10^4\cdot4169.5\cdot8.4\cdot10^5\cdot0.48}{0.170\cdot98\cdot122}+\frac{98\cdot122\cdot17.218}{1.98\cdot469.5^2}}=470.76\ ^\circ\text{K}$$

The subscript 8, 9 signifies that we are concerned with the effect the droplets from section 8 have on vapor condensation in section 9.

At 470.76 °K the saturated vapor pressure of sulfuric acid above a plane surface (equation (5.44)) and above a droplet (equation (1.9)) is $p_\infty(T_{r,8,9}) = 5.252$ mm Hg and $p_r(T_{r,8,9}) = 17.997$ mm Hg, respectively.

Inserting these figures in equation (1.67), we find the mass of the sulfuric acid vapor condensing on the droplets imported from section 8 ($N_8 = 0.15$ cm^{-3}) during the time $\tau_9 = 7.26 \cdot 10^{-4}$ sec these droplets spend in section 9:

$$g_{f,8,9} = \frac{4 \cdot 3.14 \cdot 0.170 \cdot 1.25 \cdot 10^{-7} \cdot 98 \cdot 0.15 \cdot 7.26 \cdot 10^{-4}}{82.06 \cdot 469.50 \cdot 760 \cdot 171} \cdot (18.547 - 17.997) = 3.18 \cdot 10^{-19} \text{ g/cm}^3$$

The following equations give the mass of the liquid in these droplets

$$g_{8,9} = g'_{d,8} + g_{f,8,9} = 2 \cdot 10^{-21} + 3.18 \cdot 10^{-19} = 3.2 \cdot 10^{-19} \text{ g/cm}^3$$

and the droplet radius

$$r_{8,9} = \sqrt[3]{\frac{3 \cdot g_{8,9}}{4\pi\rho N_8}} = \sqrt[3]{\frac{3 \cdot 3.2 \cdot 10^{-19}}{4 \cdot 3.14 \cdot 1\,663 \cdot 0.15}} = 6.7 \cdot 10^{-7} \text{ cm}$$

The total number of droplets leaving the 9th section is given by

$$N_{tot,9} = 0.15 + 22.3 = 22.4 \text{ cm}^{-3}$$

the total mass of liquid in these droplets is

$$g_{tot,9} = 2.55 \cdot 10^{-19} + 3.20 \cdot 10^{-19} = 5.75 \cdot 10^{-19} \text{ g/cm}^3$$

the mean radius of the droplets is

$$\bar{r}_9 = \sqrt[3]{\frac{3 \cdot 5.75 \cdot 10^{-19}}{4 \cdot 3.14 \cdot 1.663 \cdot 22.4}} = 1.5 \cdot 10^{-7} \text{ cm}$$

The above procedure is repeatedly applied to calculate all the sections to section 19, inclusive; in each of these sections new embryos form continuously, and the number of different groups of droplets therefore increases from section to section.

Embryos also form in some sections after the 20th section (those where $I > 1$). These embryos, however, are ignored: they evaporate as the gas temperature increases.

Table 5.10 lists the parameters of droplets leaving the first four sections where embryos form. The number density of each group of droplets is virtually constant, but the droplet radii increase markedly from one section to the next.

As the gas moves and progressively greater quantities of vapor condense on the droplets, the ratio of the droplet radii for groups originating in adjoining sections approaches unity and different groups are therefore combined into one group (p. 54).

TABLE 5.10. Droplet parameters at the end of successive sections

Section No.	Radius, cm	Number density, cm^{-3} (NTP)
8	$r_8 = 1.25 \cdot 10^{-7}$ $\bar{r}_8 = 1.25 \cdot 10^{-7}$	$N_8 = 0.15$ $N_{8,tot} = 0.15$
9	$r_{8,9} = 6.7 \cdot 10^{-7}$ $r_9 = 1.2 \cdot 10^{-7}$ $\bar{r}_9 = 1.53 \cdot 10^{-7}$	$N_{8,9} = 0.15$ $N_9 = 22.3$ $N_{9,tot} = 22.5$
10	$r_{8,10} = 8.7 \cdot 10^{-7}$ $r_{9,10} = 5.8 \cdot 10^{-7}$ $r_{10} = 1.1 \cdot 10^{-7}$ $\bar{r}_{10} = 1.6 \cdot 10^{-7}$	$N_{8,10} = 0.15$ $N_{9,10} = 22.3$ $N_{10} = 4.6 \cdot 10^3$ $N_{10,tot} = 4.6 \cdot 10^3$
11	$r_{8,11} = 5 \cdot 10^{-6}$ $r_{9,11} = 2.9 \cdot 10^{-6}$ $r_{10,11} = 3.6 \cdot 10^{-7}$ $\bar{r}_{11} = 1.1 \cdot 10^{-7}$ $\bar{r}_{11} = 2.9 \cdot 10^{-7}$	$N_{8,11} = 0.15$ $N_{9,11} = 22.3$ $N_{10,11} = 4.6 \cdot 10^3$ $N_{11} = 2.8 \cdot 10^4$ $N_{11,tot} = 3.3 \cdot 10^4$

TABLE 5.11. Process parameters along the condensation pipe

Section No.	Temperature t, °C	H_2SO_4 vapor pressure p, mm Hg	Mass concentration of fog g, g/cm^3	Mean radius $\bar{r}$, cm	Rate of nucleation, $cm^{-3} \cdot sec^{-1}$	Supersaturation S	Total number of droplets at NTP, N, cm^{-3}	Pipe length L, mm
0	300.0	30.2	—	—	—	0.25	—	—
1	284.5	28.1	—	—	—	0.34	—	100
3	255.6	24.3	—	—	—	0.67	—	300
5	224.2	20.6	—	—	—	1.56	—	500
7	199.0	18.8	—	—	$1.2 \cdot 10^{2}$*	3.42	—	650
8	196.5	18.5	$2.1 \cdot 10^{-21}$	$1.3 \cdot 10^{-7}$	$1.8 \cdot 10^{4}$	3.71	0.15	670
9	193.1	18.3	$5.8 \cdot 10^{-15}$	$1.6 \cdot 10^{-7}$	$7.3 \cdot 10^{6}$	4.16	22.4	690
10	191.4	18.2	$1.4 \cdot 10^{-16}$	$1.6 \cdot 10^{-7}$	$9.1 \cdot 10^{7}$	4.40	$4.6 \cdot 10^{3}$	700
11	190.5	18.1	$5.7 \cdot 10^{-15}$	$2.9 \cdot 10^{-7}$	$2.9 \cdot 10^{8}$	4.54	$3.3 \cdot 10^{4}$	705
12	189.7	18.0	$4.0 \cdot 10^{-13}$	$7.7 \cdot 10^{-7}$	$8.5 \cdot 10^{8}$	4.67	$1.2 \cdot 10^{5}$	710
13	188.9	18.0	$1.7 \cdot 10^{-11}$	$1.8 \cdot 10^{-6}$	$2.4 \cdot 10^{9}$*	4.80	$3.9 \cdot 10^{5}$	715
14	188.1	17.9	$5.4 \cdot 10^{-10}$	$4.1 \cdot 10^{-6}$	$6.1 \cdot 10^{9}$	4.94	$1.1 \cdot 10^{6}$	720
15	187.4	17.8	$2.6 \cdot 10^{-9}$	$4.9 \cdot 10^{-6}$	$1.2 \cdot 10^{10}$	5.05	$3.1 \cdot 10^{6}$	725
16	186.6	17.8	$1.1 \cdot 10^{-8}$	$5.1 \cdot 10^{-6}$	$3.0 \cdot 10^{10}$	5.20	$6.9 \cdot 10^{6}$	730
17	185.8	17.7	$4.2 \cdot 10^{-8}$	$7.2 \cdot 10^{-6}$	$6.9 \cdot 10^{10}$	5.34	$1.6 \cdot 10^{7}$	735
18	185.0	17.6	$1.4 \cdot 10^{-7}$	$8.2 \cdot 10^{-6}$	$1.4 \cdot 10^{11}$	5.49	$3.8 \cdot 10^{7}$	740
19	184.3	17.5	$4.7 \cdot 10^{-7}$	$9.3 \cdot 10^{-6}$	$2.5 \cdot 10^{11}$	5.61	$8.3 \cdot 10^{7}$	745
20	183.7	17.3	$1.3 \cdot 10^{-6}$	$1.0 \cdot 10^{-5}$	$3.1 \cdot 10^{11}$*	5.67	$1.6 \cdot 10^{8}$	750
21	183.8	16.9	$3.5 \cdot 10^{-6}$	$1.5 \cdot 10^{-5}$	$1.5 \cdot 10^{11}$	5.56	$1.6 \cdot 10^{8}$	755
22	184.3	16.0	$8.0 \cdot 10^{-6}$	$1.9 \cdot 10^{-5}$	$9.6 \cdot 10^{9}$	5.13	$1.6 \cdot 10^{8}$	760
23	185.0	15.4	$1.2 \cdot 10^{-5}$	$2.2 \cdot 10^{-5}$	$2.0 \cdot 10^{8}$	4.78	$1.6 \cdot 10^{8}$	762
25	187.2	13.9	$2.0 \cdot 10^{-5}$	$2.6 \cdot 10^{-5}$	$5.7 \cdot 10^{4}$	3.97	$1.6 \cdot 10^{8}$	765
30	197.8	6.9	$7.6 \cdot 10^{-5}$	$4.1 \cdot 10^{-5}$	—	1.30	$1.6 \cdot 10^{8}$	775
35	187.8	3.5	$9.2 \cdot 10^{-5}$	$4.4 \cdot 10^{-5}$	—	1.10	$1.6 \cdot 10^{8}$	870
38	159.2	0.9	$1.1 \cdot 10^{-4}$	$4.5 \cdot 10^{-5}$	—	1.05	$1.6 \cdot 10^{8}$	1050
39	129.7	0.1	$1.1 \cdot 10^{-4}$	$4.5 \cdot 10^{-5}$	—	1.00	$1.6 \cdot 10^{8}$	1250
40	101.1	$3.1 \cdot 10^{-2}$	$1.1 \cdot 10^{-4}$	$4.5 \cdot 10^{-5}$	—	1.00	$1.6 \cdot 10^{8}$	1500
41	76.3	$4.8 \cdot 10^{-3}$	$1.1 \cdot 10^{-4}$	$4.5 \cdot 10^{-5}$	—	1.00	$1.6 \cdot 10^{8}$	1800
42	56.5	$1.5 \cdot 10^{-3}$	$1.1 \cdot 10^{-4}$	$4.5 \cdot 10^{-5}$	—	1.00	$1.6 \cdot 10^{8}$	2200

* According to equation (1.34), $I = 1.7 \cdot 10^{6}$, $2.4 \cdot 10^{13}$, and $3.0 \cdot 10^{15}$ $cm^{-3} sec^{-1}$ in sections 7, 13, and 20, respectively.

Table 5.11 lists the results of calculations for all the sections. Figure 5.10 is a graphical plot of the numerical findings. Minimum section lenghts are introduced in the region of maximum supersaturation and immediately downstream from that region, where the processes of nucleation and vapor condensation on embryos and droplets are the most intensive.

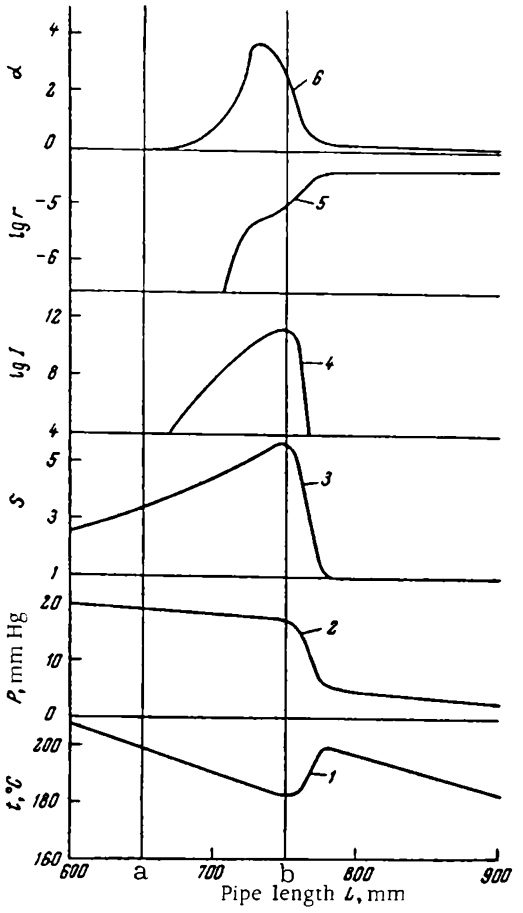

FIGURE 5.10. Parameters of condensation along a pipe:
1) gas temperature t, °C; 2) vapor pressure p, mm Hg; 3) supersaturation S; 4) rate of nucleation I, $cm^{-3}sec^{-1}$; 5) mean droplet radius $\bar{r}$, cm; 6) variability factor α (equation (1.83)).

It follows from Table 5.11 and Figure 5.10 that as the gas moves along the pipe, the supersaturation of the sulfuric acid vapor gradually increases; at the inlet $L = 0$, the supersaturation is $S = 0.25$, while at $L = 400$ mm, $S = 1$. For $L = 650$ mm (cross section a), $S = 3.42$ (7th section), and the nucleation rate is $I = 1.2 \cdot 10^2\ cm^{-3}sec^{-1}$. Since the rate of nucleation in section 7 is fairly high, fog apparently starts forming in that section.

After the 8th section, vapor condensation on the pipe wall is accompanied by vapor condensation on the surface of already existing droplets, as well as on the surface of continually forming new embryos. However, despite the gradual increase in the total rate of vapor condensation due to the combination of the three factors above and the decrease in the H_2SO_4

vapor pressure, the supersaturation S retains its upward trend for some time. The maximum supersaturation $S = 5.67$ is attained for $L = 750$ mm (cross section b, Figure 5.10, Table 5, section 20). The rate of nucleation is also maximal in that section, $I = 3.1 \cdot 10^{11}$ cm^{-3}sec^{-1}. As the gas moves further down the pipe, the supersaturation drops rapidly. Embryos form in a short section of a pipe, which is no longer than 100 mm.

The condensation of sulfuric acid vapor on the pipe wall initially produces a very gradual decrease in vapor pressure (Figure 5.10). When $S = S_{max}$ and $I = I_{max}$ have been attained, however, the vapor pressure drops abruptly due to the substantial increase in the total rate of vapor condensation in the gas volume, mainly by condensation on the surface of already existing droplets. The abrupt change gives way to a more gradual variation, when the vapor condenses simultaneously on the pipe wall and on the surface of the fog droplets.

The temperature of the gas at first displays a gentle downward trend. When droplets start forming (cross section b), the temperature slightly increases over a small section of the pipe due to intensive condensation of sulfuric acid vapor on the fog droplets and the release of a large quantity of heat. In this section the temperature of the droplets is higher than the temperature of the gas, and the entire heat of condensation is eventually transmitted from the droplet to the gas and thence to the pipe walls.

The mean droplet radius and the drop size distribution are highly variable along the pipe (see Tables 5.10, 5.11, and 5.12), since new minute embryos form continuously in the gas mixture and the existing droplets rapidly grow by condensation. The fog monodispersity, representable by the variability coefficient α (equation (1.83)), therefore also varies between wide limits along the pipe (see Figure 5.10, curve 6). The coefficient α is maximal at $L = 730$ mm ($\alpha = 3.6$). After that the continued condensational growth of the droplets (for $r \gg l$ the growth rate decreases as the radius is increased, see equation (1.70)) levels out the differences in the droplet radii and a virtually monodisperse fog is obtained ($\alpha = 0.17$).

Thermal (Brownian) coalescence influences neither the concentration nor the radius of the droplets, since the number density is comparatively low ($N = 1.6 \cdot 10^8$). This also follows from the coalescence equation

$$N = \frac{N_0}{1 + K\tau N_0} \tag{5.61}$$

where N_0, N are the initial and final number densities, cm^{-3}; K the coalescence constant, $K = 4 \cdot 10^{-10}$ cm^{3}sec^{-1} (see Appendix III); τ time, sec. The gas moves from section 20 (where nucleation has stopped) to the end of the pipe in $\tau = 0.05$ sec. Substituting N_{tot}, K, τ in equation (5.61), we obtain

$$N' = \frac{1.6 \cdot 10^8}{1 + 4 \cdot 10^{-10} \cdot 0.05 \cdot 1.6 \cdot 10^8} \approx 1.6 \cdot 10^8$$

The effect of eddy coalescence on droplet concentration and radius is also negligible in this case. The higher frequency of occurrence of aerosols in turbulent streams than in static media and in laminar flow is mainly attributable to the high difference between the density of the medium and the density of the fog droplets. On account of this difference, the

droplets are partly entrained by the eddy pulsation, so that particles of different sizes move with different velocities and collisions are more frequent.

During the nucleation stage the droplet radii range between very wide limits (from $2.3 \cdot 10^{-7}$ cm to $4.8 \cdot 10^{-5}$ cm, see Table 5.12), but since the droplets are very small ($\bar{r} = 1.04 \cdot 10^{-5}$ cm), the effect of eddy coalescence is negligible /26/.

TABLE 5.12. Drop size distribution

Drop radius, cm		Number of droplets in each group N, cm^{-3}
nucleation end-point (section 20)	pipe outlet	
$4.8 \cdot 10^{-5}$	$6.4 \cdot 10^{-5}$	$6.9 \cdot 10^{6}$
$2.1 \cdot 10^{-5}$	$4.4 \cdot 10^{-5}$	$9.3 \cdot 10^{6}$
$6 \cdot 10^{-6}$	$3.7 \cdot 10^{-5}$	$2.1 \cdot 10^{7}$
$1.6 \cdot 10^{-6}$	$3.2 \cdot 10^{-5}$	$4.5 \cdot 10^{7}$
$2.3 \cdot 10^{-7}$	$2.7 \cdot 10^{-5}$	$7.8 \cdot 10^{7}$
$\bar{r} = 1.04 \cdot 10^{-5}$, $\alpha = 2.8$	$\bar{r} = 4.5 \cdot 10^{-5}$, $\alpha = 0.17$	$N_{tot} = 1.6 \cdot 10^{8}$

At the end of the process the droplets become somewhat larger, but the size distribution is considerably more uniform (range of radii from $2.7 \cdot 10^{-5}$ to $6.4 \cdot 10^{-5}$ cm, see Table 5.12). Eddy coalescence again fails to take over /14/.

It is interesting to trace the variation of the mass ratio of the vapor condensing on droplets to the vapor condensing on the pipe wall. We see from the graph in Figure 5.11 that this ratio is maximal not when the nucleation rate attains its highest value (I_{max}), but later, when vapor condenses abundantly on droplets which have somewhat grown.

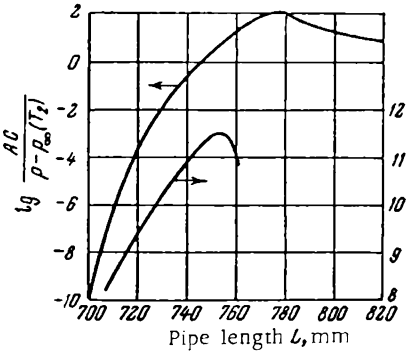

FIGURE 5.11. Ratio of the rates of condensation on droplets and on the pipe surface.

The mass concentration of the fog at the pipe outlet ($L = 2200$ mm) is $g = 1.1 \cdot 10^{-4}$ g/cm^3 or 0.744 kg/hr, which is 54% of the total quantity of sulfuric acid vapor at the inlet (see Table 5.9).

The reliability of our numerical data on the final number density and mass concentration of fog essentially depends on the accuracy with which the nucleation rate and the rate of vapor condensation on fog droplets during the nucleation stage have been determined. When nucleation has stopped, the number density of the fog remains virtually constant (the effect of thermal and eddy coalescence is negligible), so the bulk of the sulfuric acid vapor remaining in the gas mixture condenses on the surface of the drops.

From all the preceding we see, in particular, that tentative information on the mass concentration of fog (and also on the mean droplet radius at the end of the process) can be obtained if the maximum S is known (in our case the calculations should be made using the data for section 20, see

Table 5.11). It should be assumed, however, that the remaining vapor condenses in its entirety on the droplets. The calculations that follow confirm this assumption.

For section 20, $p = 17.3$ mm Hg, $N = 1.6 \cdot 10^8$ cm^{-3}, and $g = 1.3 \cdot 10^{-6}$ g/cm^3 (at NTP). The mass of sulfuric acid vapor in the gas at NTP is

$$g_v = \frac{17.3 \cdot 98}{(760 - 17.3) \cdot 22.4 \cdot 10^3} = 1.1 \cdot 10^{-4} \text{ g/cm}^3$$

If we assume that all the vapor condenses on the droplets, the mass concentration of the fog (at NTP) at the end of the process will be

$$g = 1.3 \cdot 10^{-6} + 1.1 \cdot 10^{-4} \approx 1.1 \cdot 10^{-4} \text{ g/cm}^3$$

i.e., as in Table 5.11.

The droplets on which vapor condensed were regarded as if suspended in a still medium. But in a turbulent stream the droplets grow faster, since vapor is transferred by convective, as well as molecular, diffusion. Convective diffusion arises because the droplets are only partly entrained by the eddy pulsations.

Since even the largest droplets are very small (the droplets grow to $4.5 \cdot 10^{-5}$ cm at the end of the process; the newly formed embryos have radii of $1 \cdot 10^{-5}$ cm on the average, see Table 5.12), the effect of eddy diffusion is small enough to be ignored.

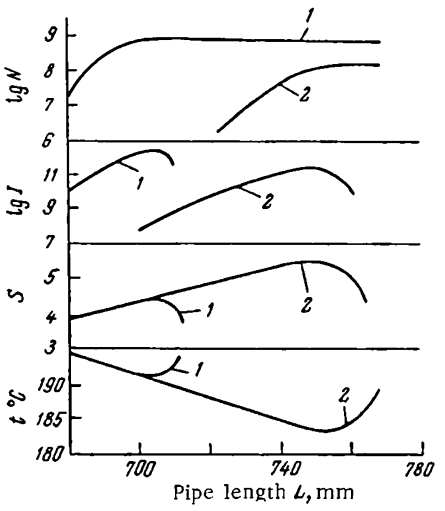

FIGURE 5.12. Condensation parameters for different nucleation rates: 1) nucleation rate calculated from the Becker-Doering equation; 2) from the Frenkel equation

In the preceding calculations we neglected the heat transmitted by radiation from the droplets to the gas (since the droplets are minute, the radiative heat transfer is vanishingly small /26/) and the heat radiated from the hot droplets to the pipe wall. The relative contribution from radiative heat transfer in the nucleation region is very small, since the mean droplet radius is not greater than $1 \cdot 10^{-5}$ cm (see Table 5.12). At the end of the process, when the droplets will have grown to $4.5 \cdot 10^{-5}$ cm on the average, the heat transfer from the droplets to the pipe wall becomes noticeable. The difficulties involved in calculations with radiative heat transfer, however, are not justified, since the correction introduced in the mass concentration of the fog and in the droplet radii is small, while the number density remains unchanged.

We also ignore the Stefan flow in our calculations, since the ratio of vapor pressure to the total pressure of the gas in the nucleation region is small ($p/P = 0.033$) and the correction is less than 1% /26/.

Figure 5.12 plots the fundamental condensation parameters in the nucleation region with the rates of nucleation computed from the Frenkel (1.53) and the Becker-Doering (1.34) equations. These graphs disclose the relation among the different parameters at the instant of embryo buildup and throw some light on the effect of I on the drop size distribution of the fog.

The curves plotting the variation of the fundamental parameters along the pipe in the region of maximum nucleation follow the same general trend, but the final outcomes are essentially different. The values of I obtained from the Becker-Doering equation are several orders of magnitude higher than the corresponding values from the Frenkel equation. The final number density, however, increases much less markedly: as I increases, the number of embryos forming per unit time becomes proportionately higher and a progressively higher mass of vapor is consumed by these forming and growing droplets. The supersaturation therefore diminishes rapidly and the nucleation ceases earlier than according to the Frenkel equation.

PREVENTION OF FOG DURING FREEZING OUT OF VAPOR

Chemical analysis of gases and various laboratory tests often require preliminary freezing out of the vapor from the gas mixture. In industry, vapor freezes out if the gases are cooled rapidly.

In laboratory, the vapor is typically frozen out in a U-shaped trap immersed in a cooling liquid. When a vapor-containing gas is passed through the trap, the vapor condenses on the walls. It is assumed that the vapor pressure in the gas mixture issuing from the trap corresponds to saturation at the temperature of the cooling liquid. A fairly complete separation of vapor can therefore be achieved if the trap is cooled to a sufficiently low temperature (using a mixture of some liquid with CO_2 ice or liquid air).

It follows from the preceding, however, that supersaturated vapor forms almost invariably when vapor condenses on a surface. Part of the supersaturated vapor condenses into liquid droplets in the gas volume and the resulting aerosol is entrained by the gas stream emerging from the trap. The content of the freezing component in the outgoing gas mixture is thus naturally higher than that corresponding to the saturated vapor pressure; it is equal to the sum of the mass concentrations of the aerosol and the vapor.

The velocity of the gas in the trap is generally small, and the temperature of the issuing gas, as well as the temperature of the trap walls, is equal to the temperature of the coolant medium. Equations (5.7) and (5.8) can therefore be used in vapor trap calculations.

As the temperature of the gas mixture in the trap decreases, the supersaturation rises to a maximum and then falls off. If the maximum supersaturation is greater than the critical value, the theoretical maximum is not attained, since as soon as the critical supersaturation is reached vapor starts condensing in the gas volume and aerosol droplets form. The supersaturation rapidly decreases due to vapor condensation on the aerosol particles.

Figure 5.13 plots the concentration of ethanol vapor and mist in air as a function of temperature, obtained by approximate calculations. The curves represent the behavior of the vapor-gas mixture as it progresses through the trap /27, 28/.

The following initial data were assumed in the calculations: coolant temperature $T_2 = 213$ °K, inlet air temperature $T_1 = 293$ °K, inlet vapor pressure $p_1 = 15$ mm Hg. The air at the trap inlet is thus 34.2% saturated with alcohol vapor. The calculations were made for clean, dust-free air which contained gas ions. The entire length of the U-shaped trap was divided into several sections and each was assigned an arbitrarily chosen gas temperature in a descending sequence. Equation (5.7) was then applied to calculate the ethanol vapor pressure at the corresponding temperatures.

For example, the air entering one of the sections at the temperature $T_1 = 273$ °K is assumed to have the temperature $T = 263$ °K at the end of that section. The ethanol vapor pressure in the gas entering the particular section is $p_1 = 12.4$ mm Hg (calculated from the terminal conditions of the preceding section). The vapor pressure near the condensation surface ($T_2 = 233$ °K) is $p_2 = 0.045$ mm Hg; the coefficient $\delta = 0.655$ (calculated from (5.20)) is assumed to be contant. Inserting these numerical values in equation (5.7), we find $p = 11$ mm Hg.

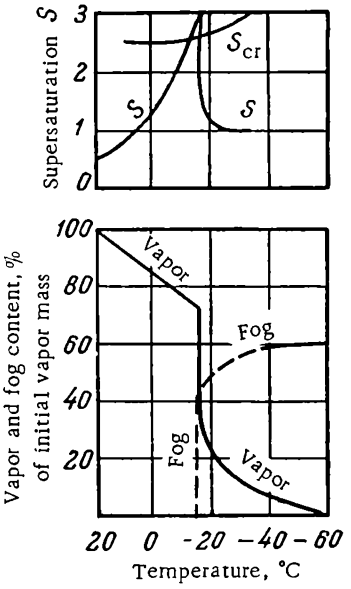

FIGURE 5.13. The content of ethanol vapor and fog vs. air temperature in the trap.
Temperature of the coolant - 60 °C; initial ethanol vapor pressure 15 mm Hg.

At 263 °K the saturated vapor pressure of ethyl alcohol is $p_\infty = 5.6$ mm Hg. From (1.1) we thus find $S = 1.96$. Since this supersaturation is subcritical ($S < S_{cr}$), no fog forms.

The calculations for the other fog-free sections are carried out in the same way.

At − 15 °C the supersaturation reaches the critical value and fog starts forming. In this and all the subsequent sections the vapor pressure is taken equal to the saturated vapor pressure, and the fog content in the air at the end of each section is found as the difference between the vapor pressure from equation (5.7) and the saturated vapor pressure.

There is a certain fundamental inaccuracy in these calculations, since the rate of fog formation and the heat of condensation are both ignored. The error, however, is not large, particularly in the last sections, where the mass of condensing vapor is small and the vapor mainly condenses on already existing fog droplets. The numerous droplets offer a very extensive surface, and the condensation is therefore rapid. The concentration of the fog forming in each section is determined from equation (1.87).

We see from Figure 5.13 that as the air progresses through the trap the ethanol vapor pressure first decreases almost linearly (due to vapor condensation on the trap walls), approximately along the same line as in Figure 5.10. At a certain point the smooth descent of the curve is abruptly altered, since the supersaturation has increased sufficiently for spontaneous vapor condensation to begin. Fog is formed, its mass concentration increasing by the contribution from two mechanisms:

nucleation of new droplets and vapor condensation on already existing drops. Figure 5.13 also shows that, for the particular initial conditions used in our work, the content of fog in the emerging air is nearly 60% of the total amount of ethyl alcohol in the incoming air.

It follows from equation (5.8) that as the coolant temperature T_2 is decreased, the supersaturation increases and the mass concentration of the fog forming by vapor condensation in the gas volume correspondingly increases. This conclusion is illustrated by the calculations of the ethanol mist content in the air emerging from the trap as a function of the coolant temperature (Figure 5.14). The calculations were made along the lines described above and under the same initial conditions ($T_1 = 293°K$, $p_1 = 15$mm Hg).

We see from Figure 5.14 that no fog forms in clean air at T_2 higher than 240 °K and the content of ethyl alcohol in the issuing air therefore corresponds to the saturated vapor pressure at the coolant temperature. Fog starts forming at $T_2 = 240$ °K, its mass at the trap outlet increasing as the temperature is further decreased. At $T_2 = 193$ °K, more than 70% of the initial mass of ethyl alcohol is converted into fog which emerges from the trap with the air stream.

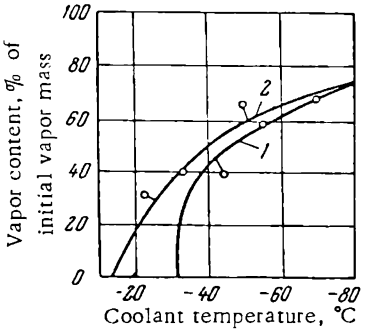

FIGURE 5.14. Ethanol fog content in the emerging air as a function of coolant temperature: 1) cleaned air; 2) without cleaning.

Unfiltered air generally contains condensation nuclei of $10^{-4}-10^{-5}$ cm (see Figure 1.7). The critical supersaturation for these particles, according to equation (1.9), is close to unity. In uncleaned air vapor starts condensing in the gas volume earlier and a larger mass is converted into fog. Curve 2 (Figure 5.14) has been plotted for uncleaned air with a critical supersaturation of unity, the other conditions remaining as before.

The results of calculations are consistent with the results of laboratory experiments /27, 28/ which measured the content of ethyl alcohol mist in the air emerging from a trap. In these experiments, dried air which contained ethyl alcohol vapors was passed through a U-shaped copper tube immersed in a coolant liquid. The air was analyzed for ethyl alcohol at the inlet and at the outlet. The experimental findings are marked by circles in Figure 5.14. The theoretical results provide a satisfactory fit to the experimental data.

To sum up: the percentage of vapor condensing inside the trap decreases as the temperature is lowered; contrary to the common belief, the separation is less complete at low temperatures.

We are now in a position to calculate the conditions of vapor condensation in a trap under which no fog forms and the separation is nearly complete.

The maximum supersaturation decreases as the coolant temperature is increased, and if the content of vapor in the gas at the trap inlet is known, we can find the coolant temperature which ensures a sufficiently low maximum supersaturation so that fog does not form. Figure 5.15 plots the limiting temperature of fog formation for different initial pressures of ethyl alcohol: at lower temperatures ethanol vapor condenses into fog.

The calculations are carried out as follows. Since the vapor pressure near the condensation surface is small in comparison with the vapor pressure in the gas mixture entering the trap, the temperature at which the maximum supersaturation is attained is found from equation (5.10).

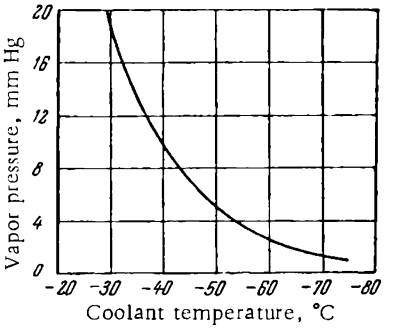

FIGURE 5.15. Limiting conditions of fog formation.

The coolant temperature and the corresponding critical supersaturation are known, so equation (5.8) is used to determine the maximum ethanol vapor pressure at the trap inlet for which fog does not form. For coolant temperature $t_2 = -60\,°C$, or $T_2 = 213.1\,°K$, we find from equation (5.10) (the coefficient E is calculated from (2.12)):

$$0.655\,T^2 - 5090T + 5090 \cdot 213.1 = 0$$

whence $T = 219.1\,°K$ or $t = -54\,°C$. The saturated vapor pressure of ethyl alcohol at this temperature is $p_\infty = 0.1$ mm Hg and the critical supersaturation is $S_{cr} = 5$. Substituting these values in equation (5.8), we find the vapor pressure at the trap inlet

$$p_1 = \frac{S_{cr}\,p_\infty - p_2}{\left(\frac{T - T_2}{T_1 - T_2}\right)^{\delta}} + p_2 = \frac{5 \cdot 0.1 - 0.045}{\left(\frac{219 - 213}{293 - 213}\right)^{0.655}} + 0.045 = 2.53\ \text{mm Hg}$$

This is the general outline of the calculations used in plotting the curve in Figure 5.15. We see from Figure 5.15 that as the coolant temperature decreases, the maximum permissible vapor pressure falls off steeply (the curve is nearly logarithmic). If the vapor content in the gas mixture at the trap entrance is known, the temperature of the coolant at which no fog forms can be read off this curve. The partially devaporized gas mixture emerging from the first trap can be passed through a second trap which is maintained at a lower temperature than the first trap. This temperature is again adjusted to ensure that the vapor condenses on the surface and no fog forms. A succession of cold traps will separate the vapor from the gas mixture with any desired degree of completeness.

If packed traps are used, the probability of fog formation substantially decreases because vapor condenses on the extensive surface of the packing. The heat of condensation warms the packing and its temperature becomes higher than the temperature of the gas. Heat is thus transferred between

the packing and the gas. The effect of the packing on the supersaturation is expressed by the coefficient K in equation (5.23). It follows from this equation that the maximum supersaturation decreases as the packing surface is increased.

These conclusions are confirmed experimentally. The trap used in the previous tests was subsequently packed with glass tubes. The content of ethyl alcohol in the emerging gas was a factor of 20 less than in experiments with unpacked traps. Industrial experiments with the condensation of sulfuric acid vapor /29/ also indicate that packing promotes vapor condensation on the surface.

It follows from the preceding that separation of vapor by freezing almost invariably leads to the development of supersaturated vapor. Vapor therefore often condenses in the gas volume and aerosol particles form. The mass concentration of the aerosol at the outlet may substantially exceed the content of vapor in the emerging gas. The freezing-out procedure should therefore be adjusted so that the vapor condenses on the trap surface only.

The simplest and most reliable technique by which aerosol formation can be prevented is the use of packed filters with a large specific surface. However, even in packed filters a large difference between the initial vapor pressure and the vapor pressure near the condensation surface may lead to spontaneous condensation and the formation of aerosol. Special calculations should therefore be made in each particular case in order to establish the conditions under which fog formation is avoided.

Some data on the maximum supersaturation which is obtained when 20 °C water vapor is cooled in a trap are listed in Table 5.13. The results were obtained by the same calculations as those applied for ethyl alcohol.

TABLE 5.13. Maximum supersaturation for the freezing out of water vapor (initial vapor pressure $p_1 = 1$ mm Hg)

Coolant temperature T_2, °K	Temperature for maximum supersaturation T_{max}, °K	Maximum supersaturation s_{max}	Coolant temperature T_2, °K	Temperature for maximum supersaturation T_{max}, °K	Maximum supersaturation s_{max}
213	220	4.7	173	175	928
193	200	58.7	153	157	110 000

We see from Table 5.13 that very high supersaturation develops even when a gas with a small vapor content (11 mm Hg) is cooled excessively. Unfortunately no data are available on the critical supersaturation of water vapor at low temperatures, and the point of incipient fog cannot be found. It is obvious, however, that the supersaturations listed in Table 5.13 are high enough for fog to form.

The above data on the conditions of fog formation in traps can also be applied to calculate the freezing out of water and carbon dioxide vapor from air in Linde columns which are generally used for air separation into oxygen and nitrogen /30, 31/. The Linde column is similar to a pipe condenser (see Figure 5.6), i.e., the air circulates through the pipes and the coolant flows between the pipes. The coolant temperature in these

columns is very low (120 — 150 °K), and the water vapor content in the atmospheric air is comparatively high, so that large supersaturations may develop (see Table 5.13). On the other hand, the freezing out should proceed under such conditions that spontaneous condensation of vapor in the gas volume is avoided and the impurities do not pass through in the form of aerosol particles. It is only under these conditions that effective cleaning can be achieved. This requires a small temperature difference (not more than 30 °C) between the gas and the pipe wall. But the efficiency of the column increases as the temperature difference is increased, and the application of theoretical findings on fog prevention at relatively large temperature differences is therefore of considerable significance in practice. For example, water and CO_2 vapors condense and crystallize on the inner pipe wall, so the heat transfer coefficient is gradually lowered and the hydraulic resistance of the pipe is increased (the gas now flows through a pipe of a narrower cross section). When the resistance rises to the maximum permissible value, the circulation is stopped and the pipes are thawed to drain the frozen water and carbon dioxide.

Equation (5.7) is applied /30 — 32/ to determine the relation of vapor pressure to gas temperature and to calculate the resulting supersaturation. An analysis of this equation and of the data on p. 111 shows that fog formation is best avoided by the use of packed towers and columns (with crossed plates arranged along the entire column, concentric cylindrical surfaces, ribs, etc.). This conclusion is confirmed by experimental findings and by the observation that needle-shaped ice crystals of water and CO_2 on the pipe walls reduce the probability of fog formation (these crystals act as a packing) /30/.

In some sulfuric acid plants, before entering the absorption tower the gas is cooled by circulating through the pipes of a heat exchanger (Figure 5.6), where cold water or air washes the external surface of the pipe. The gas entering the cooler always carries sulfuric acid vapor, which in some cases condenses into fog. The presence of sulfuric acid vapor in the gas after the contact stage is explained as follows: according to technological specifications, the SO_2 gas before reaching the catalytic chamber is dried to a water vapor content of 0.01% (0.08 g/m^3 at NTP). After the contact stage, the gas contains an excess of SO_3, which combines with the water vapor to form sulfuric acid in quantities of 0.54 g/m^3 at NTP (0.076 mm Hg).

If the water entering the cooler is cold (or the water content of the gas is high), part of the sulfuric acid vapor condenses spontaneously and fog is formed. The fog particles easily pass through the remaining stages of the installation and are emitted into the atmosphere with otherwise harmless gases.

Fog formation is prevented by raising the temperature of the water (or air) entering the cooler to 40 — 50 °C. The ratio expressed by equation (5.21) and the supersaturation are both altered. Equations (5.9) and (5.8) give the temperature of the condensation surface (and the temperature of the coolant) required to prevent fog formation.

PREVENTION OF FOG DURING THE RECOVERY OF VOLATILE SOLVENTS BY CONDENSATION

Volatile solvents (ethyl alcohol, ether, naphtha, acetone, toluene, etc.) are often used in industry to dissolve various nonvolatile compounds. The solvent typically does not participate in chemical reactions and is eventually removed from the solution. Processes of this kind are encountered in the manufacture of rubberized fabrics, leatherette, 35-mm film, artificial leather, smokeless gunpowder, etc.

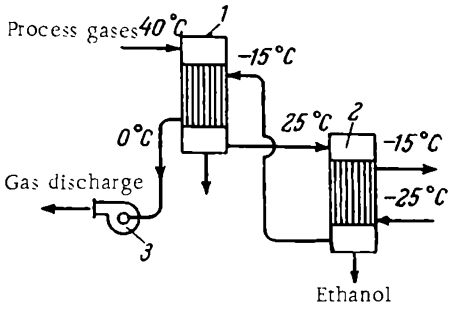

FIGURE 5.16. Solvent recovery by condensation:
1) cooler; 2) condenser; 3) ventilator.

The volatile solvent is mostly removed by heating the solution in a stream of warm air. The solvent evaporates and is carried off by the air stream. The bulk of the solvent is recovered from the carrier gases and is used again and again.

Several different industrial techniques are known for the recovery of volatile solvents, one of which — the condensation method — retrieves the solvent by cooling the gas and allowing the vapor to condense on a surface /33—35/.

As an example, let us consider the recovery of ethyl alcohol in 35-mm film industry /33/. The solvent-recovering condenser is shown in Figure 5.16. The gas is initially cooled from 40 °C to 25 °C. The higher boiling fractions (amyl acetate, butyl acetate, etc.) are separated at this stage, but ethanol vapor remains in the gaseous phase. The gases then pass on to a condenser whose pipes are cooled externally by a circulating coolant with a temperature of − 25 °C. The gases are cooled to − 15 °C and ethanol vapor condenses.

The following conditions are assumed for particular calculations:

Gas temperature	
at condenser inlet t_1, °C	25 ° (or $T_1 = 298$ °K)
at condenser outlet t, °C	− 15 (or $T = 258$ °K)
Surface temperature t_2, °C	− 30 (or $T_2 = 253$ °K)
Ethanol vapor pressure at condenser inlet p, mm Hg	47.2
Saturated vapor pressure at $T_2 - p_2$, mm Hg	2.5

From equation (5.17) we have

$$\delta = \left(\frac{D}{a}\right)^{1-m} = \left(\frac{0.102}{0.187}\right)^{1-0.4} = 0.69$$

The latent heat of evaporation of ethyl alcohol is $L = 220$ cal/g, and from (2.12) we have

$$E = 0.503 \cdot 46 \cdot 220 = 5090$$

Inserting the numerical values in equation (5.9) we obtain by successive approximations the temperature at which the maximum supersaturation is attained: $T = 260.5$ °K or $t = -12.5$ °C. Inserting this temperature in equation (5.8), we find the maximum supersaturation $S_{max} = 3.47$. The critical

supersaturation of ethyl alcohol vapor in air under these conditions is $S_{cr} = 2.3$. Since the maximum supersaturation in the condenser is higher than the critical supersaturation, vapor will condense in the gas volume and fog will form. If the recovery cycle is open, the fog escapes with the discharged gases and some ethyl alcohol is lost irretrievably. In a closed cycle the fog lowers the condenser recovery ratio and affects adversely the operating conditions of the entire installations. Similar calculations show that the recovery ratio is not improved by lowering the temperature of the coolant, since fog formation is enhanced in cold gas.

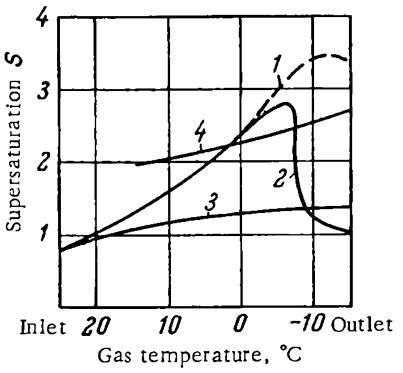

FIGURE 5.17. Supersaturation of ethanol vapor in the condenser:
1) for $t_2 = -20$ °C ignoring fog formation; 2) for $t = -20$ °C with fog formation; 3) for $t - t_9 = 5$ °C; 4) critical supersaturation.

We repeated the preceding calculations for various final temperatures in order to reconstruct the supersaturation which develops as the ethanol mixture moves through the condenser pipes. The results are plotted in Figure 5.17 (curve 1) which shows that the critical supersaturation is attained when the gas has cooled to 275 °K. At lower temperatures, the formation of embryos and fog droplets lowers both the derivative dS/dT and the function S, which decrease at an accelerated rate, similarly to what is shown in Figure 5.10.

A consistently small temperature difference between the gas and the coolant will prevent fog formation and ensure more complete condensation of ethyl alcohol. The ratio expressed by equation (5.21) is small in this case and the supersaturation diminishes in accordance with equations (5.8) and (5.9). The conditions should be so chosen that the maximum supersaturation remains less than the critical value.

These conclusions are confirmed by calculations carried out under the same conditions as previously, except for the temperature of the condensation surface, which is constantly maintained 5 °C below the temperature of the gas (Figure 5.17, curve 3). In this case, the supersaturation is invariably lower than the critical value.

Vapor is recovered by condensation also in pipes where the internal walls are cooled by a dripping liquid or in installations with plane-parallel packing /36/. These setups ensure a higher rate of heat transfer than in a pipe condenser, since the gas is in direct contact with the coolant liquid.

If the content of the condensable vapor in the gas is small, the heat of condensation can be ignored. The temperature of the condensation surface i is then a function of the temperature of the gas mixture. Equation (5.4) can therefore be integrated, which yields the relation of the vapor pressure to the gas temperature along the entire pipe.

In a countercurrent tower, with the gas mixture flowing from bottom to top and the coolant trickling from top to bottom, we have from the heat balance considerations

$$g_g c_g (T_g^0 - T_g') = g_l c_l (T_l' - T_l^0) \qquad (5.62)$$

where g_g and g_l are the masses of the gas and the liquid, kg/hr; c_g and c_l the specific heats of the gas and the liquid, kcal/kg; T_g^0 and T_l^0 the inlet temperatures of the gas and the liquid, °K; T_g' and T_l' the outlet temperatures of the gas and the liquid, °K.

Solving this equation for T_g', we find

$$T_g' = T_g^0 - \frac{g_l c_l}{g_g c_g}(T_l' - T_l^0) \tag{a}$$

For a certain pipe section, where the gas temperature is T_g and the temperature of the liquid is T_l, we similarly have

$$g_g c_g (T_g - T_g') = g_l c_l \ (T_l - T_l^0) \tag{b}$$

whence

$$T_l = \frac{g_g c_g}{g_l c_l}(T_g - T_g') + T_l^0 \tag{c}$$

Substituting T_g from equation (a) into (b), we find

$$T_l = \frac{g_g c_g}{g_l c_l}(T_g - T_g^0) + T_l' \tag{d}$$

Putting

$$\frac{g_g c_g}{g_l c_l} = a \tag{5.63}$$

and seeing that in our previous symbols (p. 63) $T_g^0 = T_1$, $T_g = T$, and $T_l = T_2$, we rewrite equation (d) in the form

$$T_2 = T_l' - a(T_1 - T) \tag{e}$$

The saturated vapor pressure near the surface can be expressed by equation (1.2):

$$p_\infty = p_2 = e^{C - \frac{E}{T_2}}$$

Inserting these expressions for T_2 and p_2 in (5.4), we find

$$\frac{dp}{dT} = \delta \frac{p - e^{C - \frac{E}{T_2}}}{T - aT - T_l' - aT_1} \tag{f}$$

Putting

$$1 - a = b \tag{5.64}$$

$$-T_l + aT_1 = C_1 \tag{5.65}$$

we rewrite (f) in the form

$$\frac{dp}{dT} = \delta \frac{p - e^{C - \frac{E}{aT - C_1}}}{bT - C_1}$$

or

$$\frac{dp}{dT} = \frac{\delta}{bT + C_1} \cdot p - \frac{\delta e}{bT + C_1} \tag{g}$$

Putting

$$-\frac{\delta}{bT + C_1} = P; \quad -\frac{\delta e^{C - \frac{E}{aT - C_1}}}{bT + C_1} = Q$$

we write for (g)

$$\frac{dp}{dT} + Pp = Q \tag{h}$$

Solving this linear equation, we find

$$p = e^{-\int PdT} \left[\int Qe^{\int PdT} dT + C_2 \right] \tag{i}$$

Substituting for p and integrating over T from T_1 to T, we write

$$\int_{T_1}^{T} PdT = -\int_{T_1}^{T_2} \frac{\delta dT}{bT + C_1} = -\ln\left(\frac{bT + C_1}{bT_1 + C_1}\right)^{\frac{\delta}{b}}$$

whence

$$e^{-\int_{T_1}^{T} PdT} = e^{\ln\left(\frac{bT + C_1}{bT_1 + C_1}\right)^{\frac{\delta}{b}}} = \left(\frac{bT + C_1}{bT_1 + C_1}\right)^{\frac{\delta}{b}}$$

and correspondingly

$$\int_{T_1}^{T} Qe^{\int_{T_1}^{T} PdT} dT = \int_{T_1}^{T} \frac{-\delta e^{C - \frac{E}{aT - C_1}} (bT_1 + C_1)^{\frac{\delta}{b}} dT}{(bT + C_1)^{1 + \frac{\delta}{b}}}$$

Substituting in equation (i), we find

$$p = \left(\frac{bT + C_1}{bT_1 + C_1}\right)^{\frac{\delta}{b}} \left[\int_{T_1}^{T} \frac{-\delta e^{c - \frac{E}{aT - c_1}} (bT_1 + C_1)^{\frac{\delta}{b}} dT}{(bT + C_1)^{1 + \frac{\delta}{b}}} + C_2 \right]$$

For $T = T_1$, $p = p_1$, and therefore $C_2 = p_1$.

Inserting this result for C_2 in the previous expression and taking the constants outside the integral, we write

$$p = (bT + C_1)^{\frac{\delta}{b}} \left[- \delta e^C \int_{T_1}^{T} \frac{e^{-\frac{E}{aT - C_1}} dT}{(bT + C_1)^{1+\frac{\delta}{b}}} + \frac{p_1}{(bT_1 + C_1)^{\frac{\delta}{b}}} \right] \qquad \text{(j)}$$

For simplicity we put

$$S = \int_{T_1}^{T} \frac{e^{-\frac{E}{aT + C_1}} dT}{(bT + C_1)^{1+\frac{\delta}{b}}} \qquad \text{(k)}$$

and make the substitution

$$\frac{E}{aT - C_1} = v \quad T = \frac{E + C_1 v}{av} \quad dT = -\frac{E dv}{av^2} \qquad (5.66)$$

Then

$$S = \int_{v_0}^{v} \frac{-e^{-v} E dv}{av^2 \left(\frac{Eb}{av} + \frac{C_1 b}{a} + C_1 \right)^{1+\frac{\delta}{b}}} =$$

$$= -\frac{1}{b} \left(\frac{a}{Eb} \right)^{\frac{\delta}{b}} \int_{v_0}^{v} \frac{e^{-v} v^{\frac{\delta}{b} - 1} dv}{\left(1 + vC_1 \frac{a+b}{Eb} \right)^{1+\frac{\delta}{b}}}$$

Putting

$$C_1 \frac{a+b}{Eb} = l \qquad (5.67)$$

we write

$$S = -\frac{1}{b} \left(\frac{a}{Eb} \right)^{\frac{\delta}{b}} \int_{v_0}^{v} \frac{e^{-v} - v^{\frac{\delta}{b}-1} dv}{(1 + vl) \left(1 + \frac{\delta}{b} \right)} = -\frac{1}{b} \left(\frac{a}{Eb} \right)^{\frac{\delta}{b}} I \qquad \text{(l)}$$

and equation (j) takes the form

$$p = (bT + C_1)^{\frac{\delta}{b}} \left[\frac{\delta}{b} e^C \left(\frac{a}{Eb} \right)^{\frac{\delta}{b}} I + \frac{p_1}{(bT_1 + C_1)^{\frac{\delta}{b}}} \right] \qquad (5.68)$$

or

$$p = \frac{\delta}{b} e^{C} \left[\frac{(bT + C_1)^{\delta}}{Eb} \right]^{\frac{\delta}{b}} I + p_1 \left(\frac{bT + C_1}{bT_1 + C_1} \right)^{\frac{\delta}{b}} \tag{5.69}$$

The integral

$$I = \int_{v_0}^{v} \frac{e^{-v} v^{\frac{\delta}{b} - 1} dv}{(1 + vl)^{1 + \frac{\delta}{b}}} \tag{5.70}$$

can be expanded in a power series. This approach, however, is much too cumbersome; it is more convenient to make use of the relation /37/

$$\int_{v_0}^{v} f(v)\, dv = \frac{3}{10} \cdot \frac{v - v_1}{6} (f_0 + 5f_1 + f_2 + 6f_3 + f_4 + 5f_5 + f_6) \tag{5.71}$$

where f_0, f_1, f_2, f_3, f_4, f_5, f_6 are the values of the integrand for equidistant points v.

We may take

$$v_1 = v_0 + \frac{1 + (v - v_0)}{6} \qquad v_2 = v_0 + \frac{2(v - v_0)}{6}$$

$$v_3 = v_0 + \frac{3(v - v_0)}{6} \qquad v_4 = v_0 + \frac{4(v - v_0)}{6}$$

$$v_5 = v_0 + \frac{5(v - v_0)}{6} \qquad v_6 = v_0 + \frac{6(v - v_0)}{6}$$

Equation (5.66) is solved to determine the value of the variable at the initial and the final temperatures T_1 and T; equation (5.70) is then applied to find the integral I and equation (5.68) readily gives the pressure of the condensable vapors in the relevant section.

When vapor condenses on the surface of the trickling liquid, the supersaturation may have a maximum. However, the relation of p to T is complex and it is very difficult to derive a practicable general equation for the calculation of the maximum supersaturation. To obtain the maximum supersaturation, p should be determined from (5.68) for several arbitrarily chosen sections and equation (1.1) should then be applied to calculate the supersaturation in each of these sections. The results are plotted in a graph which gives the maximum supersaturation. A necessary condition in all these manipulations is that the maximum supersaturation be less than the critical supersaturation, so that fog does not form.

PREVENTION OF FOG DURING VAPOR CONDENSATION IN SPRAY TOWERS

Liquid-sprayed packed towers are a conventional tool with a variety of industrial uses. They require minimum maintenance, are simple to build,

and have low hydraulic resistances. Condensation or evaporation processes often take place in these towers, so that fog formation is a common ocurrence here.

For example, coke oven gas is cooled in spray towers /38/. The vapors of high-boiling products partially condense in the gas volume and fog is formed (some 10 g/m^3), which is subsequently collected in electrostatic precipitators. Fog similarly forms when the generator gas is cleaned in metallurgical plants, or when the combustion gases of peat, wood, etc., are handled.

As an example of fog formation during evaporation we can mention the case of graduating towers, where the warm water trickling downward through the tower packing is mixed with the upward moving cold atmospheric air. The vapor evaporating from the surface of the warm water partially condenses in the stream of cold air and fog is formed.

Fog formation is particularly frequent in packed towers used for the condensation of sulfuric acid vapor. The conditions of fog formation in the sulfuric acid industry have been studied most intensively, and since the mechanism of fog formation during vapor condensation is independent of the actual vapor composition, we consider in the following some characteristic cases of H_2SO_4 mist in liquid-sprayed packed towers.

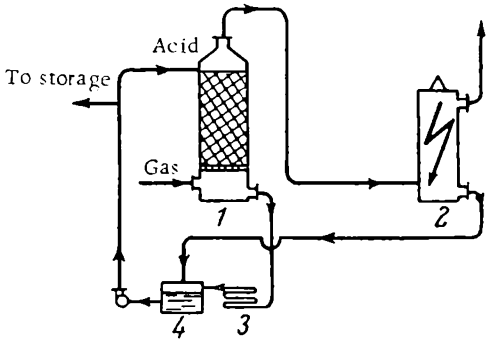

FIGURE 5.18. Spray tower for sulfuric acid condensation:
1) condenser tower; 2) electrostatic precipitator; 3) cooler; 4) acid collector.

In the wet-gas contact process, some 30% of the total output is collected in electrostatic precipitators which trap the sulfuric acid mist forming in the condenser tower when the gas is cooled and H_2SO_4 is allowed to condense /21/. The wet-gas process is technologically simple and it gives cheap sulfuric acid; these are the main reasons for the current popularity of this technique. In USSR alone over 300,000 metric tons of sulfuric acid were produced by this method in 1963.

In the wet-gas process, hydrogen sulfide is burned in atmospheric air, and the gas mixture containing SO_2, oxygen, and water vapor is then delivered without preliminary drying to a contact catalyst chamber for the oxidation of SO_2 to SO_3 /21/. The oxidized gas mixture is passed through a packed condenser tower sprayed with cold sulfuric acid (Figure 5.18). When the gas is cooled, sulfuric acid vapor forms according to reaction (5.42); these vapors condense on the surface of the sulfuric acid dripping down the walls. The excess heat is absorbed by the sulfuric acid spray, which is consequently heated in the tower. The heated acid is circulated through the cooler 3 and from the collector 4 it is pumped back into the spray tower. High supersaturation develops when the sulfuric acid condenses, and a certain proportion of the H_2SO_4 vapor therefore condenses in the gas volume in the form of fog droplets which are separated in the electrostatic precipitator 2.

We now consider some theoretical and practical data concerning the influence of various factors on the conditions of sulfuric acid condensation

in spray towers in the wet-gas contact plants. The calculations are made by the approximate numerical technique described on p. 127 for a pipe condenser. The reaction heat (5.42) and the differences in the composition of the liquid and the gas acid phases are allowed for in the process. The calculations are based on the data provided by a sulfuric acid plant with an output of 5 metric tons per hour /21/: inlet and outlet temperatures 450 and 75 °C for the gas and 50 and 80 °C for the acid; SO_3 content in the gas entering the tower 5.22% (Table 5.14); internal diameter of the tower $D_{in} = 6.1$ m; height of packing $H = 6.1$ m; total surface area provided by the packing $F = 13{,}200\ m^2$; quantity of spraying acid $N = 455{,}800$ kg/hr.

TABLE 5.14. Composition of gas at tower inlet

Components	Composition, % by vol.	Flow rates	
		m^3/hr	kg/hr
SO_3	5.22	1119	4027
H_2O	7.38	1581	1280
H_2SO_4	0.08	17	75
N_2, O_2 etc.	87.32	18683	24094
	100.00	21400	29470

The results of these calculations show that the condensation indices vary along the tower (as the gas progresses from bottom to top) approximately in the same way as in a simple pipe condenser (Figure 5.19).

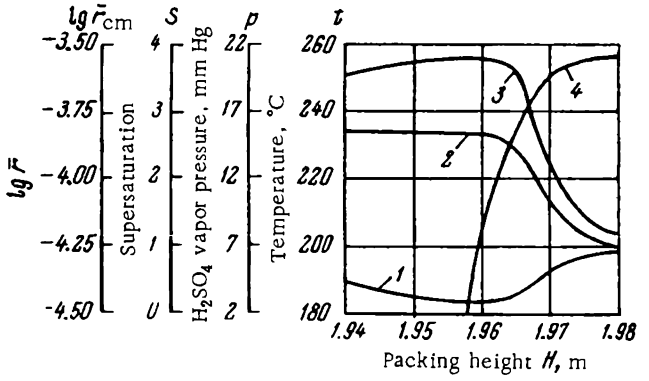

FIGURE 5.19. Variation of condensation indices along the spray tower (initial temperature of the spraying acid 50 °C, temperature of spent acid 80 °C):
1) gas temperature t, °C; 2) H_2SO_4 vapor pressure p, mm Hg; 3) supersaturation S; 4) mean droplet radius $\bar{r}$, cm.

Initially, the supersaturation is less than unity, but it rapidly increases as the gas is cooled, reaching a maximum ($S_{max} = 3.78$) at a height of $L = 1.96$ m, when the gas has cooled to 184 °C (see Figure 5.19). After that the supersaturation rapidly decreases to $S = 1$.

The mean droplet radius at the tower outlet is approximately $3.2 \cdot 10^{-4}$ cm; the droplets grow most intensively up to the 1.97 m level due to enhanced condensation of the supersaturated vapor on their surfaces. The amount

of sulfuric acid tied up in droplets in the emerging gas (the mass concentration of the fog) is 63.7 g/m^3 or nearly 30% of the total mass of sulfuric acid vapor at the tower inlet.

Over a narrow section (between the 1.96 and the 1.98 m levels) the temperature of the gas increases considerably due to the rapid condensation of the sulfuric acid vapor on the fog droplets: the heat of condensation is transmitted from the droplets to the gas.

In the wet gas process the sulfuric acid fog is collected by various filters.

Fog also forms in the gases issuing from the Glover towers in the chamber process of sulfuric acid manufacture. In this process, the burner gases (a mixture of air and SO_2) are brought in contact with a solution of nitrogen oxides in sulfuric acid (nitrous vitriol). Nitrogen oxides react with SO_2 in the presence of water to give sulfuric acid. The lower nitrogen oxides are recovered by oxidation with atmospheric oxygen /25/. The reaction mainly takes place in the liquid phase, i.e., the nitrous vitriol oxidizes the SO_2 dissolved in the acid.

Burner gases contain SO_3 and water vapor, as well as SO_2. The fumes are relatively hot (300—400 °C), and the content of sulfuric acid vapor is low in accordance with the dissociation equation (5.42). The hot gas comes in contact with the cold acid spray in the Glover tower: this causes incidental cooling of the gas mixture, the dissociation equilibrium is displaced in the direction of H_2SO_4, which subsequently condenses on the surface of the cold spraying liquid. The temperature of the condensation surface in the Glover tower varies between wide limits, and equation (5.8) therefore cannot be applied to find the maximum supersaturation. The probability of fog formation can be inferred from the available data on the gas temperature and the H_2SO_4 vapor pressure along the height of the entire tower.

We now proceed with fog calculations for a tower with an output of 75 kg/m^3 /39, 40/. The height of the tower is arbitrarily divided into several sections; heat and mass transfer equations are then applied to each section separately /41/. The partial H_2SO_4 vapor pressure over sulfuric acid at different temperatures is computed from equation (1.3).

TABLE 5.15. The coefficients A and B from equation (1.3)

Acid concentration, % H_2SO_4	A	B
85	7.751	3742
90	7.897	3685
95	8.316	3637
98	8.470	3593

Since no experimental data are available on the H_2SO_4 vapor pressure over 75.5% sulfuric acid, the coefficients A and B have been determined by extrapolating the figures listed in Table 5.15. This table was obtained by reducing the experimental data from /42/ by the method of least squares /43/. The dissociation of sulfuric acid vapor was ignored in the calculation of the coefficients in Table 5.15, and they can therefore be applied for H_2SO_4 vapor at temperatures under 250 °C. A more rigorous treatment of

the experimental data leads to complex formulas /44/ which are very difficult to use in our particular case.

The following numerical values are assumed in the calculations:

Gas temperature, °C	
tower inlet	318
tower outlet	88
Acid temperature, °C	
tower inlet	41.8
tower outlet	127.3
Concentration of sulfuric acid, %	
tower inlet	75.7
tower outlet	76.5
Gas flow rate at NTP, m^3/hr	3000
Flow rate of spraying acid, kg/hr	3400
Vapor pressure, mm Hg	
of water in the incoming gas	15
of sulfuric acid in the incoming gas	4
Heat transfer coefficient, $kcal \cdot m^{-2} \cdot hr^{-1} \cdot deg^{-1}$	3
Water evaporation coefficient, $kg \cdot m^{-2} \cdot hr^{-1} \times (mm\ Hg)^{-1}$	0.011
H_2SO_4 condensation coefficient, $kg \cdot cm^{-2} \times hr^{-1} (mm\ Hg)^{-1}$	0.027

The water evaporation coefficient β_{H_2O} and the H_2SO_4 condensation coefficient $\beta_{H_2SO_4}$ were calculated from equations (5.12) and (5.18) making use of the experimental heat transfer coefficient $\alpha = 3\ kcal \cdot m^{-2} \cdot hr^{-1} \cdot deg^{-1}$.

The equation of heat balance is written for each section:

$$Q_1 = Q_2 + Q_3 \qquad \text{(a)}$$

where Q_1 is the quantity of heat lost by the gas in the particular section; Q_2 the quantity of heat absorbed by the heating acid; Q_3 the quantity of heat expended in the evaporation and dilution of the acid.

The heat of formation of the sulfuric acid is ignored, since in the base of the tower (where the fog forms) the content of nitrogen oxides in the sulfuric acid is low and the oxidation of SO_2 is insignificant /25/. If water vapor condenses in this section, Q_3 is negative.

The three components of the heat balance are calculated from the equations

$$Q_1 = vc_g (t_g^0 - t_g') \qquad (5.72)$$

$$Q_2 = g_a c_a (t_a^0 - t_a') \qquad (5.73)$$

$$Q_3 = 1.35 \cdot 89.3 (365 - t_a')^{1/3} A \qquad (5.74)$$

$$Q_1 = \alpha F \Delta t \qquad (5.75)$$

$$A = \beta_{H_2O} F \Delta p_{H_2O} \qquad (5.76)$$

Here v is the volume of the gas mixture; c_g the specific heat of the gas mixture; t_r^0 and t_g' the temperature of the gas entering and leaving the particular section; g_a the mass of the spraying acid; c_a the specific heat of the acid; t_a^0 and t_a' the temperature of the acid entering and leaving the section; A the quantity of water evaporating in the section; 1.35 a numerical coefficient which allows simultaneously for the evaporation of water and the dilution of sulfuric acid (it is obtained by preliminary calculation);

the condensation surface in the tower; Δt the average temperature difference between the gas and the spraying acid; Δp_{H_2O} the average difference between the vapor pressure of water in the gas mixture and the saturated vapor pressure of water over sulfuric acid.

The tower is divided into short sections, and the average difference of temperatures and vapor pressures can therefore be replaced with the difference between the initial temperatures and vapor pressures at the inlet to the particular section:

$$\Delta t = t_g^0 - t_a^0 \tag{5.77}$$

$$\Delta p_{H_2O} = p^0_{H_2O,g} - p^0_{H_2O,a} \tag{5.78}$$

Inserting the numerical values in equation (a), we find

$$vc_g (t_g^0 - t_g') = g_a c_a (t_a^0 - t_a') + 1.35 \cdot 89.3 (365 - t_a')^{1/3} A \tag{5.79}$$

The following equations should also be observed:

$$vc_g (t_g^0 - t_g') = \alpha F (t_g - t_a) \tag{b}$$

$$A = \beta_{H_2O} F (p^0_{H_2O,g} - p^0_{H_2O,a}) \tag{c}$$

From (5.79) we calculate the temperature of the outgoing acid t_a'.

The sulfuric acid vapor pressure at the end of the section is obtained from the following equations:

$$B = \beta_{H_2SO_4} F (p^0_{H_2SO_4,g} - p^0_{H_2SO_4,a}) \tag{5.80}$$

$$B = \frac{VM_{H_2SO_4} (p^0_{H_2SO_4,g} - p'_{H_2SO_4,g})}{PRT} \tag{5.81}$$

where B is the quantity of H_2SO_4 vapor condensing in the section; $p^0_{H_2SO_4,g}$, $p'_{H_2SO_4,g}$ the vapor pressure of H_2SO_4 in the gas entering and leaving the section; $p^0_{H_2SO_4,a}$ the saturated vapor pressure of H_2SO_4 over liquid acid at the entrance to the section; $M_{H_2SO_4}$ the molecular weight of sulfuric acid.

Equating the right-hand sides of (5.80) and (5.81) we obtain an equation for the vapor pressure of the sulfuric acid in the gas leaving the section ($p'_{H_2SO_4,g}$):

$$\frac{\beta_{H_2SO_4} PRTF}{VM_{H_2SO_4}} = \alpha F = \frac{p^0_{H_2SO_4,g} - p'_{H_2SO_4,g}}{p^0_{H_2SO_4,g} - p^0_{H_2SO_4,a}} \tag{d}$$

In our case

$$\alpha = \frac{0.027 \cdot 760 \cdot 22.4}{3\,000 \cdot 98} = 0.001563$$

and therefore

$$0.001563\ F = \frac{p^0_{H_2SO_4,g} - p'_{H_2SO_4,g}}{p^0_{H_2SO_4,g} - p^0_{H_2SO_4,a}}$$

If the temperature of the gas leaving the section and the H_2SO_4 vapor pressure in the gas are known, equation (2.9) can be applied to find the saturated vapor pressure; the supersaturation is then obtained from equation (1.1). If fog is formed, the content of sulfuric acid in the fog

droplets is calculated from the temperature of the gas and the partial pressures of sulfuric acid and water vapor.

The concentration of sulfuric acid and the water vapor pressure in the gas at the end of each section are calculated from the equations

$$C' = C^0\left(1 + \frac{AC^0}{g_a}\right) \tag{5.82}$$

$$p'_{H_2O,g} = p^0_{H_2O,g} \pm \frac{ARTD}{M_{H_2O}V} \tag{5.83}$$

where C^0 and C' are the concentrations of the acid at the beginning and the end of the section; $p^0_{H_2O,g}$, $p'_{H_2O,g}$ the vapor pressure of water in the gas at the beginning and the end of the section; R the gas constant; T the temperature, °K; P the total pressure of the gas; M_{H_2O} the molecular weight of water.

Table 5.16 and Figure 5.20 present the results of calculations for a normally operating Glover tower.

TABLE 5.16. Specifications of a Glover tower along its height (calculated for normal operation)

Section No.	Gas temperature, °C	Acid temperature, °C	Surface F, m^2	Water vapor pressure p_{H_2O}, mm Hg	Acid concentration, % H_2SO_4	Sulfuric acid vapor pressure $p_{H_2SO_4}$, mm Hg	Fog concentration, g/m^3	Concentration of acid in the fog, % H_2SO_4	Supersaturation of H_2SO_4 vapor, S
0	318	127.3		15.0	76.5	4.0	—	—	—
1	308	126.4	17.3	18.7	76.3	3.9	—	—	—
2	288	124.7	36.4	26.8	75.9	3.7	—	—	—
3	268	122.8	40.4	33.5	75.4	3.48	—	—	—
4	248	120.8	45.4	40.8	75.0	3.26	—	—	—
5	228	118.6	51.9	47.7	74.6	3.0	—	—	—
6	208	116.1	60.3	54.3	74.3	2.73	—	95	0.52
7	188	112.8	71.8	60.1	73.9	2.44	—	91	2.12
8	168	107.8	88.0	64.0	73.7	0.29	12.1	88	7.3
9	148	98.4	109.5	63.0	73.8	0.06	13.2	84	1
10	128	79.7	133.0	52.0	74.4	0.011	13.4	80	1
11	108	54.2	136.5	33.6	75.5	0.003	13.4	77	1
12	88	41.8	122.5	29.6	75.8	0.0007	13.4	75.8	1

We see from Figure 5.20 that as the hot gas moves down the tower, the sulfuric acid vapor pressure at first decreases smoothly because of vapor condensation on the surface of the packing. The supersaturation S increases concurrently, and when it attains the critical value S_{cr} vapor starts condensing in the gas volume and fog is formed. The vapor pressure therefore drops steeply due to the combined condensation of H_2SO_4 on the packing and on the fog droplets.

Fog forms approximately half way down the tower and its mass concentration increases, first rapidly and then at a slower rate, to a value of 13.4 g/m^3 at the outlet from the tower. The concentration of sulfuric acid in the fog droplets diminishes as the gas moves along the tower, dropping to 75.8% at the outlet.

Fog formation is confined to a very narrow section of the tower, the supersaturation rapidly increasing between sections 7 and 8 (Table 5.16). The variation of the fundamental condensation indices (the gas temperature t, the sulfuric acid vapor pressure p, the supersaturation S, and the mean droplet radius $\bar{r}$) during fog formation is approximately the same as in a spray tower in the wet-gas contact process (Figure 5.19). The absolute values for the two processes are somewhat different, however: the vapor pressure of sulfuric acid at the entrance to the Glover tower is substantially less than at the entrance to the condenser tower in the wet-gas process.

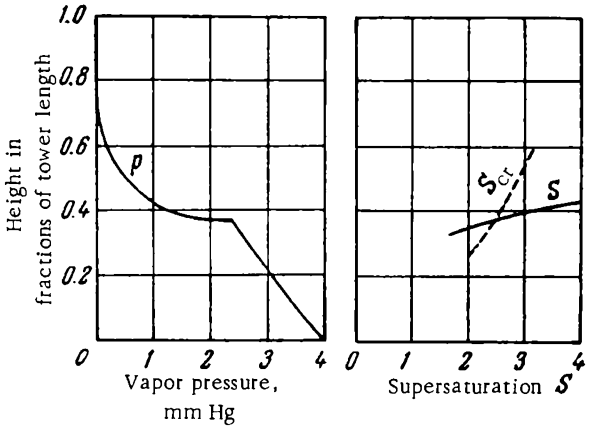

FIGURE 5.20. H_2SO_4 vapor pressure and supersaturation in a normally operating Glover tower (theoretical).

As we have previously observed the vapor pressure above a droplet is higher than above a plane surface, but with droplets of $0.5 \cdot 10^{-5} - 5 \cdot 10^{-5}$ cm radius the difference is a mere 1—5% (calculated from equation (1.9)), and is therefore ignored.

SO_2 is oxidized in fog droplets and sulfuric acid forms, so that the content of H_2SO_4 in the emerging fog is higher than the calculated figure and also higher than the concentration of sulfuric acid in the incoming gas. This is confirmed by numerous data provided by sulfuric acid plants (Table 5.17) and by laboratory tests /39/ which have measured the decrease of SO_2 concentration in a reaction vessel filled with a gas mixture of H_2SO_4 mist, nitrogen oxides, and SO_2. The results of these tests show that the oxidation of SO_2 in fog droplets increases as the concentration of nitrogen oxides in the gas mixture is increased and decreases as the concentration of H_2SO_4 in the fog droplets is raised.

TABLE 5.17. A survey of towers

Tower No.	Tower volume, m^3	Internal surface, m^2	Fog concentration at the outlet, g/m^3	Time spent in the tower, sec
1	17	647	24.0	10
2	77	2530	40.0	41
3	55	1819	20.1	31
4	50	1730	13.3	28
5	50	1730	7.0	28
6	60	1890	6.3	35
7	37	1430	5.2	21

Note. The content of H_2SO_4 in the incoming gas is $14\ g/m^3$

The amount of SO_2 oxidized to sulfuric acid in the fog droplets cannot be found unless the total surface of the droplets and the H_2SO_4 concentration in the droplets are known: these factors have a decisive effect on the rate of SO_2 oxidation in the chamber process. The total surface area of spherical droplets increases as the droplet radius is decreased (equation (1.88)). There are, however, no published data on the size of fog droplets which form in the sulfuric acid industry; the few reports which are available on the subject do not specify the conditions of fog formation, its lifetime, or mass concentration. Since the size of the droplets changes continuously by coalescence, this information is of little value.

Results of calculations show that the number density of fog droplets at the end of the nucleation stage in the Glover tower is $N = 10^8\,cm^{-3}$, dropping to $N = 0.8 \cdot 10^8\,cm^{-3}$ at the outlet due to coalescence. If we accept this figure, as well as the data listed in Table 5.17, we find that the total surface area of the fog droplets is nearly $10\,m^2/m^3$. The surface of the packing (ceramic rings measuring 50×50 mm) is $110\,m^2/m^3$ /25/.

Despite the comparatively large surface of the fog droplets, the quantity of SO_2 oxidized in the droplets is small (see Table 5.17). This is so because the concentration of the acid in the fog droplets is higher than the concentration of the spraying acid (see Table 5.16), while the rate of SO_2 oxidation, as we have previously observed, decreases as the acid concentration is increased.

At this stage we cannot determine the effect of acid concentration in the fog particles on the rate of SO_2 oxidation, since the published data display a considerable divergence /45/. It is therefore impossible to determine the mass concentration of fog in the gas mixture emerging from the tower.

We see from Table 5.17 that due to the conversion of SO_2 to sulfuric acid in fog droplets the mass concentration of the fog in the gas leaving the first tower is twice as high as the theoretically calculated figure ($24\,g/m^3$, and not $13.4\,g/m^3$). The oxidation of SO_2 in fog droplets continues in the second tower as well, and the total quantity of sulfuric acid in the droplets rises to $40\,g/m^3$ (see Table 5.17).

The sulfur fumes contain dust particles which may act as condensation nuclei. It is readily seen, however, that the dust does not have a noticeable effect on fog formation. Indeed, according to technological specifications /25/, the content of dust in the gas passed through dry electrostatic precipitators should not exceed $0.1\,g/m^3$ or $1 \cdot 10^{-7}\,g/m^3$.

The density of the dust collected in dry electrostatic precipitators is $3\,g/cm^3$. Calculations show that nearly 75% of all the dust particles have radii greater than $1.7 \cdot 10^{-3}$ cm; we therefore take $e_d \approx 1 \cdot 10^{-3}$ cm. From equation (5.85) we thus have $N_d = 10\,cm^{-3}$, i.e., each cubic centimeter of the gas mixture entering the Glover tower contains about 10 dust particles. This dust content can hardly affect the process of fog formation: the number density of embryos in the first instant of nucleation is $N \approx 10^8\,cm^{-3}$, as we have previously observed.

The bulk of sulfuric acid fog which forms in the Glover tower is precipitated in subsequent chambers and towers, but part of it nevertheless escapes into the atmosphere with the discharge gases. The concentration of fog in the emerging gases is nearly $5\,g/m^3$, i.e., the losses of sulfuric

acid are about 1.5% of the total output. Electrostatic precipitators are installed in some sulfuric acid plants which recover the H_2SO_4 fog from the exhaust gases and thus lower the process losses. These precipitators, however, are a costly piece of equipment, and the engineers should try to reduce the acid losses by alternative techniques, specifically by suppressing the formation of fog in the Glover tower.

The supersaturation decreases as the temperature of the condensation surface (i.e., the temperature of the spraying acid) is increased, because the ratio (5.21) decreases. The reduction in supersaturation lowers the quantity of fog forming in the Glover tower.

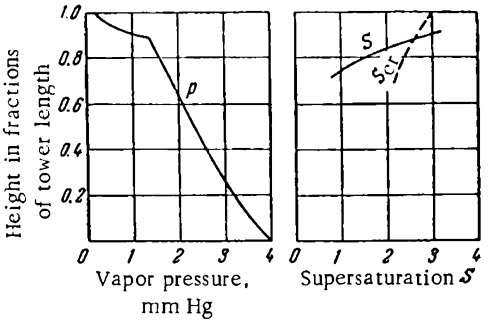

FIGURE 5.21. H_2SO_4 vapor pressure and supersaturation in a Glover tower sprayed with concentrated sulfuric acid (theoretical).

Figure 5.21 plots the results obtained for an acid-sprayed Glover tower. The temperature of the acid is higher than in the previously considered case. The following numerical data were assumed:

Quantity of spraying sulfuric acid g_a, kg/hr	1030
Concentration of sulfuric acid, %	
at the inlet C_2	77.9
at the outlet C_1	91
Temperature of the gas at the outlet t, °C	155
Temperature of the acid, °C	
at the inlet t_2	38.4
at the outlet t_1	189.1

Comparison of Figures 5.20 and 5.21 shows that when the Glover tower is sprayed with more concentrated sulfuric acid, fog forms at a later stage (approximately at a height of 0.9 m, and not 0.4 m). The bulk of sulfuric acid vapor condenses on the packing, and less fog is therefore formed than in a normally running Glover tower. Under the above conditions the content of fog in the gas issuing from the Glover tower is 6.9 g/m^3, i.e., half the corresponding figure in the former case.

We should also remember that as the concentration of the spraying acid is increased, the concentration of the acid in the fog particles rises to 86% and the rate of SO_2 oxidation in the droplets decreases. The content of H_2SO_4 mist in the gases issuing from a Glover tower sprayed with

concentrated sulfuric acid is therefore a factor of 3—4 less than in the gas from a normally operating tower. If part of the sulfuric acid produced in the tower is delivered to the spraying cycle in order to increase the concentration of the acid spray, fog formation is further reduced or perhaps prevented altogether. Increasing the temperature of the spraying acid raises the radius of the fog droplets and ensures better separation of the mist in the subsequent stages.

In the contact process of sulfuric acid manufacture, the fumes are scrubbed with sulfuric acid. The conditions in the first scrubbing tower are approximately the same as in a Glover tower (p. 155). The mass concentration of the scrubbed gas is therefore the same as in the gas issuing from the Glover tower /46/ (see Table 5.16).

The condensation indices in the first scrubbing tower vary approximately in the same way as in the condenser tower in the wet-gas process (see Figure 5.19).

Formation of sulfuric acid fog in the first scrubbing tower substantially complicates the contact process, and considerable efforts are therefore devoted to the development of fogless cleaning procedures. The first scrubber is sprayed with concentrated sulfuric acid which is heated to a sufficiently high temperature, to prevent the supersaturation from reaching the critical value in the tower. Fog formation is thus avoided /25, 47/. The temperature of the spraying acid is determined from equations (5.9) and (5.8). The As_2O_3 and SeO_2 fumes present in the gas mixture are absorbed by the sulfuric acid in the scrubber; they are recovered from the acid solution at a later stage. The gas emerging from the scrubbing tower is passed through a spray trap and is then delivered to the contact chamber.

The content of sulfuric acid vapor in the fumes entering the tower is low, and the heat of condensation is therefore ignored. The sulfuric acid vapor pressure in the tower is calculated from equation (5.68).

In the contact process the gas is dried in a packed tower which is sprayed with concentrated sulfuric acid. A considerable quantity of heat is released when the acid absorbs water vapor, so that the sulfuric acid heats and partially evaporates. The sulfuric acid vapor is mixed with the cold gas stream, where it condenses into fog. This process is further enhanced by the high content of water vapor (approximately 35 g/m^3 at NTP) in the gas. The equilibrium vapor pressure of sulfuric acid is thus lowered, and nearly all the H_2SO_4 vapor is converted to fog. The mass concentration of the fog forming in drying towers is therefore determined by calculating the quantity of sulfuric acid which evaporates from the H_2SO_4-wetted surface of the tower. The calculations can be made using equation (5.1) and the data available on the coefficient β_p /25/.

In the contact process fog often forms as the sulfuric acid vapor present together with SO_2 in the gases condenses in oleum and monohydrate absorption towers. Sulfuric acid vapor is formed when water vapor (which remains in the gas after drying) combines with SO_3 (produced in the contact chamber) or when the spraying acid evaporates upon mixing with the hot gas in the lower part of the absorption tower. If the content of water vapor in the gas is less than 0.01% (the technologically acceptable limit /25/) the quantity of sulfuric acid vapor is insignificant, and no fog forms in the absorber.

When the percentage drying is lowered, more sulfuric acid vapor reaches the absorption tower and fog is formed. Fog formation is minimized by absorbing the SO_3 in a monohydrate absorption tower sprayed with sufficiently hot concentrated sulfuric acid (98.3% H_2SO_4). The higher the content of water vapor in the incoming gas (0.2—0.3%), the higher the temperature of the spraying acid (80—90 °C at the inlet, 110—120 °C at the outlet).

PREVENTION OF FOG DURING VAPOR CONDENSATION IN BUBBLERS

The principal advantage of bubblers is the high rate of condensation ensured by the fast flow of the gas and especially by the fragmentation of the gas stream into a multitude of bubbles, the surface of each bubble renewing as it moves up through the liquid layer.

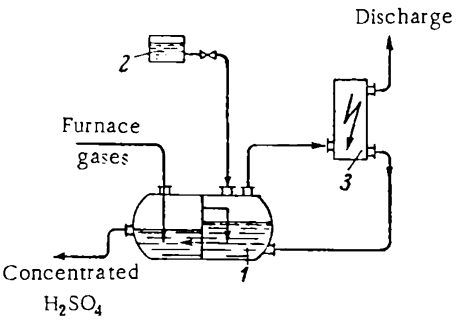

FIGURE 5.22. Bubbler for sulfuric acid concentration:
1) concentrator; 2) weak acid; 3) electrostatic precipitator.

Bubblers are used for scrubbing and cooling of gases, for the absorption of gaseous substances in liquids, for vapor condensation, etc. They are very popular in phosphoric and sulfuric acid industries: bubblers of the same design are used in the manufacture of both phosphoric and sulfuric acids. The two acids have close boiling points and they condense under very similar conditions.

A bubble concentrator is a horizontal cylinder 1 (Figure 5.22) divided into two or more separate chambers. The sulfuric acid to be concentrated is delivered from the tank 2 to the second chamber and then flows to the first chamber. Furnace gases (800—1000 °C) are injected into the first chamber through pipes immersed in the acid pool. The bubbling gases heat the acid, the excess water evaporates, and the acid becomes more concentrated. Some sulfuric acid, however, also evaporates in the process.

The gas cooled to 250—260 °C in the first chamber is delivered by pipes to the second chamber where it again bubbles through the acid layer. The sulfuric acid vapor imported by the gas from the first chamber condenses on the surface of the relatively cold sulfuric acid (130—150 °C) in the second chamber. The conditions favor spontaneous condensation and fog is formed. The fog droplets are separated in an electrostatic precipitator 3.

The quantity of sulfuric acid collecting in the electrostatic precipitators is 15—20% of the total amount of acid delivered into the concentrator. The cost of the precipitators is nearly 35% of the total cost of the concentrator, and it is therefore highly desirable to prevent fog formation altogether or to ensure that the droplets, once formed, grow to a substantial size (in order to reduce the field strength in the precipitators).

Figure 5.23 shows schematically how acid vapor condenses in a gas bubble moving up through a layer of sulfuric acid in the second chamber

of the H_2SO_4 concentrator. The inner bubble surface is cooler than the gas, and the gas loses heat. This heat causes evaporation of water molecules which diffuse from the interior of the acid volume to the bubble, and the water content of the bubbling gas mixture is increased. The temperature and the concentration of the sulfuric acid remain constant because less concentrated acid is continually delivered to the second chamber, the excess overflowing to the first chamber.

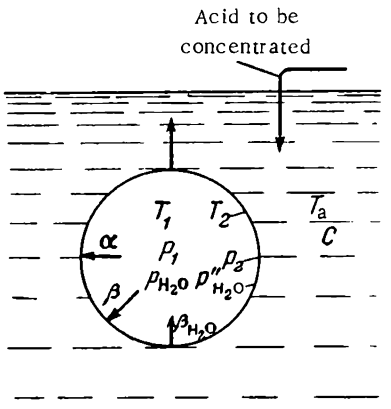

FIGURE 5.23. Condensation of sulfuric acid vapor in a gas bubble:
α is the coefficient of heat transfer from the gas for the bubble surface; β the coefficient of H_2SO_4 condensation; β_{H_2O} water evaporation coefficient; T_1, T_2, and T_a the temperatures of the gas, the bubble surface, and the acid; p_1 and p_2 acid vapor pressure in the gas and near the bubble surface; p_{H_2O} and p''_{H_2O} water vapor pressure in the gas and near the bubble surface; C acid concentration.

The gas bubble on its way up passes through new layers of acid, and the temperature of the inner surface of the bubble (on which the sulfuric acid vapor condenses) therefore remains constant. Vapor condensation in bubblers is thus calculated using equations (5.7) and (5.8). These calculations show /48/ that if the concentrator has two chambers, the supersaturation of the sulfuric acid vapor in the second chamber (where the temperature of the vapor is drastically reduced) is high enough for fog condensation to occur.

Table 5.18 and Figure 5.24 describe the variation of the condensation indices in a gas bubble on its way up through the acid in the second chamber.

The supersaturation attains its maximum at a temperature of 215 °C and H_2SO_4 vapor pressure of 6.1 mm Hg (Table 5.18). Previous data on vapor condensation in a pipe (see Table 5.10) suggest that when the gas is cooled further, the bulk of the sulfuric acid vapor condenses on the surface of already existing fog droplets. The content of sulfuric acid mist in the gas leaving the second chamber is therefore calculated from (5.26); in the case on hand the calculations give $g = 35\ g/m^3$.

It follows from equation (5.8) that as the temperature of the acid (T_2) and the H_2SO_4 vapor pressure over the acid (p_2) are increased, the supersaturation decreases. Fog can therefore be prevented if the bubbler is divided into several chambers, the temperature and the concentration of the acid being gradually lowered from one chamber to the next. The number of chambers and the particular operating conditions depend on the acid content before and after concentration and on the permissible percentage of acid losses in the discharge gases. Optimal conditions ensuring minimum supersaturation should be determined theoretically.

TABLE 5.18. Vapor conditions in a gas bubble in the second concentrator chamber

Position in Figure 5.24	Temperature, °C	H_2SO_4 vapor pressure, mm Hg	Supersaturation
3	250	7.5	0.9
4	230	6.7	1.7
5	215	6.1	$S = S_{cr} = 2.7$
6	143	Fog, 35 g/m³ at NTP	

Figure 5.25 is a schematic diagram of a concentrator which consists of four bubbling chambers in a series. The sulfuric acid is mainly concentrated in the first chamber, while the other three chambers serve for preliminary concentration and separation of sulfuric acid vapor.

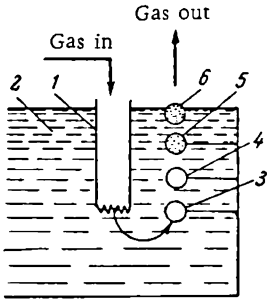

FIGURE 5.24. Schematic diagram showing how sulfuric acid vapor condenses in the second bubbler compartment:
1) bubbling tube; 2) 72.5% H_2SO_4 at 140 °C; 3—6) gas bubbles.

The furnace gases pass successively through the four chambers; each chamber is fed with 68.6% H_2SO_4 through a separate pipe. The fortified acid from all the chambers is delivered to the first chamber, which also receives a small quantity of weak acid. The output of the first chamber is 93% H_2SO_4.

The process is controlled so that no fog should form in the subsequent stages of sulfuric acid separation. This is achieved by adding weak sulfuric acid to all the chambers, so the acid concentration in the bubbler remains constant.

Table 5.19 lists the results of some calculations which indicate that the bulk of the sulfuric acid vapor (65%) is trapped in the second chamber; 19% condenses in the third chamber and some 11% in the fourth. The emissions thus contain 2.2 g/m³ of sulfuric acid, which is less than 0.5% of the total output. If a fifth chamber is added to the installation (a case not covered by Table 5.19), the H_2SO_4 emissions drop to 0.5 g/m³ at NTP.

A succession of four chambers (where the first chamber acts as the main acid concentrator) is therefore sufficient for separating nearly all H_2SO_4 vapor from the gas, so that no fog is formed.

The number of successive chambers can be reduced if the temperature of the gas is raised by adding hot furnace gases at each stage of the concentration process. A more uniform temperature is thus maintained in

all the chambers, the supersaturation of H_2SO_4 vapor is decreased, and the probability of fog formation diminishes. The supersaturation decreases because the denominator of (5.21), which enters equation (5.8), increases as the gas temperature (T_1) at the inlet is increased.

TABLE 5.19 Stages in sulfuric acid concentration with furnace gases injected into the first chamber

	1st chamber	2nd chamber	3rd chamber	4th chamber
Gas temperature, °C				
inlet	800	240.7	211	201
outlet	240.7	211	201	181
Acid concentration, % H_2SO_4				
incoming	71.3	68.6	68.6	68 6
outgoing	93	89.2	88.2	84.2
Temperature of acid in the chamber, °C	232	210	200	180
H_2SO_4 vapor pressure at the outlet, mm Hg	7.5	2.6	1.2	0.4
Acid intake, % of the total	83.6	10.4	1.2	4 8
Maximum supersaturation	—	1.74	1.99	2.23
Critical supersaturation	—	1.76	2.0	2.26
Supersaturation at the outlet	0.67	1.31	1.11	1.26
Efficiency	0.9	0.9	0.9	0.9

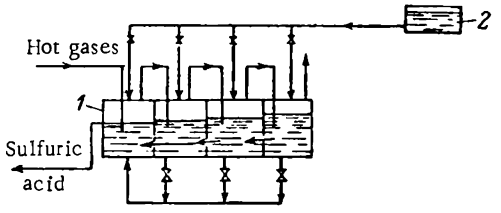

FIGURE 5.25. Sulfuric acid concentrator:
1) concentrated acid; 2) weak acid.

Figure 5.26 is a schematic drawing of a sulfuric acid concentrator where hot gas is added in different stages. The temperature and the concentration of the acid are adjusted to ensure the required conditions, i.e., the temperature of the gas entering each successive chamber is raised by injecting hot gas and the acid concentration is regulated by dilution with some weak acid.

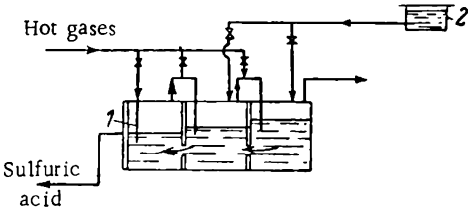

FIGURE 5.26. Sulfuric acid concentrator with hot gas injected into the second and the third chambers:
1) concentrated acid; 2) weak acid.

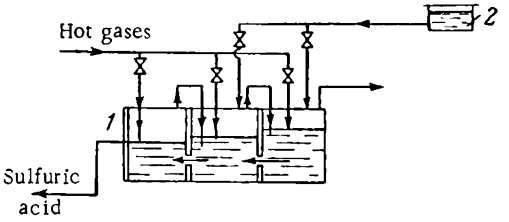

FIGURE 5.27. Sulfuric acid concentrator with hot gas injection to the second and the third chambers through separate pipes:
1) concentrated acid; 2) weak acid.

Calculations of the three-chamber concentrator show that if the gas is heated before entering each successive chamber (by adding 46% of hot gases at the entrance to the second chamber and 22% at the entrance to the third chamber), the partial pressure of H_2SO_4 vapors is 0.66 mm Hg after the second chamber and 0.09 mm Hg (0.48 g/m^3) after the third chamber. Comparison of these data with the figures listed in Table 5.19 indicates that the addition of hot gas substantially improves the process of concentration. The condensation of sulfuric acid vapor in the second and the third chambers is more complete than without hot gas injection.

The preceding calculations ignore the acid spray which is carried over from one chamber to the next. This effect is of no significance when all the hot gas is injected into the first chamber (Figure 5.25), as it only slightly alters the acid feed of each chamber.

An important modification is a concentrator with hot gas injection into the second and subsequent chambers through separate pipes (Figure 5.27). Each chamber thus receives two gas streams which bubble independently through the acid layer. Different processes occur in each stream. The gas stream coming from the first chamber contains sulfuric acid vapor which is mostly converted into fog. The separately admitted hot furnace gas contains no sulfuric acid vapor. Therefore no fog forms when this gas mixes with the cold acid: it is only saturated with acid vapor. Since the concentration of the acid in the second chamber is low, the mass of H_2SO_4 vapor in the gas is small and the saturated vapor pressure is substantially less than in the first chamber (it is 8.4 mm Hg in the first chamber and only 0.17 mm Hg in the second). When the two streams are eventually mixed, the concentration of sulfuric acid fog in the gas mixture is less than that without hot gas injection.

TABLE 5.20. The content of sulfuric acid in the gas after the third chamber in a concentrator with separate hot gas injection

Hot gas injection, %			H_2SO_4 content in the gas leaving the third chamber, g/m^3		
1st chamber	2nd chamber	3rd chamber	as fog	as vapor	total
57	27	16	9.0	1.0	10.0
32	46	22	4.1	0.2	4.3
16	51	33	4.1	0.3	4.4

Note. Temperature of furnace gas 820 °C, content of sulfuric acid vapor after the 1st chamber 43.3 g/m^3 at NTP.

Table 5.20 lists the results of calculations on the content of fog and sulfuric acid vapor in a gas mixture emerging from the third chamber in a concentrator with separate hot gas injection into the second and the third chambers. We see that as the quantity of hot gas injected into the second and the third chambers increases, the content of sulfuric acid first decreases and then starts increasing. It is thus possible to calculate the optimal concentration conditions in this case.

It also follows from the above that sulfuric acid can be concentrated without fog formation by direct contact with hot gases if certain conditions are observed. The concentration should be split into several successive stages, and fog can be prevented more easily if these stages are comparatively numerous. The number of successive stages can be reduced if the gas is heated before moving from one chamber to the next or if hot furnace gases are injected into each chamber through a separate pipe.

The validity of our calculations is supported by the operating indices of industrial installations. In a two-chamber concentrator /49/, with hot furnace gases passing successively through the two chambers, the concentration of sulfuric acid mist in the gas leaving the second chamber was 35—40 g/m^3 (this result is consistent with the theoretical figures listed in Table 5.18). If, however, the furnace gases were injected simultaneously into each chamber, the fog content dropped by more than a factor of three to 11 g/m^3 (at NTP). In wet-gas processes sulfuric acid vapor is sometimes separated not in a packed tower (p. 153), but in a bubbler /21/ which is analogous to the three-chamber bubbling concentrator described in this chapter. The first chamber receives gas with a certain content of sulfuric acid vapor, the vapor condensing in the same way as in the second chamber of the concentrator (p. 163). Since the saturated vapor pressure in the chamber is sufficiently high, no fog is formed.

REFERENCES

1. AMELIN, A. G. — ZhTF, 16:1409. 1946.
2. AMELIN, A. G. — ZhTF, 19:1136. 1949.
3. MIKHEEV, M. A. Osnovy teploperedachi (Principles of Heat Transfer). — Gosenergoizdat. 1959.
4. KUTATELADZE, S. S. and V. M. BORISHCHANSKII. Spravochnik po teploperedache (Heat Transfer Handbook). — Gosenergoizdat. 1959.
5. RAMM, V. M. Adsorbtsionnye protsessy v khimicheskoi promyshlennosti (Adsorption in Chemical Industry). — Goskhimizdat. 1951.
6. ACKERMAN, G. — Forschungsheft, 1:382. 1937.
7. COLBURN, A. P. and T. B. FRANS. — Am. Inst. Eng., 33:197. 1937.
8. COLBURN, A. P. and A. EDISSON. — Ind. Eng. Chem., 33:457. 1941.
9. CHILTON, T. H. and A. P. COLBWIN. — Ind. Eng. Chem., 26:1183. 1934.
10. BERMAN, L. D. — ZhTF, 2:148. 1939.
11. BERMAN, L. D. — Izvestiya VTI, No. 10—11:17. 1940.
12. BERMAN, L. D. Isparitel'noe okhlazhdenie tsirkulyatsionnoi vody (Evaporative Cooling of Circulating Water). — Gosenergoizdat. 1949.
13. DUKHIN, S. S., B. V. DERYAGIN, and M. L. MIKHEL'SON. — DAN SSSR, 105:1229. 1955.
14. LEVICH, V. G. Fiziko-khimicheskaya gidrodinamika (Physicochemical Hydrodynamics). — Fizmatgiz. 1959.
15. FUKS, N. A. Mekhanika aerozolei (Mechanics of Aerosols). — Izdatel'stvo AN SSSR. 1955.
16. BAKANOV, S. P. and B. V. DERYAGIN. — Kolloidnyi Zhurnal, 21:377. 1959.
17. FUKS, N. A. Uspekhi mekhaniki aerozolci (Advances in Aerosol Mechanics). — Izdatel'stvo AN SSSR. 1961.

18. AMELIN, A. G. and M. I. BELYAEV. — Kolloidnyi Zhurnal, 24 : 374. 1962.

19. COLBWIN, A. P. and O. A. HOGEN. — Ind. Eng. Chem., 26 : 1178. 1934.

20. SMITH, I. C. — Ind. Eng. Chem., 34 : 1248. 1942; 134 : 1495. 1942.

21. AMELIN, A. G. Proizvodstvo sernoi kisloty iz serovodoroda po metody mokrogo analiza (Wet-Gas Contact Process for the Production of Sulfuric Acid from Hydrogen Sulfide). — Goskhimizdat. 1960.

22. AMELIN, A. G. — Kolloidnyi Zhurnal, 25 : 146. 1963.

23. AMELIN, A. G. and E. V. YASHKE. — Kolloidnyi Zhurnal, 25 : 3. 1962.

24. DERYAGIN, B. V. and G. Ya. VLASENKO. — DAN SSSR, 63 : 155. 1948; Kolloidnyi Zhurnal, 13 : 249. 1951; Vestnik AN SSSR, 5 : 76. 1951; Priroda, 29. 1953.

25. AMELIN, A. G. Proizvodstvo sernoi kisloty (Sulfuric Acid Industry). — Khimiya. 1964.

26. FUKS, N. A. Isparenie i rost kapel' v gazoobraznoi srede (Evaporation and Growth of Droplets in a Gaseous Medium). — Izdatel'stvo AN SSSR. 1958.

27. AMELIN, A. G. — Soobshcheniya o nauchnykh rabotakh chlenov VKhO im. D. I. Mendeleeva, No. 46. 1949.

28. AMELIN, A. G. and Z. B. BORODASTOVA. — ZhPKh, 24 : 529. 1950.

29. AMELIN, A. G. — ZhKhP, No. 10 : 14. 1940.

30. VASYUNINA, G. V. and L. S. AKSEL'ROD. — Trudy VNIIKIMASh, 4 : 184. 1961.

31. VASYUNINA, G. V. and L. S. AKSEL'ROD. — Trudy VNIIKIMASh, 6 : 8. 1963.

32. HAUSEN, H. — Angew. Chem., 20 : 12. 1948.

33. GLADKOV, N. G. Kurs rekuperatsionnoi tekhniki (Regeneration Techniques). — Izdatel'stvo Leningradskogo Krasnoznamennogo khimiko-tekhnologicheskogo instituta. 1934.

34. PLATTI, L. Recovery of Volatile Solvents. [Russian translation. 1934.]

35. PUZHAI, N. S. — ZhKhP, No. 20 : 21, 22. 1931.

36. PLANOVSKII, A. N., V. M. RAMM, and S. Z. KOGAN. Protsessy i apparaty khimicheskoi tekhnologii (Processes and Equipment in Chemical Industry). — Goskhimizdat. 1962.

37. SCARBOROUGH, J. B. Numerical Mathematical Analysis. — London, Oxford Univ. Press. 1930.

38. VOL'FKOVICH, S. I., A. P. EGOROV, D. A. EPSHTEIN, et al. Obshchaya khimicheskaya tekhnologiya (General Chemical Engineering), Vol. 1. — Goskhimizdat. 1953.

39. CHEREPKOV, I. F. — ZhKhP, No. 3 : 19. 1940.

40. SHUL'TS, V. N. — ZhKhP, No. 16 : 807. 1936.

41. AMELIN, A. G. and A. I. BARANOVA. — ZhKhP, 22 : 1225. 1949.

42. THOMAS, J. S. and W. E. BORKER. — J. Chem. Soc., 127 : 2820. 1925.

43. AMELIN, A. G. — Dissertation. Moskva. 1946.

44. ABEL, E. — J. Phys. Chem., 50 : 260. 1946.

45. MALIN, K. M. Tekhnologiya sernoi kisloty (Sulfuric Acid Technology). — Goskhimizdat. 1950.

46. AMELIN, A. G. — Khimicheskaya Promyshlennost', No. 2 : 28. 1960.

47. AMELIN, A. G. — Soviet patent 105414, 11 Feb. 1940; Byulleten' Avtorskikh Izobretenii, No. 2 : 11. 1957.

48. AMELIN, A. G. and Z. B. BORODASTOVA. — ZhPKh, 18 : 664. 1956.

49. RYBNIKOV, G. S. and A. S. TITOV. — Khimicheskaya Promyshlennost', No. 8 : 54. 1961.

Chapter Six

FORMATION OF SUPERSATURATED VAPOR AND FOG AS THE RESULT OF CHEMICAL REACTIONS OF GASES IN THE VOLUME

DERIVATION OF WORKING FORMULAS FOR SUPERSATURATION

Supersaturated vapor develops in a chemical reaction between gaseous components only if the saturated vapor pressure of the reaction products is less than the saturated vapor pressure of the starting components. Chemical reactions in a gaseous phase are triggered by the collision of the reactive molecules due to turbulent or diffusive mixing of the gases or by various external agents, such as heat, light, X rays, radioactive radiations, ultrasound, etc.

Molecular collisions between SO_3 and H_2O, NH_3 and HCl, and between other gaseous components result in the formation of vapors of new chemical compounds (H_2SO_4, NH_4Cl, etc.) with lower saturated vapor pressures. High supersaturations are thus obtained and the vapors condense spontaneously tc give fog droplets.

Gaseous $Fe(CO)_5$ and $Ni(CO)_4$ decompose when heated. Metal vapors are released, they condense spontaneously and settle in the form of metal powder. Some hydrocarbons are similarly decomposed when heated in the absence of oxygen or in an excess of oxygen. The decomposing hydrocarbons release carbon vapor which condenses in minute particles — finely divided soot (p. 187).

When $SiCl_4$ and SiF_4 react with water vapor at around 1000 °C, the starting compounds are hydrolyzed (p. 191) and SiO_2 vapor is formed. It condenses into silica smoke — fine silica powder, commercially known, e.g., under the German trade-name Aerosil.

The present theory of formation of supersaturated vapor in chemically reacting gases is fairly rudimentary, and we therefore present but a limited discussion of a few aspects of this highly significant problem.

The working equations for the supersaturation change depending on the particular chemical reaction and on the processes which trigger the reaction. If the reacting gases are allowed to collide in turbulent streams, the vapor pressure of the reaction products and the temperature of the resulting gas mixture are determined by the same factors as those previously considered in the section on vapor-gas mixtures (Chapter Three). The supersaturation, however, depends on many other factors, and the corresponding equation is more complex than for the mixing of vapors and gases:

$$S = f(n, k_1, Q_1, V. \ . \ . \ .) \qquad (6.1)$$

where n is a parameter defined by equation (3.1); k_1 the rate constant of the reaction; Q_1 the reaction heat; V the total volume of the gas mixture (which may vary in the course of the reaction).

No general equation for the supersaturation has been derived. In particular cases, however, the effect of some factors can be ignored and the supersaturation equation is then obtained in a fairly convenient form.

If the reaction is described by the equation

$$\nu_1 A_1 + \nu_2 A_2 = \nu A + Q \tag{6.2}$$

where A_1 and A_2 are the reacting components; A the reaction product; ν_1, ν_2, ν the stoichiometric coefficients, the following expression can be obtained for the vapor pressure p of the reaction products in the mixture by balancing the components as in the derivation of (3.4):

$$p = \frac{p_2 bn}{(1 + bn) - \frac{p_2 bn}{P}(\nu_1 + \nu_2 - \nu)} \tag{6.3}$$

where p_2 is the vapor pressure of the component A_2 in the second gas stream; P the total pressure of the gas mixture; b a coefficient defined by equation (3.3); n a parameter defined by relation (3.1). The last term in the denominator of (6.3) allows for the change in volume due to the reaction between the components.

Equation (6.3) is in force as long as

$$p_2 \leqslant \frac{\nu_1 p_1}{\nu_2 bn} \tag{6.4}$$

where p_1 is the vapor pressure of the component A_1 in the first gas stream. As the content of the component A_2 increases, the reaction continues as long as there is any A_1 in the gas mixture. Once the entire quantity of the first component has reacted, further addition of A_2 cannot increase the concentration of the reaction product. Its concentration is actually decreased by the addition of this, now indifferent gas to the mixture. The vapor pressure of the reaction product in the region where equation (6.3) does not apply is expressed as

$$p = \frac{p_1}{(1 + bn) - \frac{p_1}{P}(\nu_1 + \nu_2 - \nu)} \tag{6.5}$$

The vapor pressure of the reaction product in the mixing region, where the parameter n varies from zero to infinity, is thus plotted by a curve with two intersecting branches (Figure 6.1) /1/. The left-hand branch is expressed by equation (6.3) and the right-hand branch by equation (6.5). The intersection point of the two branches corresponds to the maximum vapor pressure p_{max} of the reaction product in a given gas mixture. Equating the right-hand sides of (6.3) and (6.5) and simplifying, we obtain the value of the parameter n in the region of maximum vapor pressure:

$$n = \frac{p_1}{p_2 b} \tag{6.6}$$

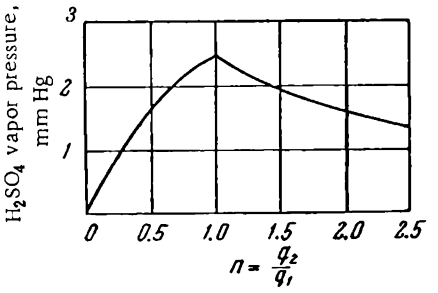

FIGURE 6.1. H_2SO_4 vapor pressure vs. the mass ratio of mixing air streams containing SO_3 and water vapors.

Substituting the parameter n from (6.6) into (6.3) or (6.5), we obtain the maximum vapor pressure after mixing:

$$p_{max} = \frac{p_1 p_2}{(p_1 + p_2) - \frac{p_1 p_2}{P}(\nu_1 + \nu_2 - \nu)} \tag{6.7}$$

If the concentration of the reacting components is low, the volume of the gas mixture does not change appreciably when the reaction takes place, so equations (6.3) and (6.5) can be written as

$$p = \frac{p_2 bn}{1 + cn} \tag{6.8}$$

$$p = \frac{p_1}{1 + bn} \tag{6.9}$$

For the maximum vapor pressure we have

$$p_{max} = \frac{p_1 p_2}{p_1 + p_2} \tag{6.10}$$

The temperature of the gas after mixing can be determined as in the derivation of (3.7) by balancing the heat currents:

$$g_1 c_1 T_1 + g_2 c_2 T + Q_p = T(g_1 c_1 + g_2 c_2) \tag{6.11}$$

where Q_p is the heat released when the new product is formed.

Equation (6.11) does not allow for the effect of the reaction product on the specific heat of the gas mixture, since the corresponding change is small in systems with a low content of reacting gases. The quantity of heat released by the chemical reaction can be expressed as

$$Q_p = \frac{pMQ}{P}\left(\frac{g_1}{M_1} + \frac{g_2}{M_2}\right)$$

where Q is the heat of the reaction (6.2); M the molar mass of the reaction product; M_1 and M_2 the molar masses of the reacting components.

Inserting this expression for the Q_p in the heat balance equation (6.11) and making use of relations (3.3) and (3.6), we find

$$T = \frac{T_1 + T_2 an + \frac{pMQ}{PM_1c_1}(1 + bn)}{1 + an} \tag{6.12}$$

If the reaction heat is ignored, equation (6.12) reduces to equation (3.7).

The supersaturation in the mixing region is represented by a curve of the same general shape as the vapor pressure graph, i.e., two intersecting branches. The left-hand branch corresponds to n between 0 and p_1/bp_2 (the vapor pressure according to equation (6.3)), and the right-hand branch to n varying from p_1/bp_2 to infinity (the vapor pressure according to equation (6.5)).

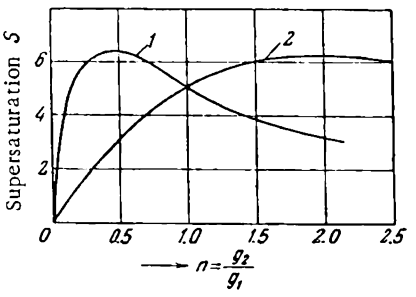

FIGURE 6.2. Supersaturation of sulfuric acid vapor as a function of the mass ratio of the mixing air streams containing SO_3 and water vapor.

The complex dependence of the temperature and the vapor pressure on the mass ratio of the mixing components obstructs the derivation of a general equation expressing the supersaturation as a function of n. Practical calculations are therefore best made by the graphical method.

Figure 6.2 presents the results calculated for the mixing of two air streams containing water vapor and SO_3 /1/. The SO_3 vapor pressure is 5 mm Hg. Curve 1 corresponds to the mixing of air streams with $t_1 = 100\,°C$ and $t_2 = 140\,°C$, curve 2 to air streams with $t_1 = 140\,°C$ and $t_2 = 100\,°C$. We see from Figure 6.2 that in both cases the supersaturation vs. n curves have a maximum.

If the volume and the temperature of the gas mixture are assumed to remain unaffected by the chemical reaction, the supersaturation in the mixing region can be found from equation (3.10). The parameter n corresponding to the maximum supersaturation is then calculated from (3.13). Two separate regions, however, should be considered, with the parameter n varying from 0 to p_1/bp_2 and from p_1/bp_2 to infinity. In the former region we put in (3.10) and (3.13) $p_1 = 0$, and in the latter region $p_2 = 0$. Substituting $p_1 = 0$, we find

$$S = \frac{p_2 bn}{(1 + bn)\, p_\infty(T)} \tag{6.13}$$

$$A = \frac{2T_1T_2 + E(T_1 - T_2)}{Eb(T_1 - T_2) + aT_2^2} \qquad B = \frac{T_1^2}{Eab(T_1 - T_2) + aT_2^2} \tag{6.14}$$

Putting $p_2 = 0$, we obtain

$$S = \frac{p_1}{(1 + bn)\, p_\infty(T)} \tag{6.15}$$

$$A = \frac{2T_1T_2 - E(T_1 - T_2)}{aT_2^2} \qquad B = \frac{bT_1^2 - Ea(T_1 - T_2)}{a^2bT_2^2} \tag{6.16}$$

The supersaturation, the drop size distribution, and the radii of the fog particles are primarily dependent on the rate of the reaction which produces the condensable compound, i.e., on the parameter $dp/d\tau$.

When nucleation occurs, the supersaturation is diminished by the condensational growth of the droplets. The longer the droplets stay in the supersaturated region, the greater the supersaturation decrement. The dispersity and the number density of the fog forming in chemical reactions therefore both depend on the derivative $dS/d\tau$, and equations (1.91) and (1.92) apply in this case.

FORMATION OF FOG WHEN SO_3 IS ABSORBED BY AQUEOUS H_2SO_4 SOLUTIONS

Two distinct regions should be distinguished in the absorption of SO_3 by aqueous solutions of sulfuric acid, according as the acid is more or less concentrated than 98.3% H_2SO_4 (the azeotropic point, where the boiling point is maximal). At low concentrations (below the azeotropic point) the gaseous phase contains H_2SO_4 and H_2O vapors, while at high concentrations (above the azeotropic point) H_2SO_4 and SO_3 vapors are liberated from the solution. Therefore when some SO_3 is externally injected into a gas phase in equilibrium with 98.3% H_2SO_4, the excess SO_3 is absorbed by the sulfuric acid. This process can be calculated using the ordinary equations for the absorption of readily soluble gases in liquids. The effect of various factors on the absorption rate was determined in laboratory tests /2/. The numerical value of the rate constant for packed towers is known from industrial surveys /3/.

If some SO_3 vapor is injected externally into the gas phase in equilibrium with sulfuric acid of less than 98.3% H_2SO_4, the SO_3 is partly absorbed by the sulfuric acid and partly reacts with the H_2O vapor forming gaseous H_2SO_4. The sulfuric acid vapor pressure in the gas phase increases above the saturated vapor pressure; the equilibrium is displaced and H_2SO_4 starts condensing on the surface of the liquid. On the other hand, the reaction of water molecules with SO_3 leads to a H_2O deficiency in the gas phase, and some water evaporates from the surface of the sulfuric acid.

To sum up, when a gas mixture containing SO_3 comes in contact with a sulfuric acid solution of less than 98.3% H_2SO_4, the SO_3 gas reacts with water forming supersaturated H_2SO_4 vapor. If the resulting supersaturation exceeds the critical value, the vapor will condense spontaneously and sulfuric acid fog is formed. The aerosol particles subsequently coalesce and settle out under the action of gravity, centrifugal forces, etc. Since the absorption of SO_3 vapor by sulfuric acid of less than 98.3% concentration is invariably accompanied by condensation of H_2SO_4 vapor, the ordinary equations of gas absorption are inapplicable in this case.

The total quantity of the sulfur trioxide absorbed from the gas mixture is expressed by the equation

$$G = g_1 + g_2 + g_3 \qquad \text{(a)}$$

where g_1 is the quantity of sulfur trioxide absorbed as SO_3; g_2 the quantity of sulfur trioxide absorbed as H_2SO_4 vapor; g_3 the quantity of sulfur trioxide absorbed as H_2SO_4 fog.

If the absorption of SO_3 by sulfuric acid takes place at temperatures under 100 °C, when the equilibrium vapor pressure of H_2SO_4 is very small,

g_2 can be ignored. The quantity of H_2SO_4 fog settling out in absorption towers is negligible, and in practice we may therefore put $g_3 = 0$. The amount of sulfur trioxide absorbed by sulfuric acid from the gas atmosphere is therefore mainly determined by the first component, i.e., its absorption as SO_3 gas.

The rate of this process depends not only on the rate of absorption of SO_3 by sulfuric acid, but also on the rate of formation of H_2SO_4 vapor in the reaction between SO_3 and H_2O in the gas phase. The rate of formation of sulfuric acid vapor depends, on the one hand, on the rate of evaporation of water from the solution surface and, on the other hand, on the rate of the reaction between SO_3 and H_2O in the vapor phase. It has been shown /4, 5/ that the reaction between H_2O and SO_3 vapors is almost instantaneous; therefore as long as the gas mixture contains SO_3, it holds no water vapor. The rate of formation of H_2SO_4 from SO_3 and H_2O in the vapor phase is thus determined only by the rate of evaporation of water from the surface of the sulfuric acid solution. This can be expressed by the equation

$$\frac{dp_{H_2O}}{d\tau} = \frac{\beta_2}{\rho}(p_{H_2O,\infty} - p_{H_2O}) \qquad (6.17)$$

where p_{H_2O} is the water vapor pressure in the gas mixture; τ time, sec; β_2 the evaporation coefficient of water, cm/sec; ρ the mean radius of the interstices in the packing, cm; $p_{H_2O,\infty}$ saturated vapor pressure of water at the temperature of the liquid surface.

In our case p_{H_2O} is very small, since the water vapor combines instantaneously with SO_3. Equation (6.17) is therefore written as

$$\frac{dp_{H_2O}}{d\tau} = \frac{\beta_2}{\rho} p_{H_2O,\infty} \qquad (b)$$

The rate of absorption of SO_3 by sulfuric acid in the absence of water vapor is expressed by the equation /2/

$$\frac{dp_{SO_3}}{d\tau} = \frac{\beta_1}{\rho}(p_{SO_3} - p_{SO_3,\infty}) \qquad (6.18)$$

where p_{SO_3} is the SO_3 vapor pressure in the gas mixture; $p_{SO_3,\infty}$ the saturated vapor pressure of SO_3 at the temperature of the liquid surface; β_1 the absorption coefficient of SO_3 by sulfuric acid, cm/sec.

The saturated vapor pressure of SO_3 over sulfuric acid of less than 98.3% H_2SO_4 is negligibly small at temperatures under 100 °C. Equation (6.18) can therefore be written in the form

$$\frac{dp_{SO_3}}{d\tau} = \frac{\beta_1}{\rho} p_{SO_3} \qquad (c)$$

The quantity of SO_3 which combines with water vapor — an essential component in the total absorption balance — can be found from equation (b). Substituting this correction in (c), we write

$$-\frac{dp_{SO_3}}{d\tau} = \frac{\beta_1}{\rho} p_{SO_3} + \frac{\beta_2}{\rho} p_{H_2O,\infty} \qquad (d)$$

Putting

$$\frac{\beta_1}{\rho} = N \quad -\frac{\beta_2 p_{H_2O,\infty}}{\rho} = M$$

and inserting these expressions for the constants in (d), we obtain an ordinary linear differential equation

$$\frac{dp_{SO_3}}{d\tau} + Np_{SO_3} = M$$

The general solution of this equation is

$$p_{SO_3} = e^{-N\tau}\left(\frac{Me^{N\tau}}{N} + C\right) = \frac{M}{N} + \frac{C}{e^{N\tau}} \qquad \text{(e)}$$

For $\tau = 0$ the SO_3 vapor pressure (p_{SO_3}) is equal to the SO_3 vapor pressure in the starting mixture ($p^0_{SO_3}$). Therefore

$$p_{SO_3} = p^0_{SO_3} = \frac{M}{N} + C$$

whence

$$C = p^0_{SO_3} - \frac{M}{N} \qquad (6.19)$$

Inserting the appropriate expressions for the constants N, M, C in equation (e), we find

$$p_{SO_3} = \frac{p^0_{SO_3} + \frac{\beta_2}{\beta_1} p_{H_2O,\infty}}{e^{\beta_1\tau/\rho}} - \frac{\beta_2 p_{H_2O,\infty}}{\beta_1} \qquad (6.20)$$

Equation (6.20) gives the SO_3 vapor pressure in the gas mixture at any time τ. Putting $p_{SO_3} = 0$ in equation (6.20), we find the time for all the sulfur trioxide to be absorbed from the gas mixture:

$$p_{SO_3} = 0 = \frac{p^0_{SO_3} + \frac{\beta_2}{\beta_1} p_{H_2O,\infty}}{e^{\beta_1\tau/\rho}} - \frac{\beta_2 p_{H_2O,\infty}}{\beta_1}$$

where

$$e^{\beta_1\tau/\rho} = \frac{\beta_1 p^0_{SO_3}}{\beta_2 p_{H_2O,\infty}} + 1$$

or

$$\tau = \frac{\rho}{\beta_1} \ln\left(\frac{\beta_1 p^0_{SO_3}}{\beta_2 p_{H_2O,\infty}} + 1\right) \qquad (6.21)$$

Thus only part of the SO_3 is absorbed by the sulfuric acid. The rest combines with water molecules forming H_2SO_4 vapor. At temperatures under 100 °C, the H_2SO_4 vapor pressure is very small. All the gaseous H_2SO_4 therefore condenses spontaneously into fog droplets which are entrained by the gas stream. The absorbed SO_3 can be expressed as the difference between the initial content of sulfur trioxide in the gas mixture and the SO_3 combining with water vapor.

If the total volume of the gas mixture remains constant despite absorption (this is true for the low concentrations of SO_3 commonly encountered in practice), the degree of SO_3 absorption is expressed by the equation

$$\eta = \frac{100\,(p^0_{SO_3} - p_{H_2O})}{p^0_{SO_3}} \qquad (f)$$

where η is the degree of absorption, %; $p^0_{SO_3}$ the initial vapor pressure of SO_3 in the gas mixture; p_{H_2O} the water vapor pressure under the hypothetical condition that the water evaporating from the acid does not react with SO_3.

Integrating equation (b) over p_{H_2O} from 0 to p_{H_2O} and over τ from 0 to τ, we find

$$p_{H_2O} = \frac{\beta_2}{\rho} p_{H_2O,\,\infty} \qquad (g)$$

and inserting for τ its expression from (6.21)

$$p_{H_2O} = \frac{\beta_2 p_{H_2O,\,\infty}}{\beta_1} \ln\left(\frac{\beta_1 p^0_{SO_3}}{\beta_2 p_{H_2O,\,\infty}} + 1\right) \qquad (6.22)$$

Inserting this expression for p_{H_2O} in equation (f), we find

$$\eta = 100\left[1 - \frac{\beta_2 p_{H_2O}}{\beta_1 p^0_{SO_3}} \ln\left(\frac{\beta_1 p^0_{SO_3}}{\beta_2 p_{H_2O,\,\infty}} + 1\right)\right] \qquad (6.23)$$

From (5.19) and (5.28) we have

$$\frac{\beta_1}{\beta_2} = \left(\frac{D_1}{D_2}\right)^{1-m} \qquad (6.24)$$

where D_1 is the diffusivity of SO_3 vapor; D_2 the diffusivity of water vapor.

Making use of (6.24), we obtain from (6.23)

$$\eta = 100\left[1 - \frac{p_{H_2O,\,\infty} D_2^{1-m}}{p^0_{SO_3} D_1^{1-m}} \ln\left(\frac{p^0_{SO_3} D_1^{1-m}}{p_{H_2O,\,\infty} D_2^{1-m}} + 1\right)\right] \qquad (6.25)$$

Equation (6.25) applies when the gas mixture remains in contact with the sulfuric acid surface until all the SO_3 is removed from the gas phase (equation (6.21)).

Equation (6.23) provides a satisfactory fit to experimental data on the absorption of SO_3 by aqueous solutions of sulfuric acid /5, 7/. The experiments were carried out in a vertical absorption column packed with glass marbles and sprayed with sulfuric acid of different concentrations. The column was immersed in an electric furnace which ensured the required temperature conditions along the entire height. Dry air containing 0.67% SO_3 (5.1 mm Hg) was injected into the base of the column. The degree of absorption was calculated from the SO_3 contents at the inlet and the outlet.

One series of experiments was carried out under isothermal conditions, i.e., the temperature was constant along the entire column. The results of these experiments (Figure 6.3) indicate that the experimental findings are in fairly poor agreement with the theoretically calculated data. The divergence observed at the higher temperatures shows that the simplifications adopted in the derivation of (6.23) have a detrimental effect on the accuracy of the calculations.

The time for complete removal of SO_3 from the gas mixture decreases as the saturated vapor pressure of water ($p_{H_2O,\infty}$) over sulfuric acid increases (equation (6.21)). It is zero when the water vapor instantaneously binds all the SO_3 molecules diffusing to the surface of the sulfuric acid (this can be achieved if the water vapor pressure over H_2SO_4 is sufficiently high).

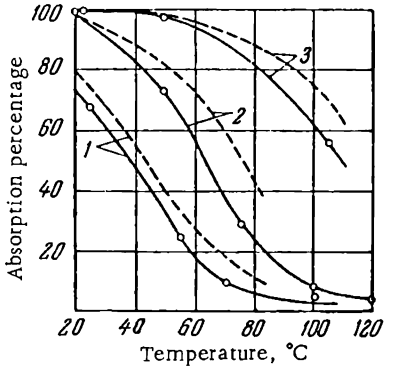

FIGURE 6.3. Degree of absorption of SO_3 by sulfuric acid solutions in a constant-temperature absorption column:
1) 85% H_2SO_4; 2) 90% H_2SO_4; 3) 95% H_2SO_4; solid line — experimental data, dashed line — calculated data.

This binding is instantaneous if the rate of SO_3 absorption is equal to the rate of evaporation of water. In this case, proceeding from equations (b) and (c), we write

$$\frac{\beta_2 p_{H_2O,\infty}}{p} = \frac{\beta_1 p^0_{SO_3}}{p}$$

whence

$$p_{H_2O,\infty} = \frac{\beta_1 p^0_{SO_3}}{\beta_2} \qquad (6.26)$$

The saturated vapor pressure over sulfuric acid can be expressed by equation (1.3)

$$\lg p_{H_2O,\infty} = A - \frac{B}{T}$$

Taking the logarithm of (6.26) and equating the right-hand side with that of equation (1.3) above, we find

$$A - \frac{B}{T} = \lg \frac{\beta_1 p^0_1}{\beta_2}$$

or

$$T_{cr} = \frac{B}{A - \lg \frac{\beta_1 p^0_{SO_3}}{\beta_2}} \qquad (6.27)$$

The temperature defined by equation (6.27) can be called critical: it corresponds to the conditions when the absorption of SO_3 by the sulfuric acid ceases.

Making use of equation (6.24), we write equation (6.27) in the form

$$T_{cr} = \frac{B}{A - \lg p^0_{SO_3}\left(\frac{D_1}{D_2}\right)^{1-m}} \qquad (6.28)$$

Table 6.1 lists the critical temperatures for various vapor pressures of SO_3 in the gas mixture.

TABLE 6.1. Critical temperature (°C) of SO_3 absorption

H_2SO_4 concentration, %	Critical temperature for different SO_3 vapor pressures		
	5.1 mm Hg	38 mm Hg	75 mm Hg
95	142	191	207
90	99	144	164
85	—	105	120

Actually some SO_3 is always absorbed even at the critical temperature, since sulfuric acid fog is allowed to settle out. We see from Figure 6.3 that curves 1 and 2 do not quite reach the abscissa axis at the critical temperature.

The above theory explains the phenomenon which is observed when dry air mixed with SO_3 is passed through a horizontal glass tube with a water drop in it /8/. Fog forms abundantly around the drop, but straight above the drop there is a transparent gas layer where the water vapor prevents direct contact of the SO_3 molecules with the liquid surface.

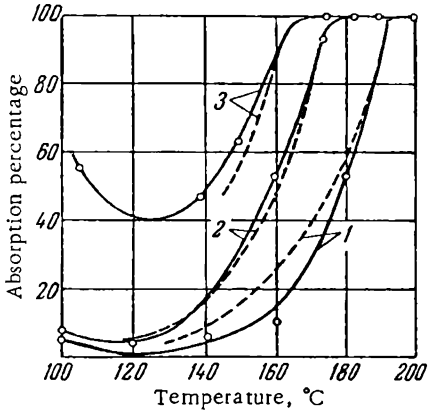

FIGURE 6.4. Degree of absorption of SO_3 by aqueous H_2SO_4 solution in a variable-temperature absorption column:
1) 85% H_2SO_4; 2) 90% H_2SO_4; 3) 95% H_2SO_4; solid line — experimental; dashed line — theoretical.

Good agreement between the theory and the experiment was obtained in the second series of experiments dealing with SO_3 absorption in sulfuric acid /5, 7/. In distinction from the first series of experiments (where the temperature was constant along the entire column), the temperature at the outlet, i.e., in the upper part of the tower, was always 100 °C. The temperature at the base of the column was higher than 100 °C, and it decreased uniformly as the gas progressed upward through the column. The results of the second series of experiments are plotted in Figure 6.4 (the abscissa axis gives the temperature in the base of the column). The same figure also gives the absorption curves of SO_3 calculated from equation (6.29).

We see from Figure 6.4 that the degree of absorption rises as the base temperature is increased, reaching a maximum at a certain temperature for each particular concentration of the acid. Since the temperature in the base of the absorption column is higher than the critical temperature, SO_3 is not absorbed. The entire sulfur trioxide combines with water vapor evaporating from the surface of the sulfuric acid, and H_2SO_4 vapor is formed. It should be noted that at these high temperatures the H_2SO_4 vapor pressure is subcritical and no fog develops. As the gas moves upward, its temperature decreases and sulfuric acid vapor condenses on the surface of the packing, so that a high degree of absorption is recorded.

These results are supported by supersaturation calculations for the absorption column with 95% H_2SO_4 (inlet temperature 173 °C, outlet temperature 101 °C, Table 6.2).

TABLE 6.2. Supersaturation of H_2SO_4 vapor along the absorption column

Temperature along the column, °C	H_2SO_4 vapor pressure in the gas		Supersaturation	Critical supersaturation
	mm Hg	N/m^2		
173 (inlet)	5.1	678	—	—
159	2.0	267	2.4	3.4
144	0.8	106	2.0	4.0
130	0.4	53	1.8	4.4
115	0.16	21	1.78	5.0
101 (outlet)	0.07	9	1.75	5.4

If the temperature at the column base is such that the supersaturation of the H_2SO_4 vapor is higher than the critical value, vapor condenses spontaneously and fog is formed, the degree of absorption of SO_3 diminishing steeply. In the second series of experiments, when fog formation was prevented by providing an extensive condensation surface (a packed column), the percentage absorption of SO_3, η, is expressed by the equation

$$\eta = \frac{(p^0_{SO_3} - p_{H_2SO_4,\infty}) \cdot 100}{p^0_{SO_3}} \qquad (6.29)$$

where $p^0_{SO_3}$ is the SO_3 vapor pressure at the inlet; $p_{H_2SO_4,\infty}$ the saturated vapor pressure of H_2SO_4 at the outlet.

If the H_2SO_4 vapor is supersaturated at the outlet, sulfuric acid fog is formed. The fog droplets are entrained by the emerging gas, and the resultant degree of absorption diminishes.

The above relations are sufficiently accurate for calculating the degree of absorption of sulfur trioxide in the monohydrate absorption tower in the contact process. The results can be presented as a function of spraying acid concentration and temperature (Figure 6.5) /3/. The calculations for spraying acid of less than 98.3% H_2SO_4 allowed for losses in the SO_3 form (due to incomplete absorption of the SO_3 gas), in the form of sulfuric acid mist (forming from water vapor and SO_3), and in the form of H_2SO_4 vapor (evaporated sulfuric acid). For spraying acid of more than 98.3% H_2SO_4 the losses were in the form of SO_3 and H_2SO_4 vapor only.

No published data are available on the partial vapor pressure of H_2O, H_2SO_4, and SO_3 over sulfuric acid in the 95—98.3% and 98.3—100% concentration range. The curves in Figure 6.5 are therefore approximate at these concentrations.

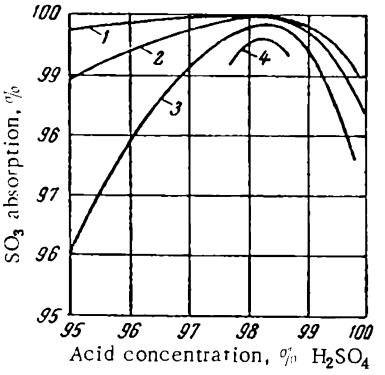

FIGURE 6.5. Degree of absorption of SO_3 in the monohydrate absorption tower:
1) temperature $t = 60$ °C; 2) $t = 80$ °C; 3) $t = 100$ °C; 4) $t = 120$ °C.

We see from Figure 6.5 that the absorption is peaked for 98.3% H_2SO_4. The degree of absorption of sulfur trioxide decreases to either side of the azeotropic point, and the curves become progressively steeper as the temperature is increased.

PHOTOELECTRIC NEPHELOMETRY

The development of fog in chemical reactions between gases is utilized for quantitative analysis of gases /9, 10/. The method is based on the so-called Tyndall effect: the fog particles scatter and attenuate the transmitted light /11/.

The sensitivity of the nephelometric gas analysis is very high, since fogs of extremely low density can be detected photoelectrically. Photoelectric nephelometers have been reported /12/ to measure mass concentrations of 0.005 g/m^3, or nearly 0.0004% of fog by weight. In previously described experiments with the development of supersaturated vapor in a free jet (p. 71), fog concentrations of 0.0002% by weight were determined.

This high-sensitivity method ensures reliable quantitative determination of a variety of compounds and is therefore of considerable applied interest. Particularly high sensitivities are attained if the photoelectric nephelometer is made to count the light pulses produced by individual particles crossing the light beam /12, 13/. These pulses are picked up by electric counters associated with photomultipliers. Concentrations of $\sim 10^{-10}$ g/m^3 can be determined by this technique. If the particles and the individual molecules are allowed to grow by condensation in the supersaturated vapor, the sensitivity increases still further to 10^{-14} g/m^3 /14/.

In nephelometric analysis, a gas mixture containing the test component is mixed with another gas which reacts with the component of interest (gas or vapor). A new substance is formed upon mixing, whose saturated vapor pressure is lower than that of the starting components. The chemical reaction between the gaseous components thus leads to the formation of supersaturated vapor and aerosol. For example, the water content of a gas can be determined by injecting it with some sulfur trioxide and measuring the concentration of the sulfuric acid mist which forms. Hydrogen chloride is similarly determined in a gas mixture by adding some ammonia and measuring the density of the ammonium chloride fumes.

The application of this method in practice involves a certain difficulty: the size of the fog droplets is a function of the conditions under which the fog is formed. Moreover, the size and the number density of the droplets vary with time; this introduces an additional unaccountable optical effect which complicates the actual measurements.

These difficulties, however, can be eliminated if the tests and the measurements are made under identical standard conditions. Since the concentration of the test component is determined by measuring the scattering or the absorption of light by the reaction product, which is present in the form of an aerosol, it is essential that the reaction be completed before the gas mixture is delivered to the sample cell for measurements. The conditions should moreover favor the conversion of the bulk of the reaction products to fog.

Reactions between gases are generally very fast; spontaneous vapor condensation and fog formation are also among the nearly instantaneous processes, so the entire process of fog condensation in mixing gases is completed in our case in fractions of a second.

When gas streams containing equal amounts of water vapor and SO_3 are mixed /15/, the reaction of sulfuric acid vapor formation runs to completion in $3 \cdot 10^{-4}$ sec. In one of the experiments, the content of sulfuric acid vapor in the mixture was 0.02% by vol., which corresponds to a partial pressure of 0.15 mm Hg. The saturated vapor pressure of H_2SO_4 at 20 °C is $2 \cdot 10^{-4}$ mm Hg. Therefore, once the water vapor has reacted with sulfur trioxide, the sulfuric acid vapor has a supersaturation of 750 (equation (1.1)). The H_2SO_4 vapor is almost entirely converted to fog, since the critical supersaturation for sulfuric acid in this case is nearly 12.

The above considerations are confirmed by actual measurements of the water content of gases /16/: SO_3 is added to the wet gas and the fog concentration is determined photoelectrically. When the air streams containing SO_3 and water vapor are mixed, the gas mixture is fed to a horizontal cell (Figure 6.6a) with plane-parallel end windows illuminated by an electric bulb. The transmitted light is picked up by a phototube in series with a galvanometer. The illuminance at the phototube varies as a function of fog concentration, and the photocurrent is recorded by the galvanometer.

These photoelectric measurements of fog concentration are inaccurate, since some fog droplets always settle on the end windows introducing a permanent bias into the galvanometer readings. In later experiments /17/ the cell design was modified so that the end windows were continually washed by the incoming gas mixture (Figure 6.6b). The reliability of the galvanometer readings increased correspondingly.

Quantitative determinations based on photoelectric measurements of fumes are carried out in a cell without end windows (Figure 6.6c); the pressure in the cell is lower than the ambient-pressure, so that no fumes escape from the open ends. The fumes develop when hydrogen chloride is added to an ammonia-containing air mixture. In principle, the phenomenon is governed by the same mechanism as the formation of fog in a mixture of wet air with sulfur trioxide.

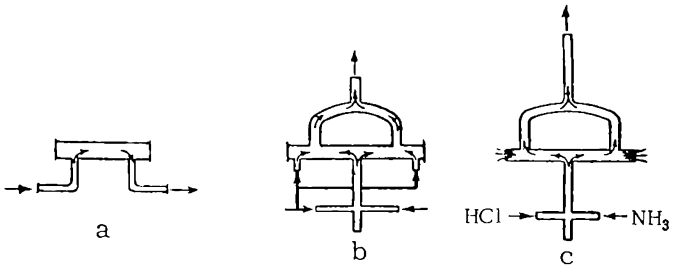

FIGURE 6.6. Sample cells for photoelectric nephelometry.

The cell without end windows can be recommended for use if the wet air entering the sample cell at the open ends does not produce aerosols upon mixing with the test gas.

The experience gained in the laboratory was applied to develop a special instrument /10, 17/ for measuring the absorption of sulfur trioxide in the monohydrate absorption tower in the contact process. Laboratory tests and the results obtained with pilot installations provided the basis for the design of the automatic industrial photoelectric nephelometer AFT-3 /18, 19/. It is used for automatic determination of H_2SO_4 and SO_3 fog in the discharge gases of the contact process (after the monohydrate absorber).

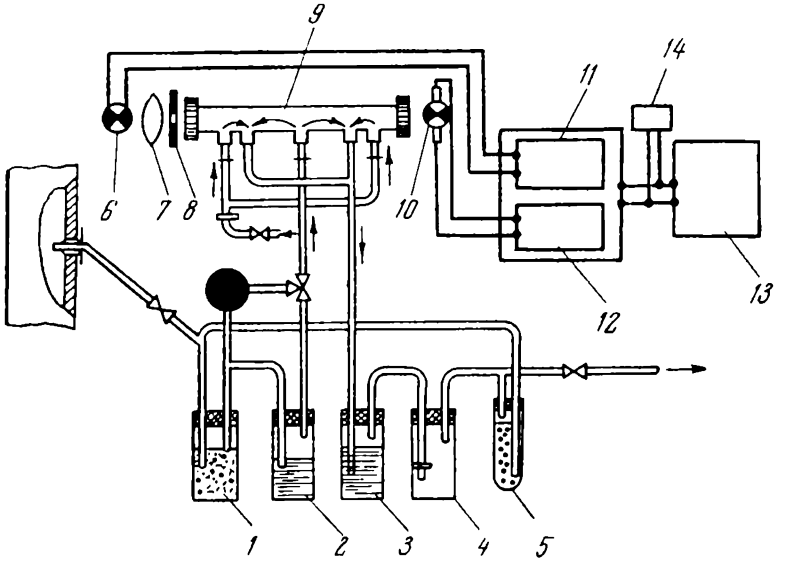

FIGURE 6.7. Functional diagram of the AFT-3 nephelometer:
1, 4) spray traps; 2) humidifier; 3) sulfuric acid; 5) manostat; 6) light source; 7) condenser lens; 8) aperture; 9) sample cell; 10) phototube; 11) voltage stabilizer; 12) current amplifier; 13) electron tube potentiometer; 14) galvanometer.

In the AFT-3 nephelometer the sample gas is passed through a spray trap 1 (Figure 6.7) and is then delivered to a water-filled humidifier 2. Sulfur trioxide combines with water vapor to give sulfuric acid mist which is entrained by the gas into the sample cell 9 (the cell is shown separately in Figure 6.6b). The gas carrying the sulfuric acid fog enters the cell through the central pipe and leaves through the lateral pipes. Clean air protecting the end windows from the precipitation of dust, spray particles, and sulfuric acid mist is pumped through the inlets at the two ends of the cell. The gas emerging from the sample cell passes through a jar 3 with 96% H_2SO_4 and a spray trap 4 and is then discharged.

An optical system comprising a light source 6, condenser lenses 7, and an adjustable aperture 8 is provided near one of the end windows. A phototube 10 is mounted at the opposite end window: it receives the light transmitted through the sample cell. The illuminating lamp is supplied by a source of stabilized voltage 11. The photocurrent is passed through the amplifier 12 whose output is coupled into an electron tube potentiometer 13 and a direct reading galvanometer 14. The galvanometer is connected intermittently, to adjust the zero point of the nephelometer.

The nephelometers are manufactured with a scale $0-1\ g/m^3$ H_2SO_4 /19/. The relative error in these measurements is ±10%. Additional errors caused by mains voltage instability and fluctuations of ambient temperature are ±8%. The flow rate of the sample gas through the cell is 1—1.5 liter/min. The delay time is no greater than 1.5 min.

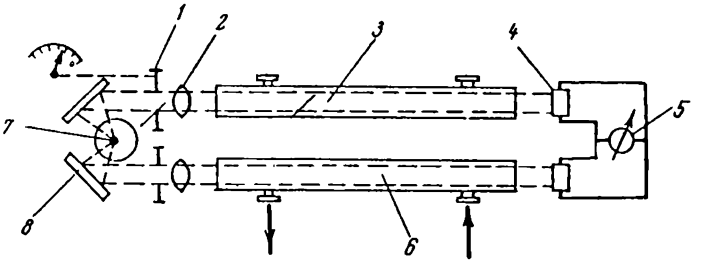

FIGURE 6.8. The "Vlagomèr" photoelectric hygrometer: 1) adjustable aperture; 2) lens; 3) reference cell; 4) phototube; 5) null galvanometer; 6) indicator cell; 7) light source; 8) mirror.

The results of photoelectric nephelometry /16/ were utilized in the design of the "Vlagomer"* photoelectric hygrometer. This instrument monitored the humidity of air during the drying of sulfur dioxide by sorbents /20/. The hygrometer has two colorimetric sample cells (Figure 6.8): an air-filled reference cell 3 and an indicator cell 6 filled with the fog mixture.

The photoelectric part of the equipment is based on the differential principle with optical compensation. The readout is provided by the calibrated aperture scale. The instrument is highly sensitive and will determine the dew point of water vapor at − 62 °C.

* [In Russian, "hygrometer".]

Similarly designed instruments based on the conversion of vapor-gas mixtures to fog were used for the determination of ammonium sulfate in the discharge gases of a liquid SO_2 plant (sensitivity 0.06 g/m^3) /21/, for the determination of the water content of hydrocarbon gases /22/, humidity of chlorine, etc.

Figure 6.9 is a diagram of the photoelectric instrument measuring the critical supersaturation. The fog is formed by mixing gases in a free jet /9/. No particles can settle on the walls, because the mixing chamber is made large enough for the entire jet to be confined to the axial region.

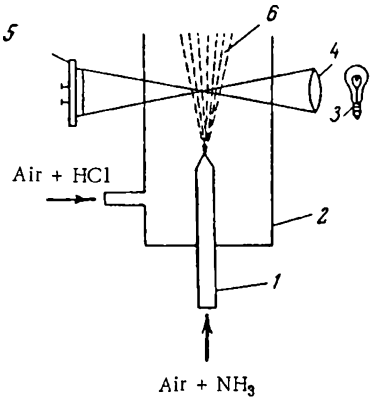

FIGURE 6.9. Setup for measuring the critical supersaturation:
1) nozzle; 2) mixing chamber; 3) light source; 4) lens; 5) phototube; 6) free jet.

It follows from the hydrodynamics of free jets (Chapter Three) that if the nozzle velocity is sufficiently high, the concentration of the reaction products (and consequently the concentration of the fog in the jet) is virtually independent of the flow velocities, being determined by the mass ratio of the reacting gases. The accuracy of the analysis is therefore dependent on the sensitivity of the photocell.

FORMATION OF CONDENSATION NUCLEI IN THE ATMOSPHERE AS THE RESULT OF CHEMICAL REACTIONS OF GASES IN THE VOLUME

The atmospheric gases react between themselves forming new compounds with a lower saturated vapor pressure than the starting components. The reaction products thus condense spontaneously into liquid or solid particles — atmospheric condensation nuclei (Chapter One) which play an important role in the development of clouds.

Active formation of atmospheric condensation nuclei has been discussed mainly in connection with the problems of artificial precipitation and harmful air pollution. Nitric and sulfuric acids, as well as some of their compounds, are among the principal agents which lead to the formation of condensation nuclei in the atmosphere. Gaseous substances are emitted into the atmosphere with industrial discharge gases or are produced by natural processes.

Pollutants of artificial origin (which take part in chemical reactions in the atmosphere) are very numerous and diversified. They are classified according to concentration and the origin of the emissions: automotive transport, tractors, ships, locomotives and diesel engines, factories, oil-processing plants, chemical and metallurgical industries, thermal power stations, etc. There is hardly an industrial installation which does not emit gaseous pollutants into the atmosphere.

Lightning and the ultraviolet radiation of the sun produce various nitrogen oxides and ozone (a vigorous oxidant) in the atmosphere. When nitrogen oxides, oxygen, ozone, and water vapor are present together in the air, a chain of chemical reactions is triggered culminating in the formation of nitric acid:

$$NO + O_3 = NO_2 + O_2 \quad (a)$$
$$2NO + O_2 = 2NO_2 \quad (b)$$
$$2NO_2 + H_2O = HNO_3 + HNO_2 \quad (c)$$

Reaction (b) is displaced to the right at temperatures under 140 °C; the rate constant of this reaction increases as the temperature is decreased /23/. The results obtained for reaction (c) show /24/ that it occurs in the gaseous phase, and nitric acid mist develops if the HNO_3 vapor is supersaturated.

Burner fumes are nearly always polluted with sulfur dioxide, since the conventional fuels (coal, oil, fuel gas, etc.) always contain sulfur. Sulfur dioxide is emitted into the atmosphere in large quantities with the discharge gases of ferrous and nonferrous metallurgical plants, where sulfide ores and ores of ferrous and nonferrous metals are roasted. Sulfur dioxide also forms by oxidation of atmospheric hydrogen sulfide, which is emitted into the air by decaying organic substances and products.

The worldwide annual consumption of coal is in the neighborhood of $2.0 \cdot 10^9$ metric tons; the average content of sulfur in coal is 1.5% /25/. The quantity of sulfur dioxide which forms when coal is burned is thus

$$2 \cdot 10^9 \cdot 0.015 \cdot 64/32 = 6 \cdot 10^7 \text{ metric tons per annum}$$

(i.e., an annual output of 60 million metric tons). There are also other forms of sulfur-containing fuel which are burned in industry, as well as the gases ejected by volcanic eruptions, so that the total quantity of sulfur dioxide emitted into the atmosphere is nearly 100 million metric tons per annum. This enormous amount of sulfur dioxide is converted to sulfuric acid and its salts, which eventually settle to the ground in the form of liquid or solid particles (aerosols) or with rain drops (which have formed by condensation of water vapor on these nuclei).

Sulfuric acid is formed in the atmosphere by photochemical oxidation of sulfur dioxide /26, 27/, the sulfur trioxide combining with water vapor:

$$2SO_2 + O_2 = 2SO_3 \quad (d)$$
$$SO_3 + H_2O = H_2SO_4 \quad (e)$$

Ammonia is liberated when organic substances burn or decay. The nitric and the sulfuric acids in the air react with ammonia to give

ammonium salts /28/:

$$NH_3 + HNO_3 = NH_4NO_3$$
$$2NH_3 + H_2SO_4 = (NH_4)_2SO_4$$

Laboratory tests have shown that gaseous hydrocarbons react photochemically with NO_2, SO_2, and O_3 forming fog droplets in the gas phase /29/. If the gas contains NO (and not NO_2), the fog appears somewhat later, apparently due to the preliminary oxidation of NO to NO_2.

Homogeneous condensation of reaction products in a gaseous phase enhances the development of fog and smog in cities and large industrial centers, where the air is daily polluted by large quantities of exhaust gases containing SO_2, nitrogen oxides, etc. The reaction products forming in the air are generally hygroscopic and they act as active condensation nuclei on which water vapor condenses with $S<1$.

The pollutants emitted with discharge gases spread through the air by processes of molecular and eddy diffusion. When fog is formed, the harmful substances are concentrated in the heavy droplets which settle from the upper atmospheric layers to the ground air layer, where they may remain for a fairly long time (particularly in still weather) creating a serious (and sometimes fatal) health hazard to the local inhabitants. The dangers of smog are vividly illustrated by the events which took place in London between 5 and 9 December 1952. Heavy smog saturated with the fumes of central heating installations and industrial plants formed in a period of calm, windless weather. The incidence of sickness and the mortality rate rose steeply, particularly among the elderly people and the children. During one week, 2464 people died in London, the mortality reaching the level of the 1866 plague /30/.

PRODUCTION OF SOOT, SILICA SMOKE, AND Al_2O_3 POWDER

Soot is an extremely fine black powder which consists of minute particles of carbon with a mean radius of $10^{-6}-10^{-5}$ cm. The specific surface of the soot (i.e., the total surface area of the particles in 1 g of soot) is from 10 to 200 m^2/g; the greater the specific surface, the higher the quality of the soot.

The soot has an intense black color and good technological properties. It is therefore in the manufacture of inks (since antiquity), in printing industry, and in the production of various paints and varnishes. Soot is an indispensable component of rubber mixtures: it makes the rubber wear-resistant and elastic and enhances its mechanical strength. Soot is also employed in the manufacture of carbon arc electrodes, electrodes and brush contacts for electric motors, dry and wet cells, in artificial leather industry, in plastic industries (oilskins, linoleum, ebonite, long-playing records, etc.).

Soot is prepared from hydrocarbons which are burned in an oxygen-deficient atmosphere or thermally decomposed. The minute carbon particles which form in the process coalesce into larger aggregates.

No reliable data have been published on the mechanism of soot formation /31/. It seems that the vaporous carbon which is produced by the chemical reactions condenses spontaneously in the gas volume in accordance with the general rules governing homogeneous condensation of vapor.

We now proceed to apply the theory of homogeneous condensation to the thermal decomposition products of methane, which are utilized in the production of soot. The previously discussed data on the development of fog are then applied to determine the optimal conditions under which finely divided soot can be obtained.

In the thermal method of soot production /31/, methane (the natural fuel gas having methane as one of its principal constituents) is passed through a packing which has been heated to ~1670 °K. The hot methane decomposes to carbon and hydrogen:

$$CH_4 = C + 2H_2 - 17\,900 \text{ cal} \qquad \text{(a)}$$

The carbon condenses partly on the packing and partly forms a suspension of spherical particles of solid carbon. These particles — the soot — settle out, and hydrogen is marketed as a byproduct of the soot industry.

The main reaction is accompanied by subsidiary reactions, which have no immediate bearing on the principal process and are thus not considered here.

Since the decomposition of CH_4 is an endothermic reaction, the packing is gradually cooled as soot is being formed. When the temperature of the packing has dropped to 1473 °K, the CH_4 feed is stopped, the packing is reheated, and another cycle begins. The soot becomes progressively coarser as the temperature is decreased.

The dispersity of soot (as of any aerosol) increases with the increase of S (p. 37). The vapor supersaturation (1.1), however, is under the influence of two conflicting temperature-dependent factors: it shows a tendency to increase because of the increase in the rate of carbon formation at higher temperatures and to decrease because of the increase in the saturated vapor pressure of carbon (equation (1.2)). S and $dS/d\tau$ as functions of temperature therefore have a certain maximum, and the finest soot is obtained at some optimal temperature. No reliable data are available at present concerning the effect of different factors on the formation of soot, and it is therefore impossible to derive a general equation for $dS/d\tau$ which takes into consideration the development of carbon vapor (and the supersaturation S), the rate of nucleation in the gas (the surface tension of carbon and the exact aggregate state of the forming embryos are unknown), the rate of growth of the embryos, and other factors.

To obtain an approximate solution of the problem, the derivatives $dp/d\tau$ and $dT/d\tau$ which ignore the nucleation of embryos are substituted in equation (1.7). This simplification is partially justified because in the initial period of nucleation the embryos are too small (with a radius of $\sim 10^{-7}$ cm) to cause a substantial reduction in p and a noticeable increase in T.

The rate of formation of gaseous carbon according to reaction (a) is expressed by an ordinary differential equation /32/

$$\frac{dp}{d\tau} = k\frac{p_1(p_1 - p)}{p_1 + 2p} \qquad \text{(b)}$$

where p_1 is the initial pressure of methane; p the vapor pressure of carbon; k the rate constant

$$k = Ae^{-\frac{B}{T}} \tag{c}$$

T the absolute temperature; A, B are coefficients.

The vapor pressure of carbon during nucleation is very low, and we may therefore take

$$\frac{p_1(p_1 - p)}{p_1 + 2p} \approx p_1 \tag{d}$$

The temperature is a linear function of time during the active part of the cycle, and so

$$\frac{dT}{d\tau} = M = \text{const} \tag{e}$$

Inserting the expressions for (b), (c), (d), and (e) for the corresponding quantities in equation (1.7), we write

$$\frac{dS}{d\tau} = \frac{p_1 Ae^{-\frac{B}{T}}}{p_\infty(T)} - \frac{pE}{T^2 p_\infty(T)} M \tag{f}$$

To find the maximum of the function $dS/d\tau = f(T)$, we differentiate equation (f) and write

$$\frac{d}{dT}\left(\frac{dS}{d\tau}\right) = \frac{p_1 Ae^{-\frac{B}{T}}}{T^2 p_\infty(T)}(B - E) - \frac{ME}{T^4 p_\infty(T)}[NT^2 - p(E + 2T)] \tag{g}$$

where

$$N = \frac{dp}{dT}$$

Putting the right-hand side of this equation equal to zero, we find

$$Ap_1 e^{-\frac{B}{T}}(B - E) = EM\left[N - p\left(\frac{E}{T^2} + \frac{2}{T}\right)\right] \tag{h}$$

From (b), (c), (d), and (e) we have

$$N = \frac{dp}{dT} = \frac{p_1 A}{M} e^{-\frac{B}{T}} \tag{i}$$

Inserting this expression for N in (h) and manipulating, we find

$$e^{\frac{B}{T}} = \frac{Ap_1(2E - B)}{EMp\left(\frac{E}{T^2} + \frac{2}{T}\right)} \tag{j}$$

The numerical values of the parameters entering equation (j) are the following:

$$M = \frac{T_2 - T_1}{t}$$

where T_1 and T_2 are the absolute temperatures of the gas at the inlet and the outlet of the reaction chamber, $T_1 = 293\,°K$, $T_2 = 1673\,°K$; t is the time the gas spends in the reaction chamber, taken equal to 1 sec; thus

$$M = \frac{1673 - 293}{1} = 1390 \text{ deg/sec};$$

$$A^{32} = 10^{12};\ B^{32} = \frac{79\,000}{1.98} = 39\,900;$$

$$E^{38} = 37\,100 \cdot 2.3 = 85\,300 \text{ (see Appendix II)};$$
$$p_1^{31} = 760 \cdot 0.937 = 712 \text{ mm Hg } (9.5 \cdot 10^{-4}\ N/m^2);$$
$$p = 10^{-2} \text{ mm Hg (approximately)}.$$

Substituting in (j), we find

$$T_{opt} = 1150\,°K$$

Similar calculations indicate that $S = S_{max}$ at $T = 1175\,°K$.

The temperature of the furnace is brought up to 1570—1670 °K at the beginning of each cycle /31/, and the packing gradually cools to 1370—1470 °K during the active stage. The calculated optimal temperature is thus lower than the operating temperatures, but we must not forget that our calculations are highly approximate, and in view of this the fit between theory and experiment is apparently satisfactory.

There are some published data /31, 33/ which indicate that the dispersity of the soot increases with the increase of temperature (i.e., the radius of the soot particles is decreased), but there is no mention of optimal temperatures. The existence of an optimal temperature follows from an analysis of laboratory tests.

The curve in Figure 6.10 plots the dispersity of the soot (obtained by burning natural methane gas under laboratory conditions) as a function of temperature /31/; the dispersity distinctly increases as the temperature is increased. The upward trend, however, almost stops at 1500 °C, and a further increase in soot dispersity can hardly be expected at higher temperatures.

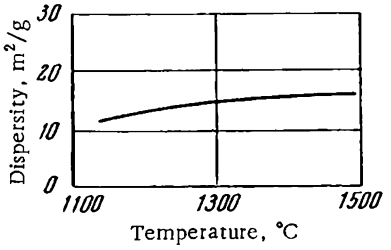

FIGURE 6.10. Soot dispersity vs. temperature.

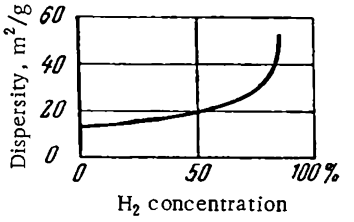

FIGURE 6.11. Soot dispersity vs. concentration of hydrogen in the mixture.

In industry, the fineness of the soot is increased by adding 2—3 volumes of hydrogen to each volume of the methane gas fed into the furnace; the exact action of hydrogen is not clear /31/. The beneficial effect of hydrogen in the gas mixture is also confirmed by laboratory tests (Figure 6.11).

Previous data (p. 38 and 124) and the conclusions reached in Chapter Seven (p. 206) indicate that the particle size decreases as the vapor pressure is decreased: the condensational growth of the embryos is less intensive under these conditions.

The dependence of the soot dispersity on temperature and hydrogen concentration supports the previous suggestion that soot is formed as the result of homogeneous condensation of vapor.

Finely divided silicon dioxide — silica smoke or Aerosil — is used as a reinforcing agent in the manufacture of heat-resistant rubber from silicone rubber. The highly active silica smoke is almost completely dehydrated silicon dioxide which is also used as a filler in the leather industry, in the production of polyether and epoxy resins, heat-resistant lubricants, dye-stabilizing glues, etc.

Silica smoke is produced from silicon tetrachloride /35—37/. $SiCl_4$ vapors are hydrolyzed in a hydrogen flame or a methane flame. The hydrolysis occurs in the initial section of the jet, and the reaction is completed in a furnace at a temperature of some 1273 °K. The resultant effect is expressed by the equation

$$SiCl_4 + 2H_2O \rightleftarrows SiO_2 + 4HCl - 30\,100 \text{ cal} \qquad (k)$$

At the reaction temperature (1273 °K) the saturated vapor pressure of SiO_2 is low /38/, being of the order of 10^{-8} mm Hg, and the supersaturation in this process is therefore high. The SiO_2 vapor condenses spontaneously in the form of smooth spherical particles which measure from one millimicron to a few millimicrons. The aerosol emerging from the furnace is allowed to aggregate into largish flakes which are then separated in filters. Hydrogen chloride is recovered from the filtered gases. The specific surface of the particulate end product varies between 50 and 450 m^2/g, depending on the particular process conditions.

Silica smoke can also be manufactured by oxidizing volatile silicon compounds in a gaseous phase (organochlorosilanes, tetraethyl orthosilicate, silicon tetrachloride, etc.), hydrolysis of gaseous silicon tetrafluoride /36/, etc.

Thermodynamic calculations indicate that at temperatures of 400—1600 °K reaction (k) virtually runs to completion /36/. The optimal temperature conditions are therefore adjusted to ensure maximum dispersity of the silica smoke. To this end, the derivative $dS/d\tau$ should be made as large as possible. It is, however, obvious from equation (1.1) that the supersaturation is determined by two conflicting factors: as the temperature is increased, the supersaturation on the one hand shows a tendency to increase due to the increase in the rate of formation of silicon dioxide, while on the other hand, the supersaturation is lowered by the increase in the saturated vapor pressure of SiO_2 with temperature. Therefore, to choose the optimal conditions under which silica particles of minimum size are obtained, we must consider the rate of formation of SiO_2, i.e., $dp/d\tau$, the rate of vapor condensation on the surface of droplets expressed by equation (1.67), and the rate of temperature variation $dT/d\tau$ (it is determined by the rate of oxidation of hydrogen and the rate of condensation of SiO_2, when heat is released).

The size of the embryos is approximately 10^{-7} cm. The total mass of the embryos is therefore negligibly small and the resultant reduction in vapor pressure is insignificant. The vapor pressure is mainly lowered by the condensational growth of the embryos, which is a relatively gradual process. The change in vapor pressure is thus felt only when the number density of the fog has increased sufficiently. Both the vapor pressure of SiO_2 and the temperature of the gas are therefore assumed to remain unaffected by condensation of vapor during the nucleation stage. The equation for the rate of formation of SiO_2 is written in the form

$$\frac{dp_1}{d\tau} = k_1 (p^0 - p_1) \tag{l}$$

where p^0 is the initial pressure of $SiCl_4$; p_1 the pressure of SiO_2 in the gas; k_1 the rate constant of the $SiCl_4$ hydrolysis.

Since the saturated vapor pressure of SiO_2 at the process temperature is very low, the nucleation begins at a low p; furthermore, the reduction in p^0 at the initial stages of homogeneous condensation is insignificant, since the embryos are minute and the quantity of condensing SiO_2 is negligible. We may thus take

$$p^0 - p_1 \approx p^0$$

The rate constant of the $SiCl_4$ hydrolysis is

$$k_1 = A_1 e^{-\frac{B_1}{T}} \tag{m}$$

Making use of the above relations we write

$$\frac{dp_1}{d\tau} = p^0 A_1 e^{-\frac{B_1}{T}} \tag{n}$$

The gas mixture is heated by the oxidation of hydrogen (a reaction of second order):

$$2H_2 + O_2 = 2H_2O + 57\,800 \text{ cal} \tag{o}$$

If the heat of condensation of SiO_2 is ignored, the rate of change of the temperature is expressed by the equation

$$\frac{dT}{d\tau} = -\frac{M dp_2}{d\tau} = M k_2 (p_2^0 - p_2') \tag{p}$$

where p_2^0 is the initial pressure of hydrogen in the gas mixture; p_2 the current pressure of hydrogen; p_2' the pressure of water vapor produced by the oxidation of hydrogen; M a coefficient; k_2 is the rate constant of the reaction (o):

$$k_2 = A_2 e^{-\frac{B_2}{T}} \tag{q}$$

During the nucleation stage, the concentration of hydrogen is fairly constant and equation (p) is approximately written as

$$\frac{dT}{d\tau} = N k_2 = N A_2 e^{-\frac{B_2}{T}} \tag{r}$$

where

$$N = M(p_2^0 - p_2')^2 = \text{const}$$

Substituting from (l), (m), (n), and (r) in equation (1.7), we find

$$\frac{dS}{d\tau} = \frac{p^0 A_1}{p_\infty(T)} e^{-\frac{B_1}{T}} - \frac{N p_1 E A_2}{T^2 p_\infty(T)} e^{-\frac{B_2}{T}}$$

Differentiating $dS/d\tau$ with respect to temperature (as a first step in the determination of S_{max}), we write

$$\frac{d}{dT}\left(\frac{dS}{d\tau}\right) = \frac{p_0 A_1 (B_1 - E) e^{-\frac{B_1}{T}} dT}{T^2 p_\infty(T)} -$$

$$- \frac{N E A_2 e^{-\frac{B_2}{T}} [T^2 dp_1 + p_1 (B_2 - E - 2T)\, dT}{T^4 p_\infty(T)} \qquad (s)$$

From (n) and (r) we have

$$dp_1 = \frac{p^0 A_1}{N A_2} e^{\frac{B_2 - B_1}{T}} dT$$

Substituting this result in (s), moving dT to the left-hand side of the equality, and putting $\frac{d}{dT}\left(\frac{dS}{d\tau}\right)$ equal to zero, we find after some manipulations

$$\frac{p^0}{p_1} \cdot \frac{A_1}{A_2} \cdot \frac{B_1 - 2E}{EM(p_2^0 - p_2')^2} T^2 e^{\frac{B_2 - B_1}{T}} = B_2 - E - 2T \qquad (t)$$

The numerical values of A_1 and B_1, unfortunately, are not known, and equation (t) cannot be solved. A simple analysis shows, however, that this equation gives a real value of T, and the derivative $dS/d\tau$ indeed has a maximum at which the SiO_2 particles are the smallest.

This conclusion is consistent with the results of laboratory tests /36/ which indicate that as the temperature is raised to 1220 °K, progressively finer SiO_2 powder is obtained, whereas at 1220—1270 °K (this temperature is attained by substituting oxygen for part of the air) the trend is reversed.

The existence of optimal temperature at which the finest SiO_2 is obtained is also confirmed by experimental data /40/ on the size of SiO_2 particles which form when SiF_4 is hydrolyzed at various temperatures. The corresponding data plotted in Figure 6.12 give the radius of SiO_2 particles as a function of flame intensity (the abscissa is the reciprocal intensity). The flow rate of the gas is not specified in /40/. If a constant volume is assumed, the temperature of the gas is directly proportional to the flame intensity (as expressed by the authors).

We see from Figure 6.12 that as the flame intensity is increased, the particle size first decreases to a minimum and then starts increasing. It follows from the preceding that the derivative $dS/d\tau$ is maximal at the point of minimum particle size.

Finely divided Al_2O_3 powder is used as an adsorbent in various laboratory investigations. One of the methods for the preparation of this powder is by

hydrolysis of gaseous Al_2Cl_6 in an oxygen-hydrogen flame:

$$Al_2Cl_6 + 3H_2O = Al_2O_3 + 6HCl + 40\,160 \text{ cal} \qquad (u)$$

The effect of various factors on the fineness of the Al_2O_3 powder formed by the reaction (u) was studied experimentally /40, 41/ in a setup which comprised an electric furnace for the evaporation of Al_2Cl_6, a burner,

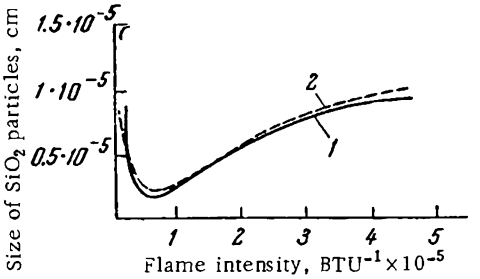

FIGURE 6.12. Size of SiO_2 particles obtained by hydrolyzing SiF_4 as a function of flame intensity: 1) commercial propane flame (CH_4 30%, C_2H_6 10%, C_3H_3 61%, C_4H_{10} 26%); 2) hydrogen flame.

and a collector for the separation of the powder from the gas. The burner had three conical nozzles (Figure 6.13): oxygen saturated with chloride vapors was delivered through the inner nozzle, hydrogen was fed through the outermost nozzle. The middle ring nozzle fed nitrogen into the flame, which screened the burner from the reaction products and prevented the clogging of the nozzles with the powdered product. The Al_2O_3 powder was separated in an electrostatic precipitator in the form of dense (nonporous) spherical particles.

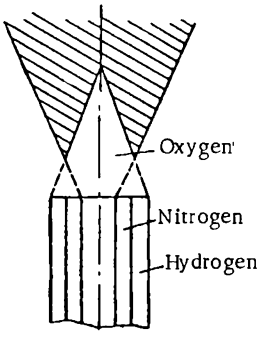

FIGURE 6.13. Burner for the production of Al_2O_3 powder.

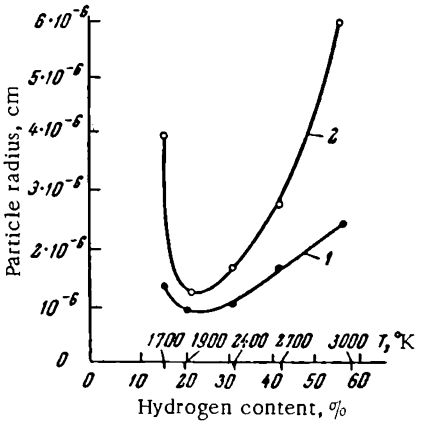

FIGURE 6.14. Radius of Al_2O_3 particles vs. flame temperature: 1) 0.01 g/l of Al_2Cl_6 in the mixture; 2) 0.1 g/l of Al_2Cl_6 in the mixture.

The results of these investigations indicate that the mechanism of formation of finely divided aluminum oxide in a hydrogen-oxygen flame according to reaction (u) is consistent with the theory of homogeneous

condensation of vapor. The saturated vapor pressure of Al_2O_3 at the process temperature is sufficiently low ($p_\infty = 1$ mm Hg at $T = 2419$ °K) /32/, and the Al_2O_3 vapor formed according to reaction (u) condenses into Al_2O_3 droplets which then solidify (the melting point of Al_2O_3 is 3131 °K).

This mechanism is identical in all particulars with the formation of soot and silica smoke, and it is therefore true in this case also that the radius of the solid Al_2O_3 particles becomes smaller as the derivative $dS/d\tau$ is increased. The derivative, when considered as a function of temperature, should have a maximum, i.e., in other words, the radius of the Al_2O_3 particles should have a minimum at a certain optimal temperature.

These considerations are confirmed by the experimental data plotted in Figure 6.14 /41, 42/. We see that the minima of the $\bar{r} = f(T)$ curves are fairly distinct at different concentrations of Al_2Cl_6 in the gas mixture, i.e., at different vapor pressures of the aluminum oxide. The increase of particle radius with the increase of vapor pressure is consistent with the general concepts of homogeneous condensation (p. 35), the implication of this being that Al_2O_3 particles form by homogeneous condensation. The experimental results show that at a constant concentration of Al_2Cl_6 in the gas mixture, the radius of the spherical Al_2O_3 particles decreases with the increase of the nozzle velocity of the burning gas. These results also agree with the theory of homogeneous condensation, according to which the derivative $dS/d\tau$ increases as the gas velocity is increased, so the droplets stay less time in the region of supersaturated vapor. Both these factors are conducive to the formation of small particles.

Fine Al_2O_3 powder can also be prepared from aluminum isopropylate, instead of from Al_2Cl_6.

Oxides of Fe, Ti, Zr and mixtures of Al and Si oxides in the form of monodisperse powders with particle radii of $3 \cdot 10^{-6} - 10^{-5}$ cm were prepared by a similar technique in a hydrogen-oxygen flame /40/.

VARIOUS CASES OF FOG FORMATION AS THE RESULT OF CHEMICAL REACTIONS OF GASES IN THE VOLUME

Petrov's mixture* is prepared by treating kerosine with sulfuric acid or gaseous sulfur trioxide /43/. SO_3 is provided by the gases from the contact installation of a sulfuric acid plant (containing some 7.5% SO_3). The reaction occurs at a temperature of 60—70 °C. Sulfur trioxide is absorbed by kerosine and sulfonaphthenic acids are formed. When the gas mixture is bubbled through naphtha, sulfonaphthenic acids form not only in the bulk liquid, but also in the gaseous phase.

The vapor pressure of the various hydrocarbons in kerosine is sufficiently high at the reaction temperature, and the liquid partly evaporates. The water generally contained in kerosine is also converted to vapor. Sulfur trioxide reacts with the gaseous hydrocarbons and with the water vapor forming sulfonaphthenic acids and sulfuric acid. These vapor-phase reaction products have exceedingly low saturated vapor pressures; high supersaturation therefore develops, the vapors condense spontaneously,

* ["Kontakt Petrova", a detergent mixture of sulfonaphthenic acids, the Russian equivalent of Twitchell reagent.]

and fog is formed. We thus have here another instance of fog formation as the result of a chemical reaction of gases in the volume. The discharge gases carry a substantial quantity of mist, and its separation involves considerable technological difficulties.

The weight of the reaction products absorbed by the liquid is expressed by equation (6.23). In our case $p^0_{SO_3}$ is the partial vapor pressure of sulfur trioxide, $p_{K,\infty}$ the saturated vapor pressure of kerosine, β_1 a coefficient signifying the rate of absorption of sulfur trioxide, β_2 the evaporation coefficient of kerosine.

As the temperature is increased, progressively less sulfur trioxide is absorbed, since the saturated vapor pressure of kerosine increases and the amount of SO_3 reacting in the vapor phase correspondingly rises. Fog also forms more abundantly at high temperatures. Temperature thus has a very marked influence on the absorption of SO_3 by liquid kerosine.

As we have previously observed (in the discussion of the absorption of sulfur trioxide by sulfuric acid of less than 98.3% H_2SO_4), a critical temperature (6.28) exists at which the absorption of sulfur trioxide is zero. In our case, the saturated vapor pressure of kerosine being high, all the sulfur trioxide combines with kerosine vapor without reaching the liquid surface.

The absorption of sulfur trioxide is improved when the SO_3 partial vapor pressure is increased (provided that the liquid surface in contact with the gas is sufficiently large). A higher output of the Petrov mixture can therefore be obtained by increasing the concentration of sulfur trioxide in the incoming gas.

The application of equation (6.28) for the calculation of the Petrov mixture production conditions involves certain difficulties, because kerosine is a mixture of several petroleum distillation products of different volatilities and different molecular weights. Hydrocarbons with the highest saturated vapor pressures are the first to evaporate, and these components combine with sulfur trioxide in the vapor phase and form fog droplets. The discharge gases emitted in the initial stages of kerosine processing therefore carry a relatively high concentration of fog. Kerosine may also contain water, whose vapor pressure is exceedingly high at the process temperature: the kerosine therefore loses nearly all its moisture and the water vapor combines instantaneously with sulfur trioxide /4/ forming fog droplets.

Actual experience gained on Petrov mixture plants shows that in the initial period the gaseous emissions contain kerosine vapor, as well as mist particles. This implies that a supercritical temperature develops virtually at the very first instant, and hardly any sulfur trioxide reaches the liquid surface at all. The losses of sulfur trioxide during the initial stages are therefore considerable.

As the volatile fractions are distilled from the kerosine, the saturated vapor pressure of the remaining hydrocarbons (p_∞) decreases, more sulfur trioxide is absorbed by the liquid, and the concentration of fog in the discharge gases decreases.

It should be noted, however, that the mist is partly absorbed by the liquid kerosine. The conditions for the entrapment of the aerosol particles are most favorable when the gases are bubbled through the kerosine pool.

SiF_4 and HF are released when phosphate ore is treated with sulfuric acid. The general content of fluorine in the fumes is 0.1—0.2 g/m³ /44, 45/. When the gases cool in an absorbing tower, SiF_4 reacts with water vapor:

$$3SiF_4 + 2H_2O = 2H_2SiF_6 + SiO_2$$

Hydrogen fluoride is also partly converted to fluorosilicic acid:

$$6HF + SiO_2 = H_2SiF_6 + 2H_2O$$

Since the discharge gases contain an excess of water vapor, nearly all the fluorosilicic acid condenses in the gas volume and fog is formed. Indeed, at temperatures of 50—70 °C, the gas contains in equilibrium a mere 0.02—0.04 g/m³ of fluorine /46/. SiO_2 vapors are also entirely converted to the aerosol state: their partial pressure at the process temperature is negligible.

There are no published data on the composition of the mist particles which form in the superphosphate industry. These are apparently hydrofluoric acid droplets holding silica gel in suspension /47/.

When superphosphate is granulated, fluorine is emitted mainly during drying: some 10—20% of fluorine admitted with the superphosphate stock are released in the process. Since the product is dried at a sufficiently high temperature, the hydrofluoric acid evaporates and escapes with the discharge gases. These gases are cooled in the absorbing tower, where vapor condenses not only on the surface, but also in the gas volume forming fog droplets (Chapter Five). This mechanism of fog formation is confirmed by laboratory tests and by industrial surveys /45, 47—50/. Ordinary absorbing towers are therefore inadequate if the fluorine is to be recovered from the discharge gases: special mist collectors should be applied for this purpose.

Hydrogen chloride is a byproduct of various chemical industries. Combining with the water vapor generally present in the process gases, it gives a very fine mist of hydrochloric acid. The presence of this mist substantially complicates the technological aspect of the process, since it is fairly difficult to separate. Hydrochloric acid fog is also formed in HCl manufacture, in organic synthesis, and in various inorganic technological processes /51/. Chlorine substitution and dehydrochlorination reactions, condensation reactions in the presence of $AlCl_3$ and PCl_3, phosgenization, hydrolysis of potassium chloride and polymineral potassium ores — all these are plagued by the development of HCl mist.

Hydrogen chloride emissions in plants may cause acute irritation and inflammation of mucous membranes and persistent cough. However, the harmful hydrochloric acid fog forms on production premises only when a substantial quantity of hydrogen chloride has been released. As the content of water in the air is increased, the HCl concentration remaining constant, the fog forms more abundantly and the hydrochloric acid becomes more dilute. At $T = 293$ °K, with a water vapor pressure of 1173 N/m² (8.8 mm Hg), which corresponds to a relative humidity of 50%, hydrochloric acid starts condensing into fog at an HCl pressure of 133 N/m² (1 mm Hg or nearly 2 g/m³ at NTP), and the concentration of the acid in the mist

droplets is some 20%. The maximum permissible concentration of HCl in the air on industrial premises is 6 mg/m^3, and hydrochloric acid mist thus forms only if the HCl concentration accidentally exceeds the admissible level by a factor of ~200.

The incipient point of fog formation is determined by calculating the dew point of hydrochloric acid for the given HCl and water contents of the gas /51/. According to laboratory data obtained for clean and pollute industrial gases, hydrochloric acid mist develops at higher temperature than what follows from the calculations of dew point /52/.

The progress in nucleonics led to the development of a new science — radiation chemistry, which is concerned with the effect of nuclear radiations on substances and chemical reactions. Radiation-chemical techniques are highly promising for industrial realizations of various chemical processes /53, 54/.

Nuclear radiations trigger various reactions in the gaseous phase, and the saturated vapor pressures of the reaction product may be lower than those of the initial components. Vapor thus condenses spontaneously and fog is formed. For example, irradiation of methane, ethane, propane, ethylene, or oxygen mixtures of these gases with a flux of fast electrons produces visible fog, whose concentration depends on the composition of the gas mixture and on the conditions of irradiation /55/.

The properties of fogs which form in radiation-chemical reactions have been studied most intensively in recent years. The test gas was irradiated with 112 keV electrons with an intensity of up to 100 μA in a 2-liter brass reaction vessel /55/. A beam of light was directed into the reaction vessel to be transmitted by the fog, thereupon striking a phototube. The photocurrent was measured with a galvanometer: the reduction in photocurrent characterized the density of the mist. The mass concentration of the fog was determined gravimetrically (by precipitating the fog droplets on a filter); the number density and the electrical properties of the mist were established in Millikan's condenser.

It follows from the results of these experiments /55—57/ that fog is formed when the energy of the radiation is absorbed by the gas, and the transmitted light is correspondingly attenuated. When the source of radiation is turned off, the intensity of the transmitted light increases: the gas is clarified by coalescence and settling out of the droplets.

The fog which forms when methane and ethylene are irradiated has oily droplets. The fog droplets in an irradiated mixture of methane with oxygen contain aqueous solutions of formic acid, formaldehyde, peroxides, and alcohols. When the intensity of the radiation is reduced to 1/10, the absorption and the scattering of light becomes a factor of 3.5 less (the number density of the fog diminishing from 1.1 to 0.3 g/m^3) /57/. The radius of the fog droplets forming in methane is $2 \cdot 10^{-5} - 6 \cdot 10^{-5}$ cm; most of the droplets are charged, carrying from 1 to 11 units of positive or negative electricity /57/. Nearly 66% of the droplets have 1—3 units of charge. The mass concentration of the fog increases as the irradiation time is increased. Figure 6.15 plots the experimental results obtained after 30 min of irradiation /57/.

A setup has been described in the literature /58/ for the production of polymethylacrylate and polymethylmetacrylate by vapor-phase polymerization

of the monomer, triggered by ultraviolet radiation in a nitrogen atmosphere. A monodisperse fog is obtained, with droplet radii of 10^{-5}—10^{-4} cm, depending on the actual operating conditions.

Metallic wires can be exploded in the air by passing sufficiently strong electric current through them (p. 97). The metal vapor is oxidized by atmospheric oxygen, the oxides condense spontaneously, and fog is formed.

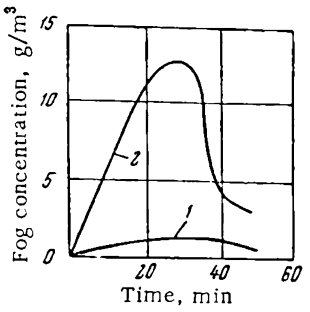

FIGURE 6.15. Mass concentration as a function of time during and after irradiation (irradiation time 30 min): 1) CH_4; 2) $CH_4 + O_2$.

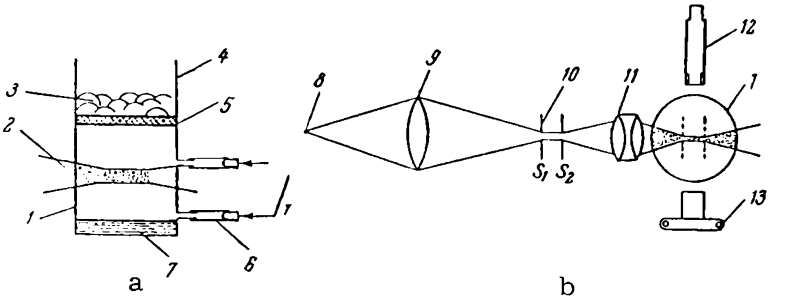

FIGURE 6.16. Schematic diagram of the setup: a — diffusion chamber; b — recording device; 1) lower cylindrical chamber; 2) illuminated region; 3) wet cotton wool; 4) upper cylindrical chamber; 5) porous partition; 6) test gas inlet and outlet; 7) HCl in water; 8) point light source; 9) condenser lens; 10) adjustable slit apertures; 11) objective lens; 12) microscope; 13) camera.

Fog formation in vapor-phase chemical reactions is utilized in the chemical diffusion method for the production of supersaturated vapor /59, 60/. Figure 6.16 is a diagram of the setup applied to study the formation of condensation nuclei of hydrochloric acid /60/. The setup comprises a diffusion chamber and a recording device.

The diffusion chamber (Figure 6.16a) is made up from two cylindrical glass vessels 1 and 4 with a porous partition 5 (Schott filter) between them. Hygroscopic cotton wool 3 soaked with water is uniformly spread on the filter 5, and an aqueous solution of hydrochloric acid 7 is poured into the vessel 1. The diffusing molecules of HCl and water vapor combine to give a mist which is observed in transmitted light with a microscope 12 (Figure 6.16b) or is photographed with the camera 13. The HCl concentration in the solution is high enough to create a certain supersaturation in the chamber, which is sufficient to initiate a measurable rate of nucleation.

This diffusion chamber can be applied to study the formation of sulfuric acid mist (from SO_3 and water vapor), ammonium chloride fumes (from HCl and NH_3), etc.

REFERENCES

1. AMELIN, A. G. — DAN SSSR, 58:1673. 1947.

2. TURKHAN, E. Ya. and V. I. YUDINA. — ZhKhP, No. 2:12. 1938.

3. AMELIN, A. G. — Khimicheskaya Promyshlennost', No. 9:1. 1945.

4. GOODEVE, C. F., A. S. EASTMAN, and A. DOOLEY. — Trans. Faraday Soc, 30:163, 1127. 1934.

5. AMELIN, A. G. — ZhPKh, 18:509. 1945.

6. TURKHAN, E. Ya. and E. A. ANDREEVA. — ZhKhP, No. 6 : 8. 1939.

7 AMELIN, A. G. — ZhPKh, 17 : 319. 1944.

8. DOOLEY, A. and C. GOODEVE. — Trans. Faraday Soc., 32 : 1209. 1936.

9 AMELIN, A. G. Soviet patent 75155, 11 Dec. 1947.

10. AMELIN, A G. Soviet patent 85513, 6 July 1949.

11. VAN de HULST, H. C. Light Scattering by Small Particles. — New York, Wiley. 1957. [Russian translation. 1961.]

12. WHYTLAW-GRAY, R., and H. S. PATTERSON. Smoke. — London, Arnold and Co. 1932.

13. DERYAGIN, B. V. and G. Ya. VLASENKO — In: "Novye idei v oblasti izucheniya aerozolei", Izdatel'stvo AN SSSR. 1949.

14. KOGAN, Ya. I. and Z. A. BURNASHEVA. — ZhFKh, 34 : 2630. 1960.

15. PETRYANOV, I. V. and N. N. TUNITSKII. — ZhFKh, 8 : 1131. 1939.

16. AMELIN, A. G. and B. V. MIKHAL'CHUK — Zavodskaya Laboratoriya, 14 : 778. 1948.

17. AMELIN, A. G., B. V. MIKHAL'CHUK, E. V. YASHKE, and G. G. GUBANOV. — Khimicheskaya Promyshlennost', No. 2 : 54. 1950.

18. PEREVEZENTSEV, I. G. Tumanomery tipa AFT-1 i PFT-2 (AFT-1 and PFT-2 Nephelometers). — Trudy UNIKhIM, No. 6 : 46. 1958.

19. FIALKO, G. M. Avtomatizatsiya proizvodstva sernoi kisloty (Automation of Sulfuric Acid Manufacture). — Izdatel'stvo Mashinostroenie. 1964.

20. BRODSKII, Yu. P. — Khimicheskaya Promyshlennost', No. 2 : 63. 1959.

21. SELEZNEV, N. and N. BALABANOV. — Byulleten' NIITEkhim, No. 5 : 45. 1959.

22. BYK, S. Sh. and L. I. SHCHERBAK. — Khimicheskaya Promyshlennost', No. 7 : 224. 1953.

23. WEBB, H. W. Absorption of Nitrous Gases. — London, Arnold and Co. 1923.

24. GOYER, G. G. — J. Coll. Sci., 18 : 616. 1963.

25. AMELIN, A. G. Proizvodstvo sernoi kisloty is serovodoroda po metody mokrogo kataliza (Wet-Gas Contact Process of Sulfuric Acid Manufacture from Hydrogen Sulfide). — Goskhimizdat 1960.

26. GERHARD, E. R. and H. F. JOHNSTONE. — Ind. Eng. Chem., 47 : 972. 1955.

27. ENDOW, N., G. J. DOYLE, and J. Z. JONES. — J. Air Pollution Control Assoc., 13 : 141. 1963.

28. JUNGE, C. E. and J. E. MANSON. — J. Geophys. Res., 66 : 2163. 1961.

29. PRAGER, M., STEPHENS, E. R., and W. E. SCOTT. — Ind. Eng. Chem., 52 : 521. 1960.

30. RYAZANOV, V. A. Sanitarnaya okhrana atmosfernogo vozdukha (Health Hazards of Atmospheric Air). — Medgiz. 1954.

31. KEL'TSEV, V. V. and P. A. TESNER. Sazha. Svoistva, proizvodstvo i primenenie (Soot, Its Properties, Manufacture, and Applications). — Gostoptekhizdat. 1952.

32. Spravochnik khimika (Chemist's Handbook), Vol. III. — Izdatel'stvo Khimiya. 1964.

33. ZEL'BERG, G. M. — Gazovaya Promyshlennost', No. 8 : 26 1956.

34. TESNER, P. A. and I. S. RAFAL'KES. — Trudy VNIIgaz, 3 : 3. 1959.

35. WHITE, L. J. and G. J. DUFTY. — Ind. Eng. Chem , 51 : 332. 1959.

36. NIKOLINA, V. Ya. — Khimicheskaya Promyshlennost', No. 1 : 48. 1962; also Candidate Dissertation, Khar'kov. 1965.

37. German Federal Republic patents 877891, 886446, 947789, 952891, 103601; USA patent 2798792; British patents 655647, 707389, 726250, 778705, 778706; Swedish patent 151931; Swiss patents 265192, 272991; Japanese patent 1514.

38. Spravochnik khimika (Chemist's Handbook), Vol. I. — Goskhimizdat. 1962.

39. British patents 438782, 630182, 675341, 728094, 793054; USA patents 2535036, 2631083, 2886414; French patent 1025837; German Federal Republic patent 1047756.

40. British patent 793054, 9 April 1958.

41. CAILLAT, R , J. P. CUERT, J. ELSTON, F. JUILLET, R POINTUD, M. PRETTRE, and S. TEICHER — Bull. Soc. Chem. France, No. 1 : 152. 1959.

42. CUERT, J. P., J. ELSTON, and S. TEICHNER — Bull. Soc. Chem. France, No 1 : 81. 1961.

43. MARKIN, N. E. — Azerbaidzhanskoe Neftyanoe Khozyaistvo, No. 6 : 25 1940.

44. BOGUSLAVSKII, I. M and L. D. KIOSSE. — Soobshcheniya o Nauchno-Issledovatel'skikh Rabotakh NIUIF, 2 : 54. 1957.

45. SAFIULIN, N. Sh. — Khimicheskaya Promyshlennost', 6 : 77. 1959.

46. ILLARIONOV, V. V., T. I. SOKOLOVA, Z. S. KULAGINA, and I. T. KNYAZEVA. — Soobshcheniya o Nauchno-Tekhnicheskikh Rabotakh NIUIF, 2 : 48. 1957.

47. LUNDE, K. E. - Ind. Eng. Chem., 50 : 293. 1958.

48. SHERESHEVSKII, A. I., L. S. GORITSKAYA, and L. N. POTAPOVA. — Soobshcheniya o Nauchno-Tekhnicheskikh Rabotakh NIUIF, 2 : 26. 1957.

49. LIMONOV, V. E. and V. E. VARLAMOV. — Nauchnye Zapiski Odesskogo Politekhnicheskogo Instituta, 3 : 41. 1962.

50. VARLAMOV, M. V., A. A. ENIAN, and L. M. KOZAKOV. — Vestnik Tekhnicheskoi i Ekonomicheskoi Informatsii NIITEkhim, 7 : 53. 1960.

51. POZIN, M. E. Tekhnologiya mineral'nykh solei (Technology of Mineral Salts). — Goskhimizdat. 1961.

52. VARLAMOV, M. L. and K. K. BELENAVICHUS. — ZhPKh, 36 (4) : 697. 1963.

53. Sbornik rabot po radiatsionnoi khimii (Collection of Papers in Radiation Chemistry). — Izdatel'stvo AN SSSR. 1955.

54. MIKHAILOV, B. M., L. V. TARASOVA, and V. S. BOGDANOV. — In: "Deistvie ioniziruyushchikh izluchenii na neorganicheskie i organicheskie sistemy. Izdatel'stvo AN SSSR. 1958.

55. BOGDANOV, V. S. — ZhFKh, 34 : 1044. 1960.

56. BOGDANOV, V. S. — DAN SSSR, 136 : 121. 1961.

57. BOGDANOV, V. S. — In: "Trudy II Vsesoyuznogo soveshchaniya po radiatsionnoi khimii". Izdatel'stvo AN SSSR. 1962. [English translation, "Proceedings of the Second All-Union Conference on Radiation Chemistry", published by Israel Program for Scientific Translations, Jerusalem 1964 (AEC-tr-6228).]

58. PEARSON, R. and G. LANGER. — Nature, 187 : 235 1960.

59. VOLLRATH, R E. — Rev. Sci. Instrum., 7 : 409. 1936.

60. TWOMEY, S. — Geofis. pura e appl., 43 : 227, 243. 1959.

Chapter Seven

FOGS WITH CONTROLLED NUMBER DENSITY AND DROP SIZE DISTRIBUTION

The frequent development of fog in industry is a highly undesirable byproduct which may lead to severe losses of valuable raw materials, catalyst spoilage, etc. The data presented in the preceding chapters of this book can be applied to created controlled conditions which prevent the formation of fog in industrial processes. Fog prevention, however, often entails a reduction in process rate. The main objective of condensation processes in industry is to recover the maximum quantity of liquid at a minimum cost. It is therefore economically expedient to speed up the process and to provide special collectors and filters for subsequent separation of the fog particles.

The degree of separation of fog in filters is highly sensitive to the droplet radius. The effectiveness of electrostatic precipitators, for example, is directly proportional to the droplet radius; the degree of separation by centrifugal force is proportional to the square of the radius, while the separation in inertial filters is even more sensitive to the droplet radius /1/.

The concentration of the fog remaining in the filtered gas is proportional to the number density of the fog before filtering; effective separation therefore requires a low starting concentration of the fog in the incoming gas.

If the fog is produced artificially (the pesticide aerosols, p. 91), its number density and drop size distribution lie between rigidly defined limits. Droplet radii and number densities are particularly significant in the manufacture of soot, metal powders, artificial condensation nuclei, monodisperse aerosols, etc. Laboratory experiments are meaningless without strict control of drop size and number density, because these two parameters actually determine the properties of the aerosols.

Control of drop size distribution and number density is thus essential whenever fog is allowed to develop: if these two factors are controlled appropriately, the properties of the fog can be changed in a desired direction.

DROP SIZE AND NUMBER DENSITY AS A FUNCTION OF SUPERSATURATION

The dispersity of the fog is represented by its drop size distribution, and approximately by the mean droplet radius (p. 33). In homogeneous condensation of vapor, the drop sizes are determined by the conditions of nucleation and by the condensational growth of the embryos. We have

already noted that the embryos are minute particles (with radii of some 10^{-7} cm), and in order to grow by condensation to largish droplets of $10^{-5}-10^{-3}$ cm radius (the modal radii for industrial fog droplets), their volumes should increase by a factor of $10^{6}-10^{12}$. This enormous growth is practicable only if the embryo (and then the droplet) remains for a sufficient length of time in a supersaturated vapor. The fog observed at the end of the nucleation stage is polydisperse, since the older droplets will have grown to larger sizes than the recently formed embryos. The polydispersity of the fog diminishes as all the droplets continue to grow by condensation after the nucleation has stopped, and the differences in droplet radii are gradually leveled out. It follows from equation (1.67) that the time rate of condensational growth of a droplet is inversely proportional to its radius:

$$\frac{dr}{d\tau} = \frac{DM}{kTr\varphi}[p - p_r(T_r)]$$

Whenever fog is formed by homogeneous condensation, the dispersity of the fog is determined by the maximum supersaturation in the system: progressively finer droplets are observed as the derivative $dS/d\tau$ is increased. The process of fog formation can be divided into three stages according to the variation of S: in the first stage S varies from S_{cr} to S_{max} ($dS/d\tau$ is positive); in the second stage S varies from S_{max} to S_{cr} ($dS/d\tau$ is negative); and in the last stage the supersaturation changes between the limits $S_{cr} > S > 1$.

During the first stage two processes occur simultaneously — formation of embryos (nucleation) and their condensational growth. The rate of nucleation increases with time. A polydisperse fog is obtained at the end of the first stage, since the old droplets will have grown to a greater extent than the recently nucleated embryos. These two processes also persist during the second stage, but the rate of nucleation is smaller because of the reduction in S, while the condensational growth is more intensive because of the increase in r and the decrease in φ (equation (1.67)). During the third stage, condensational growth is the only active process and the fog becomes more monodisperse.

The derivative $dS/d\tau$ depends on the rate of the main process which raises the supersaturation S. In adiabatic expansion of vapor-gas mixtures, it is the rate of expansion that is of decisive significance (the coefficient B, equation (2.13)). When a vapor-gas mixture is mixed with a colder indifferent gas in a free jet, the supersaturation is determined by the nozzle velocity u_1 of the gas (p. 81). If vapor is allowed to condense in an externally cooled pipe, the velocity of the vapor-gas mixture w is the decisive factor (p. 117); when fog forms in a chemical reaction, the reaction rate or the rate of mixing of the reacting components are the fundamental parameters, etc.

In a previously considered example of fog developing in an adiabatically expanding vapor-gas mixture (see Figure 2.1), the first stage of fog formation corresponds to the expansion of the mixture in the time interval from $\tau_0 = 0.5 \cdot 10^{-2}$ sec to $\tau_1 = 10^{-2}$ sec; in this brief period the supersaturation jumps approximately from 5 to 15. The second stage is between $\tau = 10^{-2}$ sec and $\tau = 1.4 \cdot 10^{-2}$ sec, when supersaturation varies approximately from 15 to 7. The third stage begins at $\tau = 1.4 \cdot 10^{-2}$ sec, when $S = S_{cr}$, and persists until the vapor pressure in the vapor-gas mixture has dropped to the saturated

vapor pressure over droplets of least radius (in accordance with equation (1.9)). Isothermal distillation begins after the third stage, i.e., gradual evaporation of the smallest droplets and continued growth of the larger droplets. The isothermal distillation is explained by the difference in saturated vapor pressures over droplets of different radii: it is higher over small droplets than over large ones.

The reduction in supersaturation during the second and the third stages of fog formation is attributable to the reduction in vapor pressure and the heating of the gas mixture (heat of condensation is released continually as new embryos nucleate and the droplets grow). The embryos, however, are minute, so the reduction in vapor pressure due to nucleation and the temperature increment produced by the heat of nucleation can be ignored. The supersaturation therefore diminishes appreciably only when the number density of fairly large droplets has reached a sufficiently high value.

The excess liquid corresponding to the difference in supersaturations at the end of the second stage (when $S=S_{cr}$) and at the end of the process ($S \approx 1$), when the system is in equilibrium, condenses on the existing droplets. The mean radius of the droplets at the end of the process can therefore be inferred from the data obtaining at the end of the second stage (p. 139).

The embryos coalesce during nucleation, and the effect of coalescence on fog formation is expressed by equation (1.86). In practice, this factor is negligible, since nucleation takes but a very short time.

Fog formation during the condensation of vapor on a colder surface (p. 117) follows nearly the same pattern as the process of fog formation in an adiabatically expanding vapor-gas mixture, but the absolute values of the process indices are different in the two cases. The first stage occupies a pipe section ~ 100 mm long (from point a to point b, see Figure 5.10), where S varies from 3.4 to 5.6. The second stage is very brief (taking place in a section ~ 20 mm long), since the supersaturation diminishes not only due to spontaneous condensation of vapor in the gas volume (as is the case with adiabatically expanding mixtures), but also due to vapor condensation on the pipe surface. The third stage is the longest, occupying a pipe length of over 1000 mm, but the mass of vapor condensing on the surface of the droplets at the end of the process is insignificant, and their radius therefore hardly changes. The variability coefficient α describing the monodispersity of the fog (equation (1.83)) at first increases to some maximum and then subsides (see Figure 5.10). The fog emerging from the pipe is virtually monodisperse ($\alpha = 0.17$).

The formation of fog in a free jet, when two vapor-gas streams of different temperature are mixed (p. 66), is a much more complex process, since the supersaturation is variable across and along the jet (the and y axes). The division of the process into a sequence of three stages is meaningless in this case, since the different stages occur simultaneously in different jet sections. However, if high-speed gas streams are mixed in a three-way joint /2, 3/, the mixing may be regarded as instantaneous to first approximation ($dS/d\tau=\infty$). The first stage of the process is therefore disregarded, and the development of fog is assumed to commence with the second stage, when $S=S_{max}$. The length of this stage depends on the rate of homogeneous condensation of the vapor, i.e., the rate of nucleation I (equation (1.53)), and the rate of condensation on the surface of already

existing droplets (equation (1.67)). During the third stage, as in all processes of fog formation, the existing droplets continue to grow by condensation. The total mass of vapor condensing on the droplets at this stage is equal to the excess vapor removed from the gas phase as the supersaturation has dropped from $S=S_{cr}$ to $S \approx 1$. The duration of the third stage naturally increases as N and r diminish.

In some cases, the derivative dp/dT can be used to obtain an equation for the temperature dependence of the vapor pressure and the supersaturation. These data can also be applied to determine the conditions for maximum supersaturation (p. 95, 107).

The following expressions were obtained for the derivative dp/dT in different processes, in stages when $S<S_{cr}$:

adiabatic expansion

$$\frac{dp}{dT} = \eta T^{\frac{1}{k-1}} \tag{2.10}$$

$$\eta = \frac{k p_1 T_1^{\frac{k}{1-k}}}{k-1} \approx \text{const} \tag{2.11}$$

turbulent mixing

$$\frac{dp}{dT} = \mu \left(\frac{p-p_2}{T-T_2}\right)^2 \tag{3.11}$$

$$\mu = \frac{b}{a} \cdot \frac{T_1 - T_2}{p_1 - p_2} \approx \text{const} \tag{3.12}$$

condensation of vapor between parallel plates

$$\frac{dp}{dT} = \frac{p_1 - p_2}{T_1 - T_2} = \text{const} \tag{4.11}$$

condensation of vapor on the surface

$$\frac{dp}{dT} = \delta \frac{p-p_2}{T-T_2} \tag{5.4}$$

$$\delta = \rho c \frac{\beta}{\alpha} \approx \text{const} \tag{5.6}$$

For $S>S_{cr}$, dp/dT is expressed by considerably more complex equations, since two simultaneous processes occur in the system: formation of embryos and condensation of vapor on the surface of existing droplets and embryos. For the cases of adiabatic expansion of vapor-gas mixtures and condensation of vapor in an externally cooled pipe, the derivative dp/dT for $S>S_{cr}$ is expressed by the very complicated equations (2.27) and (5.38), respectively. The solution of the equations for $dS/d\tau$ involves still greater difficulties (see, e.g., equation (2.28)).

We see from these examples that, although dp/dT and $dS/d\tau$ are the principal factors governing drop size distribution and number density of fog in various processes where the supersaturation S increases, the general equations for these derivatives are much too complicated to be solved in a routine manner for purposes of fog control.

CONTROL OF DROP SIZE DISTRIBUTION AND NUMBER DENSITY OF FOGS

In accordance with previous observations (p. 203), the drop size distribution and the number density of the fog are determined by the maximum supersaturation S_{max} (dependent on the derivative $dS/d\tau$) and the vapor pressure p at the instant of fog formation.

The vapor pressure governs the condensational growth of the droplets. Its effect is expressed by equations (1.87) and (1.88), which give

$$\bar{r} = \sqrt[3]{\frac{3G}{4\pi\rho N}} = \sqrt[3]{\frac{3M[p - p_\infty(T)]}{4\pi\rho RTN}} \qquad (7.1)$$

where p and $p_\infty(T)$ are the vapor pressure and the saturated vapor pressure at point of incipient fog, mm Hg; N is the number density of the fog.

By varying S_{max}, $dS/d\tau$, and p, we may control the dispersity and the number density of the fog. To increase the mean droplet radius (other parameters remaining constant), the derivative $dS/d\tau$ is decreased (in order to reduce the supersaturation S), the number density is lowered, and the vapor pressure at the point of incipient fog is raised. To make the drop size distribution more homogeneous, S_{max} and $dS/d\tau$ are increased (numerically) in the first and the second stages and the duration of the third stage is lengthened, while maintaining $S_{cr} > S > 1$.

In the course of our discussion, we have repeatedly encountered various cases when drop sizes and number densities are controlled by adjusting one or several of the condensation parameters. We see from the data plotted in Figure 2.2 (curves 1 and 2), for example, that increasing the expansion ratio of a vapor-gas mixture raises the number density of the fog. When fog develops during vapor condensation on the surface, the mean droplet radius diminishes as the thermal conductivity of the gas mixture, which determines the value of the coefficient δ (equation (5.17)), is increased (see Figure 4.4). We have shown in Chapter Five (p. 124) that the dispersity and the number density increase to a certain maximum with the increase of the condensable vapor pressure, and then start decreasing. In Chapter Six we have reproduced some data concerning the influence of temperature and vapor concentration on the dispersity of soot (p. 188). All this implies that the functional relation $\bar{r} = f(T)$ has a minimum (see Figure 6.10). The existence of the minimum on the $\bar{r} = f(T)$ curve was established experimentally for silica smoke and Al_2O_3 powder (see Figures 6.12 and 6.14).

In addition to these data, Figure 7.1 plots some curves which represent the variation with time of the mean droplet radius and number density of the fog forming in adiabatically expanding vapor-gas mixtures with different expansion ratios $\frac{V_2}{V_1}$ and expansion times t. The curves are based on the results of calculations made by the procedure outlined on p. 51.

We see from Figure 7.1 that as the expansion ratio increases from 1.4 to 1.6 (curves 1, 2, and 3), the derivative $dS/d\tau$ increases and the maximum supersaturation S_{max} correspondingly rises from 9 to 23. The number density of the fog increases from $8 \cdot 10^5\,cm^{-3}$ to $3 \cdot 10^9\,cm^{-3}$ (curves 1 and 3) and the mean droplet radius diminishes from $7 \cdot 10^{-5}$ cm to $5 \cdot 10^{-6}$ cm.

The dependence on the process indices on the rate of expansion, i.e., the time t (equation (2.13)), can be established by a comparison of curves 4 and 2. It is seen from the analysis of these curves that as t rises from 0 to 10^{-2} sec, the derivative $dS/d\tau$ drops from ∞ to 4000 (curve 2). N correspondingly decreases from $6 \cdot 10^8$ cm^{-3} to $5 \cdot 10^8$ cm^{-3} (curves 4 and 2), and the mean droplet radius increases from $8 \cdot 10^{-6}$ cm to $9 \cdot 10^{-6}$ cm.

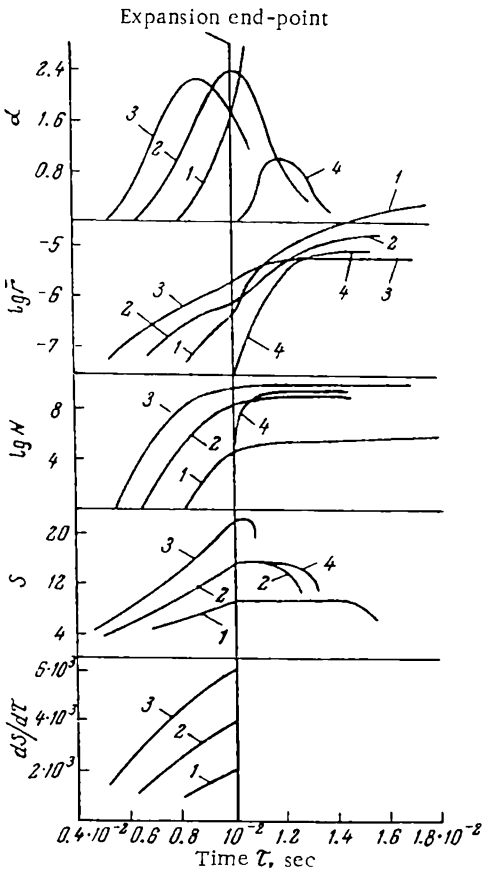

FIGURE 7 1. Process indices vs. time in adiabatic expansion:

1) $\frac{V_f}{V_0} = 1.4$, $t = 10^{-2}$ sec, $S_{max} = 9.0$;

2) $\frac{V_f}{V_0} = 1.5$, $t = 10^{-2}$ sec, $S_{max} = 15.2$;

3) $\frac{V_f}{V_0} = 1.6$, $t = 10^{-2}$ sec, $S_{max} = 23.2$;

4) $\frac{V_f}{V_0} = 1.5$, $t = 0$, $S_{max} = 15.2$.

As t is further increased to 1 sec, the quantity of vapor condensing on the surface of the droplets becomes so large that for $V/V_1 = 1.45$ the supersaturation, having reached a maximum, starts decreasing and nucleation stops (see Figure 2.3). The number density of the fog at the end of the process is now $2 \cdot 10^8$ cm^{-3} (and not $5 \cdot 10^8$ cm^{-3} as for $t = 10^{-2}$ sec).

The effect of expansion conditions on the drop size distribution is expressed by the upper graph in Figure 7.1, which plots the variability coefficient $\alpha = f(\tau)$ (equation 1.83)). In all cases, the polydispersity first increases with the expansion of the vapor-gas mixture and then, having reached a maximum, starts decreasing due to condensational growth of the droplets. As t is decreased (the rate of expansion is increased), α decreases (monodisperse fog is obtained), since the nucleation stage is shortened; the coefficient α is smallest for $t = 0$ (see Figure 7.1, curve 4). This peculiarity is utilized for the generation of a monodisperse aerosol: a vapor-gas mixture is mixed with a colder indifferent gas in a three-way joint, the two gases flowing at high velocities /3/.

The terminal droplet radius can be increased by additionally expanding the vapor-gas mixture (after the third stage), always keeping $S_{cr} > S > 1$. The dependence of the terminal radius on the additional expansion ratio is easy to determine, since no new droplets form and the excess vapor condenses on already existing droplets. The purpose of Figure 7.1 is not only to illustrate the dependence of fog dispersity and number density on various particular factors: it can be actually applied to devise techniques for the control of aerosol systems under a variety of conditions. Analogous curves plotting the effect of various factors on the derivative $dS/d\tau$ and the supersaturation S, as well as on fog dispersity and number density can be constructed for other cases when supersaturated vapor develops (in mixing gas streams, in chemical reactions, etc.).

In the following we consider some of the techniques which are commonly applied in practice for fog control. In approximate calculations the reduction in vapor pressure due to condensation of vapor in the volume is often ignored. By putting the right-hand sides of equations (1.7) and (1.8) equal to zero, we may then find the conditions for maximum supersaturation and minimum droplet radius.

CONTROL OF DROP SIZE IN MEDICAL AEROSOLS AND PESTICIDE SPRAYS

The effectiveness of sprayed pesticides depends primarily on the coefficient of precipitation of the droplets on the object surface and on the uniformity of the pesticide film on the surface. The settling out of droplets from a cloud of mist has not been studied theoretically, and at present a mere 20% of the sprayed pesticide precipitates on the surface of the leaves, while the other 80% is lost irretrievably /4/.

Calculations and experiments show that uniform spreading of the pesticide on the surface of the plant is possible only if the liquid film is extremely thin. This condition can be observed if the aerosol droplets are very fine, but as the droplets are made smaller, they show less tendency to precipitate, and a higher percentage of the pesticide is lost.

The optimal size of the spray droplets depends on the nature of the treated object and the particular conditions of treatment. One of the principal requirements to be met by spray guns and particle generators is that the drop size should be controllable.

In thermal spraying, the mist is formed in a jet; the technique for controlling the size of the droplets has been discussed previously (p. 81). High supersaturation develops in the free jet emerging from the nozzle (see Figure 3.15). Therefore despite the presence of condensation nuclei in the atmospheric air, the formation of fog in the spray gun is entirely conditioned by nucleation processes during homogeneous condensation. This is indeed so, since the number density of condensation nuclei in the air in rural areas is a mere $10^4\,cm^{-3}$ (see Table 1.6), whereas the number density of the embryos forming by homogeneous condensation of vapor is as high as $10^9-10^{10}\,cm^{-3}$. Because of the high speed of the gas in the jet and the high number density of the fog, the process of droplet formation is sensitive to eddy coalescence.

Two processes thus occur concurrently in the jet emerging from an aerosol generator (see Figure 3.15): new droplets nucleate and existing droplets grow by vapor condensation and coalescence. The final size of the droplets, i.e., the dispersity of the mist, therefore depends on the ratio of nucleation and growth rates.

It follows that in order to increase the mean radius of the fog droplets forming in the jet, the conditions should provide for the condensation of the bulk of the vapor on the surface of comparatively few droplets. The probability of nucleation should be radically suppressed. Conversely, in order to reduce the mean droplet radius, the conditions should ensure abundant nucleation of new primary droplets, simultaneously limiting the condensation of vapor on already existing droplets.

By adjusting the nozzle velocity of the vapor-gas mixture, we can create suitable conditions for nucleation in the initial section of the jet, the forming embryos then acting as condensation nuclei in the principal section. This is a practical technique for controlling the dispersity of thermally generated aerosols.

The above considerations are confirmed by experimental findings /5/. Air heated to 311 °C ($V = 0.6\ m^3/hr$ at NTP) is saturated with glycerine vapor ($p = 88$ mm Hg) and is ejected through nozzles of varying diameter (2.5, 7.5, 15, 30, and 50 mm) into the ambient air (20 °C). As the nozzle diameter is increased, the nozzle velocity of the vapor-gas mixture decreases and larger fog droplets are obtained. The drop size distribution (Table 7.1, Figure 7.2) and the mean droplet radius (Figure 7.3) are found by counting the droplets in a cloud sample and measuring their radii /6/.

TABLE 7.1. Drop size distribution in a glycerine aerosol for various nozzle diameters (nozzle velocities)

Nozzle diameter, mm	Nozzle velocity of gas, m/sec	Drop count in different radius intervals, % of the total						Mean droplet radius $\bar{r}$, cm
		0—0.5 10^{-4} cm	0.5·10^{-4}—1·10^{-4} cm	1·10^{-4}—2·10^{-4} cm	2·10^{-4}—4·10^{-4} cm	4·10^{-4}—8·10^{-4} cm	8·10^{-4}—16·10^{-4} cm	
2.5	83	77.7	19.9	2.4	—	—	—	0.8·10^{-4}
7.5	9	48.4	32.3	11.3	0.97	0.03	—	1.5·10^{-4}
15	2.3	19.3	34.4	27.3	18.0	1.0	—	2.8·10^{-4}
30	0.6	—	24.5	26.7	43.1	5.6	—	3.7·10^{-4}
50	0.2	14.1	30.4	19.0	26.1	10.0	0.4	5.0·10^{-4}

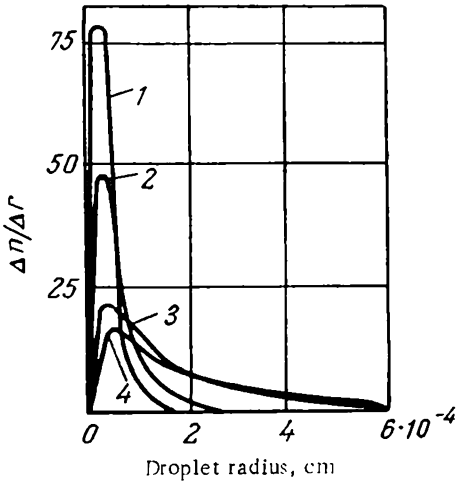

FIGURE 7.2. Differential drop size distributions:
1) nozzle diameter 2.5 mm; 2) 7.5 mm; 3) 15 mm; 4) 30 mm.

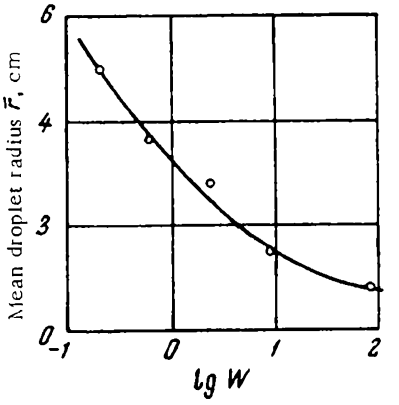

FIGURE 7.3. Mean droplet radius vs. nozzle velocity (w, m/sec).

The results of these experiments indicate that the dispersity of a fog generated by vapor condensation in a jet can be controlled between wide limits. The mean droplet radius calculated for a 2.5-mm nozzle is $\bar{r} = 1.3 \cdot 10^{-4}$ cm (the experimental figure is $\bar{r} = 0.8 \cdot 10^{-4}$ cm, Table 7.1).

In calculations, the field of the free jet along the x axis is divided into several arbitrary sections Δx; the parameters u, T, p, S, I, and $\bar{r}$ are determined for each section separately, and an average value is assumed for each section. The higher theoretical value of the mean droplet radius is attributable to this averaging. The supersaturation varies substantially across the jet (see Figure 3.7) and the rate of nucleation in each section changes correspondingly. The larger mean radius is possibly also explained by exaggerating the contribution from coalescence, since no reliable data are available for the calculation of the coalescence constant under these conditions.

The dispersity of the fog forming in a free jet can also be controlled by alternative techniques. As we have previously observed (p. 65, Figure 3.1), the supersaturation increases as the temperature difference between the mixing gases is raised, and the drop radius correspondingly decreases. The droplet radii can therefore be controlled by altering the temperature of the gas in the nozzle.

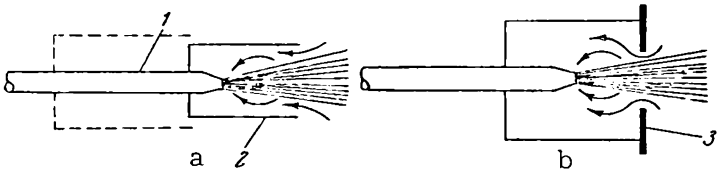

FIGURE 7.4. A device for controlling fog dispersity: 1) nozzle; 2) moving cartridge; 3) aperture.

A special device is available for the control of fog dispersity (Figure 7.4). The nozzle is enclosed in a cylindrical cartridge 2, which can be moved along the jet axis. When the cartridge is in position shown in Figure 7.4a (the solid outline), the reduction in pressure diverts part of the gas from the principal section back to the initial section (the motion of the gas is shown by arrows in Figure 7.4). Since the temperature of the diverted gas is fairly high and it contains fog droplets, the process of fog formation in the jet is essentially altered: the supersaturation decreases and the imported fog droplets act as condensation nuclei.

Figure 7.4b is a device for controlling the size of fog droplets by means of an adjustable aperture 3. As the aperture is contracted, a smaller proportion of the jet is diverted and comparatively fine droplets are formed.

In tests with the industrial mist generator /7/ operating on the principle schematically shown in Figure 3.15, the sample is withdrawn from several points of the same cross section (for different y); the sampling cross section is distant 1 meter from the nozzle ($x = 1000$). The mass concentration of the fog in the jet was determined for four separate fractions:

1st fraction $\bar{r} = 5 \cdot 10^{-4}$ cm, 2nd fraction $\bar{r} = 1.3 \cdot 10^{-4}$ cm,
3rd fraction $\bar{r} = 0.8 \cdot 10^{-4}$ cm, 4th fraction $\bar{r} = 0.5 \cdot 10^{-4}$ cm.

The droplets were tagged by dyeing the liquid before spraying. The primary droplets generated by mechanical spraying of the liquid contained more dye than the original liquid (the increased concentration is attributed to partial evaporation), whereas droplets forming by condensation carried an insignificant amount of the dye.

Figure 7.5 plots the results of the tests in a gas with a nozzle temperature of 550 °C. It follows from the graph that nearly 20% of all the liquid is concentrated in the form of large primary droplets ($\bar{r} > 5 \cdot 10^{-4}$ cm) of mechanical origin (mechanical spraying of the liquid), and nearly 60% is in the form of minute droplets ($\bar{r} = 0.5 \cdot 10^{-4}$ cm) of condensational origin. The drop size distribution of the fog across the jet (the y axis) is fairly constant.

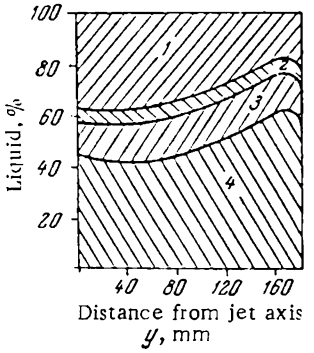

FIGURE 7.5 Percentage of liquid in droplets of different fractions:
1) $\bar{r} > 5 \cdot 10^{-4}$ cm; 2) $\bar{r} = 1.3 \times 10^{-4}$ cm; 3) $\bar{r} = 0.8 \cdot 10^{-4}$ cm; 4) $\bar{r} = 0.5 \cdot 10^{-4}$ cm.

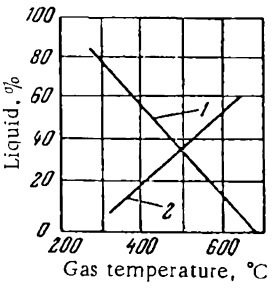

FIGURE 7.6. Liquid content of droplets vs. temperature:
1) $\bar{r} > 5 \cdot 10^{-4}$ cm; 2) $\bar{r} = 0.5 \cdot 10^{-4}$ cm.

As the nozzle temperature of the gas is increased, the liquid content of the large droplets decreases, and a higher percentage of the liquid is concentrated in the fine droplets (Figure 7.6). This is so because, on the one hand, the supersaturation in the jet increases while, on the other hand, the large droplets of mechanical origin evaporate more intensively. At gas temperatures near 600 °C, the 1st fraction disappears entirely from the fog, which implies complete evaporation of the liquid with subsequent condensation into fine droplets. The polydispersity of the fog generated by the thermomechanical method decreases while the plants are being sprayed, because the small droplets evaporate in the ground air layer and the large drops settle out near the spray gun. At some distance from the spray gun the cloud of mist therefore consists of droplets of nearly uniform radius.

We now proceed to calculate the quantity of pesticide evaporating in the air. The pesticide is sprayed at a rate of $Q = 360$ liter/hr, the spray gun moving at a speed of $w = 3600$ m/hr along the treated section. The effective radius of the sprayed pesticide is $L = 100$ m, the height of the aerosol cloud $H = 10$ m, air temperature 20 °C. We further assume that the aerosol is uniformly spread in the ground air layer (over the treated section). In this case, the hourly output of the spray gun is contained in

the following air volume:

$$V = wLH = 3.6 \cdot 10^6 \text{ m}^3$$

The concentration of the pesticide in the ground air layer is therefore

$$\Pi = \frac{Q}{V} = 10^{-4} \text{ liter/m}^3$$

Diesel fuel, a mixture of several hydrocarbons having differen saturated vapor pressures, is often used as a pesticide. An exact calculation of evaporation in this case is very laborious; to simplify the calculations, we assume that pure pentadecane ($C_{15}H_{32}$) is sprayed. The molecular weight of pentadecane is $M = 212.3$, density (at 20 °C) $\rho = 0.78$ g/cm^3, boiling point 276.6 °C; the vapor pressure of pentadecane (in mm Hg) is expressed by the equation /9/

$$\lg p = 7.312 - \frac{1973 \cdot 3}{t + 176.6}$$

At 20 °C, the saturated vapor pressure according to this equation is $p = 1.9 \cdot 10^{-3}$ mm Hg, which corresponds to a concentration of vapor $q = 2.4 \cdot 10^{-2}$ g/m^3. The fraction π of the solvent which is converted to vapor (by the evaporation of droplets) is thus

$$\pi = \frac{q \cdot 100}{10^3 \cdot \Pi\rho} = 30\%$$

We see from Figure 7.6 that at a nozzle temperature of 550 °C, some 60% of the solution occurs in the form of droplets with an average radius $\bar{r} = 0.5 \cdot 10^{-4}$ cm (4th fraction). This applies to the aerosol cloud near the nozzle. As the mist moves over the treated section and the cloud is diluted with air, the smallest droplets of this fraction are the first to evaporate. The polydispersity of the fog at some distance from the nozzle is therefore smaller than initially. The precipitation of the large droplets soon after ejection is also conducive to this homogenizing trend.

The above calculation is approximate, since the pesticide droplets do not spread through the entire air volume in the treated section. Eddy pulsations and wind currents distend the cloud, which occupies only part of the treated volume. A fairly complete reconstruction of the drop size distribution in the cloud of aerosol moving away from the spray gun can be obtained only if the various factors influencing the behavior of the aerosol in the ground air layer are taken into consideration and an appropriate numerical coefficient allowing for the spread of the mist particles through the treated volume is introduced.

The isothermal distillation in the aerosol cloud (p. 204) also operates to reduce the polydispersity of the fog as the spray moves away from the nozzle. The effect of isothermal distillation becomes more pronounced as the output of the aerosol generator is increased, since the effective radius of the spray cloud increases and the cloud of mist stays longer in the ground air layer (allowing more time for isothermal distillation).

The above considerations are confirmed by results obtained under field conditions.

CONTROL OF FOG DISPERSITY DURING VAPOR CONDENSATION ON THE SURFACE

Vapor is made to condense on the surface in a variety of industrial processes as a technique for the separation of water from the gas phase (p. 105). If fog develops during vapor condensation, the conditions should be so controlled that large droplets form, which are easy to separate in subsequent stages (p. 121).

The principal techniques for the prevention of fog during vapor condensation on the surface or for the growing of large fog droplets have been discussed in Chapter Five. We now proceed to describe a method which promotes the formation of large droplets by reducing the maximum supersaturation S_{max} during the first stage of fog development, without altering the principal technological parameters of the process.

The vapor-gas mixture is cooled until homogeneous condensation somewhat raises the number density of the fog. The process is then so conducted that the vapor mainly condenses on the surface of already existing droplets. The vapor-gas mixture can be cooled in heat exchangers or by mixing.

Let us consider the formation of monodisperse fog in a heat exchanger. The analysis will be based on the initial data applied for the condensation of sulfuric acid vapor in an externally cooled pipe (p. 126).

It follows from Table 5.11 that in section 13 the number density of the fog is $N = 3.9 \cdot 10^5$, the mean droplet radius is $\bar{r} = 1.8 \cdot 10^{-6}$ cm. If the gas leaving this section is directed to an empty insulated chamber (free volume), the supersaturation will drop rapidly due to vapor condensation on the surface of existing droplets, the temperature of the gas somewhat rising on account of the heat released by the condensing vapor (Figure 7.7).

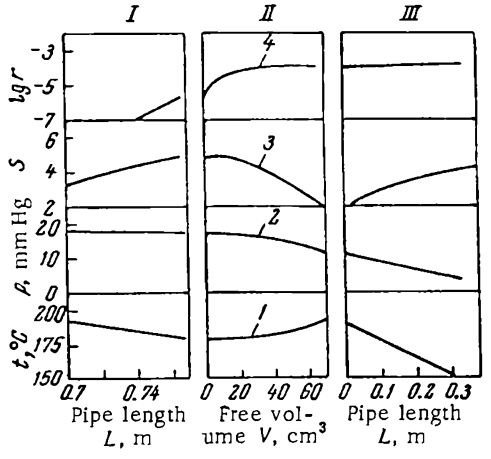

FIGURE 7.7. Condensation of sulfuric acid vapor in a condenser with free volume: I — condensation in the upper part of the condenser; II — condensation in the free volume; III — condensation in the lower part of the condenser; 1) temperature t; 2) vapor pressure p; 3) supersaturation S; 4) mean droplet radius $\bar{r}$.

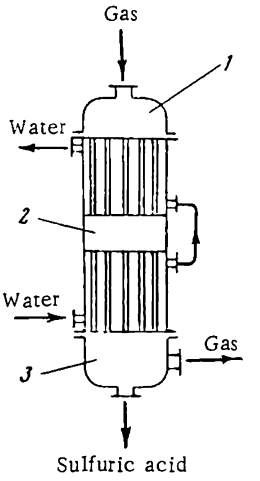

FIGURE 7.8. Condenser permitting drop size control: 1) top chamber; 2) free volume; 3) bottom chamber.

If the vapor-gas mixture emerging from the empty chamber is again directed into a pipe (where the previous conditions of cooling are maintained), the supersaturation, though rising, will remain subcritical. No new droplets therefore form in the gas. The existing droplets steadily grow in the supersaturated vapor which condenses on their surface.

Given a chamber of 60-cm^3 capacity, the gas remains 0.02 sec in the free volume, and this brief interval is sufficient to raise the mean radius of the droplets emerging at the end of the pipe from $4.5 \cdot 10^{-5}$ cm (Table 5.11) to $3.4 \cdot 10^{-4}$ cm (with $N = 3.9\ 10^5\ cm^{-3}$, as compared to the original $1.6 \cdot 10^8\ cm^{-3}$). The volume ratio of the chamber to the entire pipe is $66.8/265.4 = 0.25$.

The mean radius of the fog droplets can be regulated by changing the chamber's position along the pipe. As the chamber is moved closer to the pipe inlet, the number density of the fog droplets at the outlet decreases and the mean droplet radius of the emerging fog increases (provided that no additional droplets have formed).

In industry, the free-volume technique can be adapted to a conventional pipe condenser: the tower should be built from two separate sections with an empty space in between (Figure 7.8). The vapor-gas mixture is delivered to the chamber 1 and then to the pipes in the upper part of the condenser. The gas emerging from the pipes enters the free volume 2, where vapor condenses on the existing droplets and the supersaturation diminishes. From the free volume 2 the gas is fed into the pipes of the lower condenser section.

The coolant water circulating in the tower bypasses the free volume and enters between the pipes in the upper part of the condenser. The temperature of the coolant can be so adjusted that the zone of fog formation is displaced appropriately and the fog in the gas reaching the free volume has the required number density.

When sulfuric acid vapor condenses in a packed tower (p. 152), the conditions should favor maximum growth of fog droplets, in order to facilitate separation of the mist from the gases. The conventional approach is to lower the supersaturation by heating the condensation surface and reducing the ratio expressed by equation (5.21). This can be achieved either if the quantity of spraying acid is reduced or if the acid is heated to a higher temperature. In the first case the temperature of the condensation surface is raised by the heating of the acid in the tower base (i.e., in the initial stage of the process), where vapor condenses in the volume; the surface temperature moreover depends on the process conditions, which affect the terminal size of the droplets. In the second case the temperature of the condensation surface is raised along the entire tower height, so the spraying density is higher than in the first case and the wetting of the packing is more complete and more uniform.

Figure 7.9 plots the variation of condensation indices of H_2SO_4 for different temperatures of the spraying acid. These data were obtained by approximate numerical calculations using the initial data listed on p. 156. Curves 1, 2, and 3 correspond to an inlet acid temperature of 50 °C and outlet temperatures of 80, 150, and 200 °C, respectively; the inlet temperature of the acid in curve 4 is 100 °C and the outlet temperature is 200 °C. We see from Figure 7.9 that as the temperature of the condensation surface is increased, the development of fog is deferred to a later stage and its

mass concentration correspondingly diminishes. The droplet radius increases with the increase in the temperature of the condensation surface.

An important practical conclusion follows from the preceding discussion: by heating the spraying acid or by reducing its quantity, we can increase the radius of the forming droplets, lower the number density of the fog, and even prevent the development of fog altogether if the conditions are right. Fog prevention can be achieved with one or several serially connected towers, the number of towers depending on the vapor content of the incoming gas.

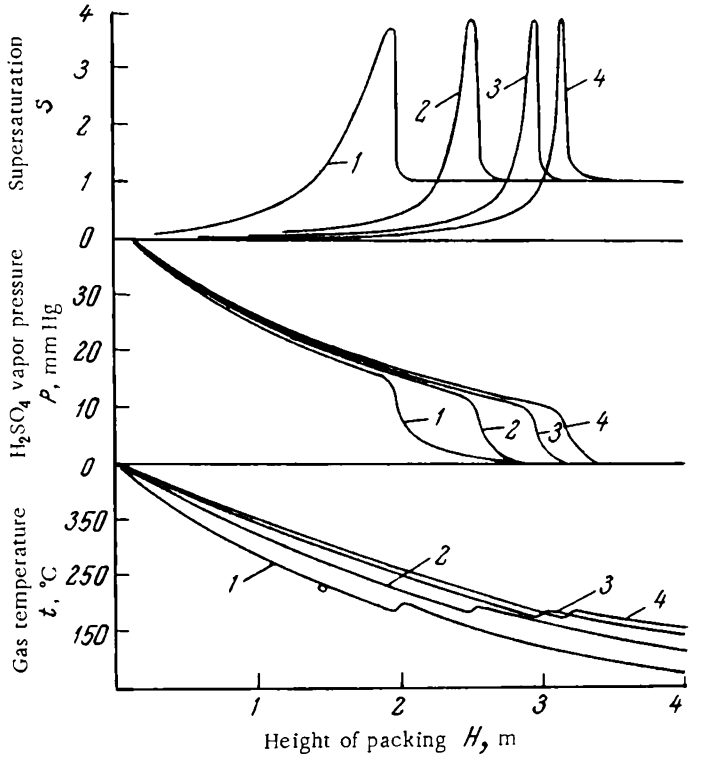

FIGURE 7.9. Condensation of sulfuric acid vapor in a packed tower: 1) inlet acid temperature 50 °C, outlet temperature 80 °C; 2) inlet temperature 50 °C, outlet temperature 150 °C; 3) inlet temperature 50 °C, outlet temperature 200 °C; 4) inlet temperature 100 °C, outlet temperature 200 °C.

As the temperature of the condensation surface is raised, the height of the packing should be increased in order to achieve the required degree of condensation, since the rates of mass and heat transfer diminish with the decrease of the differences $(p-p_2)$ and $(T-T_2)$ in equations (5.1) and (5.2). The expediency of heating the condensation surface therefore depends on economic factors. In each particular case special calculations should be made in order to find the point of balance between the increased cost of the larger condenser tower and the saving achieved by introducing cheaper filters (the mist being coarser, low-power gas filters may be used) or the reduced cost of a smaller tower and the more expensive high-power filters.

GENERATION OF ARTIFICIAL CONDENSATION NUCLEI AND MONODISPERSE FOG

Artificial condensation nuclei on which droplets form and grow are produced by condensing various substances with a characteristically low saturated vapor pressure. Any of the previously described processes in which supersaturated vapor develops can be applied for this purpose. Condensation nuclei are commonly generated by blowing a relatively cold gas past a heated surface coated with the substance from which the nuclei are to be formed /10/. The conditions in this setup ensure the development of high supersaturation and formation of minute liquid or solid particles.

The radii and the number densities of the condensation nuclei in principle can be calculated by solving the set of equations which relate the vapor pressure to temperature (equation (5.38)), the rate of nucleation (equation (1.53)), and the rate of growth of the embryos in the supersaturated vapor (equation (1.67)). No satisfactory methods have been developed for simultaneous solution of these equations, and the fundamental parameters of the condensation nuclei are therefore determined experimentally in each particular case.

It follows from the previous data on the relation of fog droplet radii to supersaturation (p. 202) that homogeneous condensation of vapor in the volume invariably produces a whole spectrum of nuclei. To obtain a more homogeneous, monodisperse distribution, high values of the derivative dS/dr should be maintained in the first and the second stages of fog formation (in order to level out the size differences between droplets of different "ages") and proper conditions should be created for the condensational growth of the droplets to the required size, keeping $S_{cr} > S > 1$.

A nichrome or platinum wire spiral is coated with a thin layer of substance from which the condensation nuclei are to be generated. The spiral is immersed in a gas stream at room temperature and electric current is passed through the wire. The temperature of the spiral and the evaporation of the coating film are controlled by adjusting the strength of the current. The molecules evaporating from the surface diffuse through the boundary layer and mix with the colder gas. High supersaturation develops, and the vapor condenses spontaneously into embryos, which grow to droplets that may eventually crystallize. Since the spiral is a very thin wire, the heat released by the metal is insignificant and the heating of the gas is negligible. The vapor therefore almost entirely condenses in the volume.

Condensation nuclei are often generated from sodium chloride (NaCl), a substance with a low saturated vapor pressure /9/:

Temperature t, °C	422	487	539	599	670	800
Saturated vapor pressure p_∞, mm Hg	10^{-6}	10^{-5}	10^{-4}	10^{-3}	10^{-2}	Fusion

Silver iodide, lead iodide, and other condensation nuclei are used in the seeding of clouds; the nuclei are produced by mixing the vapors of these compounds with atmospheric air in a free jet (p. 87).

Condensation nuclei consisting of minute water crystals can be applied for the same purpose. These crystals are formed by seeding the clouds with solid carbon dioxide at a temperature of − 78.5 °C. The CO_2 particles evaporate, and the carbon dioxide vapor mixes with atmospheric air, which

contains water vapor. The water condenses spontaneously forming minute crystals which act as condensation nuclei /11, 12/.

Finely divided aerosols (which may be regarded as condensation nuclei) are formed when a wire is exploded in an inert gas or in the air /13/. The explosion occurs when high-voltage electrical current is passed through the wire. Ag, Au, Pt wires exploding in argon generate nearly pure metal aerosols, whereas wires of common metals exploded in air give oxides in aerosol form.

When the wire explodes, the melting metal is pulverized into minute droplets. A certain proportion of the melt is evaporated, and the metal vapors mixing with the cold gas condense in the volume. The thinner the wire and the higher the voltage, the greater is the proportion of metal that evaporates. The fine condensation droplets are therefore more numerous.

Generation of artificial condensation nuclei and the study of their properties have occupied many scientists, who have been mainly concerned with seeding of atmospheric clouds and production of fogs. The main contributions in this field are reviewed in specialized literature /12, 14/.

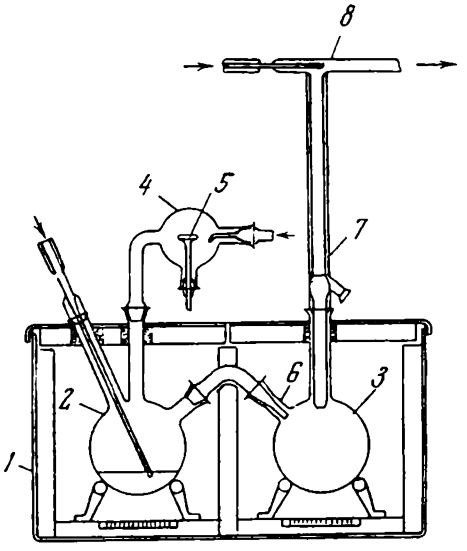

FIGURE 7.10. Aerosol generator of the heat-exchanger type:
1) thermostat; 2) evaporator; 3) reheater; 4) ionizer; 5) nichrome wire spiral; 6) nozzle; 7) condenser; 8) mixer.

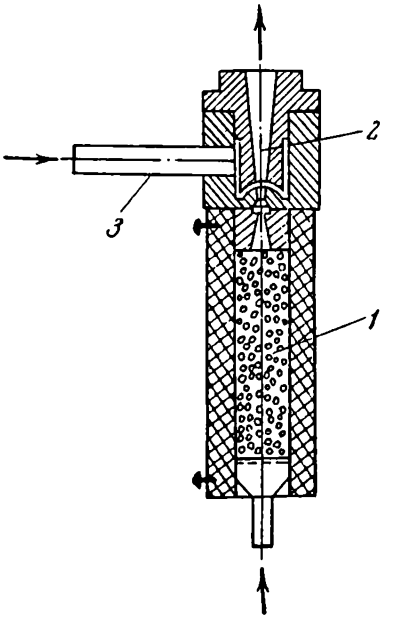

FIGURE 7.11. Aerosol generator of the mixer type:
1) evaporator; 2) nozzle; 3) cold gas in.

The fundamental properties of a fog depend primarily on the size of the constituent droplets. Experimental investigations should preferably be carried out on monodisperse fogs, with droplets of uniform size. Monodisperse fog can be obtained by condensation of supersaturated vapor on nuclei /15/. A gas stream containing artificial condensation nuclei is saturated with the vapor of the substance which is to be converted to fog, and the vapor-gas mixture is then cooled in a pipe. The cooling can be achieved in a laminar flow of gas (particle generator of the heat exchanger

type), by mixing the carrier with a colder indifferent gas in a turbulent jet (mixer-type generator), as described in Chapter Three (p. 85), or by adiabatic expansion (Chapter Two).

The gas is cooled to such an extent that the supersaturation is insufficient for homogeneous condensation, but adequate for the condensation of vapor on nuclei (heterogeneous condensation).

Figure 7.10 is a schematic diagram of the Sinclair—La Mer aerosol generator of monodisperse fog which operates on the heat-exchange principle /16, 17/. Filtered air (or nitrogen) is delivered in two currents (at a rate not exceeding 4 liter/min) to the evaporator 2 — a two-liter flask with the evaporating liquid, immersed in the thermostat 1. One of the air currents is enriched with condensation nuclei: it is first passed through the ionizer 4 where the active element is a heated nichrome wire spiral 5 coated with a layer of common salt. The second current is bubbled through the liquid in the evaporator 2. The vapor-laden gas mixes with the gas from the ionizer, and the mixture issues through a narrow nozzle 6 into the reheater 3, placed in the second temperature-controlled chamber. The gases are additionally mixed in the reheater, and the spray entrained by the air bubbling through the liquid layer is evaporated (the temperature in the second thermostat compartment is higher than in the first).

From the reheater 3 the vapor-gas mixture containing condensation nuclei is delivered to a condensation pipe 7 with an internal diameter of 2 cm, which is enclosed in an air-cooled sleeve. The vapor-gas mixture is cooled in the condenser, and vapor condenses on the pipe walls. The supersaturation thus gradually increases (p. 105), and vapor starts condensing on the nuclei. The mist emerging from the condenser is diluted in the mixer 8 with filtered air to prevent coalescence of droplets. The flow velocities and the temperatures decide the terminal radius of the droplets.

Other generators of the heat-exchanger type /18—20/ differ only in particulars, such as the method of liquid evaporation, the generation of condensation nuclei, etc.

In a mixer-type generator /21/ (Figure 7.11) the filtered air is passed at a rate of 1 liter/min through a constant-temperature evaporator 1 filled with large-porous silica gel, saturated with the evaporating liquid. The air issues in a narrow jet through the conical nozzle 2 of the mixer. A cold gas with condensation nuclei is delivered at a rate of 4 liter/min through the pipe 3 and a narrow annular slot (of adjustable width) to the same nozzle. The degree of supersaturation in the mixer is controlled by adjusting the mixer temperature, the flow velocities, and the width of the ring slot.

In another mixer-type generator /3/, the gas with condensation nuclei, before being mixed with the vapor-laden gas, is heated to the temperature of the vapors and then delivered to the condenser.

Condensation nuclei vary in size (p. 216), but as the quantity of condensing vapor increases, the differences in droplet radii diminish and when the droplets have grown to a radius of $(3-5)\cdot10^{-4}$ cm a virtually monodisperse fog is obtained. This is illustrated by calculations of sulfuric acid vapor condensation in a pipe (see Figure 5.10). When nucleation has stopped (at point b, Figure 5.10), $\bar{r} = 1\cdot10^{-5}$ cm and $\alpha = 2.3$. The droplets continue to grow by condensation and the variability coefficient α decreases, so at the pipe outlet $\bar{r} = 4.5\cdot10^{-5}$ cm and $\alpha = 0.17$.

It follows from the preceding that the uniformity of the fog droplets becomes more pronounced as the initial radius of the condensation nuclei is decreased and the terminal radius of the droplets is increased.

The liquid fog droplets produced by the above method contain the condensation nuclei as an impurity. The mass concentration (%) of these impurities is expressed by the equation

$$m = \left(\frac{r_1}{r_2}\right)^3 \frac{\rho_1}{\rho_2} \cdot 10^2 \qquad (7.2)$$

where r_1, r_2 are the radii of the condensation nuclei and the fog droplets; ρ_1, ρ_2 the density of the condensation nuclei and of the liquid droplets. The ratio r_1/r_2 is typically less than 10^{-2}, and the impurity content is therefore negligible ($\sim 10^{-4}$ %), but in some cases even this low figure is inadmissible.

Impurity-free monodisperse fog can be produced with the aerosol generator of the heat-exchanger type recommended for controlling the drop size of fogs (p. 213). The fog droplets which nucleate and grow by condensation in the free-volume chamber act as condensation nuclei in the process.

A mixer-type generator for the production of impurity-free monodisperse fog is schematically shown in Figure 7.12. Cold air is injected externally into a vapor-gas mixture, which is then delivered to the free volume 1. The mass ratio of the mixing gases is such that the required number density of the droplets is formed by homogeneous condensation.

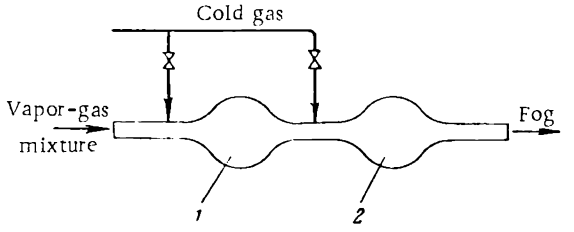

FIGURE 7.12. Mixer-type condenser: 1, 2) free volumes.

In the free volume the vapor condenses on the surface of the embryos and the supersaturation decreases. Another portion of cold air is then injected into the gas in order to reduce the supersaturation to a subcritical value. No new embryos form, and the excess vapor condenses on the surface of already existing droplets. The number of mixing stages is determined individually for each particular case, depending on the composition of the mixing gases, the content of vapor, the temperature, etc.

An analysis of the drop size distribution of fogs produced in generators of both kinds /22/, in heat exchangers /17/, and in mixers /21/ shows that the mean geometrical radii of the fog droplets are between the limits of $0.5 \cdot 10^{-4}$ and $1.25 \cdot 10^{-4}$ cm with standard deviations of 1.02 — 1.12. The size of the droplets is independent of the number density for concentrations of less than 10^4 drops/cm^3 in the mixer-type generator and 10^3 drops/cm^3 in the heat exchanger. Aerosol generators of the heat-exchanger type produce more uniform fogs than the mixer-type generators. The authors /22/ failed to explain this feature.

The supersaturation is highly variable in turbulent jets (Figures 3.7 and 3.8) and across the laminar flow of a gas in a pipe (Figure 5.2). This is apparently the main reason for the residual nonuniformity of the droplet radii in the fogs produced by these generators. The supersaturation across a pipe, however, changes between narrower limits than the supersaturation in a turbulent jet, and an aerosol generator of the heat-exchanger type therefore produces fog with a more uniform drop size distribution than the mixer-type generator. There is reason to believe that fog with even more uniform droplets will be obtained under turbulent conditions of gas flow in a generator of the heat-exchanger type, since the supersaturation remains nearly constant in the turbulent core (see Figure 5.2) and the fog droplets forming in the boundary layer (where the supersaturation is highly variable) settle out on the pipe wall without penetrating into the turbulent cone (p. 116).

It follows from the preceding data that if $S<S_{cr}$ and the supersaturation is constant throughout the generator, the monodispersity of the fog depends on the monodispersity of the condensation nuclei and on the extent of their condensational growth. Production of monodisperse condensation nuclei (which may be regarded as finely divided aerosols) is an even more formidable problem than production of monodisperse fogs (or aerosols) with droplet radii of $10^{-4}-10^{-5}$ cm: the condensation nuclei are much smaller and surface activity plays an important part in overall considerations.

REFERENCES

1. FUKS, N. A. Mekhanika aerozolei (Mechanics of Aerosols). — Izdatel'stvo AN SSSR. 1955.
2. PETRYANOV, I. V. and N. F. TUNITSKII. — ZhFKh, 13:1131. 1939.
3. FUKS, N. A. and A. G. SUTUGIN. — Kolloidnyi Zhurnal, 26:110. 1964.
4. Primenenie aerozolei v sel'skom khozyaistve (Application of Aerosols in Agriculture). Collection of translations. — IL. 1955.
5. AMELIN, A. G. and M. I. BELYAKOV. — Kolloidnyi Zhurnal, 17:1463. 1955.
6. AMELIN, A. G. and M. I. BELYAKOV. — Zavodskaya Laboratoriya, No. 12:1463. 1955.
7. DUNSKII, V. F., Z. M. YUZHNYI, and D. N. KHOKHLOV. — In: "Aerozoli v sel'skom khozyaistve", p. 28. Sel'khozgiz 1956.
8. PRONIN, A. F. Mashiny dlya bor'by s vreditelyami i boleznyami sel'skokhozyaistvennykh kul'tur (Machines for Combating Pests and Diseases of Agricultural Crops). — Izdatel'stvo Vysshaya Shkola. 1964.
9. Spravochnik khimika (Chemist's Handbook), Vol. I. — Goskhimizdat 1962
10. O'CONNOR, T. C., W. P. F. SHARKEY, and C. O'BROLCHAIM. — Geofis. pura e appl., No. 1:109. 1959.
11. AMELIN, A. G. Teoreticheskie osnovy obrazovaniya tumana v khimicheskikh proizvodstvakh (Theoretical Principles of Fog Formation in Chemical Industries). — Goskhimizdat 1951.
12. SHISHKIN, N. S. Oblaka, osadki i grozovoe elektrichestvo (Clouds, Precipitations, and Thunderstorm Electricity). — Gidrometeoizdat 1964
13. KARIORIS, F. S., B. R. FICH, and G. W. ROYSTER. — Exploding Wires, Vol. 2, p. 299. New York. 1962.
14. MASON, B. J. The Physics of Clouds. — Oxford Univ. Press 1957.
15. FUKS, N. A. and A. G. SUTUGIN — Uspekhi Khimii, 34:276. 1965.

16. SINCLAIR, D. and V. K. LA MER. — Chem. Rev., 44 : 245 1949.

17. LA MER, V. K. — Chem. Rev., 44 : 341. 1949.

18. RAPOPORT, E. and S. W. WIENSTOOK. — Experientia, 11 : 363. 1955.

19. LASSEN, L. — Z. angew. Phys., 12 : 157. 1960.

20. MARTIUS, C. — Zeiss Mitteil., 1 : 226. 1958.

21. KOGAN, Ya. I. and Z. A. BURNASHEVA. — ZhFKh, 34 : 2630. 1960.

22. FUKS, N. A. and A. G. SUTUGIN. — Kolloidnyi Zhurnal, 25 : 487. 1963.

APPENDIX I

Particle size measurement methods for different ranges of particle diameters*

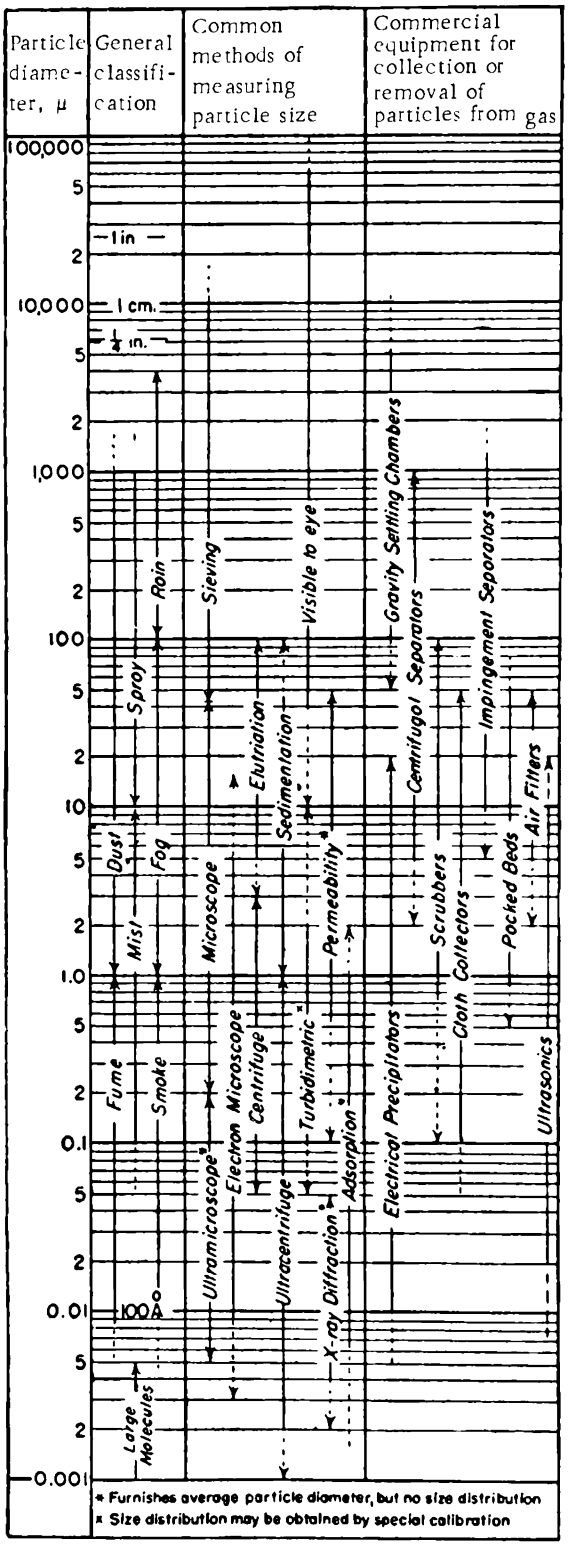

* DUECKER, W. W. and I. R. WEST. The Manufacture of Sulfuric Acid. — New York, Reinhold Publ. Corp. 1959.

APPENDIX II

Constants A and B*

Formula	Name	Temperature range, °C		A	B
		from	to		
Ag	Silver	936	2240	8 25	13700
Al	Aluminum	724	1279	8.99	15630
Al_2O_3	Aluminum trioxide	2040	2970	11.296	27320
As_4O_6	Arsenous oxide	65.5	233	13.70	6672
CO_2	Carbon dioxide	-135	-56.7	9 9082	1367.3
CaO	Calcium oxide	1360	1480	9.77	27400
Cl_2	Chlorine	-154	-103	9.950	1530
Cu	Copper	970	1083	9.232	17260
Fe	Iron	1094	1535	9.63	20000
H_2O	Water	-20	+60	9.1513	2317.7
		20	100	8.8444	2224.4
H_2S	Hydrogen sulfide	-145	-131	8.5005	1175.3
H_2SO_4	Sulfuric acid 85%	0	250	7.751	3685
	" " 90%	0	250	7.897	3685
	" " 95%	0	250	8.316	3637
	" " 98%	0	250	8.470	3593
H_2SeO_4	Selenic acid	11	31	14.130	4304
Hg	Mercury	-80	-38.87	10.383	3813
		18	360	7.20	2760
NH_4Cl	Ammonium chloride	100	400	10.0164	4360.5
NaOH	Sodium hydroxide	618	1380	7.434	7519
P	Red phosphorus	230	550	10.996	5600
Pb	Lead	483	975	7.69	9600
PbO	Lead oxide	614	878	11.58	13900
S	Molten sulfur	119.3	300	6.0489	4087.8
SO_3	Sulfur trioxide	58	17	11.44	2680
Se	Selenium	184	220	12.78	7440
		272	687	8.089	4990
CH_3OH	Methyl alcohol	40	120	5.898	1999.4
CCl_4	Carbon tetrachloride	-70	-19	8.540	1910.8
C_2H_5OH	Ethyl alcohol	-20	2120	6.266	2196.5
CH_2O_2	Formic acid	8.2	110	7.884	1860
$C_2H_4O_2$	Acetic acid	-35	10	8.502	2177.4
C	Carbon	1590	2845	10.900	37100
		2000	5000	9.330	33300

* Spravochnik khimika (Chemist's Handbook), Vol. I. — Goskhimizdat. 1962. These constants are the parameters in the equation

$$\lg p = A - \frac{B}{T} \qquad (1.3)$$

where p is the saturated vapor pressure, mm Hg; T the absolute temperature. For each particular substance this equation applies in the temperature range, as listed in the table. To convert from mm Hg to atmospheres, the constant A should be divided by 2.8808.

APPENDIX III

Coalescence (coagulation) constant of monodisperse fog of density g/cm^3 in air*

Droplet radius r, cm	Coalescence constant $K \cdot 10^{10}$, cm^3/sec	Droplet radius r, cm	Coalescence constant $K \cdot 10^{10}$, cm^3/sec
10^{-7}	4.5	$2 \cdot 10^{-5}$	4.0
$2 \cdot 10^{-7}$	6	$5 \cdot 10^{-5}$	3.4
$5 \cdot 10^{-7}$	9	10^{-4}	3.1
$1 \cdot 10^{-6}$	12	$2 \cdot 10^{-4}$	3.0
$2 \cdot 10^{-6}$	11	$5 \cdot 10^{-4}$	3.0
$5 \cdot 10^{-6}$	7.2	10^{-3}	3.0
10^{-5}	5.2		

* FUKS, N. A. Mekhanika aerozolei (Mechanics of Aerosols). — Izdatel'stvo AN SSSR. 1955.

APPENDIX IV

Supersaturation at which condensation of water vapor occurs on small ions in air*

	Ion sign	T_1 (°K)	T_2	$\frac{v_2}{v_1}$	S
Wilson (1899)	−	293	267.8	1.252	4.2
	+	293	—	1.31	6.0
Przibram (1906) . . .	−	293	—	1.236	3.7
	+	293	—	1.31	6.0
Laby (1908)	−	—	267.6	1.256	4.2
Andren (1917)	−	—	267.8	1.253	4.1
Powell (1928)	−	291	266.5	1.245	3.98
Flood (1933)	−	—	265	1.252	4.1
Loeb, Kip, and Einarsson	−	295	—	1.25	—
(1938)	+	295	—	1.31	—
Scharrer (1939) . . .	−	292	—	1.25	4.14
	+	292	—	1.28	4.87
Sander and Damkohler (1943)	−	—	265	—	3.9

* MASON, B. J. The Physics of Clouds. — Oxford Univ. Press. 1957.

Publications in Russian (in Cyrilic alphabetic order)

AMELIN, A. G Teoreticheskie osnovy obrazovaniya tumana pri kondensatsii parov (Theory of Fog Condensation). — Izdatel'stvo Khimiya. 1965. [English translation published by IPST, Jerusalem 1967.]

AMELIN, A. G. Tumany sluzhat cheloveku (Fog in the Service of Man). — Izdatel'stvo AN SSSR. 1961.

Aerozoli v sel'skom khozyaistve (Aerosols in Agriculture). Collection of papers. — Sel'khozgiz. 1956.

Aerozoli i ikh primenenie (Aerosols and Their Uses). Proceedings of the Second and Third Interdepartmental Aerosol Conferences at VASKhNIL. Published by the Ministry of Agriculture of the USSR. 1959.

BEKKERMAN, I. M. Nevidimyi ostavlyaet sled (Tracks of the Invisible). — Atomizdat. 1964.

BERKOVICH, M. T. and Ya. Z. BUKHMAN. Promyshlennaya pyl' (Industrial Dust). — Sverdlovsk, Metallurgizdat. 1960.

VEITSER, Yu. I. and G. P. LUCHINSKII. Khimiya i fizika maskiruyushchikh dymov (Chemistry and Physics of Camouflage Smokes). — Oborongiz. 1938; Maskiruyushchie dymy (Camouflage Smokes). — Goskhimizdat. 1947.

GORDON, G. M. and I. L. PEISAKHOVICH. Kontrol' pyleulavlivayushchikh ustanovok (Management of Dust-Collecting Installations). — Metallurgizdat. 1961.

GRABOVSKII, R. I. Atmosfernye yadra kondensatsii (Atmospheric Condensation Nuclei). — Gidrometeoizdat. 1956.

DERYAGIN, B. V. Aerozoli (dymy i tumany) (Aerosols — Smokes and Fogs). — Izdatel'stvo Znanie. 1961.

ELKIN, I. I. and S. I. EDEL'SHTEIN. Aerozoli antibiotikov, ikh poluchenie i klinicheskoe primenenie (Antibiotic Aerosols, Production and Clinical Uses). — Medgiz. 1955.

KOROTKIKH, G. I. Aerozoli v sel'skom khozyaistve (Aerosols in Agriculture) — Sel'khozgiz. 1960.

LEVIN, L. M. Issledovaniya po fizike grubodispersnykh aerozolei (Studies in the Physics of Coarsely Divided Aerosols). — Izdatel'stvo AN SSSR. 1961.

MEDNIKOV, E. P. Akusticheskaya koagulyatsiya i osazhdenie aerozolei (Acoustic Coagulation and Precipitation of Aerosols). — Izdatel'stvo AN SSSR. 1963.

Meteorologiya i atomnaya energiya (Meteorology and Atomic Energy). Translations from English. — IL. 1959.

Novye idei v oblasti izucheniya aerozolei (New Ideas in the Study of Aerosols). Collection of papers. — Izdatel'stvo AN SSSR. 1949.

PRECHISTENSKII, S. A. Radioaktivnye vybrosy v atmosferu (Radioactive Emissions in the Atmosphere). — Gosatomizdat. 1961.

Primenenie aerozolei v sel'skom khozyaistve (Application of Aerosols in Agriculture). Collection of translations. — IL. 1955.

Radioaktivnye chastitsy v atmosfere (Radioactive Particles in the Atmosphere). Translations from German. — Gosatomizdat. 1963.

RYAZANOV, V. A. Sanitarnaya okhrana atmosfernogo vozdukha (Health Hazards of Air Pollution). — Medgiz. 1954.

SIPYAGIN, V. A. and A. F. SACHKOV. Obespylivanie atmosfery rudnikov (Dust Removal from the Air in Mines). — Metallurgizdat. 1958.

TOMSON, N. M. Sanitarnaya okhrana atmosfernogo vozdukha (Health Aspects of Air Pollution). — Medgiz. 1959.

UZHOV, V. N. Ochistka promyshlennykh gazov elektrofil'trami (Cleaning of Industrial Gases with Electrostatic Precipitators). — Goskhimizdat. 1962.

UZHOV, V. N. Bor'ba s pyl'yu v promyshlennosti (Air Pollution in Industry). — Goskhimizdat. 1962.

FUKS, N. A. Mekhanika aerozolei (Mechanics of Aerosols). — Izdatel'stvo AN SSSR. 1955.

FUKS, N. A. Isparenie i rost kapel' v gazoobraznoi srede (Evaporation and Growth of Droplets in a Gas Medium). — Izdatel'stvo AN SSSR. 1958.

FUKS, N. A. Uspekhi mekhaniki aerozolei (Advances in Aerosol Mechanics). — Izdatel'stvo AN SSSR. 1961.

SHELEIKHOVSKII, G. V. Zadymlenie gorodov (Smoke Pollution of Cities). — Published by the Ministry of the Communal Economy of the RSFSR. 1949.

SHIFRIN, K. S. Rasseyanie sveta v mutnoi srede (Light Scattering in Turbid Media). — Tekhteoretizdat. 1951.

SHISHKIN, N. S. Oblaka, osadki i grozovoe elektrichestvo (Clouds, Precipitations, and Thunderstorm Electricity). — Gidrometeoizdat. 1964.

YARNYKH, V. S. Primenenie aerozolei v veterinarii (Veterinary Uses of Aerosols). — Sel'khozizdat. 1962.

Publications in Other Languages

Aerosols, Physical Chemistry and Applications, Proceeding of the First National Conference on Aerosols held at Liblice near Prague, October 8—13. 1962. — Publishing House of Czechoslovak Academy of Sciences, Prague, p. 943. 1965.

Air Pollution. — WHO, No. 46.

AVY, A. P. Les aérosols. — Dunod, Paris. 1956.

BEVANS, B. Math Expression for Drop Size Distribution in Sprays, Michigan. 1949.

CADLES, R. D. and P. L. MAGILL. Air Pollution Handbook, London. 1956.

DAUTREBANDE, L. L'aérosologie, Paris. 1951.

DAVIES, C. N. Dust is Dangerous. — Faber and Faber, London. 1954.

DAVIES, C. N. Recent Advances in Aerosol Research. — Pergamon Press, London. 1964.

DRINNER, P. and T. HATCH. Industrial Dust. — McGraw-Hill, London. 1954.

FETT, W. Der atmospharische Staub. — Berlin, Deutscher Verl. der Wissensch. 1958.

GOETZ, A. The Concentrometry. — McGraw-Hill, New York. 1959.

GREEN, H. L. and W. R. LANE. Particulate Clouds (Dust, Smokes and Mists). — Spon, London. 1964.

HERDAN, G. Small Particle Statistics. — McGraw-Hill, New York. 1953.

HIRTH, J. P. and C. M. POUND. Condensation and Evaporation, Nucleation and Growth Kinetics. — Pergamon Press, London. 1963.

KOULA, V. and M. DURASOVA. Aerosols in Plant Protection [in Czech. Russian translation. 1957.]

LA MER, V. K. Air Pollution. — New York. 1952.

Mc CABE, L. C. Air Pollution. — AEC, New York. 1952.

MAGIL, P. L. and F. R. HOLDEN. Air Pollution Handbook. — McGraw-Hill, London. 1956.

MANSMANN, J. Aerosole Mikro-Nebel. — Starnbery. 1958.

MARSH, A. Smoke. — Pergamon Press, London. 1957.

MASON, B. J. The Physics of Clouds. — Oxford Univ. Press. 1957.

MEETHAN, A. R. Atmospheric Pollution. — Pergamon Press, London. 1958.

NÜCKEL, H. Aerosol-Therapie, Stuttgart. 1957.

RODEBASH, W. H. Handbook on Aerosols, Washington DC. 1950.

ROSE, H. E. The Measurement of Particle Size in Very Fine Powders. — Constable and Co., London. 1958.

SHELUDKO, A. Colloid Chemistry [in Bulgarian. Russian translation. 1960.]

SINCLAIR, D. Handbook of Aerosols. — AEC, Washington. 1950.

SPURNÝ, K., Č. JECH, B. SEDLÁČEK, and O. ŠTORCH. Aerosols [in Czech. Russian translation. 1964.]

VAN de HULST, H. C. Light Scattering by Small Particles. — New York, Wiley. 1957.

VOLMER, M. Kinetik der Phasenbildung. — Leipzig. 1939.

WHYTLAW-GRAY, R. and H. S. PATTERSON. Smoke. — London, Arnold and Co. 1932.

Absorption
column 163, 177, 180, 197; also see Tower
of SO_3 by H_2SO_4 174 ff, 196
critical temperature 179
percentage 180
of thermal radiation 59
Absorptivity 59
Accommodation coefficient 10, 13, 14, 19, 27 ff
Adiabatic
expansion 22, 25, 35, 37, 43 ff, 51 ff, 85, 98, 203, 205, 218
parameters 55
processes 58 ff
Aerosil 170, 191; also see Silica smoke
Aerosol ix, 141, 174, 182 ff, 186, 191
generators 91, 92, 212, 217 ff
prevention 145; also see Fog prevention
Aerosols
medical 208 ff
monodisperse 202, 207
pesticide 91, 202, 211 ff
Aggregates, molecular; also see Embryo
critical size of 11, 12
size distribution of 12
Air pollution 22, 185 ff; also see Emissions, air polluting
Aircraft trails 89
Aitken nuclei 21
Aitken counter 22
Ash, volcanic 21
Azeotropic point 174, 181

Becker-Doering equation 10, 14, 15, 26, 48, 124 126, 140, 141
Blackbody 59
"Blackness" 59
Boltzmann's constant 4
Boundary layer 115, 116, 220
Brownian coalescence 138
Bubble, gas 164, 165
Bubblers 122, 163 ff
Bubbling concentrator 163 ff
equipment 105, 121
pipes 122
Burner fumes (sulfur) 155, 186

Catalyst, contact 153
Central cone of jet, thermodynamic parameters 67
Centrifugal force 202
Chamber
cloud 18, 22, 24-25, 45, 55 ff, 85, 98
contact catalyst 153
diffusion 19, 94, 98, 99, 114, 199
expansion, see Chamber, cloud
free-volume 219
modified expansion 56
process 155
Wilson cloud 18; also see Chamber, cloud
Clausius—Clapeyron equation 1
Cloud
chamber 18, 22, 24-25, 45, 55 ff, 85, 98; also see under Chamber
formation 99
radioactive 59
seeding 87, 216
systems 88
Coagulation constant, see Coalescence
Coalescence 33, 34, 97, 160, 198, 204, 210, 218
constant 34, 210, 224
eddy 138, 139, 208
thermal (Brownian) 138
Cold front 88
Collectors 202
mist 197
Collisions, molecular 170
Column; also see Tower
absorption 177, 180
Linde 145
Combustion gases 21, 22
Concentration, see Fog, Number density, Vapor
Concentrator, acid 163 ff
bubbling 168
Condensation
between plates 205
heat 25, 26, 31, 204
heterogenous 3, 26
in a jet 210
in a pipe 121 ff
homogeneous 3, 9, 15 ff, 36, 37, 43, 47, 68, 100, 121, 123, 163, 182, 195, 203, 204, 208, 213, 216, 219
nuclei 20 ff, 121, 185 ff, 202, 216 ff

Condensation (cont.)
on a surface 117 ff, 205, 206, 213 ff
parameters 136, 137, 140, 206
rate 29, 204
spontaneous, see Condensation, homogeneous
theory of 15
Condensational growth 203, 206, 207, 216
Condenser
for drop size control 213
Millikan's 198
pipe 121 ff, 214
surface 122
Conduction
thermal 94, 98, 101, 103, 105
Cone
of constant flow velocities 66
Contact process 162
Convection 94
current 19, 99
Cooling
radiative 43, 58, 60
total rate of 51
Core, turbulent 115 ff, 220
Correction
factor, Lothe and Pound's 16
Fuks's 29
Cosmic rays 23
Counter
Aitken 22
Nolan—Pollak 22
Scholtz 22
Counters
electric 181
nucleus 22, 84
Crystallization point 38
Current
convection 19, 99
of embryos 12
Cyclotron 99

Decay, organic 186
Degree of freedom
rotational 16
translational 16
Detector, optical 71
Dew point 101, 184
Diffusion 97, 116
chamber 19, 94, 98, 99, 114, 199
coefficient 31; also see Diffusivity
coefficient of vapor 29
convective 30, 31
eddy 61, 98, 103, 105, 187
molecular 61, 94 ff, 101, 105, 187
of vapor 36
rate 36
Diffusive force 97, 116
Diffusivity 31, 94, 96, 103, 110
thermal 94, 96, 98, 103, 108
Discharge gases, industrial 185 ff
Dispersity 35, see Drop size distribution
of fog 33 ff, 38, 203, 210
of soot 188, 190, 191
Distillation, isothermal 49, 87, 204, 212
Distribution
equilibrium 11
of droplet sizes, see Drop size distribution
steady-state 12
Drop(s)
"ages" 216
electric charge 5, 6, 90, 198
number 48
parameters 32, 136
radius 38
mean 33, 202, 209, 210, 219
rate of formation 16, 132
rate of growth 83, 84
size control, in a condenser 213
distribution 11, 55, 80 ff, 97, 121 ff
202, 209; also see Dispersity
controlled 206 ff
Dynamic equilibrium 11, 12

Eddy coalescence 138, 139, 208
diffusion, see Diffusion, eddy
pulsations 30, 31, 116, 139, 212
Electric charge of droplets 5, 6, 90, 198
counters 181
field strength 84
furnace 177, 194
Elements, radioactive 23
Embryo(s); also see Nucleation
current of 12
liquid 3
number of molecules in 10
radius 18
rate of formation 9, 10, 25
rate of growth 97
Emissions, air polluting 21, 22, 92, 185 ff
Emissivity 59
Energy
free 7, 8, 15, 16
nucleation 15
surface 7
Equation
Becker—Doering 10, 14, 15, 26, 48, 124, 126, 140, 141
Clausius—Clapeyron 1
conduction and diffusion 94
Frenkel 11, 14 ff, 18, 24, 26, 48, 58, 124, 126, 132, 140, 141
Kelvin 3, 7, 20
Maxwell 29
nucleation 34
coalescence (coagulation) 34
Equilibrium
constant 130

Equilibrium
distribution 11
dynamic 11, 12
Eruptions, volcanic 186
Evaporation coefficient 27, 28
Evaporator 125, 217, 218
Exhaust gases, see Emissions, air polluting
Expansion
adiabatic 22, 25, 35, 37, 43 ff, 85, 98, 203, 205, 218
chamber 85, 98
modified 56
rate 203
ratio 46 ff, 206, 207
time 52, 207
Exploding wires 217
Explosion, nuclear 59

Fallout, radioactive 59
Field
magnetic 57
electric 84
Filters 121, 145, 215; also see Collectors, Precipitators
inertial 202
First law of thermodynamics 43
Flow
cone of constant velocities 66
laminar 99, 109, 115, 116, 217, 220
rate 72 ff, 130
turbulent 108, 109, 113, 115, 116, 120
velocity 72, 73, 74, 130
Fluctuations, statistical 57; also see Eddy pulsations
Flux of radiant energy, attenuation of 59
Fog
appearance 17
concentration, see Number density and Fog, mass concentration
control 205, 208 ff
degree of separation 202
dispersity 33 ff, 38, 203, 210
control of 210
fluorosilicic acid 197
formation, adiabatic expansion 43 ff
chemical reactions 170 ff
diffusion processes
molecular 94 ff
eddy 105 ff
heat conduction processes
molecular 94 ff
eddy 105 ff
in the atmosphere 89, 90, 101
prevention of 112, 141 ff, 202
radiative cooling 58, 101
turbulent mixing 61 ff, 113 ff
hydrochloric acid 197
mass concentration 33 ff, 82, 90, 160, 162 198, 210
monodisperse 33, 114, 138, 203, 204, 213, 216 ff
polydisperse 33, 81, 203, 207, 212
prevention 112, 141-168, 202
production of monodisperse fog 217
radioactive 101 ff
sulfuric acid 141 ff, 174 ff
weight concentration, see Fog, mass concentration
Force
centrifugal 202
diffusive 97, 116
thermophoretic 97, 116
Free energy 7, 8, 15, 16
organic radicals 20
Free-volume chamber 219
technique 214
Freezing out of vapor 141 ff
Frenkel's (thermodynamic) equation 11, 14 ff, 18, 24, 26, 48, 58, 124, 126, 132, 140, 141
Front (Frontal surface) 88
Froth systems 121, 122
Fuks's correction 29
Fumes, sulfur, 155, 186
Furnace
electric 177, 194
gases in H_2SO_4 concentration 163, 165 ff

Galvanometer 182, 184, 198
Gas bubble 164, 165
Gases
combustion 21, 22
diatomic 58
furnace 163, 165
industrial emissions 21, 22, 92, 185 ff
ion-free 17, 86
monoatomic 47, 58
polyatomic 59
turbulent mixing of 61, 205
Generator
aerosol 91, 92, 212, 217 ff
heat-exchanger type 217 ff
mixer-type 217 ff
monodisperse fog 217
particle 208, 217
Glover tower 155, 158-162
Graduating towers 87, 153
Grid towers 121
Growth by condensation 203, 206, 207, 216

Heat
balance 62, 156, 172, 173
conduction 105
exchanger 122, 213, 217 ff
aerosol generator 217 ff
molar specific 31

Heat (cont.)
of condensation 25, 26, 31, 204
latent 36, 43, 50, 133
of evaporation, molar 2
specific 2, 106, 172
of reaction 172, 173
transfer, see Transfer
Hydrochloric acid fog 197
Hydrolysis of Al_2Cl_6 194
KCl 197
$SiCl_4$ and SiF_4 191
Hygrometer, photoelectric 184
Hygroscopic substances 17

Inertial filters 202
Insecticides 91, 92, 208 ff
Interplanetary space 59
Ion-free gases 17, 86
Ions 17, 23, 126
condensation on 5, 6
Irradiation 198
Isolines in a jet 77
Isotachs 74
Isothermal distillation, see Distillation, isothermal

Jet
boundary 72, 74
boundary layer in 115, 116, 220
condensation in 210
critical supersaturation 85-86, 90
free 19, 58, 66 ff, 83, 85, 86, 203, 204, 210
isolines in 77
pole 66, 73
turbulent 26, 72 ff, 83, 220

Kelvin equation (formula) 3, 7, 20
Kinetic factor 10, 14, 17, 28
Krakatoa 21

Light, scattering of 17, 18, 25, 85, 87, 183, 198
Lightning 186
Linde column 145
Lothe and Pound's correction factor 16

Magnetic field 57
Mass concentration 125, 199; also see Fog, Vapor
Maxwell's equation 29
Metal powders 97, 100 ff, 170, 202
Meteorites 21
Microorganisms 21
Microscope 199
Millikan's condenser 198

Mist
collectors 197
HCl 198
H_2SiF_6 196
H_2SO_4 141 ff, 174 ff
transformer oil 91
Mixer-type aerosol generator 217 ff
Mixing, turbulent 61, 205
Molar heat of evaporation 2
mass 106
mean 63, 106
specific heat 31
Molecular collisions 170
diffusion 61, 94 ff, 101, 105, 187
weight 75, 86
Monodisperse fog 204, 216 ff

Nephelometer, automatic 183 ff
Nephelometric analysis 182
Nephelometry, photoelectric 181 ff
Nolan-Pollak counter 22
Nuclear explosion 59
radiation 198
reactions 99
Nucleation (of embryos) 3, 9, 34, 124, 174, 192, 203 ff, 207, 218
equation 34
rate 9, 12, 14, 16, 17, 19, 24 ff, 37, 47, 81, 83, 84, 97, 124, 128, 199, 203, 204, 210
spontaneous 48
work 9, 16
Nuclei, condensation 20 ff, 121, 185 ff
artificial 202, 216 ff
classification 21
Nucleus counters 22, 84
Number density 14, 18, 22-23, 25-26, 33 ff, 47-48, 80-81, 83-85, 121 ff, 202
controlled 206 ff
Nusselt number 108

Oil mist 91
Optical detector 71
Oxidation, photochemical 186

Packing height 215
surface 145
Particle generators 208, 217
heat-exchanger-type 217
mixer-type 218
measurement methods 222
Particles, radioactive 59
Pesticide 91, 92
spray 208 ff
Petrov's mixture 195, 196

Photochemical oxidation 186
Photoelectric
  hygrometer 184
  measurements 87, 182, 183
  nephelometry 181 ff
Photomultiplier 181
Photosynthesis 35
Phototube 87, 182, 184, 198
Pipe
  bubbling 122
  condenser 121 ff, 214
Pollutants 186, 187
Polydispersity of fog 33, 81, 203, 207, 212
Potential, chemical 7
Powder metallurgy, see Metal powders
Prandtl numbers 108, 109, 114, 119
Precipitation
  artificial 87
  coefficient 208
  electrostatic 86
Precipitator, electrostatic 121, 153, 161, 163, 202
Pressure, partial 45; also see Vapor
Prevention of fog 112, 141-168, 202
Production of fog 217
Pulsations, eddy 30, 31, 116, 139, 212

Quantum statistics 15

Radiant energy, attenuation of 59
Radiation
  thermal 59-60
  chemistry 198
  nuclear 198
  ultraviolet 186, 199
Radiative cooling 58 ff
Radiative fogs 101 ff
Radicals, free organic 20
Radioactive cloud 59
  elements 23
  fallout 59
  particles 59
  samples 99
Rate
  of flow 130
    condensation 29, 204
    cooling, total 51
    diffusion 36
    expansion 203
    formation of droplets 16, 132
      embryos 9, 10, 25
    growth of droplets 83, 84
      embryos 97
    nucleation 12, 14, 16, 17, 19, 24 ff, 37, 47, 81, 83, 84, 97, 124, 128, 199, 203, 204, 210
Reaction, heat of 172, 173
Relaxation time 34
Resistance thermometer 57

Saturation ratio 1
Scattering of light 17, 18, 25, 85, 87, 198
Scrubbing tower 67, 105, 122, 162
Silica smoke 170, 191
    production 187 ff
Sinclair—La Mer aerosol generator 218
Smog 187; also see Air pollution
Solvents recovery 147-152
Soot 170, 202
  dispersity 188, 190, 191
  production 187 ff
Specific heat
  mean 63
  ratio 44, 45
Spray
  guns 91, 92, 208, 211, 212
  pesticide 208 ff
  towers 121, 152-163
  trap 184
Spraying
  density 214
  mechanical 211
  thermal 208
  thermomechanical 92
Statistical fluctuations 57; also see Eddy pulsations
Stefan flow 30, 116, 117, 140
Stream, turbulent, see Turbulent
Sulfuric acid
  absorption of SO_3 174 ff
  concentration 163 ff
  condensation, homogeneous 38
    in a pipe 124 ff
    in spray towers 153
      controlled 214 ff
  manufacture 153 ff
    chamber process 155
    concentrators 163 ff
    contact process 162
    Glover tower 155, 158-162
    wet-gas process 153
Supercooling 38
Supersaturation 1, 16, 34 ff, 46-47, 49, 76 ff, 111, 114, 170, 203 ff, 224
  absolute 36
  critical 3, 8, 16 ff, 65, 67, 68, 96 ff, 142, 148, 182, 185
  critical in a jet 85-86, 90
  formulas for 1, 43, 61, 94, 127, 170
  maximum 65, 82, 83, 86, 88, 95, 96 ff, 108 ff, 115, 117, 124, 125, 145, 147, 148, 152, 154, 173, 205, 208, 213
  minimum 165
  of water vapor 103
  subcritical 214, 219

Supersaturation (cont.)
supercritical 24
terminal 107, 108
zero 80
Surface
activity 220
energy 7
frontal, see Weather fronts
packing 145
tension 4, 8, 10, 15, 20, 84, 188

Temperature of absorption, critical 179
Thermal (Brownian) coalescence 138
diffusivity 94, 96, 98, 103, 108
radiation, absorption of 59
spraying 208
Thermocouples 83, 85, 86, 110
Thermodynamics, first law of 45
Thermometer, resistance 57
Thermophoresis 19, 97, 101, 116
Thermostat 89, 110, 125, 217, 218
Time
expansion 52, 207
relaxation 34
Tower
absorption 162, 163, 197
countercurrent 148
Glover 155, 158-162
graduating 87, 153
grid-packed 122
packed 121, 122, 153, 214, 215
scrubbing 67, 105, 122, 162
spray 121, 122, 152, 163
Trails, aircraft 89
Transfer
coefficient of heat transfer 106, 108, 128
coefficient of mass transfer 105, 107, 108, 128
mass and heat transfer 113, 115
Nusselt numbers 108
Prandtl numbers 108, 109, 114, 119
radiative heat transfer 59, 140
rate of heat transfer 116, 127, 215
rate of mass transfer 215
Transformer oil mist 91
Trap, vapor 141-145; also see Filter, Collector, Precipitator
Turbulent
core 115 ff, 220
flow 30, 31, 113, 115, 116, 122
jet 26, 72 ff, 83, 220
mixing of gases 61, 205
Tyndall effect 47, 67, 85, 181

Ultramicroscope 125
Ultraviolet radiation 186, 199

Vapor
diffusion coefficient 29
freezing out 141 ff
mass concentration 75
pressure 1, 3, 13, 50, 90
equilibrium 174
gradient 97, 98
maximum 171, 172
partial 90
saturated 1, 17, 45, 182
terminal 108
supersaturated 1, 12, 61 ff, 94 ff, 99, 105 ff, 170 ff
formulas for 1, 43, 61, 94, 127, 170
trail, aircraft 89
trap 141-145
Variability coefficient 33, 204, 218
Volcanic ash 21
eruptions 21, 186
Volcanoes 21

Weather fronts 88
Weight concentration, see Mass concentration
Wet-gas contact process 153 ff
Wilson cloud chamber 18
Work, nucleation 9, 16

Zel'dovich coefficient 14

EXPLANATORY LIST OF ABBREVIATIONS OF USSR INSTITUTIONS AND PERIODICALS APPEARING IN THIS BOOK

Abbreviation	Full name (transliterated)	Translation
DAN SSSR	Doklady Akademii Nauk SSSR	Proceedings of the Academy of Sciences of the USSR
Izv. AN SSSR	Izvestiya Akademii Nauk SSSR	Bulletin of the Academy of Sciences of the USSR
NIITEkhim	Nauchno-Issledovatel'skii Institut Tekhniko-Ekonomicheskikh Issledovanii po Khimii	Scientific Research Institute of Technical and Economic Research in Chemistry
NIKhIMMASh	Nauchnyi Institut Khimicheskogo Mashinostroeniya	Scientific Institute of Chemical Machine Construction
NIU GUGMS	Nauchno-Issledovatel'skie Uchrezhdeniya Glavnogo Upravleniya Gidrometeorologicheskoi Sluzhby	Scientific Research Institutes of the Main Administration of Hydrometeorological Service
NIUIF	Nauchnyi Institut Udobrenii i Insektofungisidov	Scientific Institute of Fertilizers and Insectofungicides
UFN	Uspekhi Fizicheskikh Nauk	Advances in Physical Sciences
VKhO	Vsesoyuznoe Khimicheskoe Obshchestvo	All-Union Chemical Society
VNIIgas	Vsesoyuznyi Nauchno-Issledovatel'skii Institut Prirodnogo Gaza	All-Union Scientific Research Institute of Natural Gas
VNIIKIMASh	Vsesoyuznyi Nauchno-Issledovatel'skii Institut Kislorodnogo Mashinostroeniya	All-Union Scientific Research Institute of Oxygen Machine Construction

Abbreviation	Full name (transliterated)	Translation
VTI	Vseosyuznyi Teplotekhnicheskii Institut	All-Union Thermal Engineering Institute
ZhETF	Zhurnal Eksperimental'noi Fiziki	Journal of Experimental and Theoretical Physics
ZhFKh	Zhurnal Fizicheskoi Khimii	Journal of Physical Chemistry
ZhKhP	Zhurnal Khimicheskoi Promyshlennosti	Journal of Chemical Industry
ZhPKh	Zhurnal Prikladnoi Khimii	Journal of Applied Chemistry
ZhTF	Zhurnal Tekhnicheskoi Fiziki	Journal of Technical Physics